Final Report

Development of Oil Slick Thickness Sensors

Imad H. Elhajj, Daniel Asmar, Mahdi Saleh, and Ghassan Oueidat
American University of Beirut – Lebanon

Prepared for:

U.S. Department of the Interior, Bureau of Safety and Environmental Enforcement

Versions:

Version	Reason for Change	Date	Changed by
1.0	Updated mechanical work	15 January 2018	G. Oueidat
1.1	Updated instrumentation and testing. Compiled the report	17 January 2018	M. Saleh
1.2	Reviewed the complete report	20 January 2018	D. Asmar
1.3	Included additions	20 January 2018	M. Saleh
1.4	Review and additions	21 January 2018	I. Elhajj
1.5	Additions and corrections	22 January 2018	M. Saleh
1.6	Final review	22 January 2018	I. Elhajj
1.6	Review	1 February 2018	K. McKinney
1.7	Additions and Corrections	12 February 2018	M. Saleh
1.8	Final review	14 February 2018	I. Elhajj
1.9	Final Approval	27 February 2018	K. McKinney

Submitted to:

Name	Affiliation	Authority
Kristi McKinney	Bureau of Safety and Environmental Enforcement	Contract Officer Representative (COR)

This final report has been reviewed by the BSEE and approved for publication. Approval does not signify that the contents necessarily reflect the views and policies of the BSEE, nor does mention of the trade names or commercial products constitute endorsement or recommendation for use.

This study was funded by the Bureau of Safety and Environmental Enforcement (BSEE), U.S. Department of the Interior, Washington, D.C., under Contract E17PC00001.

Executive Summary

The Bureau of Safety and Environmental Enforcement's (BSEE) Oil Spill Preparedness Division (OSPD) contracted the American University of Beirut (AUB) to develop two oil thickness sensors under BSEE Award #E17PC00001. These sensors are designed to measure the thickness of various crude and refined oils on water, and wirelessly communicate thickness information in near real-time. While the first sensor (referred to as Capacitive and shown in Figure 1) is intended to measure thickness in the range of 3mm and above, the second (referred to as Spectro) is intended for thicknesses below 3mm. The Capacitive sensor relies on measuring the capacitance of the oil/water/air that it contacts and uses this data to estimate the locations of the oil-air and oil-water interfaces. Determining instantaneous interface locations of each fluid along the probe provides the data necessary to calculate the thickness of the oil layer. The Capacitive sensor is designed to vertically mount to a skimmer, boom, or floating buoy and provide thickness readings remotely or to be hand held.

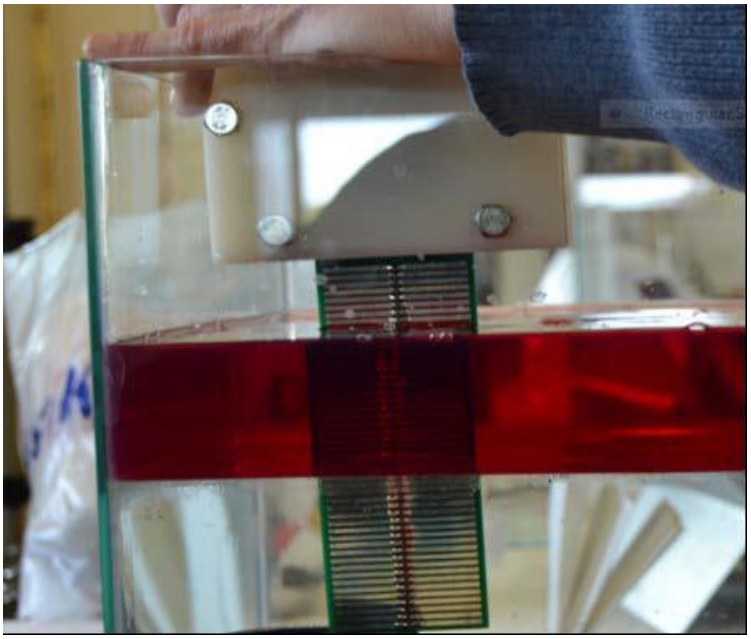

Figure 1: Capacitive Oil Thickness Sensor

The Capacitive sensor was designed to operate in a dynamic environment, where it travels through waves and measures thickness through varying water conditions. The Capacitive sensor will be used in oil spills to provide slick thickness estimates, in order to guide response operators during oil recovery operations. The Spectro sensor, shown in Figure 2, is a free-floating sensor that uses LED-based spectrometry to measure very thin layers of oil with high resolution (up to a thickness of a few millimeters). This sensor is used to determine the presence of a thin oil sheen.

This report details the main milestones of the project and is not meant to be a comprehensive log of all tasks carried out. The report discusses preliminary designs of the sensors including initial testing, experimental testbeds developed, design refinement and testing, and Ohmsett testing. The tests conducted at Ohmsett were performed as per a predefined test matrix (with exceptions); assisted by the team at Ohmsett, AUB engineers tested both Capacitive and Spectro sensors' operations and measurements. Testing of both sensors took place between November 27 and December 1, 2017.

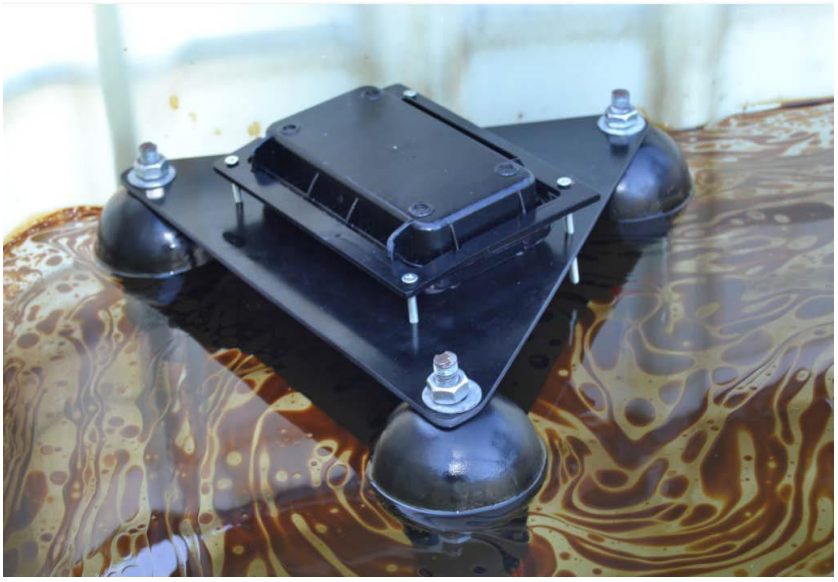

Figure 2: LED-based sensor

The testing at Ohmsett for the capacitive sensor included (1) indoor dipping tests in the small tank using four test oils, (2) outdoor dragging tests at three speeds using the movable bridge mounted over the main tank in calm water conditions using two test oils, (3) outdoor wave testing with the sensor attached to commercially available oil skimmer in the main tank and subjected to multiple wave conditions using one test oil. The testing at Ohmsett for the spectro sensor included (1) indoor free-floating tests in a small tank using two test oils, (2) outdoor free-floating tests in the main tank and subjected to multiple wave conditions using one test oil. The experimental results are discussed in detail in the Chapter 7. In general, the capacitive sensor showed very good accuracy during the indoor testing, where the average absolute error ranged from less than 1mm to around 5mm in the worst case dynamic-scenarios. Also, the sensor showed a good accuracy during the bridge-mounted dragging tests where the average absolute error was around 6mm. During the free-floating tests with waves, the capacitive sensor showed an acceptable accuracy in most of the cases where the absolute average error was less than 10mm. As expected, it was observed that the capacitive sensor accuracy dropped while testing against aggressive waves (Harbor chop), and heavy oils types, due to the significant oil-fouling. Based on the experimental results, several improvements for the sensor design are suggested at the end of this report, to enhance the sensor performance during dynamic-liquid conditions, and to further decrease the oil-fouling effect on the sensor accuracy.

For the spectro sensor, a very good accuracy was obtained during the indoor tests, especially while dealing with transparent oil sheens such as diesel, with an average absolute error of less than 400µm. During the free-floating tests, despite the high standard deviation values of the spectro measurements caused by waves, the sensor overall accuracy was also acceptable, with an average absolute error of around 500µm. However, it was observed that the sensing range of the spectro sensor was decreased to less than 1mm when dealing with opaque oil types such as HOOPS (fresh). Also, oil-fouling of the sensor lenses impacted the accuracy of the spectro device, especially at very thin oil thicknesses. It is important to note that the spectro experiments encountered a main limitation in validating the ground-truth thickness, since it was hard to obtain uniformly-distributed oil sheens at thin oil thicknesses (below 500µm). Based on the experimental results, and aiming to enhance the performance of the spectro sensor device, several suggestions are included at the end of the report for future development.

Table of Contents

List of Figures

List of Tables

Acronyms

BSEE	Bureau of Safety and Environmental Enforcement
RRB	Response Research Brand
DOI	Department of Interior
Ohmsett	Oil Spill Response Research and Renewable Energy Test Facility
AUB	American University of Beirut
GPS	Global Positioning System
LED	Light-emitting diode
RF	Radio Frequency
DC	Direct Current
USB	Universal Serial Bus
TTL	Transistor-Transistor Logic
UART	Universal Asynchronous Receiver-Transmitter
I2C	Inter-Integrated Circuit
GUI	Graphical User Interface
A/D	Analog to Digital
PCB	Printed Circuit Board

Chapter 1- Introduction

This report presents the design, prototyping, and testing of two low-cost floating oil thickness measurement instruments, that provide near real-time measurements for cleanup operations during oil spill incidents. The first sensor is designed for skimming operations, while the second is more suited for oil spill tracking, and oil volume estimation. The first sensor is designed to be installed on a skimmer (ex. TERMITE skimmer [28]), a boom or a floating buoy to help direct cleaning operation; the second sensor is designed to be mounted on a free-floating buoy. The presented experimental work and testing demonstrates the accuracy and repeatability of the proposed instruments under different environmental conditions.

1.1 Background

Sea routes are used for the transportation of oil across different countries all over the world, using large oil tankers. Given the high reliance of the world on oil and gas, and the associated high volume of traffic at sea, it is not uncommon to witness accidental oil spills[1]. Also, oil spills occur due to the release of different oil types (crude/refined) from offshore platforms, oil wells, and pipelines. These accidents have long-term hazardous effects on the environment, especially on living organisms such as birds, mammals, and fish.

Studies have revealed that in an oil spill, roughly ninety percent of the oil volume is located in ten percent of the oil spill area[2]. In addition, the appearance and thickness of slick changes with respect to time and weather conditions. Although remediation options are available during a response to an oil spill, one of the key features impacting the effectiveness of the cleaning techniques is knowing the actual thickness of oil in a slick area. For instance, when at least 1 mm of oil thickness is detected, in-situ burning is an option as a method to remove it. For denser and more emulsified oils, burning is possible only at thickness ranging from three to ten millimeters. Skimmers are widely used in oil spill response to recover floating oil; unlike other chemical based techniques such as dispersants, skimmers perform physical oil/water separation by using oil-attracting and gravity-based techniques. In addition to the sea state, presence of ice, and other environmental conditions, oil spill thickness is one of the most important factors that affects the effectiveness of skimmers[3].

To conclude, oil thickness is a critical parameter that influences the effectiveness of several oil remediation techniques, and its knowledge is essential in directing the cleanup platforms. The sensors we are presenting here, contribute to enhancing the efficiency of the currently used cleanup processes, by providing oil situational awareness, to guide cleanup crews towards the needed areas.

1.2 Related Work

Techniques used to estimate oil thickness or detect its presence can be based on either remote measurements or contact-based measurement. In what follows, we will discuss both approaches.

1.2.1 *Remote Sensing Techniques*

Remote sensing techniques, such as visual imaging and visual observation, are widely used for assessing oil spills. By utilizing airborne vehicles, visual observation—where an expert provides an estimate of the slick thickness based on color observations—is one of the simplest methods used to locate and estimate oil spill. However, due to haze and light reflection from the sea, in some cases visual inspection may be affected [4]. Furthermore, the success of visual imaging techniques is affected by the sea

conditions, as well the temperature conditions. For instance, it can be difficult to see less buoyant oil types while being swamped by waves or collecting into unpredictable shapes during rough sea surface conditions or in cold water. In the case of reflecting sunlight, ocean water may appear very bright and it may be difficult, using traditional imaging techniques, to detect thin oil films floating on the water surface.

Hyperspectral imaging from airborne vehicles [5], is another type of remote sensing technique that is widely used to detect and monitor oil spills, where experiments revealed a high correlation between oil-spill spectral reflectance values and oil-spill thickness measurements. The main limitation in hyperspectral imaging was in applying it from airborne or satellite platforms, because oil spectral measurements are highly affected by cloud coverage, lighting conditions, and sea state.

Microwave passive imaging is another technique for measuring oil thickness from airborne or satellite platforms and is somewhat unaffected by cloud coverage and adverse weather conditions. For instance, in the work of Calla et al.[6], oil spill locations were detected through temperature measurements, collected from a Special Sensor Microwave Imager (SSM/I), and an Advanced Microwave Scanning Radiometer for EOS (AMSR-E) satellite carrying passive microwave sensors. The analysis of the obtained satellite images revealed that the temperature of the oil spill area was greater than that of the surrounding unpolluted areas. Therefore, real-time monitoring for a sudden or abnormal shift in temperature within the same area may be used for detecting an oil spill accident. However, oil thickness estimation based on temperature variations could not be easily performed because the oil temperature is affected by several factors other than its thickness, such as its dielectric constant[7].

To summarize, although airborne and space borne remote sensing techniques are helpful in providing a relatively global assessment of the oil thickness, they are affected by lighting and/or atmospheric conditions, and they are relatively expensive compared to contact-based sensing techniques.

1.2.2 *Contact-based Methods*

Contact-based oil-thickness measurement methods refer to the more traditional instrumentation approaches, such as conductivity, capacitance, light arrays, electromagnetic, and vision[8] [9]. For example, in the work of Denkilkian et al. [8] conductivity and LED arrays were used in implementing a wireless oil-thickness measurement sensor; it relied on a blue LED-array to detect the variation in received blue light intensity as it propagates through oil or water. Also, a metallic array was used to detect the oil thickness based on electric conductivity; such techniques rely on the fact that different aqueous solutions feature different conductive properties. The main factor that affects the water conductivity is the concentration of dissolved salts and other chemicals in it. In contrast to seawater, which is highly conductive because of its sodium ions, oil possesses low electric conductivity. Variation in the received voltage by the conductive plates was used in estimating oil thickness. Although the implemented prototype provided acceptable results, it suffered from problems of corrosion, as well as a low resolution in the order of several centimeters.

Capacitive sensing is widely used for liquid level detection[10] [11]. The continuous capacitive measurement techniques are used mainly in measuring liquid levels in storage tanks, where accurate calibration is needed before operation [12]. Unlike the conductivity-based sensors, the capacitive sensing approach does not require direct contact between the sensor conductive plates and the examined liquid (Oil/Water). As a consequence, by avoiding direct contact electrical corrosion is also avoided. In

comparison to other contact-based oil thickness estimation techniques, capacitive-based sensing promises to be more reliable, and has a longer operating lifetime.

1.3 Selected Sensors Description

In this project, two sensors (Capacitive and Spectro) were implemented, targeting different resolutions and applications. The sensing concept used in each sensor is described briefly in the sections below. The other chapters of this report describe the detailed implementation and testing of each of the two sensors.

1.3.1 *Capacitive Array Sensor*

The capacitive liquid-level measurement technique is used to monitor, with high resolution, rapid changes in liquid amounts. Traditionally, this technique is used to detect fluid variations, by using capacitive sensors composed of a couple of conductive plates. The conductive plates are separated by a constant distance of dielectric material. The capacitance value measured by the sensor without the liquid is called the Net Capacitance `C_n'. After adding liquid into the container, the capacitance changes depending on the liquid amount and type, as $C = \mathcal{E}_r \times C_n$, where $\mathcal{E}_r$ is the relative permittivity of the liquid. The capacitive sensor plates could be shaped in different designs, including planar plates, cylindrical probes, and wires.

The capacitive sensor proposed here offers a novel design, measuring oil thickness based on a geometrical array of conductive electrodes mounted on a low-cost PCB board. This sensing methodology, which we refer to as geometrical capacitive sensing, relies on discrete values reported by an array of adjacent strips. This is in contrast to absolute measurements used in traditional capacitive liquid-level sensing applications. Oil thickness calculation is then estimated based on the geometrical dimensions of the sensor after detecting the number of electrodes immersed in oil. The change in capacitance at each electrode, caused by the change in the dielectric constant of the surrounding material, is measured independently in order to detect the type of environment (air/oil/water) it is in. The electric field formed by the electrodes is affected by the different types of environments surrounding the sensor, thus permitting the differentiation between them based on the change in the corresponding dielectric constant.

1.3.2 *Spectro-based Sensor*

The Spectro-based sensor is based on the phenomenon of light absorption to determine oil thickness. The sensor is designed for oil thickness measurements at relatively high resolutions. Oil thickness is estimated by analyzing the intensity of absorbed light passing through the examined liquid. Previous work done on the spectral analysis in[5] revealed that the correlation between oil thickness and spectral reflectance was highly affected by external lightening conditions. To address this problem, the LED-based sensor is packaged inside an enclosure to isolate the examined liquid from daylight. Our proposed design is inspired by that of that of Yeh and Tseng[13].

Chapter 2- LED-based Sensor Design and Initial Testing

2.1 Sensor Design

The LED-based sensor is composed of three main units: Processing and Communication Unit (PCU), Light Source Unit (LSU), and the Light Receiver Unit (LRU). The PCU calculates the oil thickness by analyzing the intensity of the received light signal. It acquires the location from a GPS module and sends the data to the base station through a wireless transceiver module. The overall block diagram describing the main design of the sensor is shown in Figure 3.

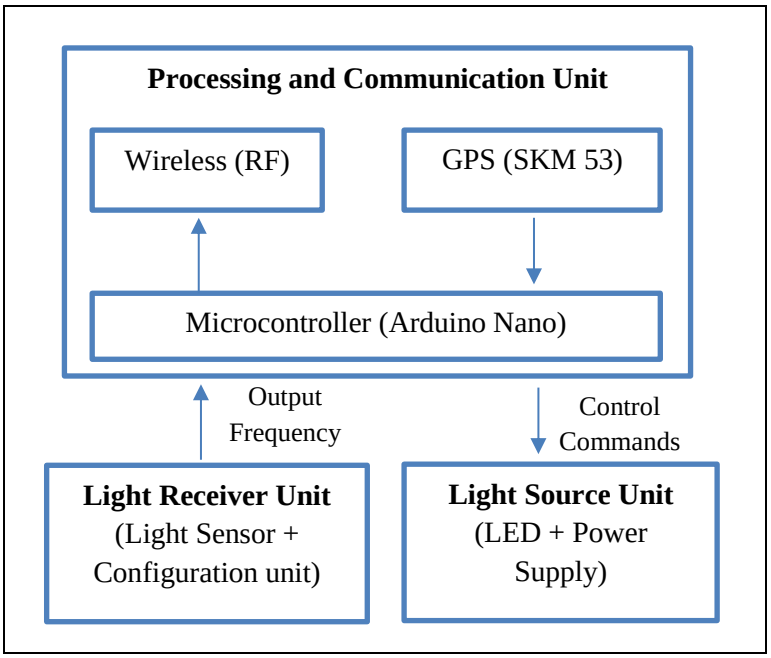

Figure 3: LED-based Sensor - Block Diagram

2.2 Sensor Components

2.2.1 *Light-to-Frequency Converter (TSL230BR)*

The main component of the LRU is the "TSL230BR-LF" (Figure 4) module provided by Texas Advanced Optoelectronics Solutions (TAOS) [14]. This module performs conversion of light intensity to frequency, at high-resolution. It was chosen due to its change its sensitivity programmatically, its low-power consumption, and its ability to communicate directly to a microcontroller. The sensitivity of the photodiode can be selected as one of three options (High, Medium, and Low) and the output frequency can be scaled to one of four values. The device responds over the light range of 320nm to 1050nm.

Figure 4 shows the TSL230BR package and its pinout description. The recommended operating conditions for this device include a supply voltage of 5V and a free-air temperature range from -25ºC to +70ºC. The three sensitivity modes (1x, 10x, and 100x) are selected using two logic inputs S0 and S1, allowing the optimization of the device response based on the intended application. The output frequency can be scaled by using two logic inputs (S2, S3), where the output is connected internally to a series of frequency dividers; divide-by 1, 2, 10, and 100 (Table 1).

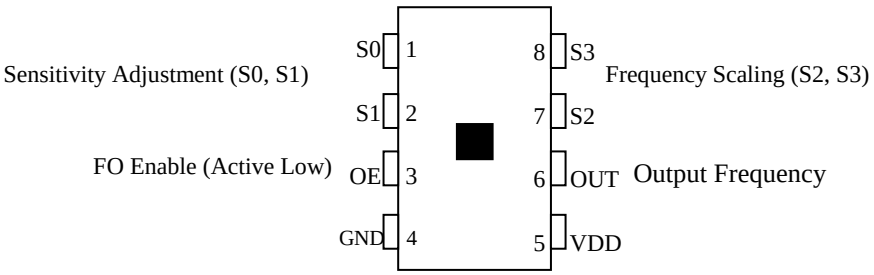

Figure 4: TSL 230BR Package (Top View)

Table 1: Sensitivity & Frequency Scaling for TSL230BR device

S1	S0	Sensitivity	S3	S2	Frequency Division Factor
L	L	Power down	L	L	1
L	H	1x	L	H	2
H	L	10x	H	L	10
H	H	100x	H	H	100

Instead of building a custom circuit to interface the TSL230BR module with the microcontroller board, the additional board "Light-to-Frequency Click" provided by MikroElektronika[15] was used. The board has a 2x5 connector (2.54mm separated pins), which simplifies its connection with any PCB or test boards[16]. Figure 5 shows the Light-to-Frequency Click module and Figure 6 shows its connections schematic.

Figure 5: Light-to-Frequency Click (Mikroelektronika)

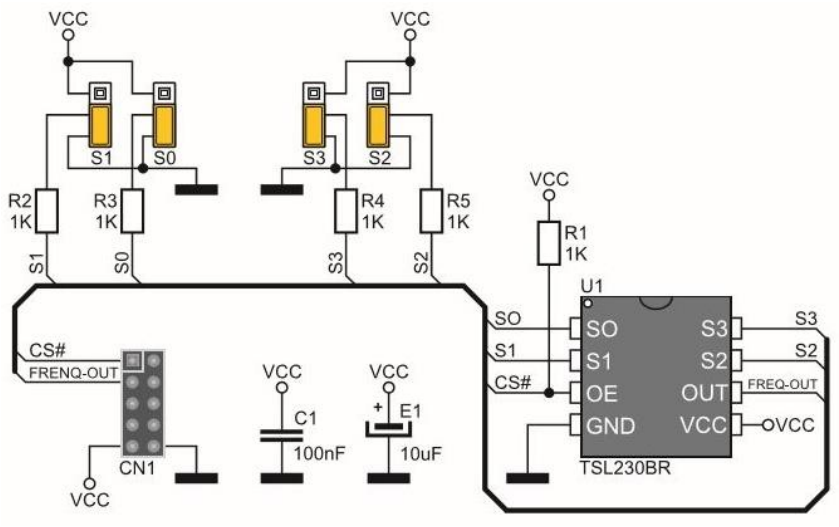

Figure 6: Connection Schematic (Light-to-Frequency Click - Mikroelektronika)

2.2.2 *GPS Module – SkyNav SKM53*

The "SkyNav SKM53" GPS module (Figure 7) provided by Skylab [17], is based on the MediaTek 3329 single-chip architecture, has an embedded antenna, and a 6-pin UART interface. This module is characterized by its high sensitivity (-165dBm), which enables GPS tracking in harsh environments. In comparison with other available GPS modules in terms of cost, power consumption, and sensitivity, the SKM53 was found to be preferable. Table 2, shows the main technical specifications of the SKM53 GPS module.

Figure 7: SKM53 GPS Module

Table 2: GPS SKM 53 – Technical Specifications

Receiver Type	L1 frequency band
Sensitivity	Tracking: -165 dbM, Acquisition: -148dbM
Accuracy	Position: 3.0m CEP50 without SA (Open Sky)
Acquisition Time	Cold/Warm Start: 36s/33s, Hot Start: 1s, Re-Acquisition: < 1s
Dimensions	30mm x 20mm x 8.5mm
Weight	10g
VCC	5V +/-5%
Current	50 mA (typical)
Operating Temp.	-40°C ~+85°C
Humidity	< 95%

2.2.3 *Processing Unit – Arduino Nano*

The Arduino Nano development board (Figure 8) is an open-source prototyping platform based on the ATmega328 microcontroller [18]. This module was selected due to its low-cost, low power consumption, and simple programmability. Main technical specifications of the Arduino Nano module are shown in Table 3.

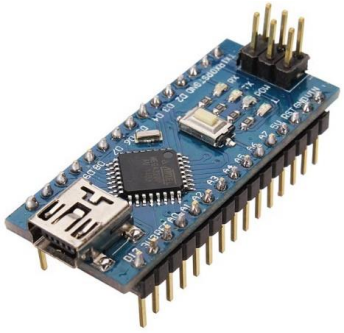

Figure 8: Arduino Nano Board

Table 3: Arduino Nano Module – Technical Specifications

Microcontroller	ATmega328
Operating Voltage	5V
Clock Speed	16MHz
DC Current (I/O pins)	40mA
Input Voltage (VIN pin)	7~12V
Power Consumption	19mA
PCB Size	18x45mm
Weight	7g
Analog I/O pins	8
Digital I/O pins	22

2.2.4 *Wireless Transceiver – TB394 2.4 GHz*

The TB394 module shown in Figure 9 is a low-cost wireless transceiver module (RS232 TTL UART) for Arduino with an IPEX antenna [19]. It operates in two modes, the AT mode and the data transmission mode. The module is configured while working in the AT mode. A serial port is used to issue basic AT commands to set the module parameters (baud rate, frequency settings, ID number, factory settings, and version information). Table 4, shows the main technical specifications of the selected wireless transceiver modules.

Figure 9: Wireless Transceiver Module (RF)

Table 4: Wireless Transceiver Module – Technical Specifications

Parameter	Specification
Operating Voltage	3.3V~5V
RS232 Interface	3.3V/5V TTL level
Frequency Range	2402-2482 MHz
Transmit power	20dBm (100mW)
Receiver sensitivity	-87dBm
Operating Temperature	-40~+85 ºC
Baud rate	9600 (Default)
Transmission distance	400m (Open Ground)
Size	32x13mm

2.2.5 *Wireless Receiver*

To receive the sensor measures wirelessly, a wireless-to-USB receiver module was implemented using the wireless RF transceiver TB394 2.4 GHz and a USB-to-TTL adapter. A 3D-printed package was implemented to fit the two modules connected together on the same PCB (Figure 10). The USB-TTL adapter is based on the CH340 chip, and supports a baud rate ranging from 50bps to 2Mbps.

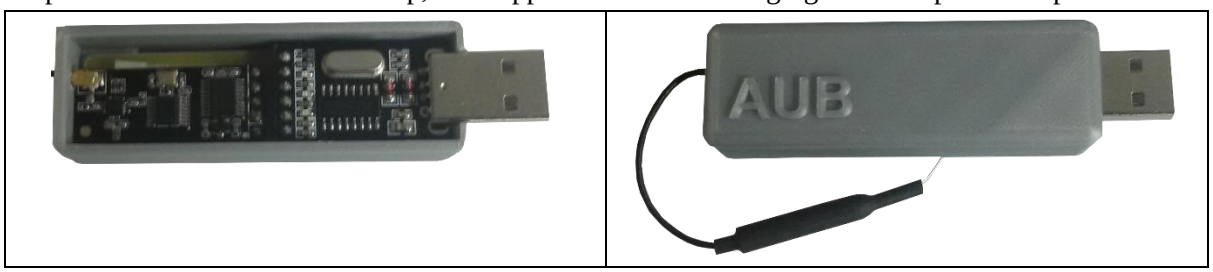

Figure 10: Wireless-to-USB receiver module

2.2.6 *Light Emitter Module*

Based on the preliminary experimental work done on the spectrometer device, the blue light was selected as the light emitting module mainly because of the high correlation observed between blue-light absorption and the oil thickness. The basic 5mm blue LED with a 30mA max current consumption and 3.4VDC forward voltage drop was selected.

2.3 Circuit Design

The control circuit of the LED-based spectrometer (Figure 11), is powered by a linear power supply composed of a voltage regulator (LM2940) with two capacitors (C1=0.47uF & C2=22uF) for filter functions. The LM2940 regulator was chosen primarily due to its low voltage drop (0.5V) which is recommended for battery-powered applications. The GPS module (SKM53) is connected to the main controller board through its serial connection pins (RX, TX) and powered with the voltage regulator output (5V) through a transistor acting as a switch. Since the GPS module is connected to digital I/O Arduino pins, a software serial library is used to replicate the serial connection functionality on those pins. The wireless transceiver module is connected to the hardware serial pins of the microcontroller (TX, RX) and powered by the regulator output voltage (5V) through a transistor acting as a switch. The use of transistors (2N3940) is essential due to the relatively high current consumption of the modules which cannot be handled by the Arduino controller pins. Resistors are used to limit the current between the Arduino digital pins and the transistors base connector.

2.4 Hardware Implementation

A double-sided PCB (Figure 12) is used to implement the LED-based sensor control circuit. The top layer of the PCB holds the microcontroller module, the GPS module, and the RF wireless transceiver. The bottom layer of the PCB holds the Light-to-Frequency converter module carrying the TSL230BR chip. The blue LED is placed in the bottom part of the buoy (directed upward) and centered with the photodiode position at the top. While the liquid mixture (Oil/Water) passes through the middle part of the sensed area, the received light is processed and converted to oil thickness based on the calibration functions.

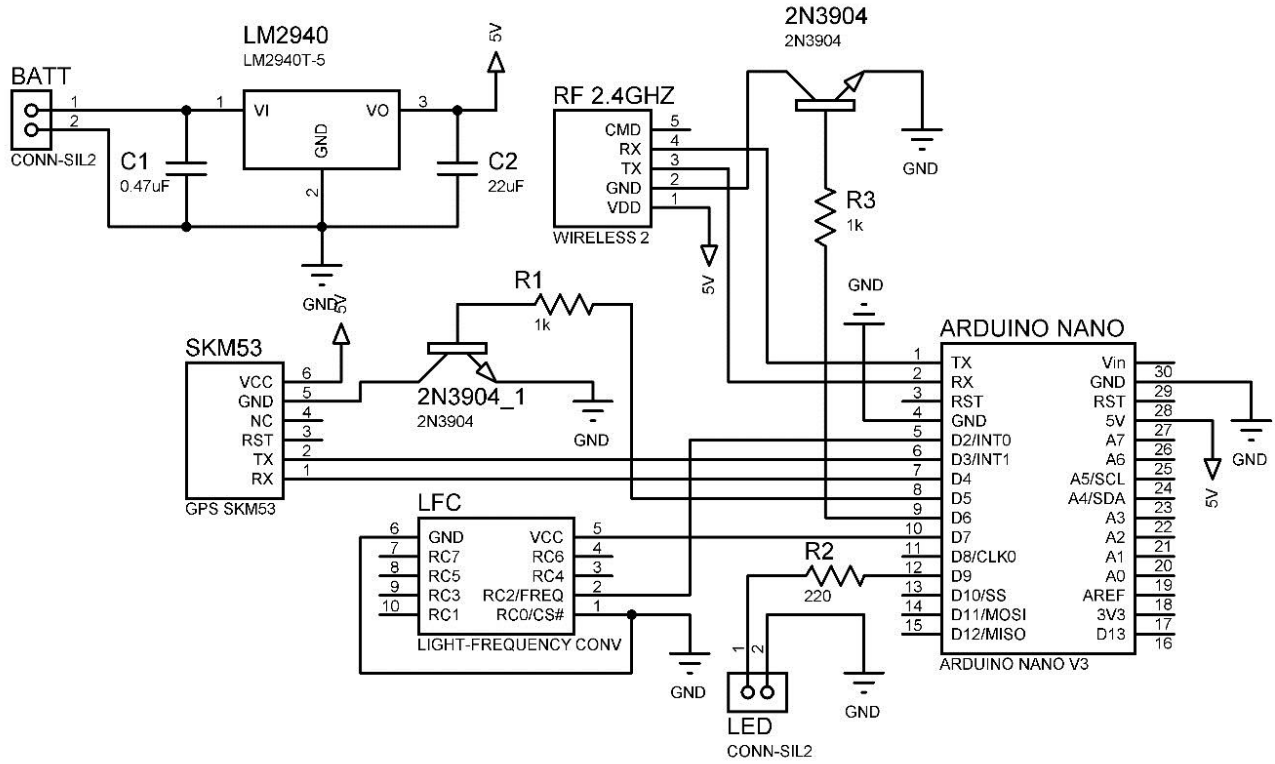

Figure 11: LED-based spectrometer control circuit schematic

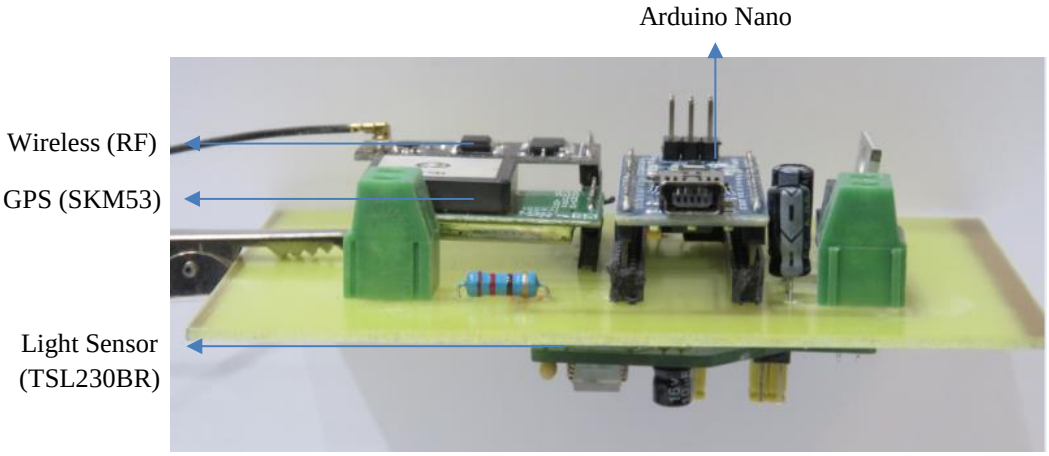

Figure 12: LED-based spectrometer PCB

2.5 Initial Experiments

Given that the LED-based sensor is intended to measure very thin oil layers, light oil types are the major target for testing. Based on past experiments presented in the project proposal, where several LEDs with different colors were tested, the blue light was found to have the maximum correlation between the absorbed light and oil thickness. To assess the effectiveness of the method in measuring different light-oil thicknesses, a small experimental platform, shown in Figure 13, was implemented representing the inner part of the sensor buoy. The light source (blue LED) is mounted in the bottom part of the platform aligned with the receiver at the top of the container. Frequency measurements were taken by the light-receiver module at different thicknesses of oil. To know the actual oil thickness, oil was added to the container with controlled amounts, by using a labeled micro-pipet. The container is closed from its sides by the black adhesive material. The black cover has one major opening in the bottom side to allow the blue light to pass, and other minor openings at the top layer kept letting some amount of light from the environment to enter to the container. This is needed because during operation, the sensing part is not isolated completely from the environment; instead, water and oil pass through the horizontal openings allowing some exterior light to enter and interfere with the measurements.

To handle the interference with the exterior light, several light measurements are taken while the LED is turned off. When activating the LED, the difference between the new measurement and the stored measurement is calculated to remove the effect of the environmental light. The frequency provided by the receiver is directly proportional to the light intensity. In other words, higher light intensities result in increased frequency of the generated square wave signal.

To control the sensitivity pins S0 and S1 are used. To decrease the noise effect, low sensitivity was set by connecting the S1 pin to GND and the S0 pin to VCC. The division factor was set to 100 by connecting S2 and S3 pins to VCC. To measure the output frequency, the output pin of the TSL230BR was connected to the Arduino second digital pin provided with an external interrupt. The frequency is calculated by counting the number of rising edges occurred at the pin for a certain interval of time (1 sec).

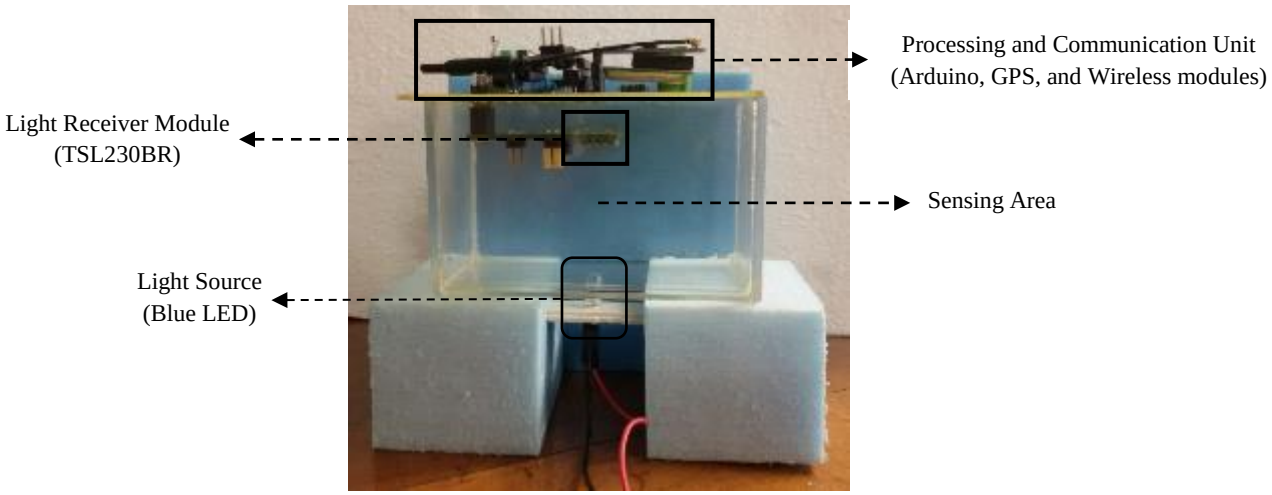

Figure 13: LED-based Sensor Sensing Section (Side View)

2.5.1 *LED-based Sensor Initial Experiment – Light Oil*

In this experiment, a lubricating oil with a viscosity of 10 centistokes (Power-10W) was tested. The received light intensity was measured successively after adding controlled amounts of oil to the

container measured by its volume. To get the corresponding oil film thickness, the volume (m3) of the added amount is divided by the area of the container (m2). The container dimensions are listed below:

- Width = 4.6cm
- Length = 8.9cm
- Height = 5.5cm
- Distance between LED and Oil: 0.3cm
- Distance between PCB and light Receiver module: 1.6mm

The statistical analysis of the experimental results of thirty-eight samples (N=38) are shown in Table 5, and the corresponding graph is shown in Figure 14.

Table 5: LED-based Sensor - Light Oil - Experiment Results

	Oil Thickness (mm)	0	1.22	2.44	3.66	4.88	6.1	7.32	8.54	9.77
Frequency (Hz/100)	Mean	69	64	56	45	38	35	31	28	24
	Standard Deviation	0.22	0.55	0.36	0.72	0.48	0.43	0.47	0.45	0.44
	Maximum	69	65	56	46	38	36	31	28	24
	Minimum	68	63	55	43	37	35	30	27	23

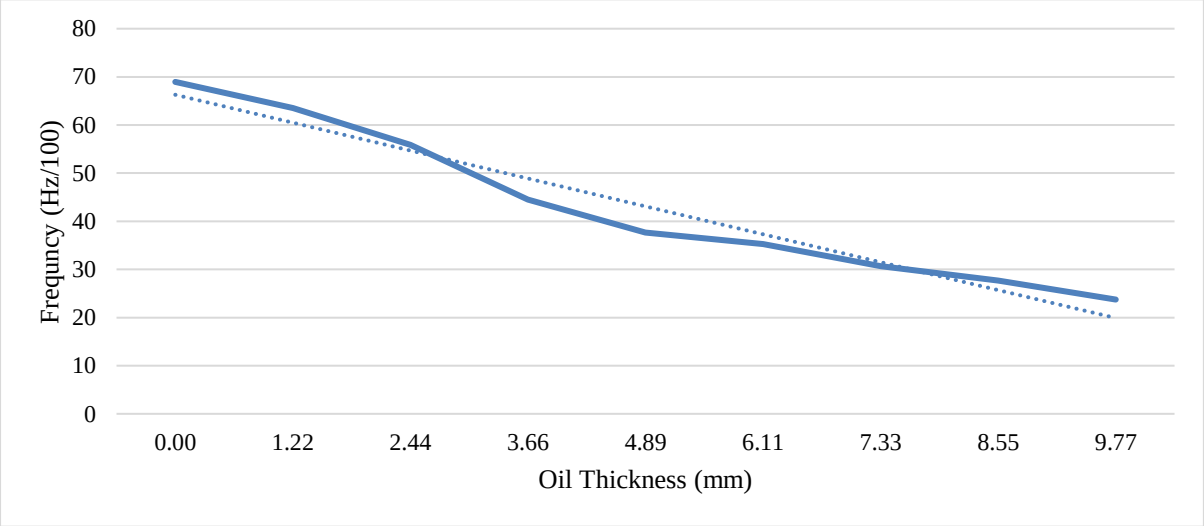

Figure 14: Output Frequency vs. Oil Thickness Plot (LED-based Light Oil Experiment)

As shown in Figure 14, the initial experiments on light oil show a linear relationship between the received frequency and oil thickness. As more oil is added to the solution, the received frequency decreases linearly since the received light intensity is decreased. The equation relating oil thickness to the received frequency is obtained by using linear regression analysis. For instance, for the experimented oil type with a viscosity of 10cSt, the calibration equation is calculated and represented by the following formula: $Y = -5.7965X + 72.073$; where Y is the output frequency and X is the oil thickness measured in mm.

2.5.2 *LED-based Sensor Initial Experiment – Heavy Oil*

Even though the heavy oil types are not the main target for the LED-based sensor, this experiment aims at monitoring the behavior of the sensor when dealing with heavy oil types. The same experimental procedure used in the light-oil experiment was repeated in this test. The light oil was replaced with a

heavy oil sample with a viscosity of 140cSt (Gear Oil). After adding controlled amounts of oil, the output frequency of the light receiver module was calculated and stored for each thickness (sample size (N) = 38). The experimental results are shown in Table 6 and the corresponding graph is shown in Figure 15.

Table 6: LED-based Sensor - Heavy Oil - Experiment Results

	Oil Thickness (mm)	0	0.48	0.73	0.97	1.22
Frequency (Hz/100)	Mean	64.60	24.57	14.65	6.57	2.31
	Standard Deviation	0.49	0.50	0.48	0.50	0.47
	Maximum	65	25	15	7	3
	Minimum	64	24	14	6	2

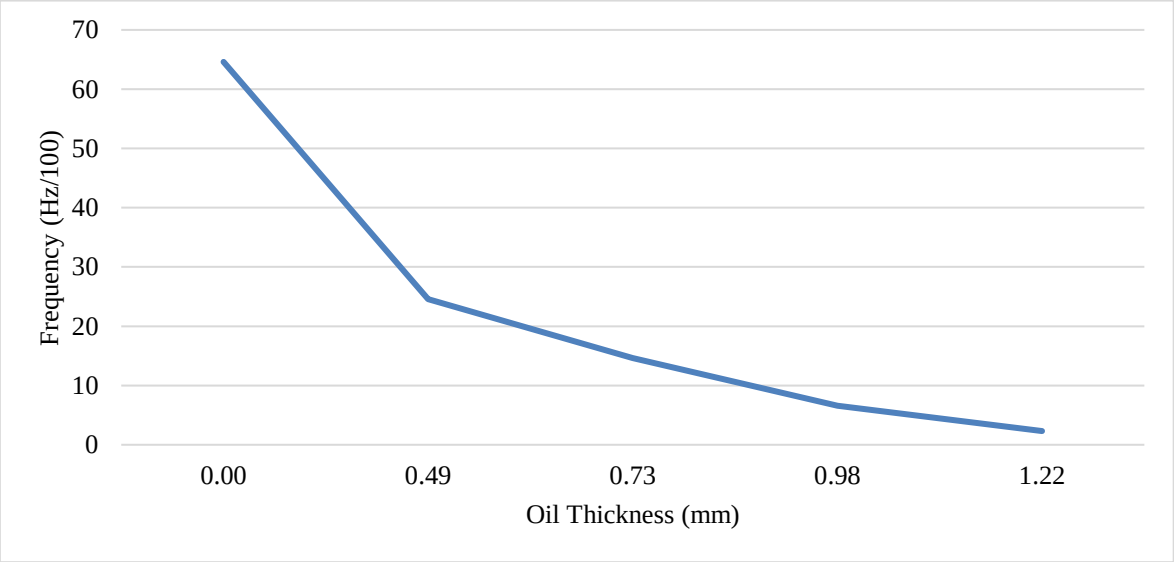

Figure 15: Output Frequency vs. Oil Thickness (LED-based Sensor - Heavy Oil Experiment)

The result of this experiment showed that the received light intensity is highly attenuated due to the use of heavy oil with a viscosity of 140cSt limiting the measurement range to around 1.2mm using the current sensitivity configuration. This result was expected due to the physical properties of heavy oils. In addition, it was observed that the relation between the oil thickness and output frequency is almost linear after 0.4mm of oil thickness.

2.6 LED-based Sensor Mechanical Design

As described before, the sensor must be able to measure thin oil film thicknesses on the surface of water based on the light absorption technique, therefore, any light coming from the environment would be undesirable. On the other hand, oil films with thicknesses in the micrometers to millimeters range are subject to breaking and separating into oil bubbles, the film thickness would be discontinuous, and bubbles will have different and non-uniform thicknesses along their spread. A package for the two-part sensor (emitter/receiver) is needed to keep water away from the electronics and the power source as well as to maintain a straight and fixed geometry of the opposing parts of the sensor, while considering the stated constraints, keeping the emitter below water at a fixed distance from the surface, and keeping stability when waves are present in the sensing environment. Multiple designs were evaluated for the

sensor package, all intended to act as buoy packages. Figure 16 shows a three-part package focused on keeping light away from the light receiver. First, by having the sensor in Compartment ‘a’ pointing downward covered by the white curved cap, second by making all other parts mat black to minimize subsea light reflection. The source/emitter is placed in Compartment ’c’, while Compartment ‘b’ serves as the floating part of the package.

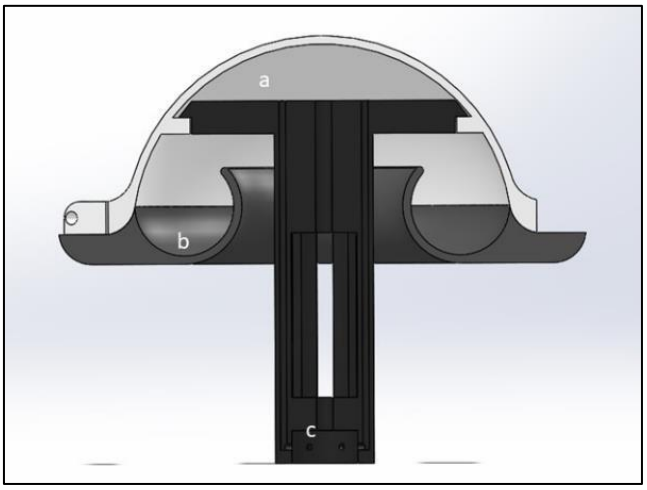

Figure 16: a) Light shield and cap, b) Light shield and floater, c) LED light channel and electronics holder

Figure 17, shows a first iteration of the model in Figure 16. For ease of manufacturing, modifications were made to simplify the design in terms of geometry. Compartment ‘a’ serves as the electronics case where batteries and the light receiver are placed, similarly to the package in Figure 16, the sensor is downward facing, it can be accessed by screwing off the cap, ‘b’ is the light shield aiming to eliminate direct sunlight from being reflected towards the sensor. Compartment ‘c’ is a hydrodynamic foam floater holding the light source, the source similarly to the case in Figure 16 is powered by the battery in ‘a’ using wires passing by ‘d’. The main design improvement in the package seen in Figure 17 is the reduction of the interfering cross-sectional area of the wire tubes with the oil film, thus reducing the film distortion caused in the case of dynamic environments.

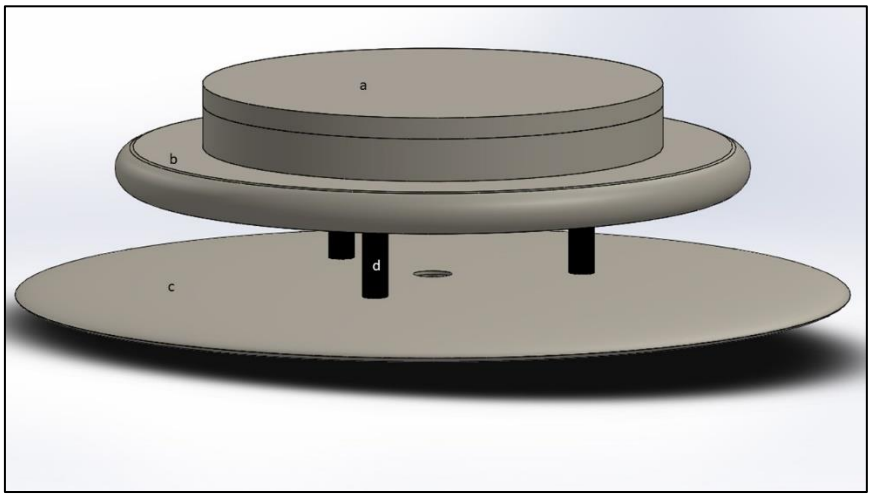

Figure 17: a) Electronics case, b) Light shield, c) Floater, d) Cable channel

Figure 18, shows the second iteration based on the two previous models. This iteration aims for minimal manufacturing cost, maximum shading, and buoy stability. Nevertheless, this iteration is not ideal in terms of robustness against film distortion.

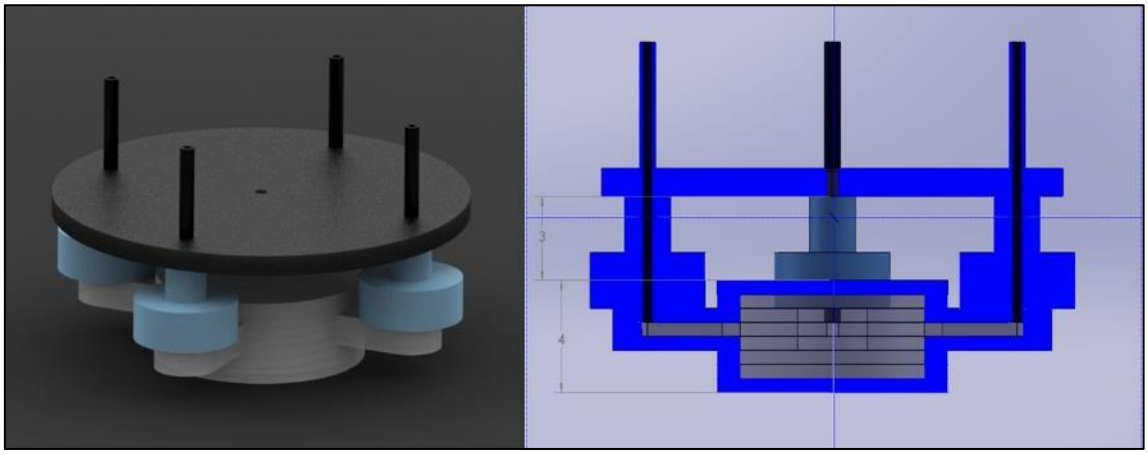

Figure 18: Maximum shading iteration (isometric view and front section plane view)

Chapter 3- Capacitive Sensor Design and Initial Testing

3.1 Sensor Design

Since oil is lighter than water, it rises to the top of the water surface and floats, thereby forming an oil layer. The capacitive sensor is composed of an array of electrodes built onto a planar PCB. Capacitance is measured at each electrode independently to detect the number of electrodes immersed in oil and calculate the thickness. Due to sea water waves and the motion of the platform holding the sensor, the height of the examined liquid may vary up and down through the sensor plates, changing the surrounding medium of the electrodes (air/oil/water), and thus changing the capacitance measured between each couple of electrodes. Figure 19 shows a cross-section of the geometrical capacitive sensor design. The main advantage of the vertical capacitive sensing arrays is that calibration against different types of oil/water is not needed on site since the sensor functions based on the difference in capacitance between electrodes, and not on the absolute capacitance values.

By using the vertical capacitive sensor array design, the presented sensor can distinguish the water/oil interface and the oil/air interface. The thickness of oil can be deduced, regardless of where along the sensor this thickness occurred. In other words, in contrast to several implemented capacitive liquid level sensors found in the literature which use a floater to maintain a fixed position of the sensor on the top of the liquid surface, the presented sensor does not require any assumptions regarding its position relative to the liquid surface. Illustration in Figure 20 demonstrates that if the sensor can deduce the two interfaces between the different mediums, the thickness can still be calculated (to within the resolution of the sensor). The application of this sensor does not require any special packaging considerations beyond waterproofing of the box in which the electronics and the battery are housed.

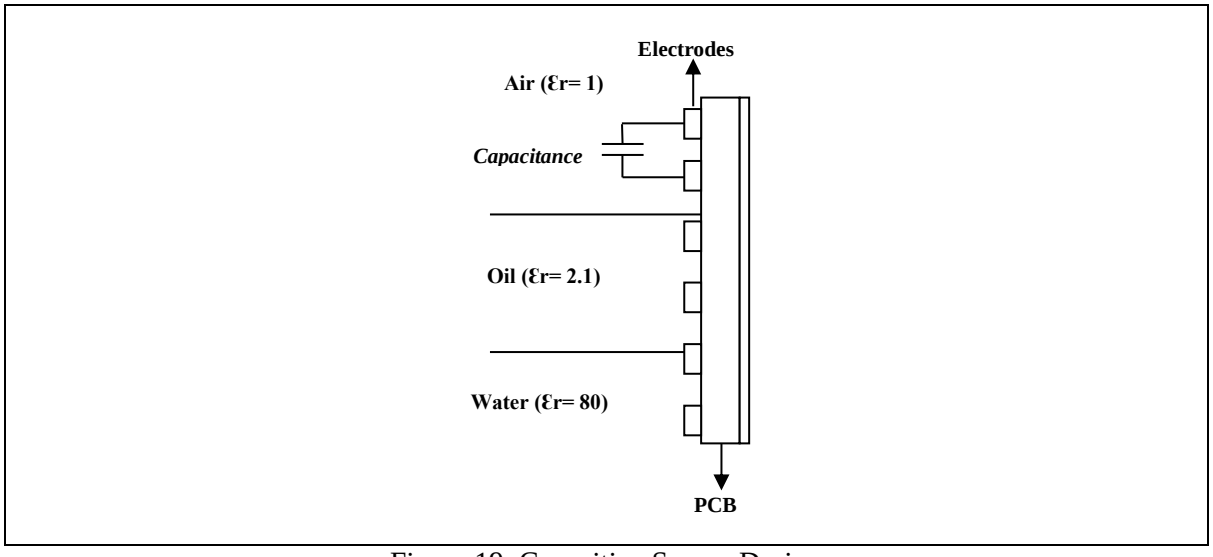

Figure 19: Capacitive Sensor Design

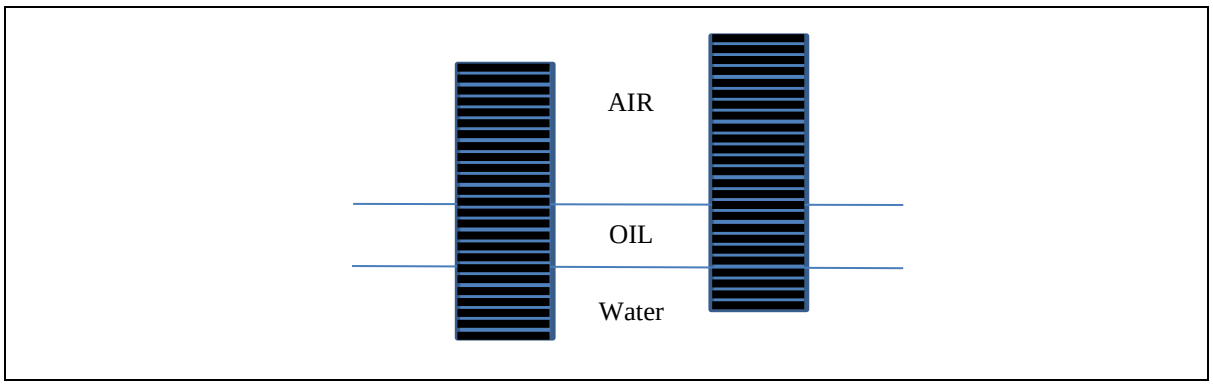

Figure 20: Illustration of vertical capacitive array at different positions

To maintain an accurate measure while the sensor is being dragged through the water and to reduce the fouling effect, the sensor is designed to be very flat (knife-like design) so that it possesses minimal resistance and drag. This way it "cuts" through water and oil whether going straight or in a turning maneuver. Since the sensing array is mounted on a slim PCB plate (1.6mm thickness) with sharp edges, water comes off easily from the sensor body while dragging, reducing the accumulation of oil on the sensing strips. This was evident throughout the tests conducted.

It is important to note that while the main use case of the presented device is to be mounted on skimmers/booms, the capacitive sensor design allows for mounting it on several other platforms including Unmanned Aerial Vehicles (UAV) and drones, since the sensor can move freely in air/oil/water layers without the need for floaters or fixed platforms. In such cases, while scanning the oil spills area, the drone can take sample measurements of the oil thickness from several locations, and produce a map showing the oil distribution in the affected area.

3.2 Capacitive Sensor Initial Implementation

3.2.1 *Capacitive Sensing Unit*

Before implementing the Capacitive sensor prototype, several PCB boards with different electrode designs (Figure 21) were implemented and tested to demonstrate the concept of using the capacitive touch sensing in measuring oil thickness. The first implementation of the complete sensing unit contains thirty-seven conductive electrodes distributed equally from top to bottom on the top layer of a double-faced PCB (Figure 22). The electrodes have the following dimensions: Width: 2mm, Length: 50mm, Vertical separation gap: 0.5mm. The bottom layer of the PCB contains the tracks connecting electrodes to the connection socket. A 37-Pin D-Subminiature PCB connector [20] [21] was selected to connect the sensing unit to the capacitive controller modules (MPR121) in the processing unit. The D-Subminiature connectors are selected due to their compact size, and the high number of pins they offer. To protect the sensing unit from the effects of direct contact with the examined liquid and to reduce fouling, the PCB was sprayed by an electrically isolating material (Nanoprotech) [22].

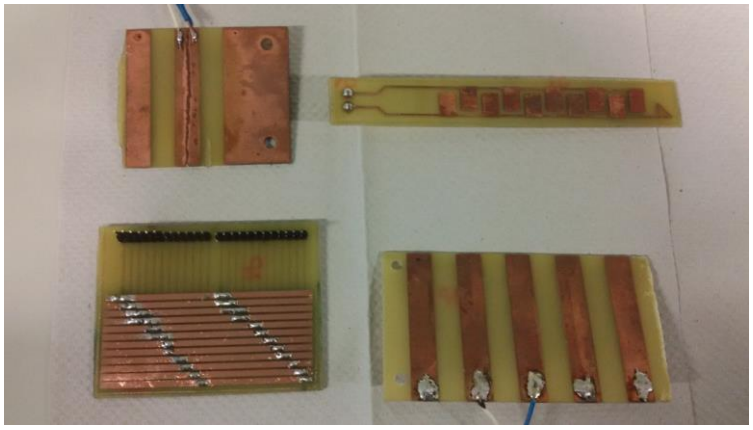

Figure 21: Initial sensing unit prototypes

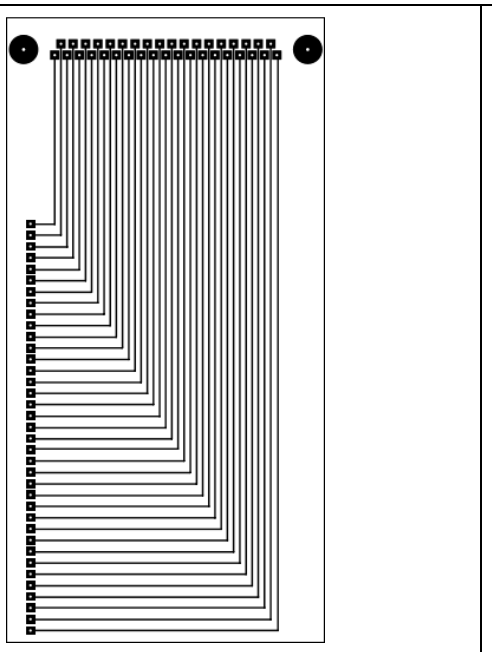

Bottom View (Tracks)

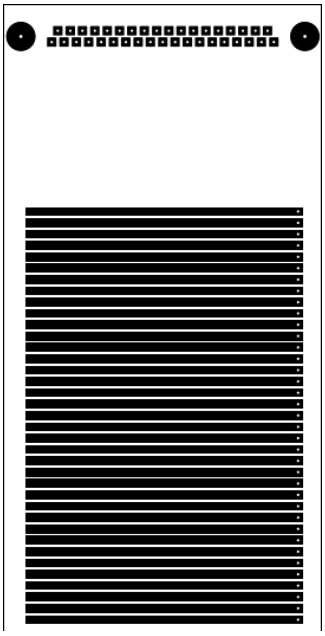

Top View (Electrodes)

Figure 22: Initial Capacitive Sensor Design

3.2.2 *Capacitive Processing Unit*

The capacitive processing unit (Figure 23) is composed of the capacitive touch controllers (MPR121), microcontroller module (Arduino Nano), and communication modules (GPS & RF). Basically, the MPR121 modules are used to measure the capacitance values of the sensor electrodes and the microcontroller board (Arduino Nano) is used to control the measurement process, calculate the oil thickness, and report it wirelessly to the base station.

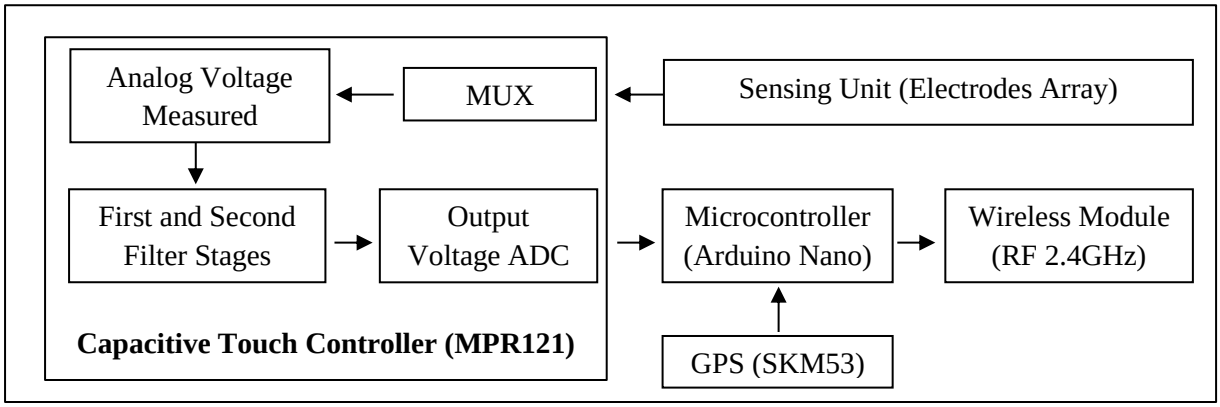

Figure 23: Capacitive Processing Unit - Block Diagram

3.2.3 *Capacitive Touch Controllers (MPR121)*

The MPR121 is a capacitive sensor controller used in touch and proximity sensing applications. It supports twelve sensing electrodes and can be connected to a microcontroller equipped with an I2C communication channel. This module normally works with an input voltage between 1.6V and 3.3V under a temperature range of -40°C to +85°C. It has a low current consumption of around 29µA at a sampling rate of 16ms. The address pin (ADD) is used to set the I2C address of the chip. By default, the ADD pin in the break out board (Figure 24) is connected to GND setting the I2C address to 0x5A [27]. The chip may be configured to three other I2C addresses by connecting the ADD pin as follows: ADD to 3.3V = 0x5B / ADD to SDA = 0x5C / ADD to SCL = 0x5D [23].

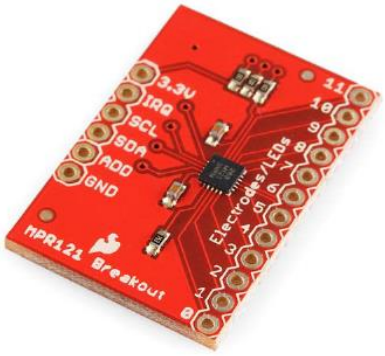

Figure 24: MPR121 Breakout Board

Three MPR121 modules were used in the initial sensor design to cover the thirty-seven electrodes in the sensing unit. Each of the controllers is set to a unique I2C address by changing the connection of the ADD pin as described before. The connection between the controllers and the Arduino is set by using two power lines and two I2C communication lines (3.3V – 3.3V / SCL – A5 / SDA – A4 / GNG – GND). The sensing pins are connected sequentially to the electrodes in the sensing card starting from top to bottom. The code scans each electrode iteratively and reads the filtered voltage value provided by the internal 10-bit Analog-to-Digital-Converter (ADC).

The MPR121 can measure a range of capacitances from around 10pF to 2000pF with a resolution of 0.01pF. The voltage measured by the chip is inversely proportional to the capacitance which is affected by the amount of charge stored in each electrode. The voltage of each electrode is measured after applying a constant amount of current for a fixed duration of time (Figure 25).

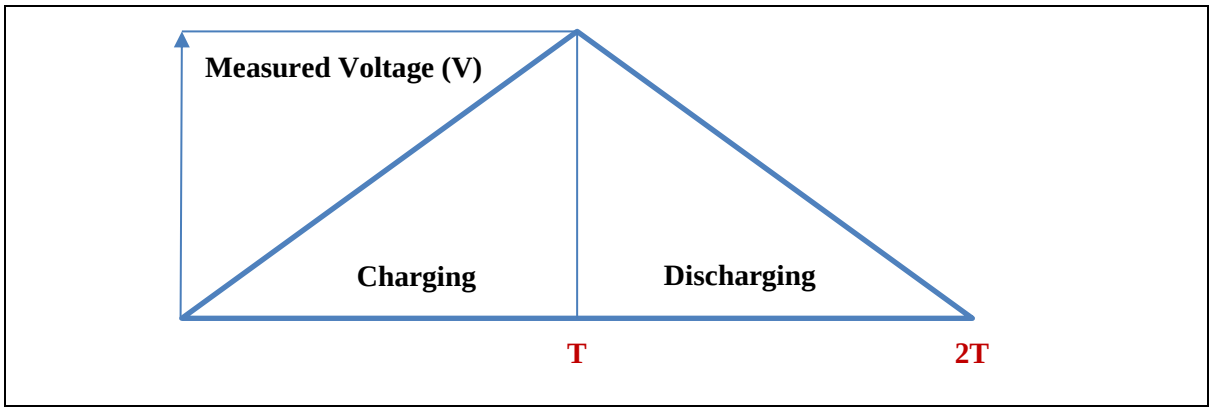

Figure 25: MPR121 Voltage Measurement Cycle

The capacitance of the electrode changes due to the change in the dielectric constant of the examined liquid, thus changing the measured voltage. The amount of current (I) and the charge time (T) are configured to set the charge amount applied to the electrodes. The peak voltage is measured after charging each electrode sequentially. The capacitance (C) is calculated as $C = Q/V = IxT/V$, Where Q is the charge amount measured in coulomb, and V is the voltage amount measured in volts.
The chip contains a set of different registers used to configure the operational parameters and to get the output data from the device. The main registers used in our application are listed as follows:

- **Electrode Filtered Data Register (0x04-0x1D):**

This register holds the filtered output data corresponding to the output of the second filter ranging from 0 to 1024. This data is obtained by measuring the voltage value of each channel and converting it from analog to digital using the internal 10-bit ADC. This register is updated every ESI x SFI and is a read-only register.

- **Filter/Global CDC Configuration Register (0x5C)**

The first two bits of this register are used to set the number of iterations for the first filter (First Filter Iterations - FFI) and may be set to the following values: 00 (6 samples - Default), 01 (10 samples), 10 (18 samples), and 11 (34 samples). The remaining six bits are used to configure the amount of charge current applied to the electrodes. This current configuration section is named the Charge Discharge Current (CDC) and can be set to a range of values between 0 and 63 (000000 (Disabled), 1 (1µA), 010000 (16µA) (Default), and 111111 (63µA)).

- **Filter/Global CDT Configuration Register (0x5D)**

The first three bits of this register are used for configuring the charging time (Charge-Discharge Time - CDT), two bits to set the number of samples taken for the second filter (Second Filter Iterations – SFI), and three bits to set up the sampling time (Electrode Sample Interval – ESI). The CDT can be set to 32µs by setting the bits to 111 and may be disabled by using 000. Other values may be set by using the following equation: CDT = 2^(n-2), where n is the decimal encoding of the three-bit binary value. The default value for the CDT bits is 001 which corresponds to 0.5µs. The SFI can be set to the following values: 00 (4 samples – Default), 01 (6 samples), 10 (10 samples), and 11 (18 samples). The ESI may be set to a value between 000 and 111 which corresponds to period value between 1ms and 128ms using the following equation period = 2^n ms, where n is the decimal encoding of the 3-bit binary value used. The 0x5C and 0x5D registers are the two main registers used in our application to

configure the MPR121 devices. All the global filtering and charging parameters are set up using these two registers. The applied settings will be utilized by all electrodes if the auto-configuration option and the individual charge/discharge feature are disabled.

3.2.4 *Initial Capacitive Sensor Prototype*

The connections between the Arduino module and the MPR121 modules are described in the schematic shown in Figure 26. Twelve input channels from each MPR121 module are connected to the electrodes of the sensing unit. The main power supply (VDD) of the MPR121 with an operational voltage range between 1.71V and 3.6V is connected to the 3.3V output pin in the Arduino board regulator and decoupled by a 0.1µF capacitor to GND. The GPS module (SKM 53) and the RF wireless transceiver (2.4GHz) is connected to the Arduino through hardware and software serial communication. Transistors (2N3904) are controlled by the microcontroller and used as a switch to power ON/OFF the GPS and wireless modules. The hardware implementation of the initial capacitive sensor prototype is shown in Figure 27.

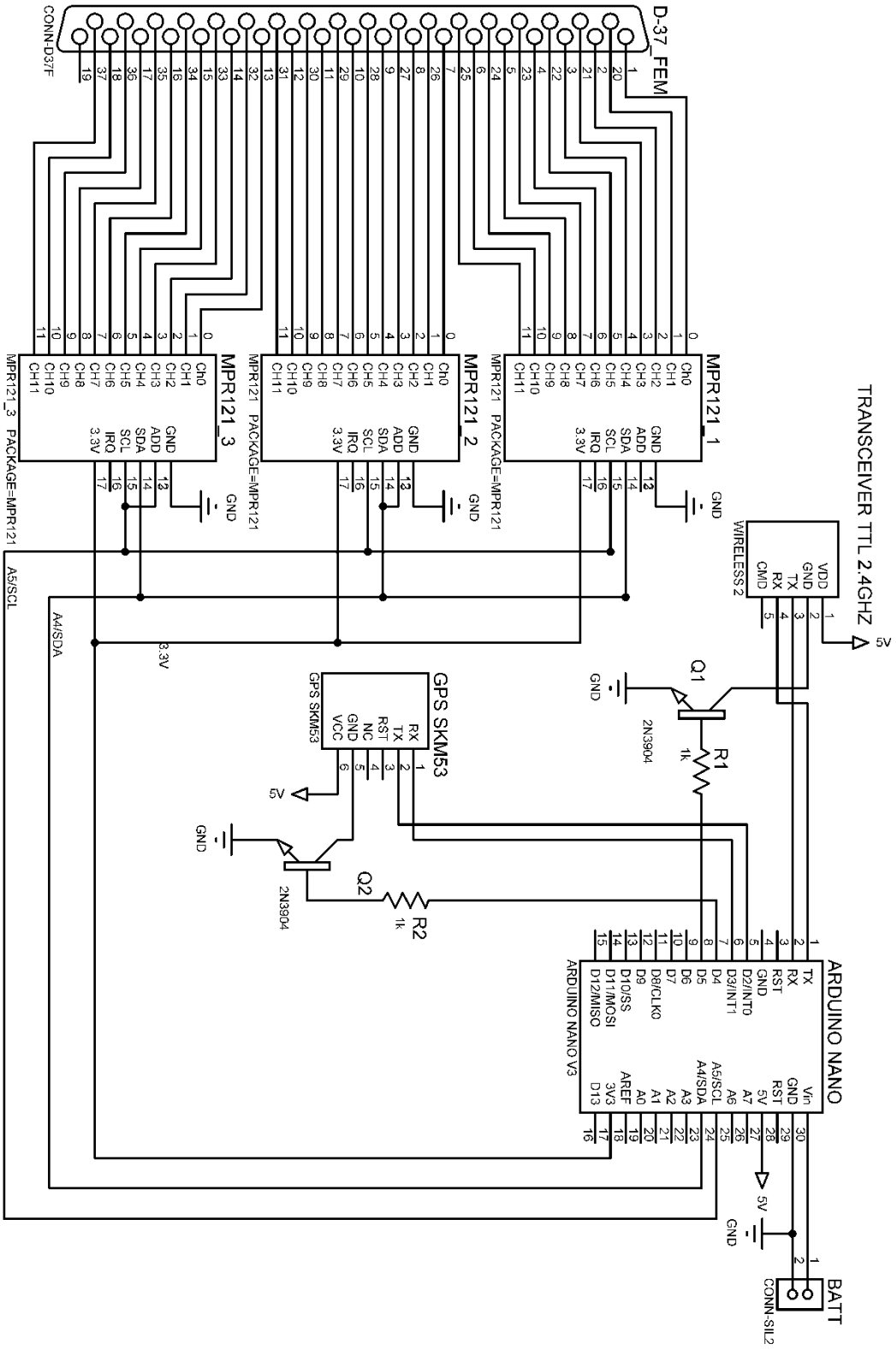

Figure 26: Capacitive Sensor - Control Circuit Schematic

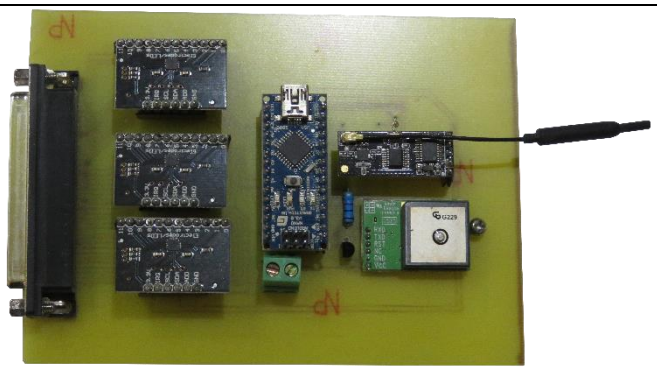

Capacitive Controller Circuit + GPS &Wireless

Capacitive Sensor (Top View - Electrodes)

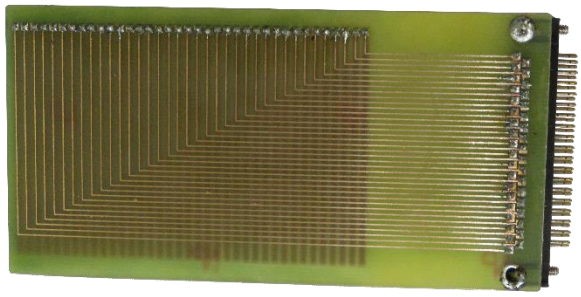

Capacitive Sensor (Bottom View – Tracks)

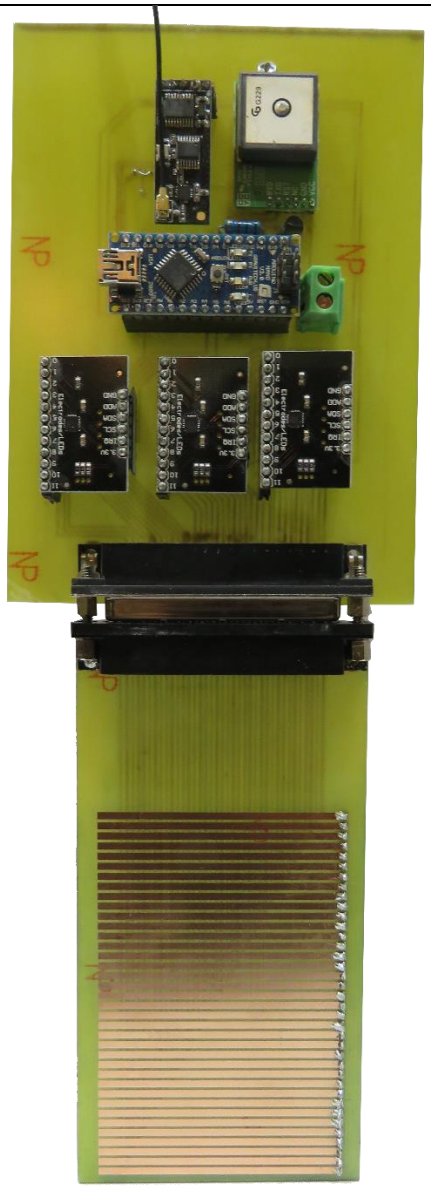

Initial Capacitive Sensor Prototype (Overall)

Figure 27: Capacitive Sensor PCBs

3.3 Capacitive Sensor Initial Mechanical Design

Preliminary design iterations have been made, modifications have been made to each design to fit a final description of an easy to manufacture and sealed package. Figure 28 is the CAD model of the very first design made with the 3D printed prototype, it represents the first iteration, and contains a sealing chamber and a sealed cap with side brackets for fixture purposes, this iteration turned out to be bulkier than expected.

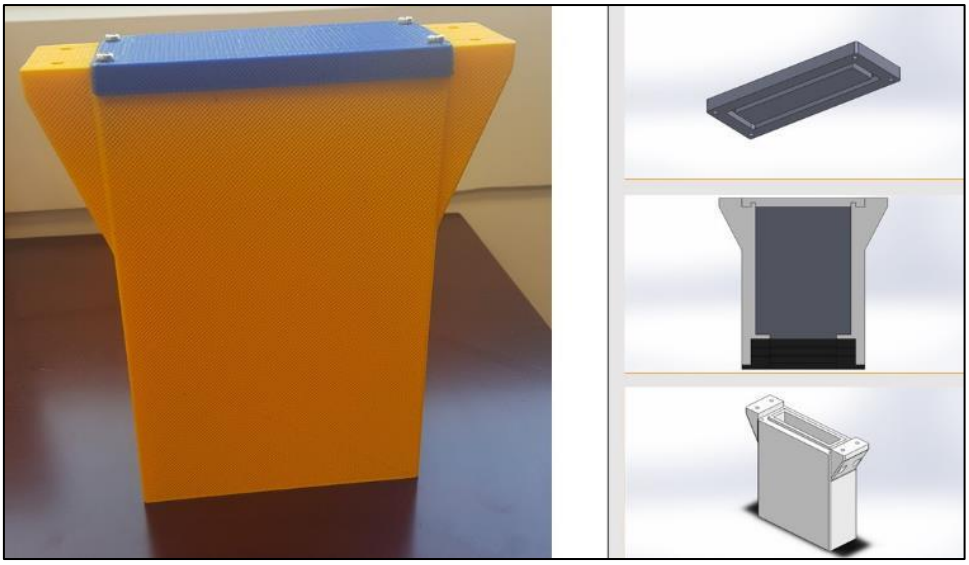

Figure 28: Capacitive Sensor Packaging - Prototype 1

Figure 29 represents the first iteration, this iteration takes into account space for vibrating motors and battery storage, it also includes sealing measures. Nevertheless, it is not efficient for manufacturing since it is made up of four parts, each requiring small tolerance which would probably cause malfunction (weak seals and loose parts). Figure 29 represents an exploded view of the package, the grey parts made of rubber for sealing purposes, since the assembly needs to withstand splashing and occasional submersion depending on the conditions under which it is operated. The white parts are machined out of Polyamide, which was chosen as a material for its durability and shock absorption properties.

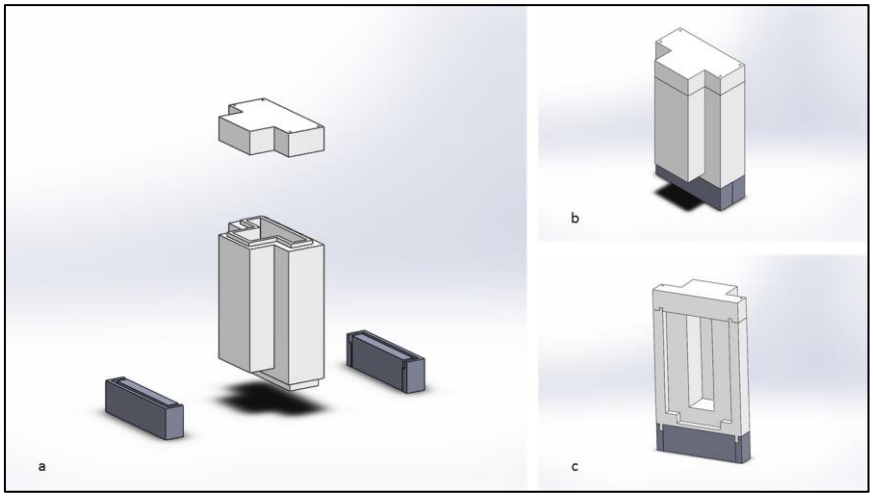

Figure 29: Capacitive Sensor Packaging - Iteration 1

The second iteration in Figure 30 takes into consideration the manufacturing process and tolerances with which this design can be achieved on the CNC mill. Sealing is achieved by applying pressure on rubber O-rings and gaskets. Figure 31 provides a close-up on the capacitive strip, control board, and the hasp lock chosen to apply pressure on the case gasket. Shop drawings with detailed dimensions for the iteration shown in Figure 30 are present in the Appendix at the end of this document.

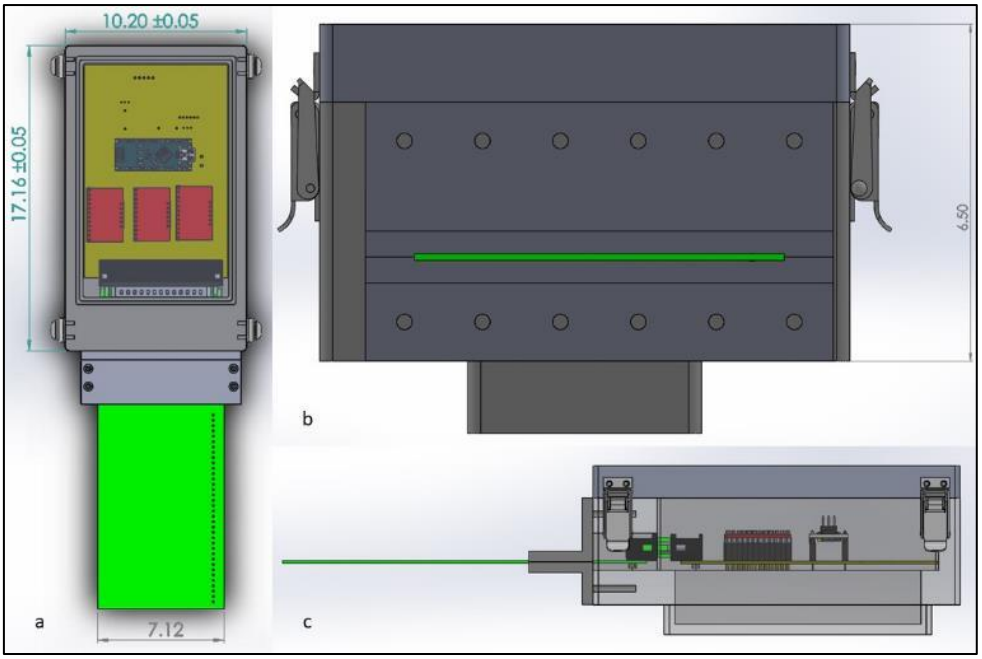

Figure 30: Capacitive Sensor Alpha Iteration (adopted for Prototype 2 machining)

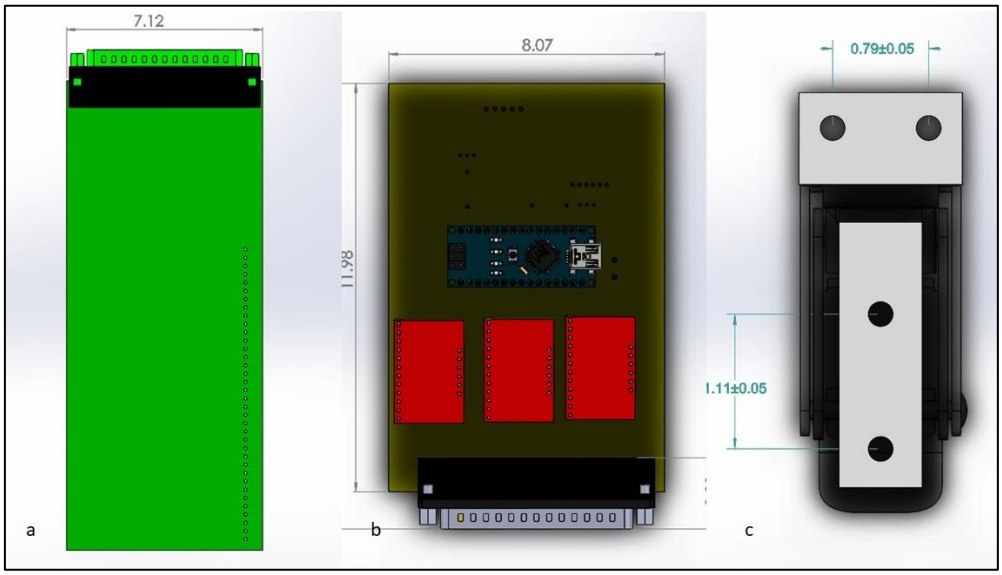

Figure 31: a) Capacitive card, b) Control board, c) Spring reinforced hasp lock

The capacitive sensor packaging has been completed and tested for waterproofing. Three tests were made twice each to determine the package's water resistance:

- Continuous water splashing for 2 minutes (passed)
- Continuous contact with running water under the sink for 2 minutes (passed)
- Submersion in water at a depth of 20cm for 30 seconds (passed)

Figure 32: Alpha package - Bottom view

Figure 33: Alpha package and extension front view

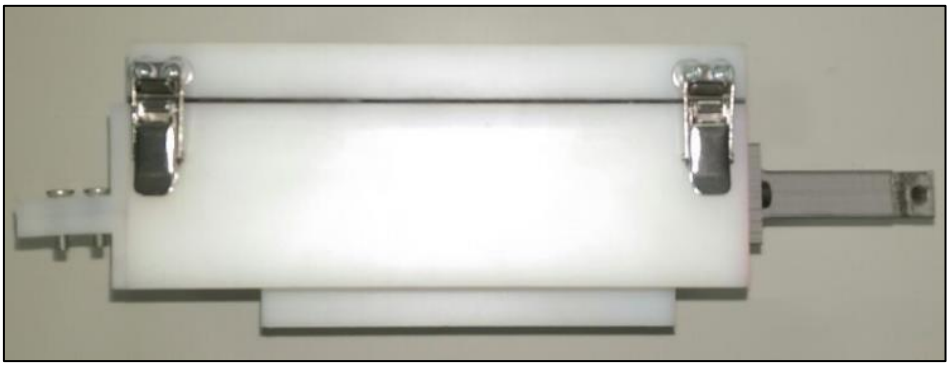

Figure 34: Alpha package and extension right view

Since all three tests were successful, a bracket/extension (Figure 32, Figure 33, Figure 34) was designed and 3D printed to fix the package to the linear actuator (part of the testbed discussed later). The package mounted on the testbed linear actuator was tested once upside down, and once in the proper orientation, the fixing bracket/extension was able to withstand the stresses, which peaked at the change in direction.

3.4 Capacitive Sensor Initial Testing

Several experiments were performed to assess the performance of the proposed capacitive sensor under different conditions and using different oil types (Heavy/Light). During the experiments, the sensor was immersed in the examined liquid (oil/water), and voltage measurements were sent wirelessly to the base station. A software application was developed to receive and save the measured voltage values.

3.4.1 *Oil Types Used in Initial Testing Experiments*

3.4.1.1 Fuel Oil

Experiments were performed to assess the performance of the proposed capacitive sensor while working with heavy fuel oil. However, first we measured the viscosity of the procured heavy fuel oil using the viscous meter available in our labs, and the results were in the range of 3300 to 3500cP. The viscosity of the fuel oil was measured using the following procedure: a spindle of a specified diameter is immersed into the oil and rotated at a precise speed, the drag measured gives the viscosity of the medium. The results of the experiment are shown in Table 7.

Table 7: Measured Viscosity (Fuel Oil)

Spindle	Speed (RPM)	Viscosity (cP)
SP R4	10	3446.4
SP R4	20	3456.1
SP R4	30	3381.7
SP R4	50	3332.6
	Average	3404.2

As shown in Table 7, while the measured viscosity is in Centipoise (cP), which represents the absolute viscosity of the oil, the kinematic viscosity is represented in Centistokes (cSt). The main difference between the two units is that the cSt (kinematic) represents the ratio of a liquid density to its absolute viscosity in cP. To convert from absolute (cP) to kinematic (cSt), the obtained values (cP) are divided by the density of the liquid. Most hydrocarbons (fuel or lubricating oil) have a density between 0.85 and 0.9. To calculate the average kinematic viscosity of this fuel oil, the average of the measured absolute viscosity (3400cP) is multiplied by the density of the oil. For a density of 0.85, the kinematic viscosity is 4000cSt. For a density of 0.9, the kinematic viscosity is 3777cSt. As a conclusion, the kinematic viscosity of the available fuel oil is between 3777 and 4000cSt measured at room temperature (around 25°C).

3.4.1.2 Light/Medium Oil

Three different single-grade oil types available in the local Lebanese market were selected for the light and medium oil experiments each with a different viscosity, as shown in Table 8.

Table 8: Viscosity of light and medium oil samples

Viscosity (cSt)	Name	Description
680 cSt	BP Energol GR-XP 680	Industrial Extreme Pressure Gear Oil
140 cSt	Power Gear 140W	Automotive Gear Oil
10 cSt	Power 10W	Engine Oil

3.4.2 *Preliminary Capacitive Sensor Experiments – Light Oil*

Experiments were first conducted on the proposed capacitive sensor to assess its ability to differentiate between air, water, and oil.

3.4.2.1 Experiment 1 – Sensor in Air

In this experiment, the sensor was surrounded only by air, the values of the first twelve electrodes were measured and logged every five seconds. An instance of the experimental results is shown in Table 9, and the corresponding graph is shown in Figure 35.

Table 9: Experiment 1 (Air) – Numerical Values

Time	E1	E2	E3	E4	E5	E6	E7	E8	E9	E10	E11	E12
10:25:30	180	170	168	172	170	175	172	175	169	171	166	170
10:25:35	180	170	168	173	171	176	172	175	170	171	166	169
10:25:40	180	170	167	173	170	176	172	176	170	172	165	170
10:25:45	180	170	168	173	171	176	172	175	169	171	166	169
10:25:50	180	169	167	173	170	177	172	175	169	171	166	169
10:25:55	180	170	167	172	170	176	172	175	169	171	166	169
10:26:00	180	170	167	173	170	176	172	175	169	171	166	170
Average	180	170	167	173	170	176	172	175	169	171	166	169

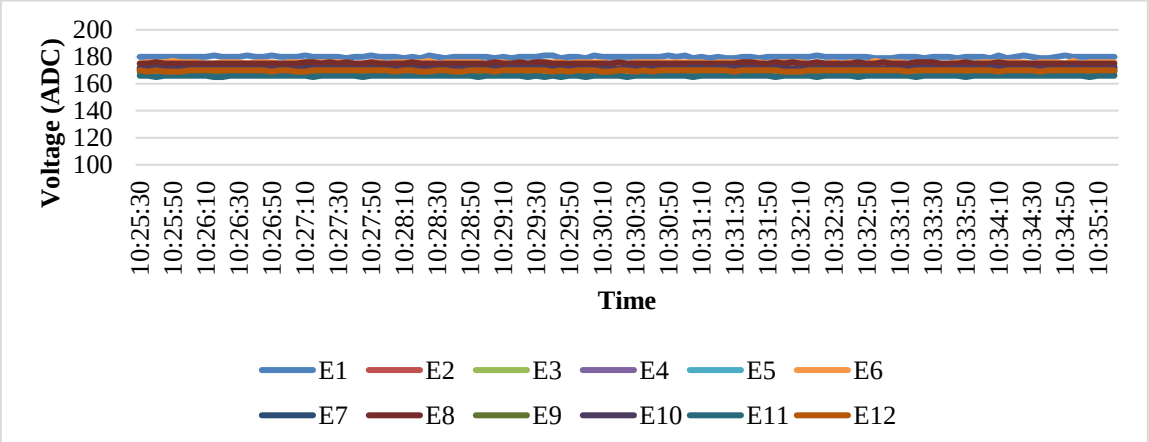

Figure 35: Experiment 1: Sensor in Air

The results of this experiment showed a difference between the absolute voltages measured by each electrode while placed in the same medium (air). This difference is primarily attributed to the resulting inevitable manufacturing inconsistencies between each electrode, including issues such as trace length, soldering, and connectors. However, since our oil thickness estimation algorithm is based on relative,

and not the absolute voltage measurements, the difference between the measured values will not affect the accuracy of our results. More importantly is the stability and repeatability of the measured values over time.

3.4.2.2 Experiment 2 – Locating the Oil/Water Interface (Light-oil)

The aim of this experiment is to monitor the effect of oil on the actual voltage value measured by each electrode. The sensor was placed initially in water, and light oil (10cSt) was gradually added to the container; this procedure ensures no oil contact with the bottom sensor electrodes during immersion. Thus, the first six electrodes from the top of the sensor were covered with oil, and the remaining electrodes are immersed in water. Voltage values of the first twelve electrodes were measured every five seconds; an instance of experimental results is shown in Table 10, and the corresponding graph is shown in Figure 36.

Table 10: Experiment 2 (Light Oil/Water) – ADC Voltage Values

Time	E1	E2	E3	E4	E5	E6	E7	E8	E9	E10	E11	E12
11:11:03	168	157	157	162	159	162	53	6	6	6	5	6
11:11:08	167	157	158	162	159	162	53	6	6	6	5	6
11:11:13	167	157	158	162	159	162	53	6	6	6	6	6
11:11:18	168	157	158	162	159	162	53	6	6	6	6	6
11:11:23	168	157	157	162	159	162	53	6	6	6	6	6
11:11:28	168	157	158	162	160	162	53	6	6	6	6	6
11:11:33	167	157	157	162	159	162	53	6	6	6	6	6
11:11:43	168	157	157	162	159	162	53	6	6	6	5	6
11:11:48	168	157	157	162	159	162	53	6	6	6	5	6
11:11:53	168	157	158	162	159	162	53	6	6	6	6	6
11:11:58	167	157	157	162	159	162	53	6	6	6	6	6
Average	168	157	157	162	159	162	53	6	6	6	6	6

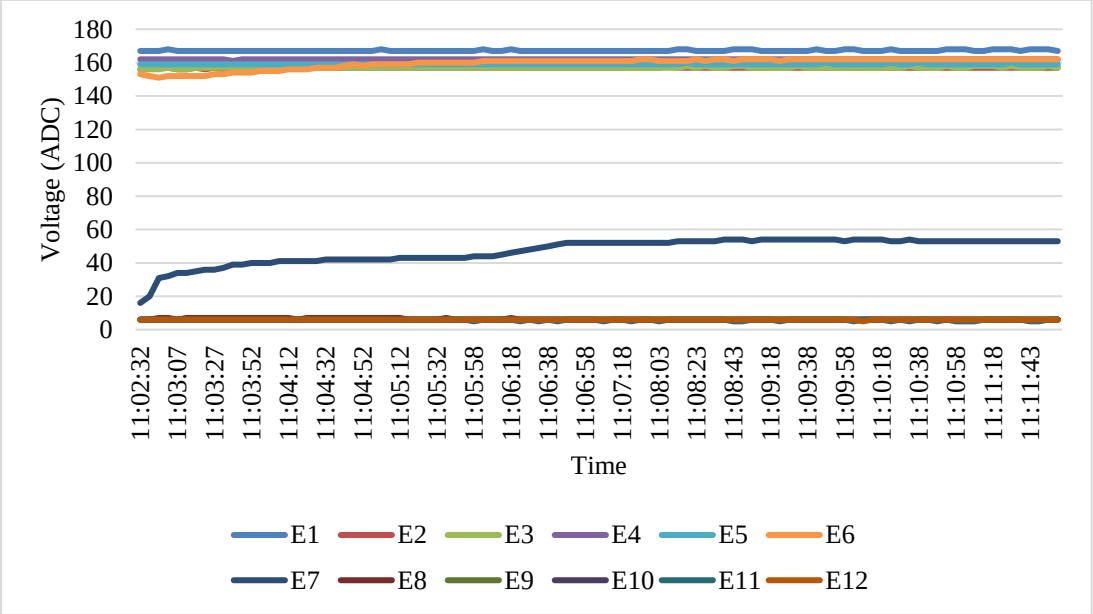

Figure 36: Experiment 2 - Light Oil / Water

As shown in Figure 36, the results show that the voltage measured by the bottom five electrodes (E8-E12) was much lower than the voltage measured by the other electrodes. This result was expected because of the relatively high conductivity of water. Also, the voltage of the first five electrodes (covered by oil) was lower than the voltage read by the same electrodes while placed in the air medium (experiment 1). The voltage measured by the seventh electrode (E7) was partially decreased because of it being located at the interface of oil and water, and accordingly being partially immersed in oil. The results of this experiment were considered encouraging since it proved the viability of our approach in differentiating between electrodes immersed in air, oil, or water.

3.4.2.3 Experiment 3 – Locating the Oil/Air Interface (Light Oil)

The aim of this experiment is to monitor the difference between the voltage measured by each of the sensor electrodes while moving the sensor between the air and oil mediums. The voltage measured by the first twelve electrodes of the sensor were recorded while moving the sensor in a random manner between the two mediums. A measurement was recorded every second. An instance of the experimental results is shown in Table 11, and the corresponding graph is shown in Figure 37.

Table 11: Experiment 3 (Air/Oil) – ADC Voltage Values

Time	E1	E2	E3	E4	E5	E6	E7	E8	E9	E10	E11	E12	Status
11:23:27	179	170	168	173	170	175	171	175	169	171	165	169	
11:23:29	179	170	168	173	170	175	171	175	169	171	165	169	
11:23:30	179	170	168	173	170	175	171	175	169	171	165	169	
11:23:31	179	170	168	173	170	175	171	175	169	171	165	169	
11:23:32	179	170	168	173	170	175	171	175	169	171	165	169	
11:23:34	179	170	168	173	170	175	171	175	169	171	165	169	Air
11:23:35	179	170	168	173	170	175	171	175	169	171	165	169	
11:23:36	179	170	168	173	170	175	171	175	169	171	165	169	
11:23:38	179	170	168	173	170	175	171	175	169	171	165	169	
11:23:39	179	169	166	171	168	172	168	172	165	167	161	165	
11:23:40	170	161	158	162	160	164	160	163	158	159	154	158	
11:23:41	170	161	158	162	160	164	160	163	158	159	154	157	
11:23:43	170	161	158	162	160	164	160	163	158	159	154	157	
11:23:44	170	160	158	162	160	164	160	163	158	159	154	157	
11:23:45	170	160	158	162	160	164	160	163	158	159	154	157	
11:23:47	170	161	158	162	160	164	160	163	157	159	154	157	Oil
11:23:48	170	160	158	162	160	164	160	163	158	159	154	157	
11:23:49	170	160	158	162	160	164	160	163	158	159	154	157	
11:23:51	170	160	158	162	160	164	160	163	158	159	154	157	
11:23:52	170	160	158	162	159	164	160	163	158	159	154	157	
11:23:53	170	160	158	162	160	164	160	163	158	159	154	157	

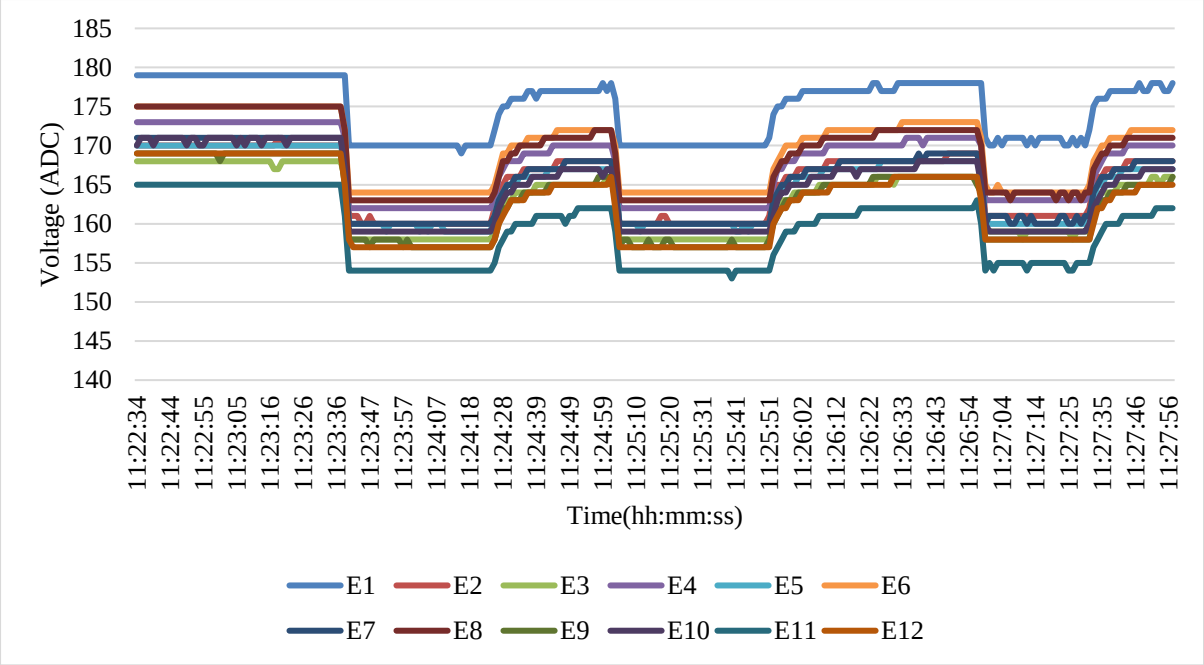

Figure 37: Experiment 3 (Air/Light Oil)

The experiment shows an immediate change in the measured voltages upon moving between the oil and air mediums. Note that although the difference is small, the measured voltage in the air is always higher than in oil.

3.4.3 *Preliminary Capacitive Sensor Experiments – Heavy Oil*

3.4.3.1 Experiment 1 – Locating Oil/Water Interface (Fuel Oil)

In this experiment, the sensor was immersed in fuel oil and water, the values of three electrodes were measured and logged every one second. The aim of this experiment is to monitor the change in the sensor voltage readings while moving the sensor electrodes between fuel oil and water. A sample of the numerical results are shown in Table 12, and the corresponding graph is shown in Figure 38 (Temperature: 23°C, RH: 60%).

Table 12: Fuel oil experiment 1- ADC Voltage Values

Time	E8	E9	E10	Time	E8	E9	E10
3:19:13	165	160	159	3:20:13	165	158	157
3:19:14	165	161	159	3:20:14	165	158	157
3:19:15	166	161	159	3:20:15	166	158	157
3:19:16	166	161	159	3:20:16	166	159	157
3:19:17	166	161	158	3:20:17	167	159	157
3:19:18	166	161	159	3:20:19	167	160	158
3:19:19	166	161	159	3:20:20	167	160	158
3:19:20	166	161	159	3:20:21	168	161	158
3:19:21	166	161	159	3:20:22	168	162	159
3:19:22	166	162	160	3:20:23	168	162	159
3:19:23	166	162	160	3:20:24	168	163	159
3:19:24	166	162	161	3:20:25	167	163	160
3:19:26	166	162	161	3:20:26	168	163	160
3:19:27	167	162	162	3:20:27	167	163	160

3:19:28	167	162	162	3:20:28	167	163	161
3:19:29	167	162	162	3:20:29	167	163	161
3:19:30	167	162	162	3:20:30	167	163	160
3:19:31	167	162	162	3:20:32	167	163	160
3:19:34	167	162	162	3:20:33	167	163	160
3:19:35	167	162	162	3:20:34	167	163	159
3:19:36	167	162	162	3:20:35	167	162	159
3:19:37	167	162	162	3:20:36	165	158	157
3:19:39	167	162	162	3:20:37	161	156	156
3:19:40	167	162	162	3:20:38	161	156	156
3:19:41	167	162	162	3:20:39	161	156	156
3:19:42	167	163	162	3:20:40	161	156	156
3:19:43	167	163	162	3:20:41	161	156	156
3:19:44	167	163	162	3:20:42	161	156	156
3:19:45	168	163	162	3:20:43	161	156	156
3:19:46	168	163	162	3:20:45	161	156	155
3:19:47	168	163	161	3:20:46	161	156	155
3:19:48	168	163	161	3:20:47	161	156	155
3:19:49	168	163	161	3:20:48	161	156	155
3:19:50	168	163	160	3:20:49	161	156	155
3:19:52	164	158	157	3:20:50	161	156	155
3:19:53	161	156	156	3:20:51	161	156	155
3:19:54	160	156	156	3:20:52	161	156	155
3:19:55	160	156	156	3:20:53	161	156	156
3:19:56	160	156	156	3:20:54	161	157	156
3:19:57	160	156	156	3:20:55	162	157	156
3:19:58	160	156	156	3:20:56	162	157	157
3:19:59	160	156	155	3:20:57	163	157	157
3:20:00	160	156	155	3:20:59	164	158	157
3:20:01	160	155	155	3:21:00	165	158	157
3:20:03	160	156	155	3:21:01	166	159	157
3:20:04	160	156	155	3:21:02	167	159	158
3:20:06	161	156	155	3:21:03	167	160	158

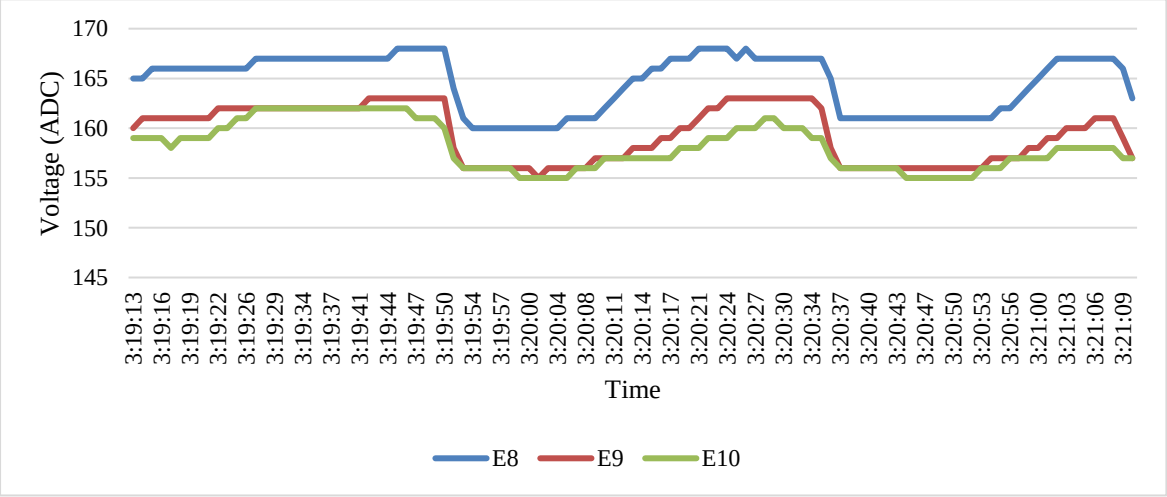

Figure 38: Fuel-oil experiment 1 – Locating oil/water interface

The results show the difference between the absolute voltage measured by each electrode while moving between fuel oil and water. The high values illustrated in Figure 38 correspond to values measured while the electrodes are in fuel-oil, and the low values correspond to values measured in water.

Although the sensor electrodes are completely covered with a thin layer of oil after being immersed in the fuel oil for the first time (Figure 39), the voltage values measured by the electrodes, while being immersed in oil are different from the values measured in the air, despite being covered with fuel oil. This difference is used in our algorithm to distinguish between oil/water interfaces.

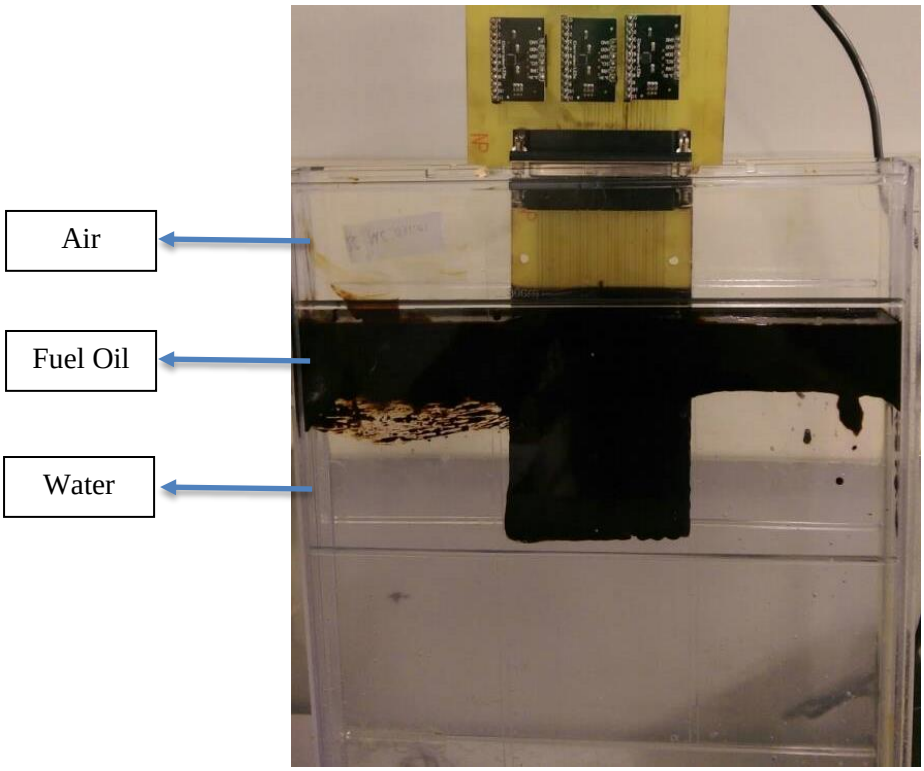

Figure 39: Capacitive Sensor - Initial Experiment (Fuel Oil) - Experimental Setup

3.4.3.2 Experiment 2 – Locating Oil/Air Interface

The aim of this experiment is to monitor the difference between the voltage measured by the sensor electrodes while moving between fuel oil and air. Voltage values of two electrodes were measured every one second; experimental results for one of the experiments are shown in Table 13, and the corresponding graph is shown in Figure 40 (Temp: 23°C, RH: 60%).

Table 13: Fuel oil experiment 2- ADC Voltage Values

Time	E6	E7	Time	E6	E7
2:21:50	172	167	2:22:26	170	165
2:21:51	172	167	2:22:27	170	165
2:21:52	172	167	2:22:28	170	165
2:21:53	172	167	2:22:29	170	165
2:21:54	172	167	2:22:30	170	165
2:21:55	172	167	2:22:31	170	165
2:21:56	172	167	2:22:32	170	165
2:21:57	172	167	2:22:33	170	165
2:21:58	172	167	2:22:34	170	165
2:22:00	172	167	2:22:35	170	165
2:22:01	172	167	2:22:36	170	165

2:22:02	172	167	2:22:37	170	165
2:22:03	172	167	2:22:39	170	166
2:22:04	172	167	2:22:40	170	165
2:22:05	172	167	2:22:41	170	166
2:22:06	170	163	2:22:42	170	165
2:22:07	166	160	2:22:43	170	165
2:22:08	164	160	2:22:44	170	166

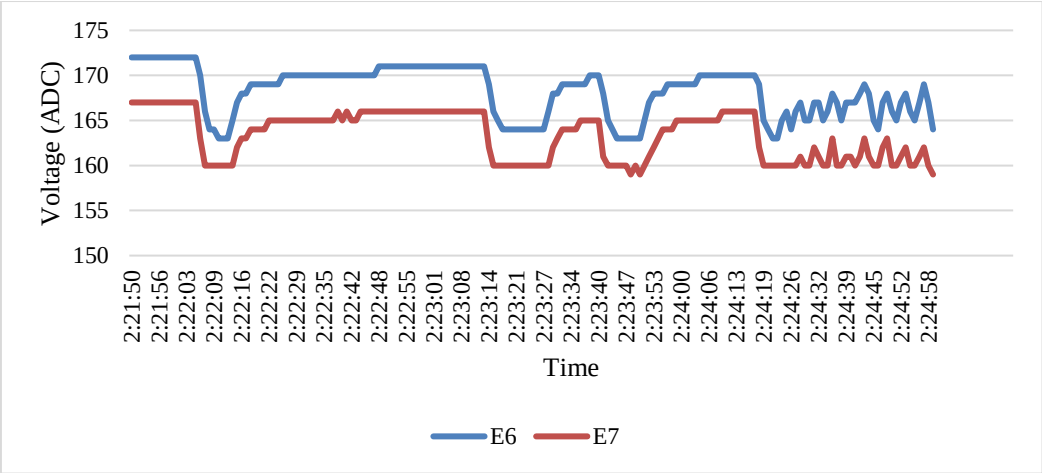

Figure 40: Fuel oil experiment 2 – Locating air/oil interface

The results show that the voltage measured by the two electrodes (E6-E7), while moving between fuel-oil and air are different. In the last part of the experiment, the rate of movement was increased thus producing a higher frequency signal as shown in Figure 40. The importance of this result lies in that it reveals that the sensor is feasible for oil types with high viscosity such as the tested fuel oil.

3.4.4 *Preliminary Capacitive Sensor Experiments - Environmental Conditions*

To assess the environmental conditions (temperature and relative humidity) effect on the measurements we conducted two experiments. In the first experiment, the sensor was placed in open air, and the readings were logged every 30 sec. During the 16-hour experiment, the relative humidity varied between 72% and 58% and the temperature ranged from 21°C to 24.7°C. The span of measurement for each electrode was very limited and didn't exceed 3.8% in the worst case.

In the second experiment, the sensor was placed in a closed room where the temperature and humidity were changing relatively fast due to air conditioning. During the experiment, the relative humidity varied between 60% and 46% and the temperature varied between 21.2°C and 24.7°C. The span of measurement for each electrode was very limited and didn't exceed 2.7% in the worst case.
As a result, these experiments provided an initial evidence that the sensor repeatability is high under different environmental conditions.

3.5 Preliminary Algorithms for Estimating Oil Thickness

Primarily, the measurement algorithms aim to calculate the oil thickness based on the dimensions of the sensor. Several approaches were evaluated to detect the most accurate and reliable method to estimate the oil thickness for all environmental cases (static/dynamic). The following sections describe the different approaches.

3.5.1 *Non-supervised Clustering Algorithm (K-Means)*

Before implementing any algorithm to estimate oil thickness we plotted the experimental results on a C vs. ΔC_t graph, where C is the difference between the baseline capacitance (in air) of each strip and its capacitance in its residing medium; ΔC_t is the transient change in C, representing how fast the oil is slipping off a strip (Figure 41).

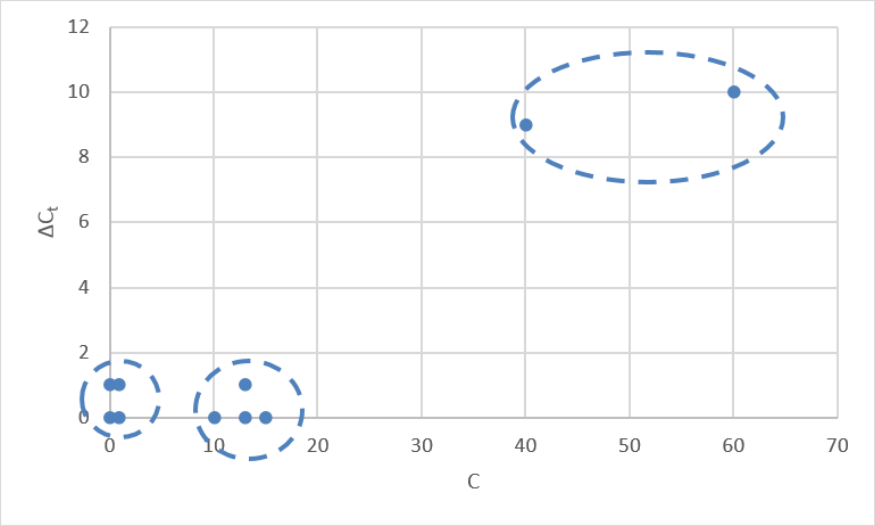

Figure 41: C vs. ΔCt

In this graph, we noted the obvious clustering of data points according to the medium they are in. Accordingly, we attempted to group data points using a clustering algorithm known as K-means[26], with a feature vector comprised of C and ΔC_t; K-means is known to produce good results when the number of clusters K is known beforehand. Here we chose three clusters, representing air, oil, and water. To implement the algorithm in real-time, the software was developed using Microsoft Windows Forms .Net (C#) framework. The results of the measurement algorithm including the estimated oil-thickness (mm) and the index of electrodes included in each cluster and the raw voltage measurements are shown in the Graphical User Interface of the application (Figure 42).

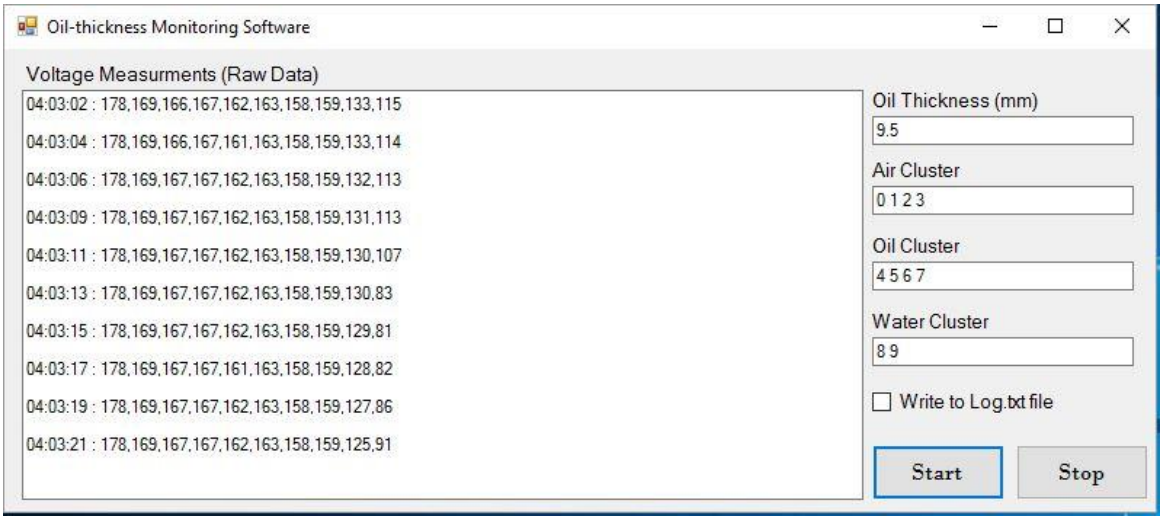

Figure 42: K-means algorithm results

As shown in Figure 42, the activated electrodes (first ten) are clustered into three different groups (air/oil/water). The index of each electrode classified into one of the three clusters is shown in the figure. From a position directly above the fluids, the sensor is lowered, in a vertical direction, into the oil/water medium. Notice that, as expected, the decreasing values of the bottom two electrodes (E8 & E9) did not affect the classification decision since the rate of change is considered as the second attribute of clustering. The estimated number of oil electrodes (4) in this case was identical to the actual number of electrodes immersed in oil, as was noted visually.

Although the results of the K-means algorithm were accurate while the sensor was not moving (static case), the results were not reliable in the dynamic case, because K-means under vertical movement results in inconsitent clustering primarily because of strips that are in transition between mediums and got fouled (e.g, oil-water).

3.5.2 *Thickness Estimation Based on Interfaces Detection*

In this approach, oil thickness was estimated based on the difference between the air/oil interface and the oil/water interface. The algorithm starts by calculating the relative change of voltage of each electrode from its calibrated value—measured while the sensor is in air. This step is essential for normalizing the voltage measurements taken by all electrodes. Then, for each electrode of index "i" we divide its voltage differential with that of its neighbor electrode of index "i+1" (lower electrode), and call this parameter "Ratios". To avoid division by zero, null deltas on the denominator are replaced by a value of one.

To test the algorithm, an experiment was conducted on a light engine oil (10W-40). The sensor was immersed in an oil/water mixture with 1cm of oil thickness. The experiment was implemented in the lab under a temperature of 24 °C and relative humidity of 59%; a sampling rate of 1/300msec was adopted. A sample of the calculated ratios is shown in Figure 43. To get the oil thickness, the algorithm proceeds by calculating the difference between the index of the electrode located at the oil/water interface layer and the index of the electrode located at the air/oil interface layer. To do so, the interfaces are identified based on the relative electrode behavior. Depending on the results shown in Figure 43, we notice a clear difference between the values before and after electrode E6. Also, electrode E10 shows a similar behavior.

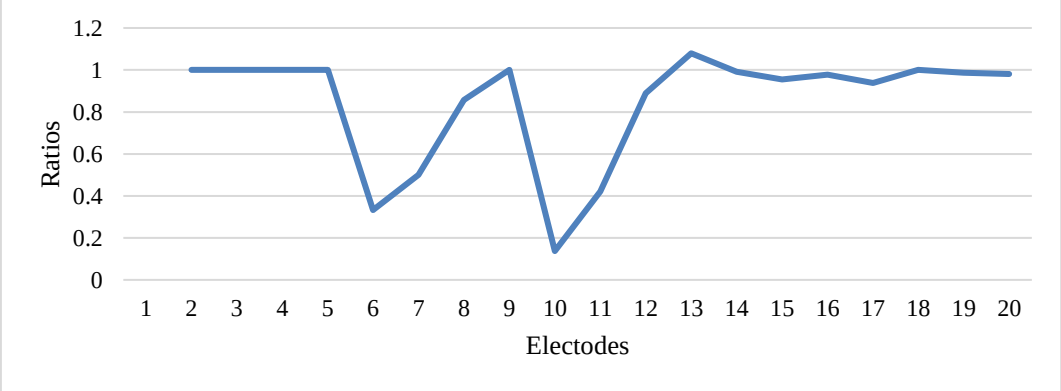

Figure 43: Interfaces detection algorithm – Ratios

The electrodes located at the interface layers (E6 and E10) show a severe drop in the computed ratios. To get the index of each interface electrode, the first two minima of the ratios series are identified. Then, the difference between the indexes of the two minimum electrodes is calculated (E10 - E6 = 4) and is used for calculating the oil thickness based on the dimensions of the electrodes.

To assess the performance of this algorithm in static cases, accuracy values were calculated after taking a set of thickness measurements. Two cases were tested in this experiment: the first case represents applying the measurement algorithm on each voltage reading without using any averaging; in the second case, a moving average of the voltage readings is used before applying the measurement algorithm. To calculate the moving average, each new voltage reading is added to the voltage measurements taken before it and the result is divided by two.

The following table presents the results, where in each case, the average of around three hundred measurements was taken. The oil used is light-oil, with a viscosity of 10 cSt. The experiment was done indoor at a temperature of around 24°C. The first case results are shown in Table 14 and the second case measurements are shown in Table 15.

Table 14: Static Experimental Results (Case 1)

Index of Oil/Water Interface	Index of Water/Oil Interface	Oil Interval	Measured Thickness (mm)	Actual Thickness (mm)	Percentage Error (%)
29	24.05	4.94	11.86	12.5	5.08

Table 15: Static Experimental Results (Case 2)

Index of Oil/Water Interface	Index of Water/Oil Interface	Oil Interval	Measured Thickness (mm)	Actual Thickness (mm)	Percentage Error (%)
29	24	5	12	12.5	4

The experimental results show that after applying the moving average (Case 2) the percentage error is reduced from 5% to 4%. As a result, this algorithm was considered acceptable for static conditions. Unfortunately, for dynamic situations, due to fouling a relatively-high error was observed in detecting the air/oil interface. Therefore, this method was deemed acceptable for static conditions, but not recommended for the dynamic cases.

Based on the results obtained from the first two methods, we concluded that the algorithm must first be capable of differentiating between the static and dynamic cases, and focus on the strips that are exhibiting change, since those would be the electrodes that are transitioning between mediums. In the next trials, the work was focused on dealing with high-dynamic conditions.

Chapter 4- Experimental Setups

In order to simulate the environments and conditions within which the sensors will be operating we designed and developed two main experimental test-beds. The experiments were organized into two categories, indoors and outdoors. Therefore, indoor testbeds and an outdoors testbed were designed, manufactured, and used to run all planned experiments. For indoors experiments two testbeds were made, one for the LED-based sensor, and another for the capacitive sensor. As for the outdoor experiments, a single testbed was made for both sensors. The testbed is a large tank made to simulate the behavior of the sensors in open sea conditions.

4.1 LED-based Sensor Testbed

The following design was used for tests conducted in our small tank; it comprises of two major parts: the fixed sensor case shown in Figure 44, and the LED/emitter case of Figure 45. The first design is intended to be suspended above the oil during tests, and the second is intended to be moved vertically, while keeping alignment between LED and spectrometer. Once the optimal distance between emitter and spectrometer is determined, it would be possible to design a third package to contain both the light source and spectrometer in their fixed validated positions. Shop drawings with dimensions of this testbed can be found in the Appendix.

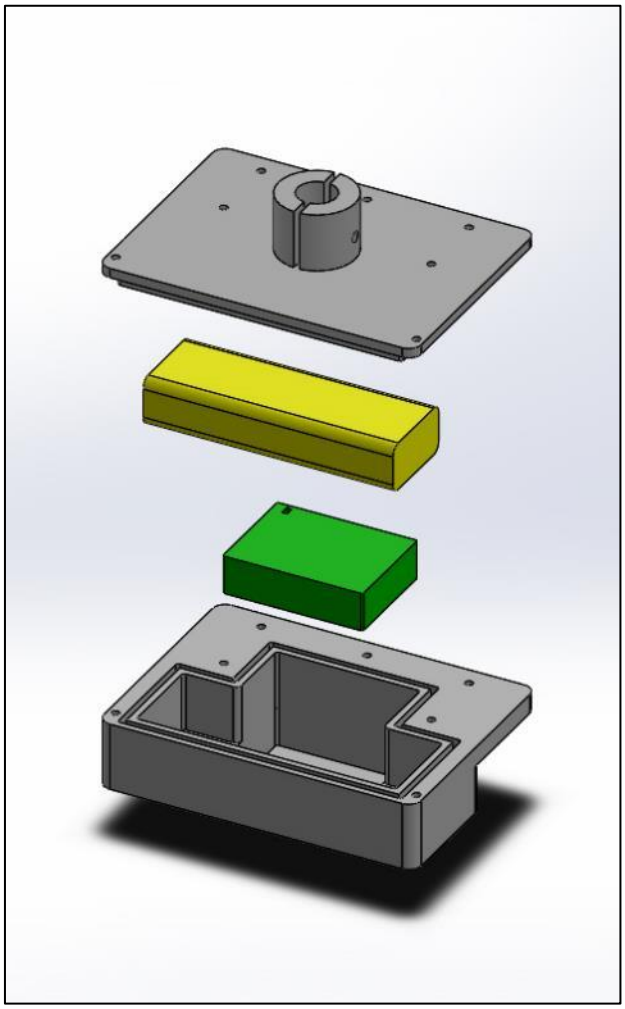

Figure 44: Exploded view of assembly fit for the spectrometer case

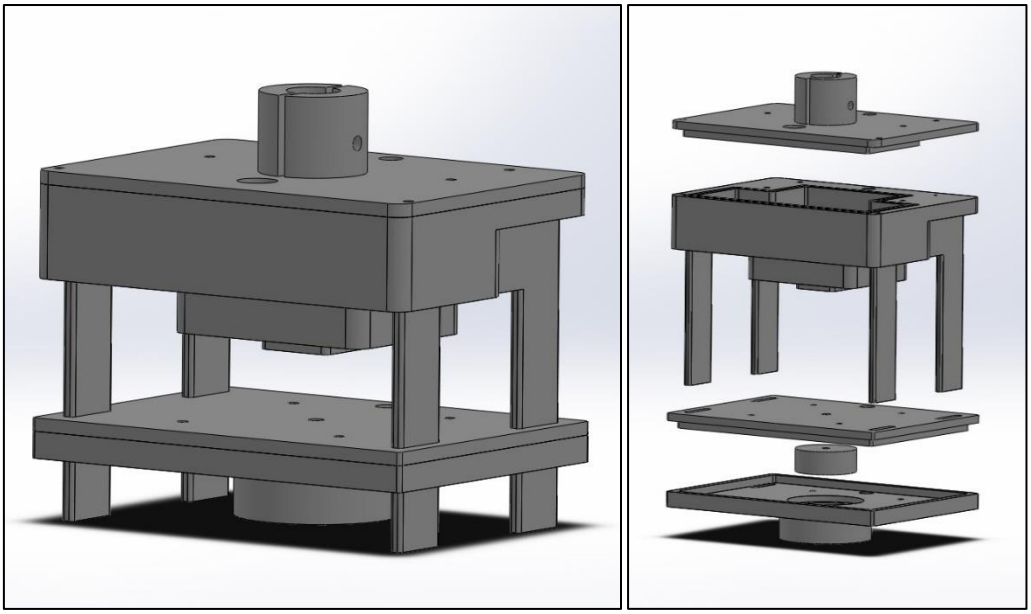

Figure 45: Experimental Spectrometer package assembly (Left) and exploded view (right)

An experimental package was designed and manufactured for the indoor lab, (Figure 46, Figure 47). The distance between light source and frequency sensor is adjustable by including slider beams on which the light source package is lowered and lifted on an M10 screw shaft that rotates around its own axis. Rotating the screw clockwise lifts the source holder with respect to the sensor box, and inherently lowering the source with respect to the sensor box by rotating counter-clockwise. The freedom to vary the distance between both parts of the setup allows the user to identify the optimal distance for reading accuracy and sensitivity to oil film thickness. The package was machined on the CNC out of polyamide, due to its ease of machinability and low friction coefficient. Figure 46 shows the experimental setup's upper part open (left) and closed (right), the upper part is a box manufactured to fit the experimental printed circuit board with the 12V battery. The system is mounted to a linear actuator in case dynamic actuation is desired in future experiments.

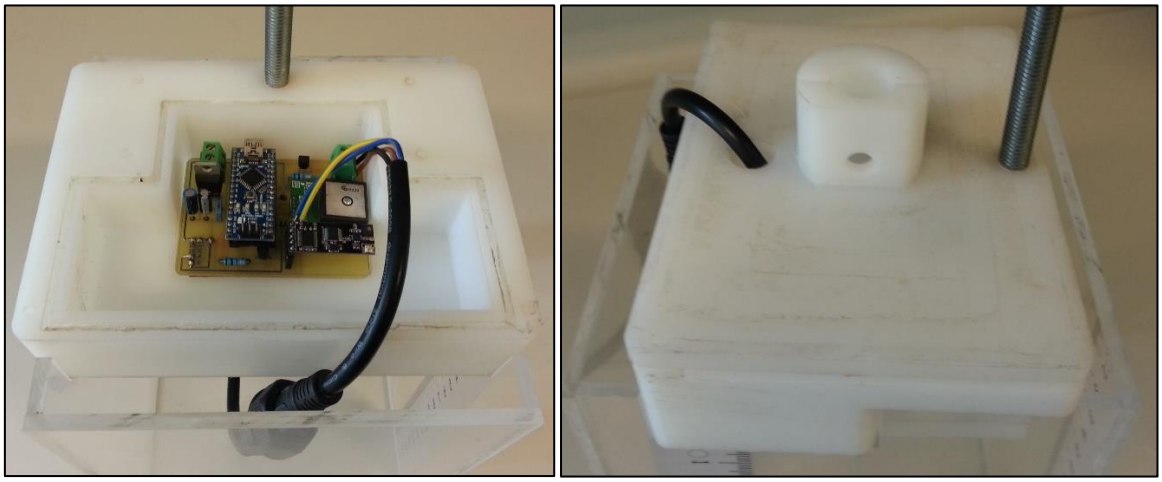

Figure 46: Sensor/battery box (left: lid off, right: lid on)

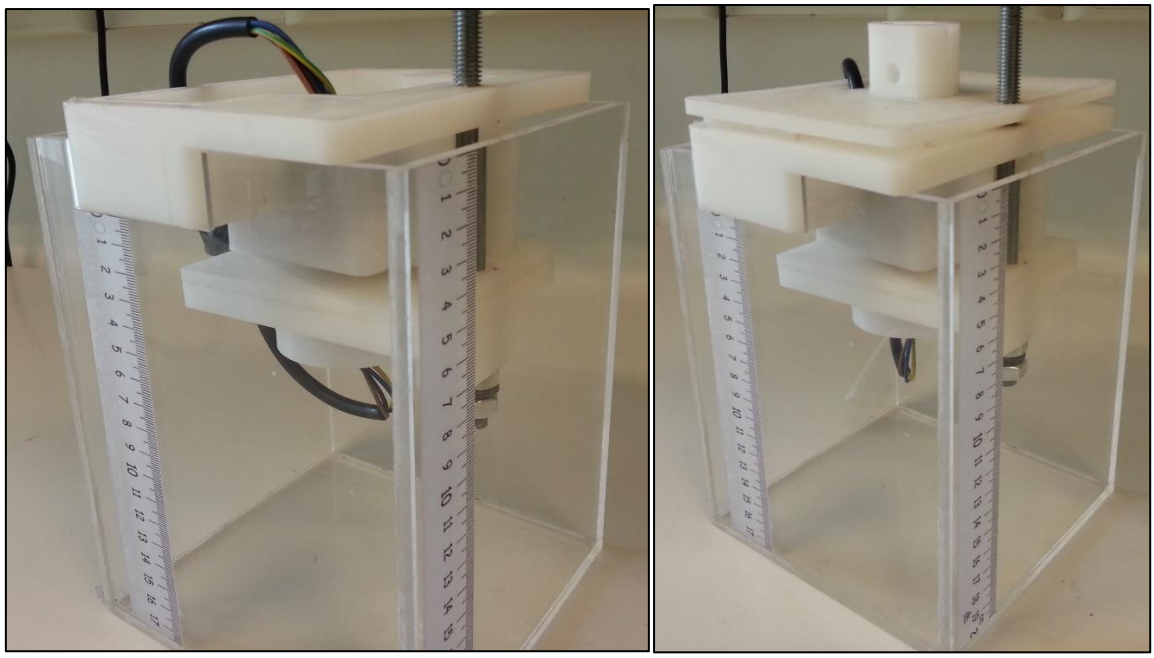

Figure 47: complete setup (left: lid off, right: lid on)

4.2 Capacitive Sensor Indoors Lab Testbed

The indoor lab tank design was implemented to test the capacitive sensor in various conditions encountered in the application environment such as waves, still water, and sensor tilting due to dragging in the sea. The tank is made of plexiglass and equipped with a mechanism for sensor actuation. The implemented lab tank is shown in Figure 48.

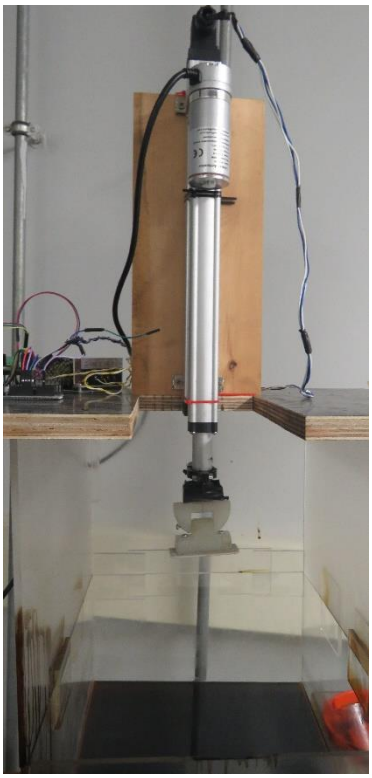

Figure 48: Capacitive Sensor Experimental Testbed - Lab tank

A 3-phase brushless DC motor (BLDC) was chosen to actuate the rack and pinion mechanism fitted on the tank, the motor specifications are as follows:

- Operating Voltage: 12V
- Motor rated speed: 3700rpm
- Motor Diameter: 36mm
- Gearbox: planetary gear reducer
- Speed: about 150rpm/s.
- Shaft length: 20mm
- Reduction ratio: 27:1
- Signal cycle pulse number: 2*27
- Control mode:
    - PWM speed control
    - Direction control
    - Feedback pulse output

The motor is interfaced with MATLAB Simulink (Figure 49) using an Arduino Mega 2560 to run real-time external mode simulations with all type speed profile input normalized to PWM range. After conducting several experiments on the motor for parameter identification purposes, it was noticed that the motor speed reaches a maximum of 150rpm at a PWM range of 150 to 255.

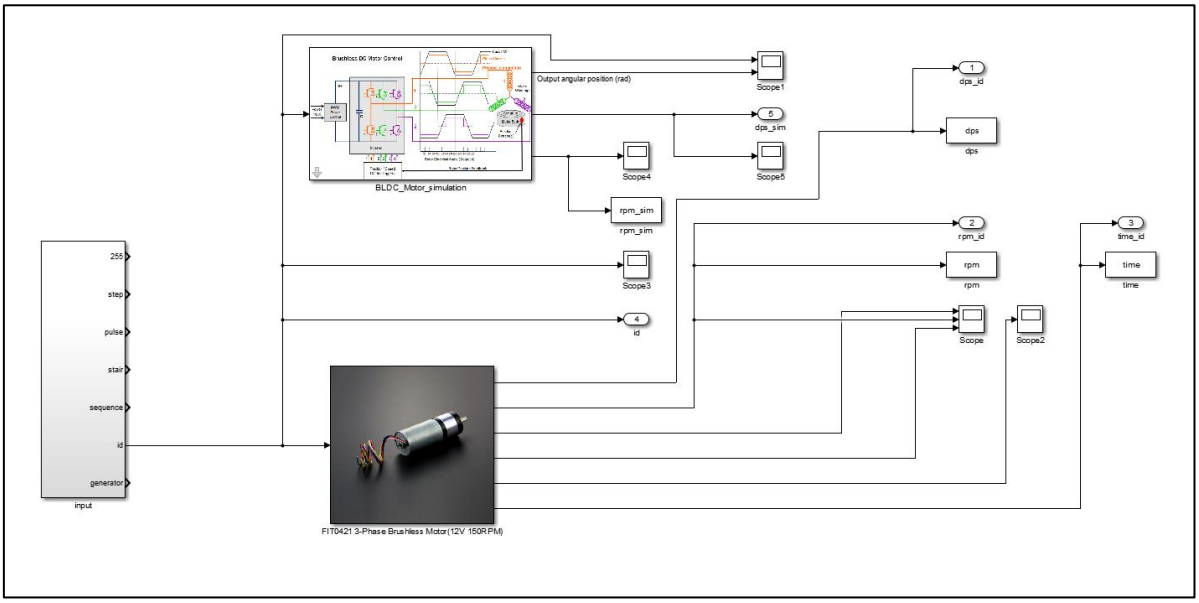

Figure 49: overall Simulink block diagram

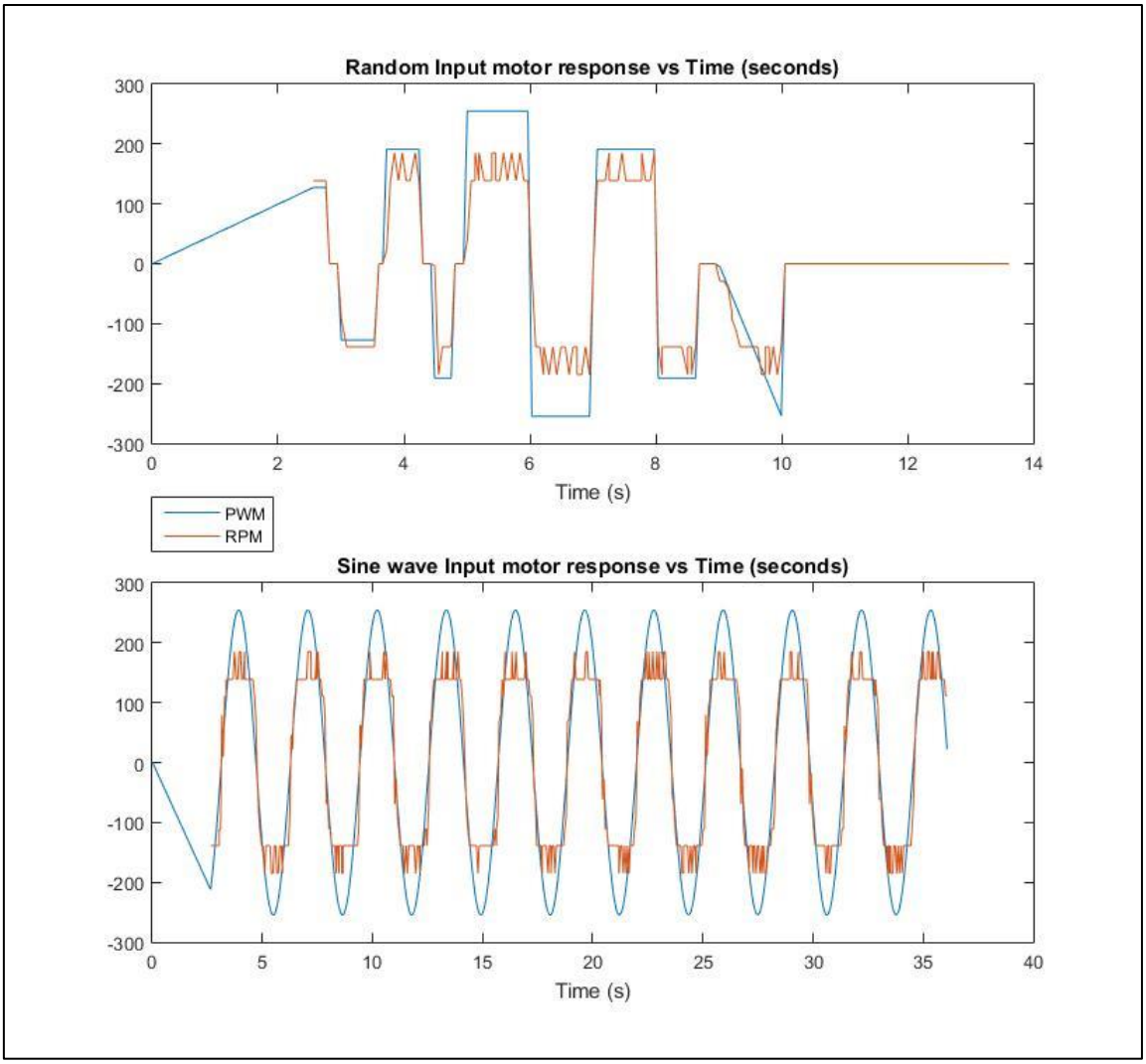

Figure 50: Motor performance

As seen in the comparison of Figure 50 the maximum speed is reached at 150PWM input for most inputs, the response is fast enough for our application. Considering that one revolution induces 3cm of travel for the rack and pinion mechanism and that the sensor capacitive card is 15cm in length, the desired wave profiles can all be realized in terms of relative amplitude travel and wave frequency using the motor at hand mounted on the designed lab tank setup. Upon testing the motor, it was noticed that due to backlash and sideways play, a non-uniform load is applied on the motor shaft by the rack and pinion mechanism causing a random change in torque. Therefore, a bang-bang controller was adopted to make the position tracking independent of such disturbances; the results of this method were much acceptable for wave amplitude simulation. A second change to the tank has been made on the software application end, allowing the user to set the frequency, amplitude, and phase shift of the simulated wave/sensor trajectory. Both the software and hardware implementation changes allowed the experiments to be performed more efficiently but one person.

4.3 Capacitive Sensor Outdoors Lab Testbed

The tank in Figure 51 shows the final design used to build the outdoors testbed; modifications were made regarding the tank partitioning, such as the inclusion of a wooden separator along the length of

the tank in order to enable testing of different conditions in the tank at the same time. The linear actuator in Figure 55 can be placed on either side of the partitions since it is not fixed on the tank rim. The tank dimensions are 1x1x3meters (three meters cubed volume), although only a fraction of the tank's volume (~50%) is filled with seawater and oil. The medium is controlled with a submersible controllable pump (Figure 52, Figure 53) in order to test various wave profiles. The complete setup was tested in rainy and sunny weather, with no complications regarding waterproofing both on the sensor and tank ends. Nevertheless, it was noticed that due to residue and debris accumulation from tree and dirt around the tank, caused the pump to clog if the tank isn't cleaned prior to testing. Manufacturing drawings of the steel tank can be found in the Appendix.

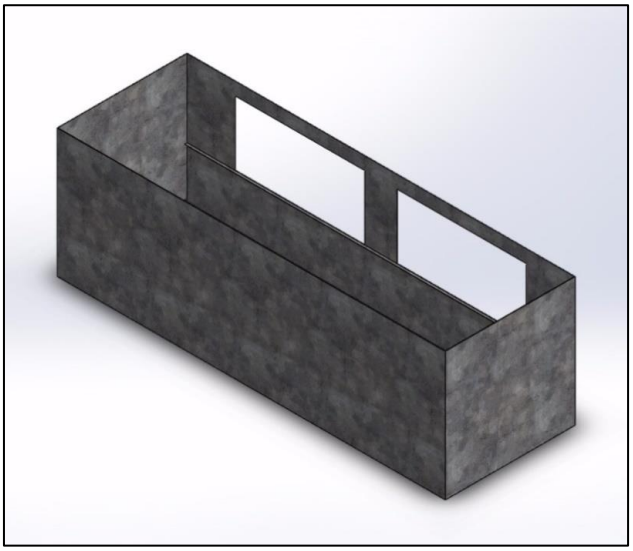

Figure 51: Large tank Galvanized steel SolidWorks design

The chosen pump model is the Abyzz A200 manufactured by VENOTEC Germany, it can deliver up to 17 l/h flow rate at a maximum speed of 5.4m/s with a maximum head of 8.8m and a maximum pressure of 1.5bar, and a power range of 4 to 200W.

Figure 52: Abyzz 200 controllable pump

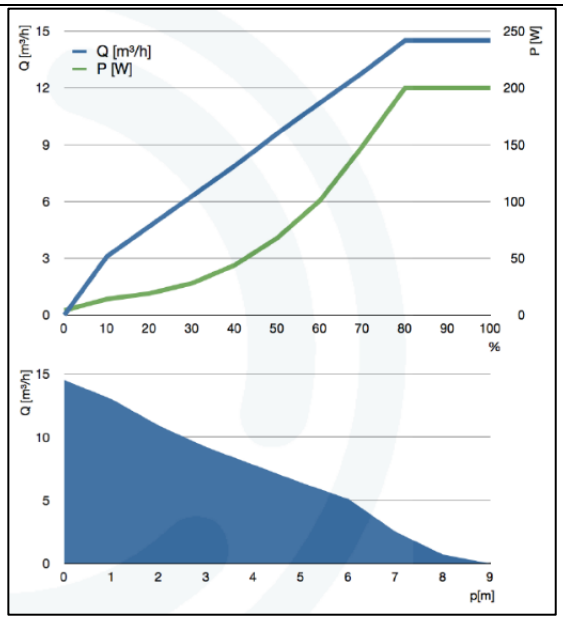

Figure 53: Pump specifications

The large wave tank was manufactured and delivered to the test location (Figure 54), the wave generating pump was also delivered, and was tested to check the resistance of the tank to waves. The pump was first set to run in positive mode from 0% to 100% (200W) power, the random mode was tested with random flow directions at random power delivery; wave mode was tested with varying flow direction time (symmetric profile and non-symmetric profile). Furthermore, the pump was tested with minimum negative flow direction (varying from 0% to 100%) as well as positive direction (minimum, to the full power positive flow direction). The tank passed all tests, welds were checked twice for leakage as well as the see-through windows, and no leaks were detected. Finally, for the sake of displacing the sensor through the tank, a linear actuator with a stroke of 1.5meters was fixed onto the tank (Figure 55).

Figure 54: Wave tank

.

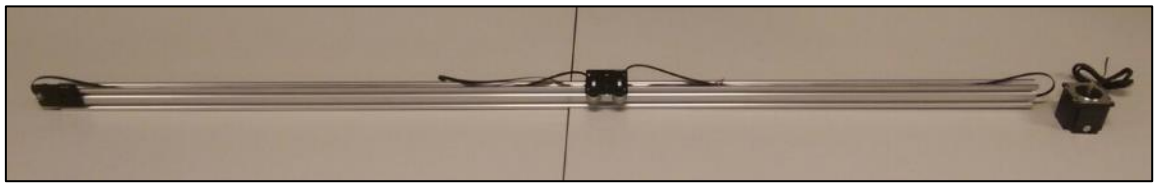

Figure 55: Linear actuator

Functionality tests were made on the large tank, where actuator, switches and control panel were waterproofed and tested in the rain while the sensor was in operation. A control panel (Figure 56) was developed for the actuator, in which the panel contained a 220VAC to 24VDC and 5VDC switching mode power supply (SMPS) to power the stepper drive. and the Atmega microcontroller; both the drive and the microcontroller were mounted on the panel as well. A potentiometer along with limit switches were added for speed control and direction change respectively.

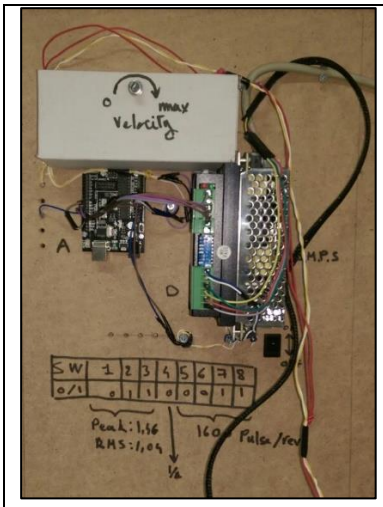

Figure 56: Control panel

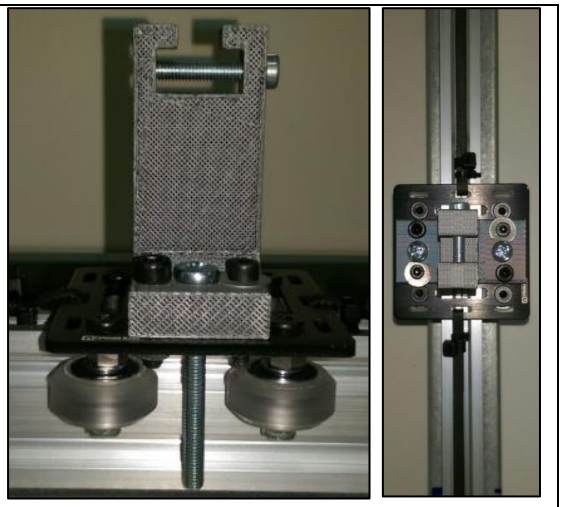
Figure 57: 3D printed extension installed on rail

A bracket/extension (Figure 57) was designed and 3D printed to fix the package with the linear actuator. The package mounted on the actuator was tested once upside down and once in the proper orientation, the fixing bracket/extension was able to withstand the stresses, which peaked at the change in direction. Figure 58, shows a photo of the initial capacitive sensor prototype mounted on the large tank actuator while dragging.


Figure 58: Photo of Capacitive sensor mounted on the large tank actuator while dragging

Chapter 5- LED-based Sensor Design Evaluation and Refinement

This chapter describes the experimental work done to evaluate the preliminary LED-based sensor design performance under different conditions. After analyzing the experimental results, design refinements were applied to the final buoy and sensor design.

5.1 Experiments for Tuning Distance

As described in the previous sections, the LED-based sensor measures the thickness of a transparent oil layer floating on water surface using the principle of light-absorption analysis. The LED-based sensor device is composed of a light source module that emits a blue light on the lower surface of the oil-water mixture and a light-to-frequency converter module to measure the intensity of the light after penetrating the oil layer. To select the optimal distance between the two modules (light-emitter and light-sensor), several experiments were performed to tune the system by recording the sensor response with respect to a set of different distances. The experimental setup shown in Figure 59 is used for this purpose, where it is composed of a graduated plexiglass container (Figure 59-Left), and a variable distance platform (Figure 59-Right). The variable distance platform is composed of two independent units connected with a waterproof cable. While the lower unit contains the light source (blue LED), the upper unit contains the sensor board. Changing the distance between the two units is done by rotating a threaded rod as described in previous chapter.

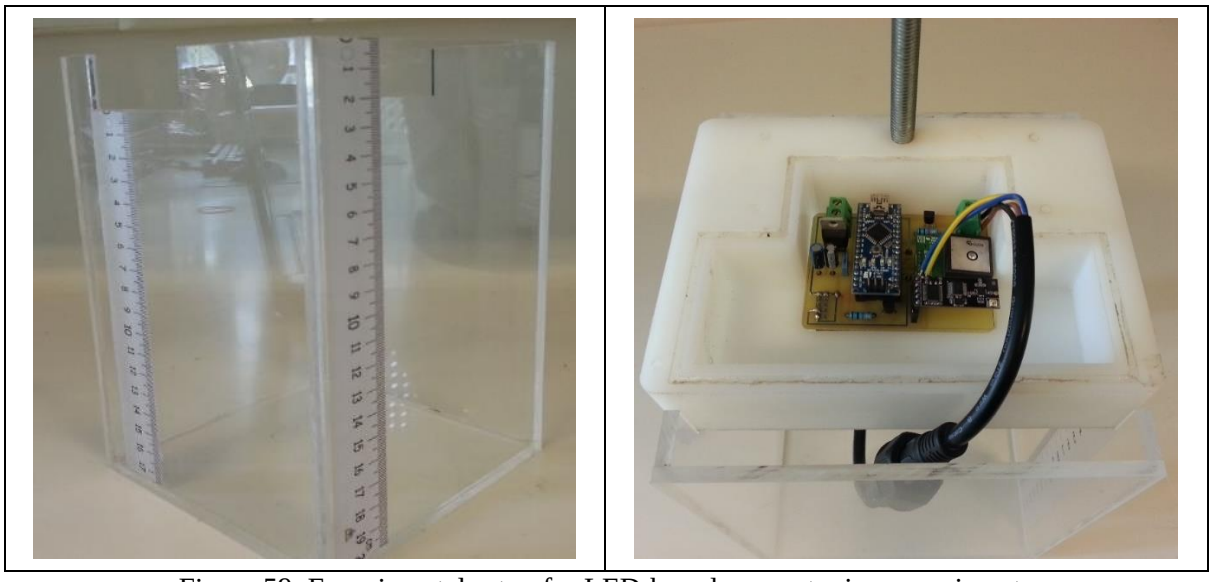

Figure 59: Experimental setup for LED-based sensor tuning experiments

5.1.1 *Distance Tuning Experiment 1 (5.8/ 6.5/ 7.4 cm - sensitivity (x100) - scaling (100))*

The first set of experiments were performed using the following distances: 5.8, 6.5, and 7.4cm. During these experiments, the sensitivity and scaling factors of the light-to-frequency converter were set to 100. The experiments were performed indoors using a light lubricating oil with a viscosity of 10cSt. The experimental results of the three experiments are shown respectively in Figure 60, Figure 61, and Figure 62.

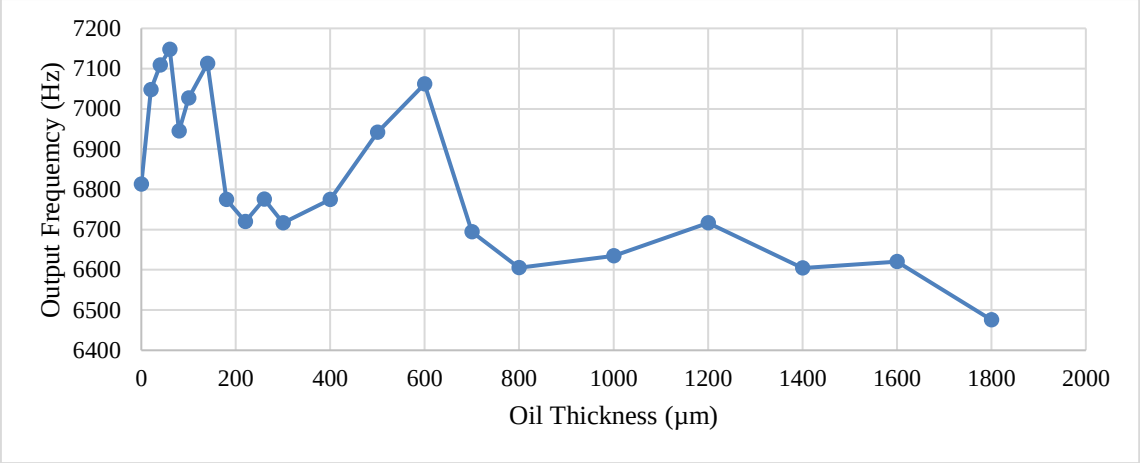

Figure 60: LED-based Sensor Tuning – Distance: 5.8 cm, Sensitivity: 100, Scaling: 100

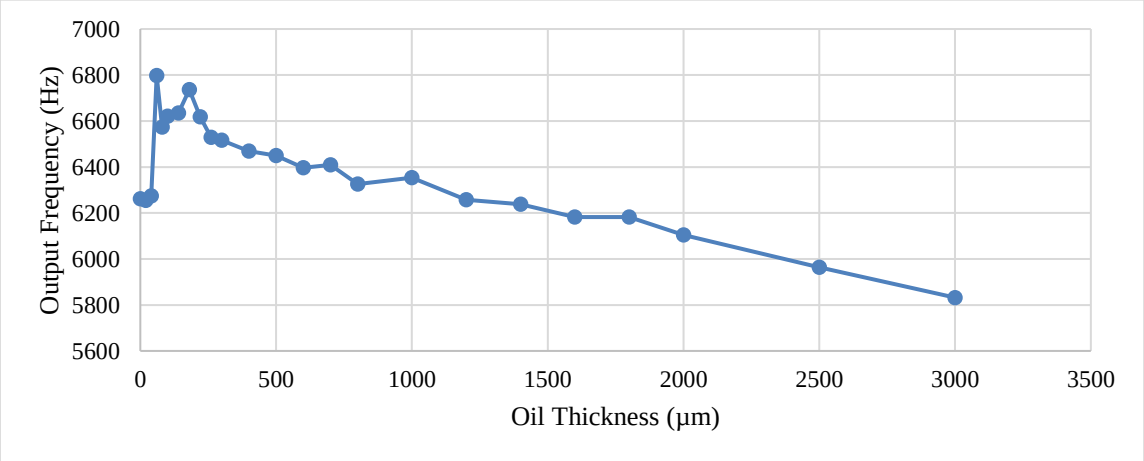

Figure 61: LED-based Sensor Tuning – Distance: 6.5 cm, Sensitivity: 100, Scaling: 100

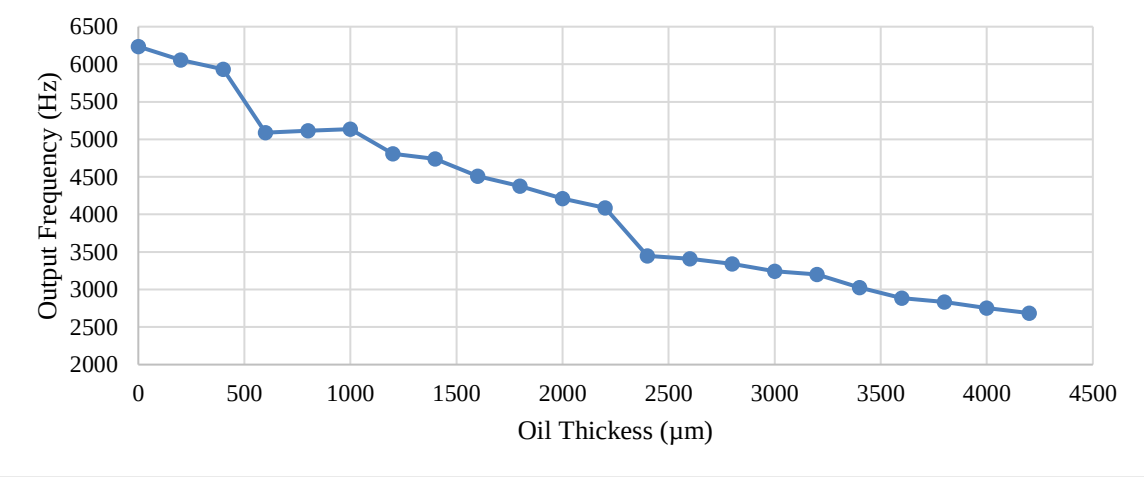

Figure 62: LED-based Sensor Tuning – Distance: 7.4 cm, Sensitivity: 100, Scaling: 100

The results of the first set of tuning experiments showed that the output frequency decreased as the oil thickness was increased. Since the output frequency is related in a direct manner to the received light intensity, it is concluded that as the oil thickness increases the penetrating light is more attenuated. However, as shown in Figure 60, and Figure 61, for distances below 7cm, major fluctuations appeared,

especially in the thicknesses below 1000µm. In contrast, results obtained from the 7.4cm experiment shown in Figure 62 show more stable and an almost linear response with respect to oil thickness.

5.1.2 *Distance Tuning Experiment 2 (7.4/8.5 cm - sensitivity (x1) - scaling (100)*

To assess the effect of different configuration parameters on the system response, several distances were tested while the sensitivity factor of the light-to-frequency converter module was decreased to 1x, and the scaling factor was set to 100. The first two experiments were done using the same light source. A resistor of 220Ω was connected in series with the blue-light LED. After that, the LED intensity was increased by replacing the series resistor by a smaller resistance of 100Ω, and the second experiment with 8.9cm distance was repeated. The experimental results of the three experiments including the frequency response with respect to the oil thickness are shown in Table 16 and the corresponding graph is shown in Figure 63.

Table 16: LED-based - Experimental Results - Distance tuning experiment 2

	Frequency (Hz/100)		
Thickness (um)	7.4cm	8.9cm	8.9cm (increased LED brightness)
0	81.921	62.581	104.167
1000	76.233	58.233	97.577
2000	73.332	54.695	92.133
3000	70.932	52.089	88.723
4000	67.421	50.173	84.578
5000	65.326	47.944	79.500

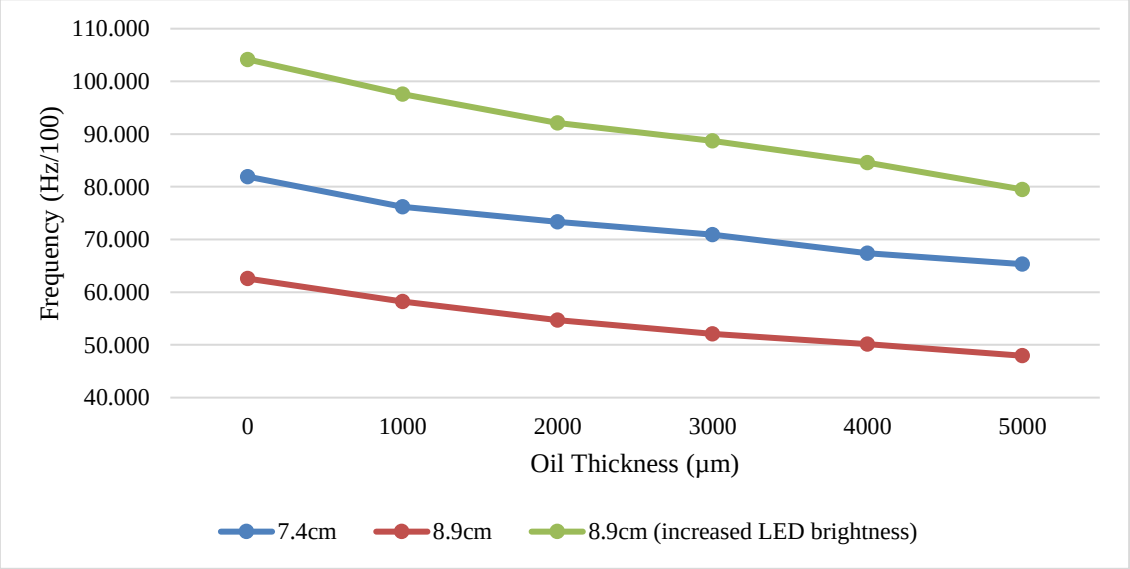

Figure 63: LED-based Sensor Tuning – Experiment 2 (Graph)

The three experiments showed an almost linear relation between the output frequency and the oil thickness, with no major fluctuations. However, major differences between the three curves were recorded regarding the threshold and slope values. To interpret the result more precisely, the average value and the average slope of each curve was calculated. The average threshold was obtained by calculating the arithmetic mean of all frequencies recorded in each experiment. Slope values were

obtained by calculating the absolute differences between consecutive frequencies, recorded by each experiment. In addition, the range of each experiment is acquired by calculating the absolute difference between the maximum and minimum frequency recorded in each experiment. The threshold, slope, and range values for each experiment are shown in Table 17 and the corresponding graph is shown in Figure 64.

Table 17: Distance Tuning Experiment 2 - Comparison

Thickness (um)	7.4cm	8.9cm	8.9cm (increased LED brightness)
Average Slope	3.319	2.927	4.933
Average Threshold	72.527	54.285	91.112
Range (Max - Min)	16.595	14.637	24.667

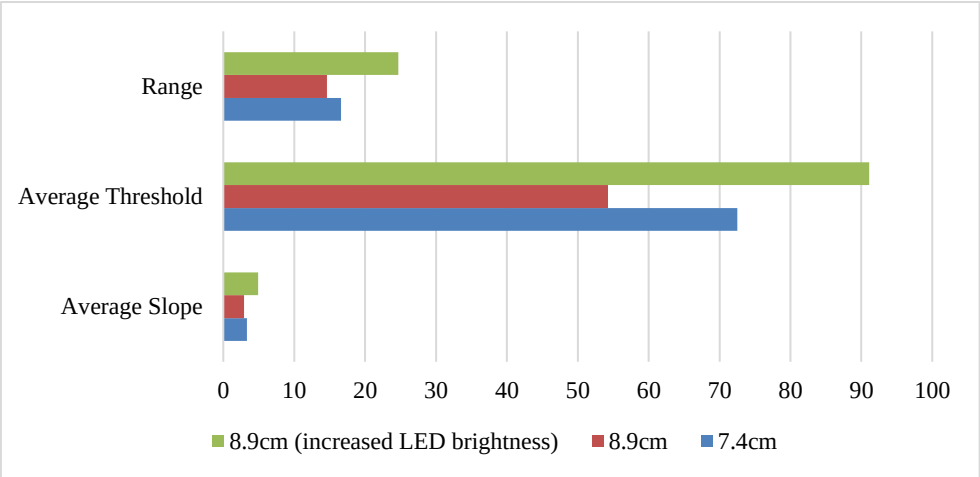

Figure 64: Distance tuning experiment 2- Comparison (graph)

The experimental results of the second set of tuning experiments showed that when the distance was increased from 7.4 cm to 8.9cm, the threshold, range, and slope values were decreased. Since working at a larger distance is more desired to protect the sensor lenses from fouling while working in dynamic sea conditions (waves), a solution was tested by increasing the LED brightness. The result of the 8.9cm experiment with enhanced LED brightness showed the maximum values of frequency slope, threshold, and range. Regarding the threshold value, the result was expected since a larger amount of light is incident on the sensor lens. The most important point is that the slope and range values representing the system sensitivity to oil thickness changes were increased. This result proved the efficiency of using distances larger than 7cm (8.9 cm) while increasing the light intensity.

5.1.3 *Distance Tuning Experiment 3 (6.5/10 cm - sensitivity (x10) - scaling (10)*

In the third set of experiments, we increased the sensitivity factor to 10x and decreased the scaling factor to 10. Two experiments were performed using two different distances (6.5cm - 10cm). The experimental results describing the frequency response with respect to the oil thickness in the two cases are shown in Table 18 and the corresponding graph is shown in Figure 65.

Table 18: LED-based - Experimental Results - Distance tuning experiment 3

	Frequency (Hz)	
Thickness (um)	**6.5 cm**	**10 cm**
0	7799.49	5910.55
100	7508.87	5651.60
200	7221.89	5776.64
300	7114.79	5556.38
400	6982.67	5474.42
500	6865.20	5385.42
1000	6582.92	5160.02
2000	6113.75	4871.74
3000	5101.94	4519.09
4000	4835.85	4168.43
5000	4621.81	3845.51

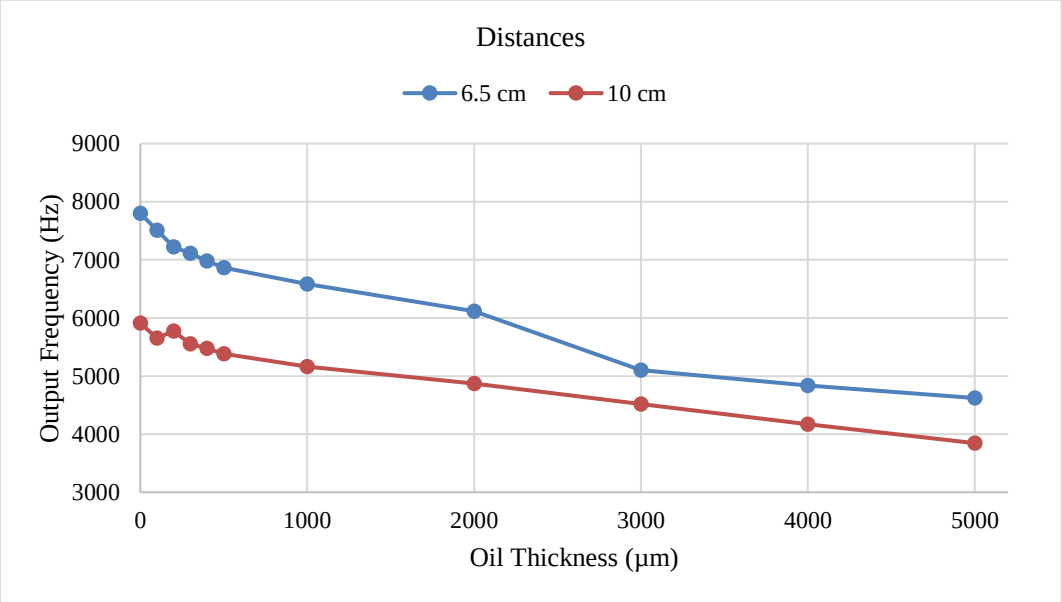

Figure 65: LED-based Sensor Tuning – Experiment 3 (Graph)

The frequency response recorded at 6.5cm and 10cm showed a similar linear relation with the oil thickness. However, it was observed that the 6.5cm frequency curve decreased in average when the distance is increased to 10cm. This result was expected since the amount of light reaching the light-to-frequency converter decreases as the distance is increased. To assess the effect of the distance increase on the sensitivity of the system, more detailed interpretation was performed by calculating the average slope, average threshold, and range of the curves obtained from the two experiments (Table 19, Figure 66).

Table 19: Distance Tuning Experiment 3 - Comparison

	Frequency (Hz)	
Thickness (um)	**6.5cm**	**10cm**
Range	3177.683919	2065.044133
Average	6431.748564	5119.987496
Average slope	317.7683919	231.5130086

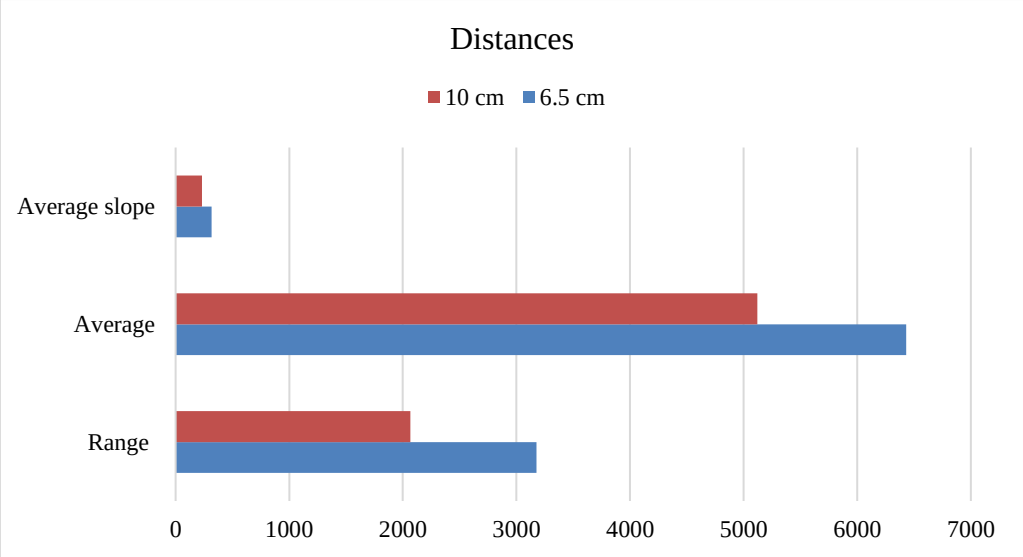

Figure 66: Distance Tuning Experiment 3 - Comparison (Graph)

The slope and the range of frequency change were also decreased with increasing the distance. This result revealed that the 6.5cm was better in terms of sensor sensitivity to changes in oil thickness. However, a tradeoff between the sensitivity and the distance was considered since larger distance contributes to protecting the sensor lenses from oil fouling during operating in the dynamic sea after conditions. Based on that and since the frequency response at 10 cm was considered acceptable also, the 10 cm was selected to be used in final sensor design with a configuration of 10x and 10 scaling factors.

5.1.4 *Diesel Experiment 4 (10 cm - sensitivity (x10) - scaling (10))*

The same experimental setup was used to evaluate the sensor performance in diesel oil instead of lubricating oil. The distance between the light-emitter and the light-to-frequency converter modules was set to 10cm. The oil thickness was added gradually through three stages, where in the first stage, the thickness was increased from 0µm to 500µm by increments of 100µm. After reaching 500µm, the thickness was doubled to reach 100µm. In the last stage, the thickness was increased from 1000µm to 5000µm with increments of 1000µm. Table 20 shows the experimental results including the sensor frequency response at each thickness level, and Figure 67 shows the corresponding graph.

Table 20: LED-based - Experimental Results - Distance tuning experiment 4

Thickness (µm)	Frequency (Hz)
0	6067.41
100	5931.47
200	5826.41
300	5741.53
400	5594.78
500	5402.47
1000	5222.15
2000	5138.92
3000	5044.20
4000	4945.12
5000	4862.07

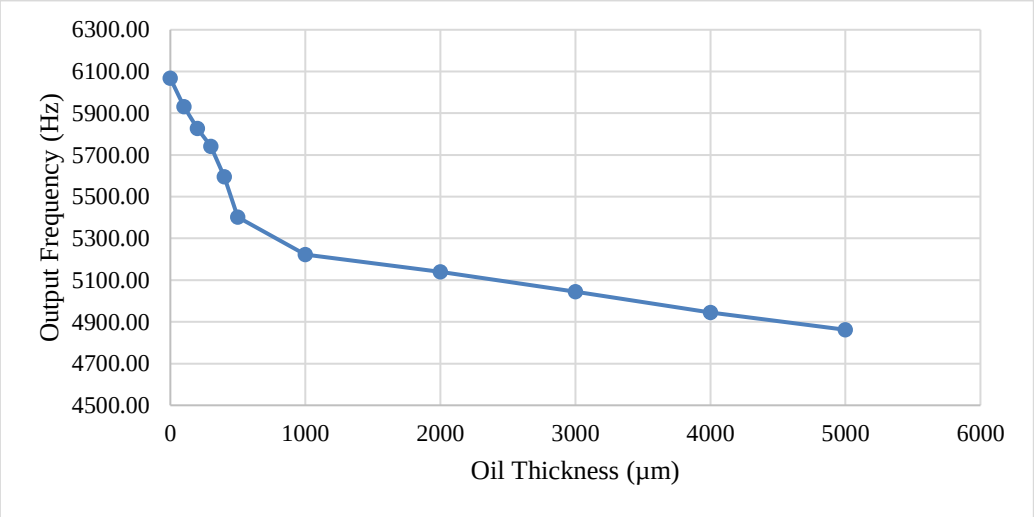

Figure 67: LED-based Sensor Tuning – Experiment 4 (Graph)

The experimental results of the diesel experiment showed a decrease in the output frequency with the increase in oil thickness. It is important to note here that a major change in the curve slope was observed past the thickness of 1000µm.

5.2 Oil-Thickness Calibration and Measurement

The aim of this experiment is to evaluate the performance of the sensor after performing calibration, which is done by recording the output frequency of the sensor against several oil thicknesses, and a piecewise linear fit to the data was performed, with the first equation between 0µm thickness and 1000µm thickness, and the second between 1000µm thickness and at 3000µm thicknesses.

To measure the oil thickness based on the calibration equations, oil was removed from the experimental setup and new amount of tap water was filled. Lubricating oil (10cSt) was added gradually to the graduated container representing several oil thicknesses ranging from 100µm to 3500µm. The sensitivity factor of the light-to-frequency converter module was set to 10x and the scaling factor to 10. The distance between the upper and lower parts of the experimental setup was set to 6.5cm. The

experimental results showing the measured oil thicknesses with respect to the actual thicknesses are shown in Table 21.

Table 21: Results of thickness measurement experiment - LED-based sensor

Actual oil thickness (µm)	Measured oil thickness (µm)	Absolute Error (µm)	Percent Error (%)
100	107.75	7.74	7.74
300	291.19	8.81	2.93
500	522.03	22.03	4.40
800	676.17	123.83	15.47
1000	1042.48	42.48	4.24
2000	2102.34	102.33	5.11
3500	3530.60	30.60	0.87

Based on the experimental results, it can be concluded that the oil thickness measurement using the current configuration settings were reliable with a maximum error of 5.1% for the values above 1000um oil thickness, and 15.5% for the values below 1000um oil thickness.

5.3 Bouy Design

A floating buoy (Figure 68) was manufactured for the LED-based sensor. Based on the critical dimensions identified in the tuning experiments, the distance between the light-emitter module and the light sensor module was set to 10cm. Mainly, the buoy structure is composed of 3 rods parallel to each other, each one holding several floaters. The rods are joined with three separate platforms. A triad of floaters was chosen for the stability of the design, waterproof light case and box were chosen for the ease of deployment and resistance to salt water wear. The buoy has an enclosing volume of a 40cm diameter cylinder with a 35cm height. The buoyancy can be increased and decreased depending on necessity and weight by adding and removing secondary foam floaters around the exposed parts of the threaded shafts. A blue LED is placed inside the light holder as a separate unit.

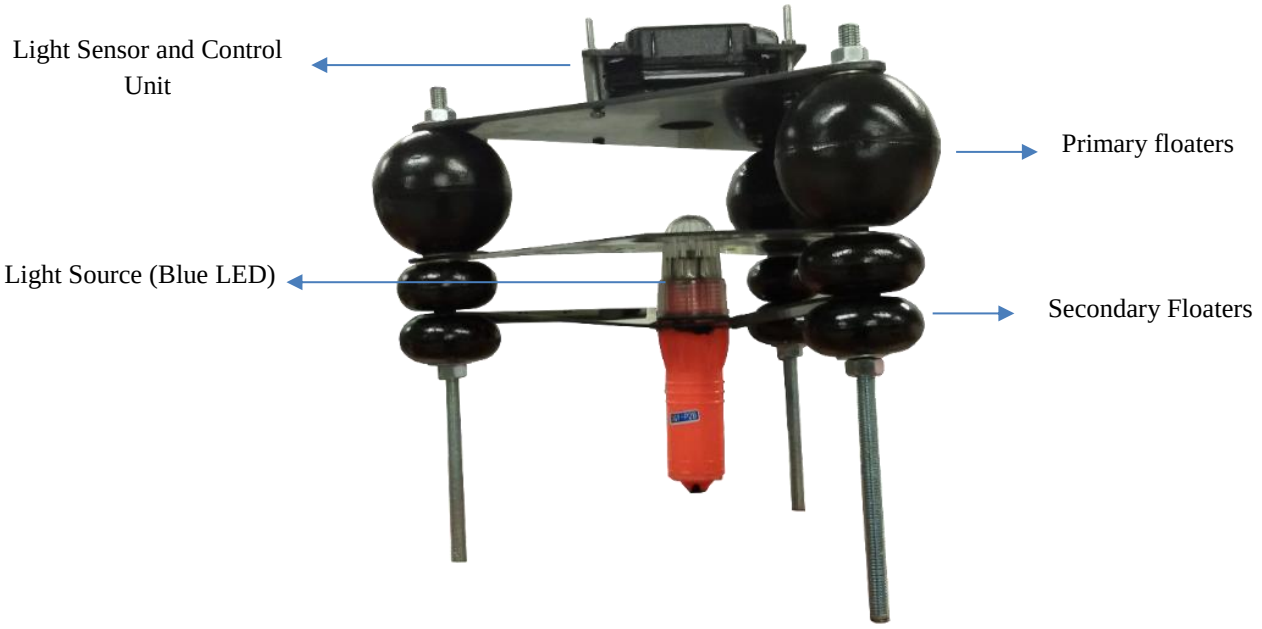

Figure 68: Spectro-based sensor - Implemented Buoy

5.4 Bouy Experiments

After designing the final sensor buoy, several experiments were performed to assess the performance of the sensor in floating conditions. The sensor was embedded into the buoy structure and a 100-Liters tank filled with seawater was used in the experiments. During the experiments, controlled amounts of lubricating light-oil with a viscosity of 10cSt was added to the container to form a set of different thicknesses. The experimental setup with the buoy installed is shown in Figure 69.

Figure 69: LED-based Buoy - Experimental Setup

Table 22: Bouy Experiment - Frequency response vs. Oil Thickness

Thickness (um)	Average Frequency (Hz)	Standard deviation
0	4910.08	15.56626
200	4847.60	217.1475
400	4758.28	105.6207
600	4703.27	19.51385
800	4540.35	26.51144
1000	4471.62	32.18685

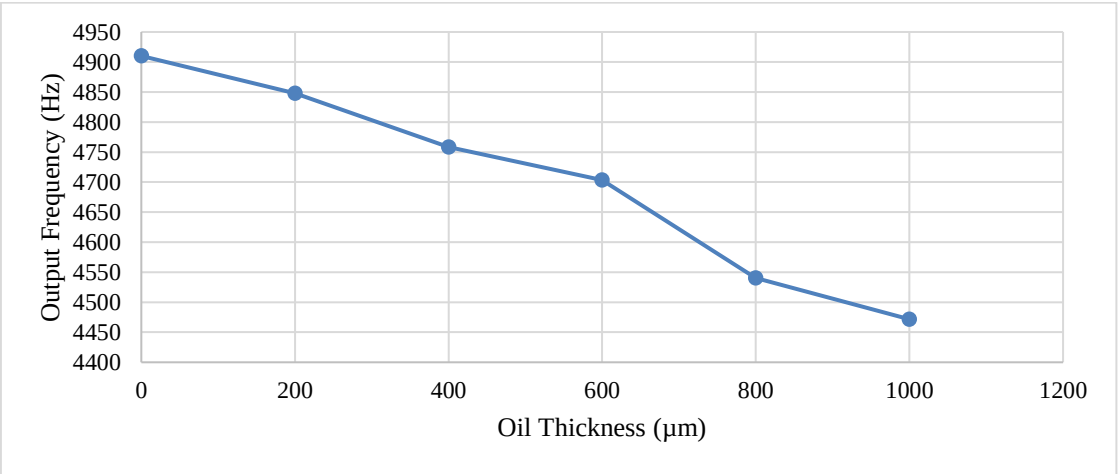

Figure 70: Buoy Experiment - Frequency response vs. Oil Thickness (Graph)

The experimental results showed an almost linear decrease of the frequency response with the increase of oil thickness (Figure 70). However, in this experiment, high standard deviation values were recorded (Table 22). Then, a set of experiments were performed to assess the effect of the water level and waves on the stability of the frequency response. The new experiments were done using several scenarios listed as the following:

- Fixed buoy (no waves)
- Changing the water level while the buoy is fixed
- Fixed buoy subjected to waves
- Floating buoy (no waves)
- Floating buoy subjected to waves

The same experimental procedure was repeated with two different oil thicknesses; 500µm and 1000µm. The output frequencies recorded from the two experiments are shown in Table 23, and Table 24 respectively.

Table 23: Floating Buoy Exp. 1 (500 µm)

Average Frequency (Hz)	Standard deviation	Condition
10247.7	24.46433	4 cm water level above led
10508.59	41.98751	7 cm water level above led
10377.53	426.8029	7 cm water level + waves
9947.77	65.60328	Floating buoy (3 cm water level)
9869.097	593.6416	Floating + waves

Table 24: Floating Buoy Exp. 2 (1000µm)

Average Frequency (Hz)	Standard deviation	Condition
10708.91	26.81183	4 cm water level above led
12033.64	67.09064	7 cm water level above led
11698.08	1146.598	7 cm water level + waves
10577.9	120.4646	Floating buoy (3 cm water level)
10283.84	476.4398	Floating + waves

It was observed that once waves are introduced, the standard deviation was highly increasing because of high-frequency fluctuations dominating the measured values. However, since the average frequency obtained at the same thickness level were almost similar with and without waves, the result was considered acceptable, and work was focused on decreasing the fluctuations algorithmically.

Chapter 6- Capacitive Sensor Design Evaluation and Refinement

This chapter describes the experimental work done to evaluate the performance of the preliminary capacitive sensor design under different conditions. After analyzing the results, design refinements were applied to the sensor layout, and the final design was implemented and tested.

6.1 Performance Testing

To evaluate the performance of the preliminary sensor design, three sensor boards with similar dimensions (Figure 71) were implemented and tested.

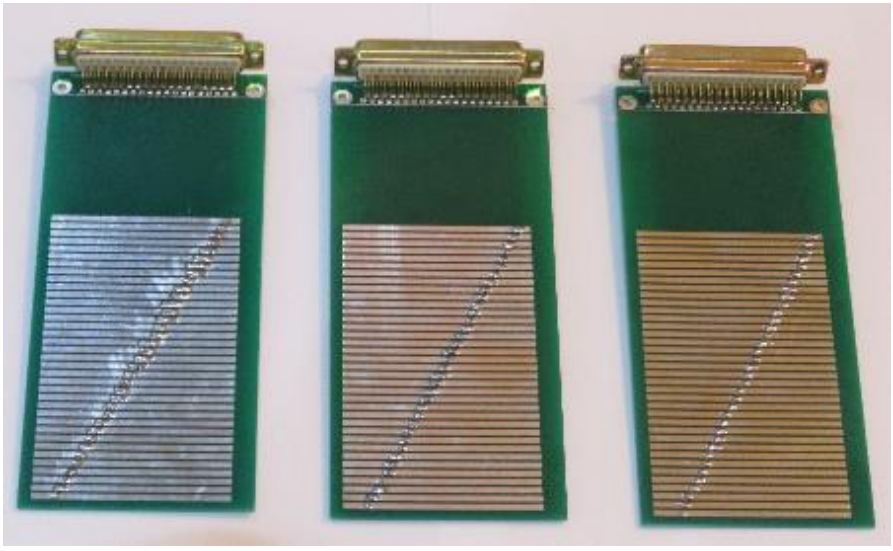

Figure 71: Sensor prototypes for repeatability testing

The three sensor boards use the D-37 male connector (shown at the top of each sensor) to connect to the controller circuit. To compare the three boards, raw voltage values were taken from each sensor in three cases: air, oil, and water. In each sensor board, 36 strips were activated, and a set of voltage measurements were recorded for each strip during the experiment.

First, the comparison of the sensors in the air medium shows that the baseline values of the three boards (A = 151, B = 154, C=149) are similar. Note that the baseline values of the sensor boards depend not only on the dimensions of the sensor board but also on the actual hardware implementation and finishing aspects in terms of soldering and copper thickness, which add to the base capacitance of the electrodes. Second, the three sensors were totally immersed in water to compare the measured voltages. In the case of immersing the board in water, a large attenuation of the voltage values of the three boards was observed. The results of this experiment showed a similar response of the three sensors while in water. With similar average values (A=2.2, B=2.3, and C=2.11), the three sensors are demonstrated to be behaving similarly.

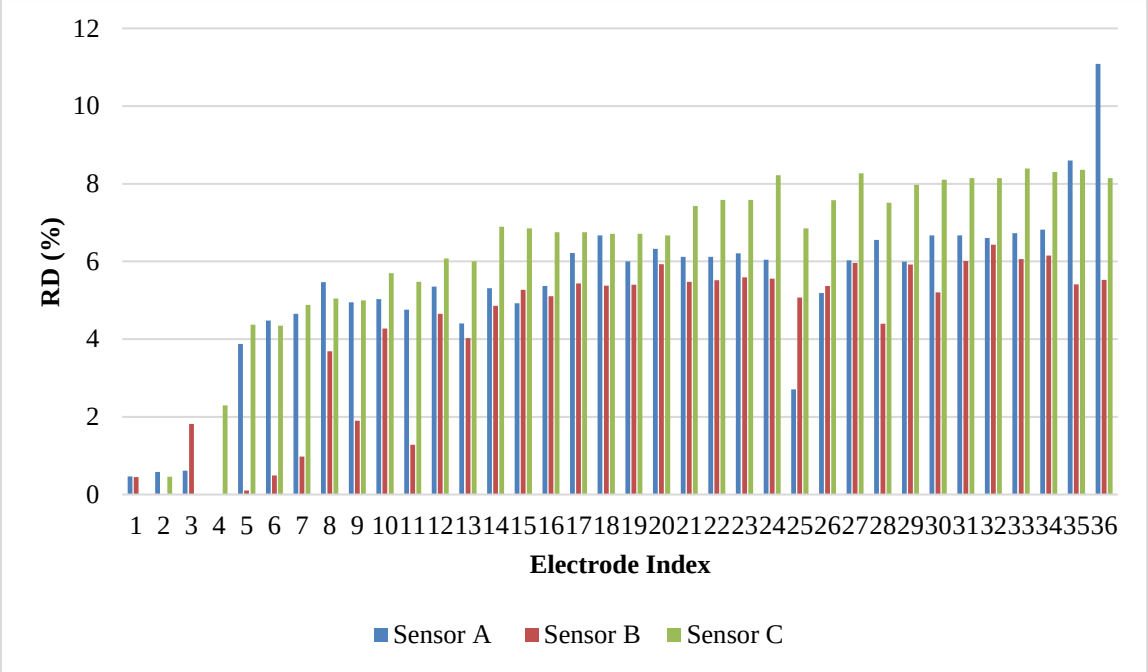

Figure 72: Capacitive Sensor Performance Experiment - Oil Case

To analyze the results in the case where the sensor is immersed in oil, the relative differences from the calibration values are calculated (Figure 72). The relative differences are divided into two categories: the first category contains the electrodes located in the air (E1 to E4), and the second category contains the electrodes immersed in oil (E5 – E36). It was noted that the relative difference of each electrode was increasing with the electrode index, since the connection tracks mounted on the bottom layer of the PCB have more length in oil when the electrode is lower. We also noted that one electrode in sensor A (E25) did not follow the expected pattern (i.e., a decrease) with its relative difference less than 4% in oil. This problem was more obvious in sensor B with several electrodes (E5, E6, E7, E8, and E11) behaving similarly to E25 in sensor A. The main difference between these electrodes and the other electrodes is that the relative difference of their values is very small, ranging from 0.1 % to 1.28% when the sensor is immersed in oil. While interpreting the experimental results, the electric connection between all the sensor components (sensing electrodes, connection tracks, male D37 connector, female D37 connector, and MPR121 controllers) was tested. A major problem was observed in the connector part (D37), where we noticed that a number of the connector pins were electrically not connected. Despite the fact that this problem was not observed initially during the preliminary experiments, it was demonstrated that it may occur after several iterations of sensor replacement (mounting/dismounting) due to connector bending and stress.

Based on the experimental results, and to avoid possible electrical connectivity problems, we decided to completely remove the connector from the design, and mount the capacitive controllers on the sensor board, instead of the controller board. By doing so, the size of the controller board size significantly decreased. The major advantage of this change is that capacitance measurements are done on the sensor boards without having any connector between the measurement channel and the sensing strip. This enhancement increases the sensitivity and the robustness of the sensor design. By removing the connector, we also avoid the issue of mechanical variations, connector bending, and aging of soldering.

6.2 Evaluating the Impact of Different Power Sources on the Sensor Performance

During the initial testing of the sensor, two main sources were used to power the circuit. First, the control circuit was powered using a USB-port on a laptop. The USB-port was used to power the Arduino module, and to retrieve the measured voltages from the MPR121 modules. The USB-port provides the Arduino with 5VDC, and the Arduino provides 3.3VDC to the MPR121 controllers through the 3.3V embedded voltage regulator. During operation, the laptop was connected to the power adapter, plugged into the AC power lines (220AC). The second source used to power the sensor was a lead-acid battery of 12VDC. To assess the effect of the two power sources on the voltages measured by the capacitive stripes, the sensor was placed at a fixed position, and a set of voltages measured by all electrodes were recorded. The sensor was set at a fixed position (surrounded by air), and a sample of 250 measures was recorded. The voltages measured by the first twelve electrodes are analyzed and presented in Table 25. Also, a graph showing voltages measured by the first electrode E1 in the two cases, is shown in Figure 73.

Table 25: Voltage (ADC) - Battery vs. USB-port Power Sources

	Electrode	Mean	Standard Deviation	Max	Min	Range
Battery Powered	E1	167.00	0.00	167	167	0
	E2	157.00	0.00	157	157	0
	E3	156.00	0.00	156	156	0
	E4	159.00	0.00	159	159	0
	E5	158.07	0.26	159	158	1
	E6	161.00	0.00	161	161	0
	E7	160.00	0.00	160	160	0
	E8	166.00	0.00	166	166	0
	E9	159.00	0.00	159	159	0
	E10	158.00	0.00	158	158	0
	E11	149.00	0.00	149	149	0
	E12	153.00	0.00	153	153	0
USB-port Powered	E1	167.43	0.50	168	167	1
	E2	157.02	0.15	158	157	1
	E3	156.00	0.06	157	156	1
	E4	159.04	0.19	160	159	1
	E5	158.58	0.49	159	158	1
	E6	161.00	0.06	162	161	1
	E7	159.50	0.50	160	159	1
	E8	162.05	0.22	163	162	1
	E9	159.00	0.00	159	159	0
	E10	158.00	0.06	159	158	1
	E11	148.70	0.46	149	148	1
	E12	153.00	0.06	154	153	1

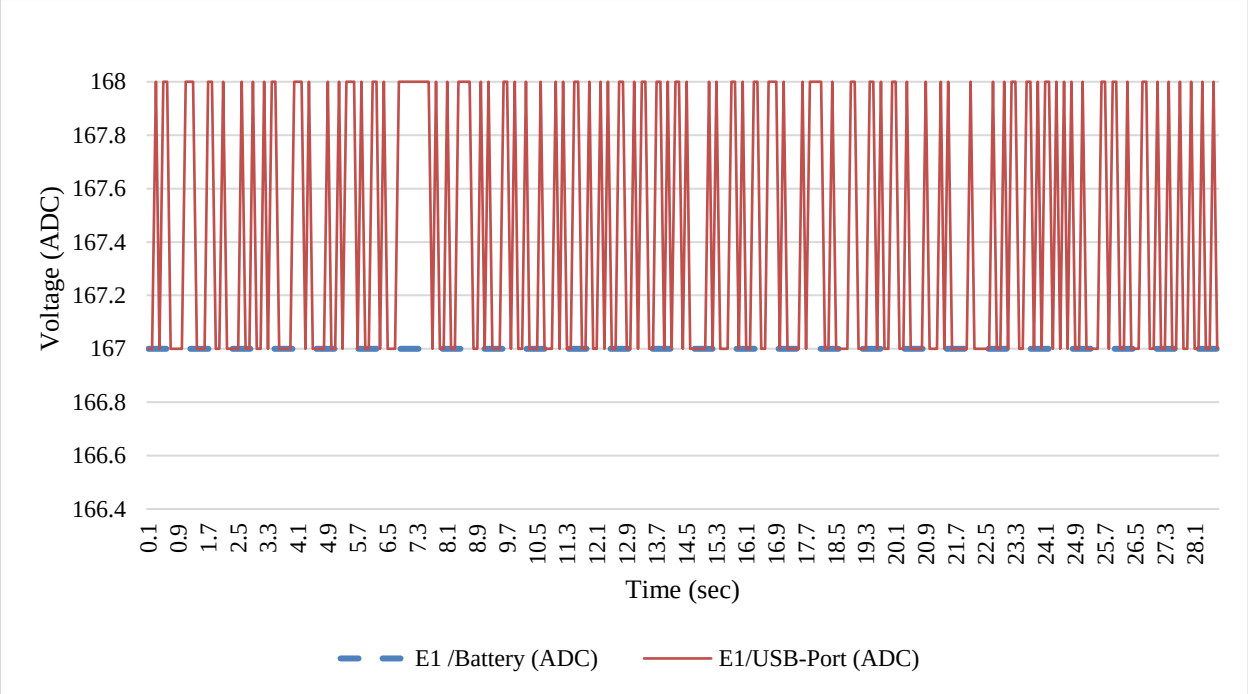

Figure 73: Voltages measured by E1 in Battery-powered and USB-powered trials

This experiment showed that using the USB-port as a power source, introduced additional noise to the measured voltage signals. This can be inferred from the increased standard deviation values shown in Table 25, and the high frequency oscillations introduced to the E1 voltage signal shown in Figure 73. Based on the experimental results, it was concluded that connecting the device to an AC power source is not recommended, to avoid inserting additional noise to the sensor measurement.

6.3 Sensor Design Refinement

As an enhancement for the preliminary sensor design, and to ensure a reliable connection between the sensor electrodes and the connection tracks, the refined design uses plugged vias embedded in a multilayer PCB, instead of using the exposed vias (double layer). The new board is composed of a 4-layer PCB, with sensor pads mounted on the top and bottom layers of the PCB, and the connection tracks are mounted in the two inner layers of the PCB. In this case, the connection tracks are completely isolated from the external material and sensing is done only by the horizontal pads. To drive power and ensure data connections to the microcontroller, the sensor board is connected to the controller board through a 4-pin connector (wire). To extend the range of the sensor, an additional MPR121 device was added to cover twelve new electrodes added to the sensing unit. The main advantage of this design is that the controller board and the sensor board become separated, connected to each other using only four wires. The updated capacitive sensor schematic is shown in Figure 74. The schematic shows the connection between four MPR121 controllers and the sensing pads numbered from 1 to 48. Addressing of the MPR121 is done using the ADD pin of the controllers. By connecting the address pin to GND, 3.3V, SDA, SCL the four controllers have the following I2C addresses respectively 0x5A, 0x5B, 0x5C, and 0x5D.

In summary, the main change regarding the sensing unit is that it includes forty-eight electrodes instead of thirty-six, the four MPR121 controllers are added to the sensing unit instead of the processing unit,

the tracks are buried inside the inner layers of a 4-layer PCB design, and the electrodes are implemented on the two layers of the PCB (bottom, top).

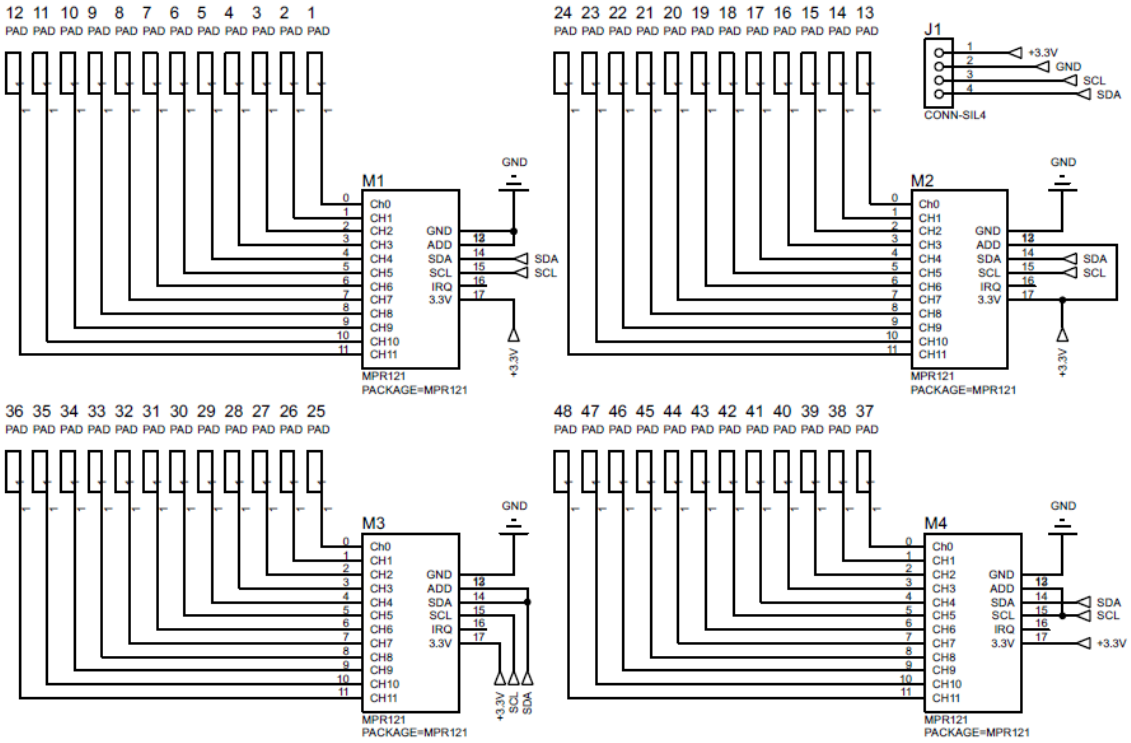

Figure 74: Capacitance Measurement Schematic - Final Design

The final version of the processing unit included a low-voltage drop regulator (LM2940), in addition to two capacitors for signal smoothing (0.47uF and 22uF). In addition, several components were added to the circuit, such as heat sinks for regulators and power jacks (3.5mm) to connect the battery packs. Three boards were implemented and tested. Figure 75 shows a sample of the implemented boards.

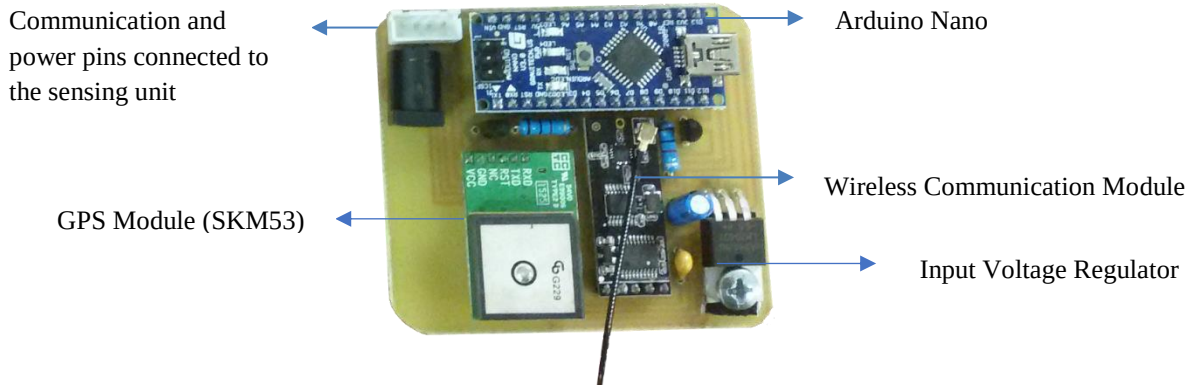

Figure 75: Processing and Communication Unit

6.4 Optimized Sensor Prototype

The final sensor design was prepared as a 4-layer PCB board (Figure 76); where connection tracks are embedded in two inner layers and sensing strips are placed on the surface layers. After adding an additional MPR121 controller to the sensor board, the number of sensing strips was increased from 36 to 48. Considering all the past experiments and design recommendations, and in order to enhance the sensitivity of the unit, increasing the width of the sensing pads with respect to the gap between the electrodes is recommended. Although the sensor measurement range is 10cm, we increased the measurement range to 14.2cm in order to have additional margins in case of maximum thickness scenario and/or wave conditions. The distance between the first sensing pad and the end of the last controller module is 3.28cm, this gap only includes hidden tracks to allow for the packaging to overlap the board and to lower the sensing stripes slightly below the package edge. The width of the sensor board is 60.0mm. The total length of the sensor board was increased to 25cm. As the capacitive controllers are embedded inside the implemented package, they will be fully isolated from water and oil. The sensing strips will be immersed in the measured mixture. The microcontroller provides the sensor with the power and Ground lines and gets the measured thickness through the data lines of a 4-pin wire. Five items from the sensor design with identical dimensions were ordered from "PCBWay" company in China (https://www.pcbway.com/).

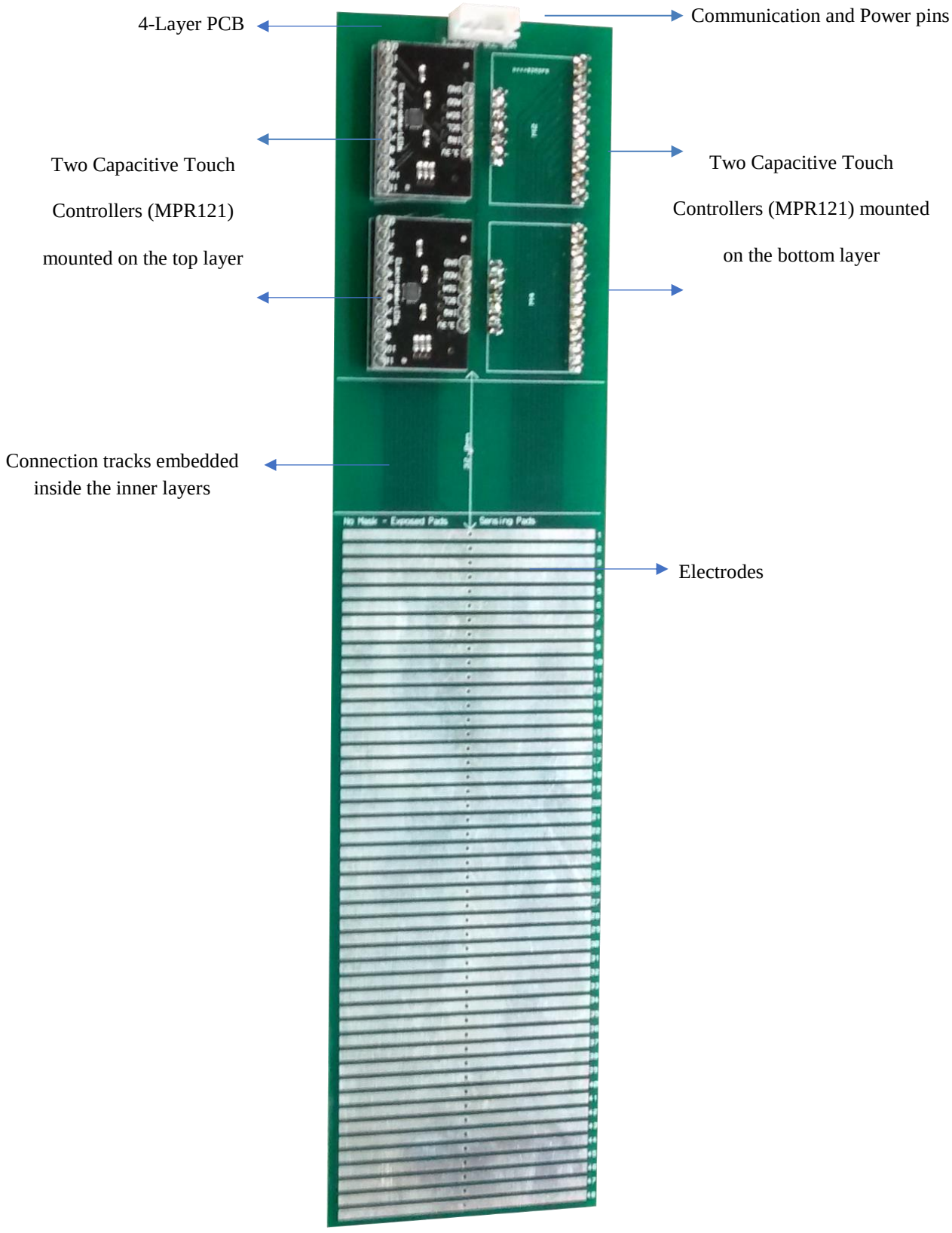

Figure 76: Optimized Sensor Prototype

6.5 Capacitive Sensor Tuning Experiments

As described before, the MPR121 controllers are used to measure the capacitance of each electrode in the sensing unit. Since the MPR121 modules use a DC charge technique to measure the capacitance, the current charge and the charge duration parameters need to be configured before operation. Based on this, tuning experiments were performed to find the best combination of the charge current and duration to be used in the final sensor design. The main aim of the tuning process is to select the combination (current/time) that maximizes the sensor sensitivity in terms of differentiation between air and oil. The voltage measurements used in the tuning experiments are taken at the output of the second filter of the MPR121 controller. The third filter output of the MPR121 controller is ignored in this project because it compares the raw voltage measurements with the baseline values used mainly for capacitive touch applications. The charge current may take a value between 1µA and 63µA, and the charge duration is set to value between 0.5µsec and 32µsec. During the experiments in which tuning was performed, the sensor was fixed on the indoor tank and immersed in a liquid that contains a layer of heavy oil (Fuel) with 20mm thickness (see Figure 77).

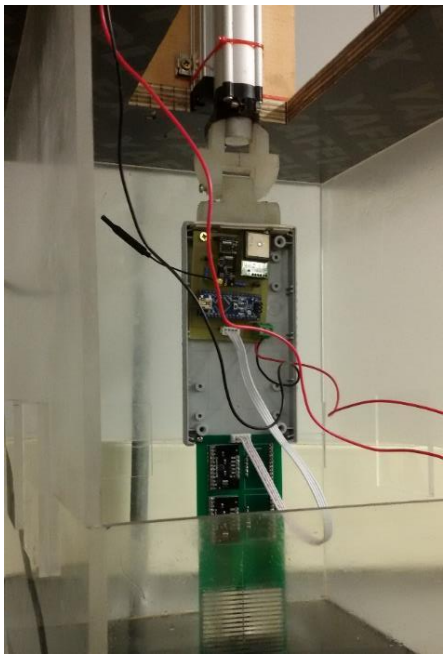

Figure 77: Experimental Installation - Tuning Experiments

6.5.1 *Current Tuning Experiments*

Current tuning was performed by setting the charge duration time to a fixed value of 0.5µsec and changing the charging current amount from 1µA to 63µA by an increment of 1µA. The experimental results are shown in Table 26 and the corresponding graph is shown in Figure 78. The vertical margins in Figure 78 indicate the interfaces between different groups of electrodes, distributed as follows:

- E1 to E25: Air
- E26: Air/Oil
- E27 to E33: Oil
- E34 to E40: Water, covered by a thin layer of oil (fouling effect)
- E41 to 48: Water.

Table 26: Current tuning experiment (Voltage (ADC) vs. Current(1-62µA))

	Current (µA)									
Electrode	1	8	16	24	32	40	48	54	62	
E1	4	52	105	159	212	265	319	358	408	Voltage (ADC)
E2	4	49	100	151	201	252	304	340	389	
E3	4	50	100	152	202	253	305	342	390	
E4	4	50	101	152	203	254	306	343	391	
E5	4	50	101	152	202	254	305	342	390	
E6	4	49	101	151	202	253	303	341	389	
E7	4	50	101	152	202	253	304	342	391	
E8	4	50	101	153	203	254	305	343	392	
E9	4	49	100	152	202	253	303	341	390	
E10	4	49	99	150	200	250	298	338	386	
E11	4	48	99	149	198	248	298	335	382	
E12	4	49	99	150	200	250	300	337	385	
E13	4	49	99	150	200	251	301	339	387	
E14	4	47	96	145	194	243	292	328	375	
E15	4	47	96	146	194	242	292	329	377	
E16	4	47	97	146	195	244	293	330	378	
E17	4	48	98	148	197	246	296	333	381	
E18	4	48	97	147	196	245	295	331	379	
E19	4	48	97	147	195	244	294	331	378	
E20	4	48	97	147	196	245	295	331	379	
E21	4	48	98	147	196	246	295	332	379	
E22	4	48	97	147	195	245	296	331	378	
E23	4	47	96	145	194	242	292	328	375	
E24	4	48	97	147	195	245	293	331	378	
E25	4	49	100	151	201	253	306	341	390	
E26	4	48	98	147	196	246	294	332	381	
E27	4	47	96	144	192	241	289	326	373	
E28	4	47	95	145	192	240	288	324	372	
E29	4	47	95	143	191	239	288	323	371	
E30	4	46	95	143	191	238	288	322	370	
E31	4	46	95	143	191	239	285	322	369	
E32	4	46	94	143	190	238	285	321	368	
E33	4	46	93	141	187	235	281	316	362	
E34	4	43	88	132	175	220	263	295	338	
E35	3	41	83	126	167	208	250	280	321	
E36	4	42	85	127	169	211	253	284	326	
E37	3	37	75	112	150	187	224	251	290	
E38	3	35	70	106	140	175	209	234	270	
E39	2	32	65	98	129	161	191	215	247	
E40	2	25	50	74	99	122	145	162	185	
E41	0	6	14	21	27	34	40	45	51	
E42	0	5	11	17	22	28	33	38	43	
E43	0	2	6	10	13	17	20	23	27	
E44	0	3	7	12	16	20	25	28	32	
E45	0	2	5	8	11	14	17	20	23	
E46	0	1	4	7	9	12	14	16	19	
E47	0	1	3	6	8	10	13	14	17	
E48	0	1	3	5	7	9	11	13	15	

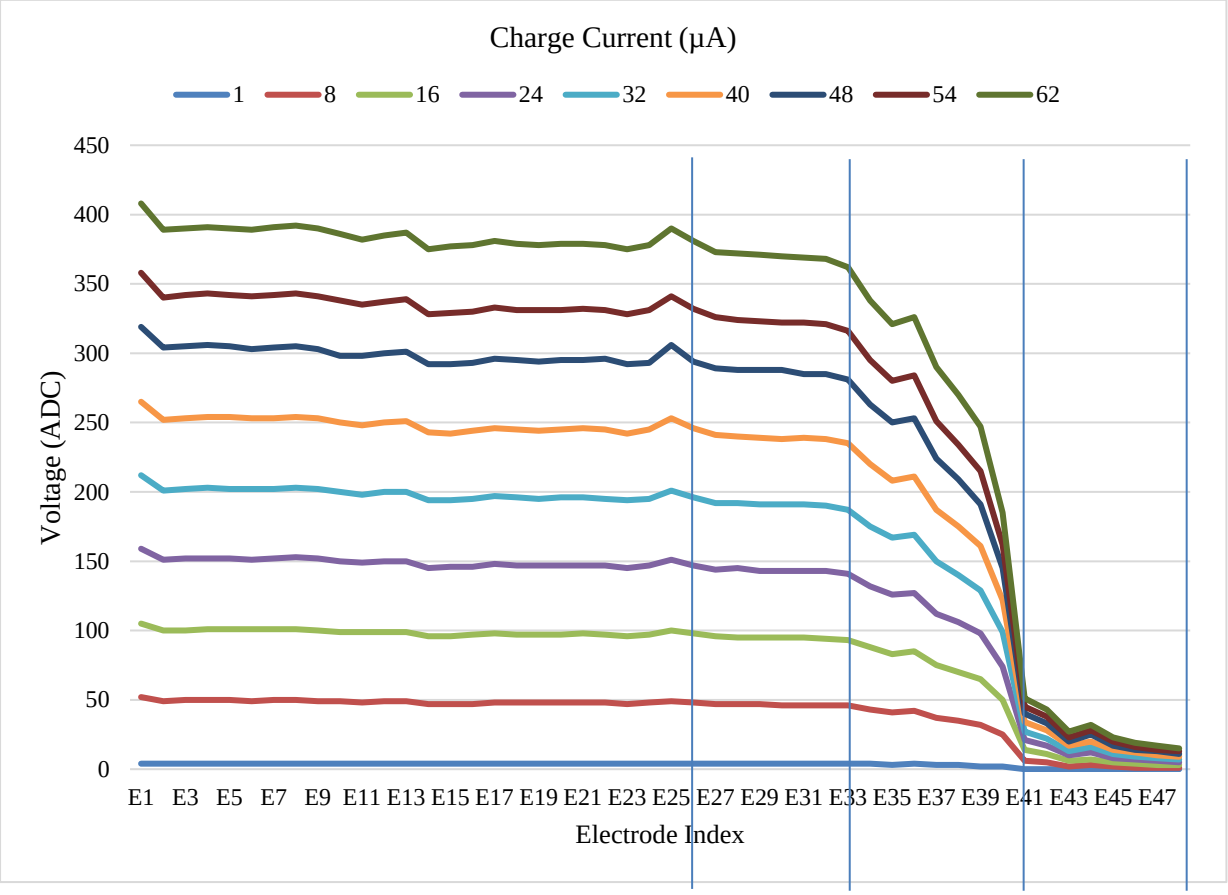

Figure 78: Current tuning – Graph (Voltage(ADC) vs. Current(µA))

Based on the tuning results, it was observed that the difference between the air and oil electrodes increase with the current in a directly proportional manner. Theoretically, this result is expected since the capacitance is directly related to the product of duration and current. However, to avoid the saturation of the 10-bit ADC contained in the MPR121, the suitable time duration parameter need to be assigned considering additional tuning experiments.

6.5.2 *Time Tuning Experiments*

In contrast to the current tuning experiments, in the time tuning experiments the current amount was set to a fixed value of 1µA and charging duration time was changed gradually from 0.5µsec to 32µsec. To do this, the CDT register included in the MPR121 controller was set with different values in order to set the needed charge time values (see Table 27). The state of the sensor electrodes is similar to the one presented in current tuning experiment section above. The experimental results are shown in Table 28 and the corresponding graph is shown in Figure 79.

Table 27: Hex values representing different charge time configurations

Charge Time (µs)	Hex Value
0.5	0x20
1	0x40
2	0x60
4	0x80

8	0xA0
16	0xC0
32	0xE0

Table 28: Time tuning experiment (Voltage(ADC) vs. Time (0.5-32 µs))

	Time (µs)							
Electrode	**0.5**	**1**	**2**	**4**	**8**	**16**	**32**	
E1	4	11	24	49	98	196	386	Voltage (ADC)
E2	4	10	22	47	93	186	368	
E3	4	11	23	46	93	187	372	
E4	4	11	23	47	94	188	373	
E5	4	11	23	47	93	187	370	
E6	4	11	23	47	93	186	368	
E7	4	10	23	47	93	186	371	
E8	4	11	23	47	94	189	373	
E9	4	10	23	47	94	188	371	
E10	4	10	22	47	92	184	366	
E11	4	10	22	46	91	182	364	
E12	5	11	23	47	93	185	366	
E13	4	10	22	54	98	190	374	
E14	4	10	22	45	92	183	364	
E15	4	10	22	46	91	184	365	
E16	4	10	22	46	92	184	368	
E17	4	10	22	46	93	187	369	
E18	4	10	22	46	93	186	368	
E19	4	10	22	46	92	185	368	
E20	4	10	22	46	93	186	368	
E21	4	10	22	46	93	186	371	
E22	4	10	22	45	92	186	369	
E23	4	10	22	45	92	184	365	
E24	4	10	23	46	93	185	368	
E25	4	10	23	47	96	191	378	
E26	4	10	22	46	93	185	371	
E27	4	10	22	44	90	180	359	
E28	4	10	21	45	90	180	357	
E29	4	10	21	44	89	179	359	
E30	4	10	21	44	90	179	356	
E31	4	10	21	44	89	180	354	
E32	4	10	21	43	89	178	354	
E33	4	10	21	43	86	172	346	
E34	2	6	14	29	59	119	237	
E35	2	4	10	22	44	87	169	
E36	2	5	12	25	51	102	202	
E37	1	4	9	20	41	82	163	
E38	1	4	9	19	39	78	153	
E39	1	3	8	17	34	70	139	
E40	0	0	1	2	3	5	9	
E41	0	0	0	0	1	2	3	
E42	0	0	0	0	1	2	4	
E43	0	0	0	0	0	1	2	
E44	0	0	0	0	0	1	2	
E45	0	0	0	0	0	0	1	

E46	0	0	0	0	0	0	0	
E47	0	0	0	0	0	0	0	
E48	0	0	0	0	0	0	0	

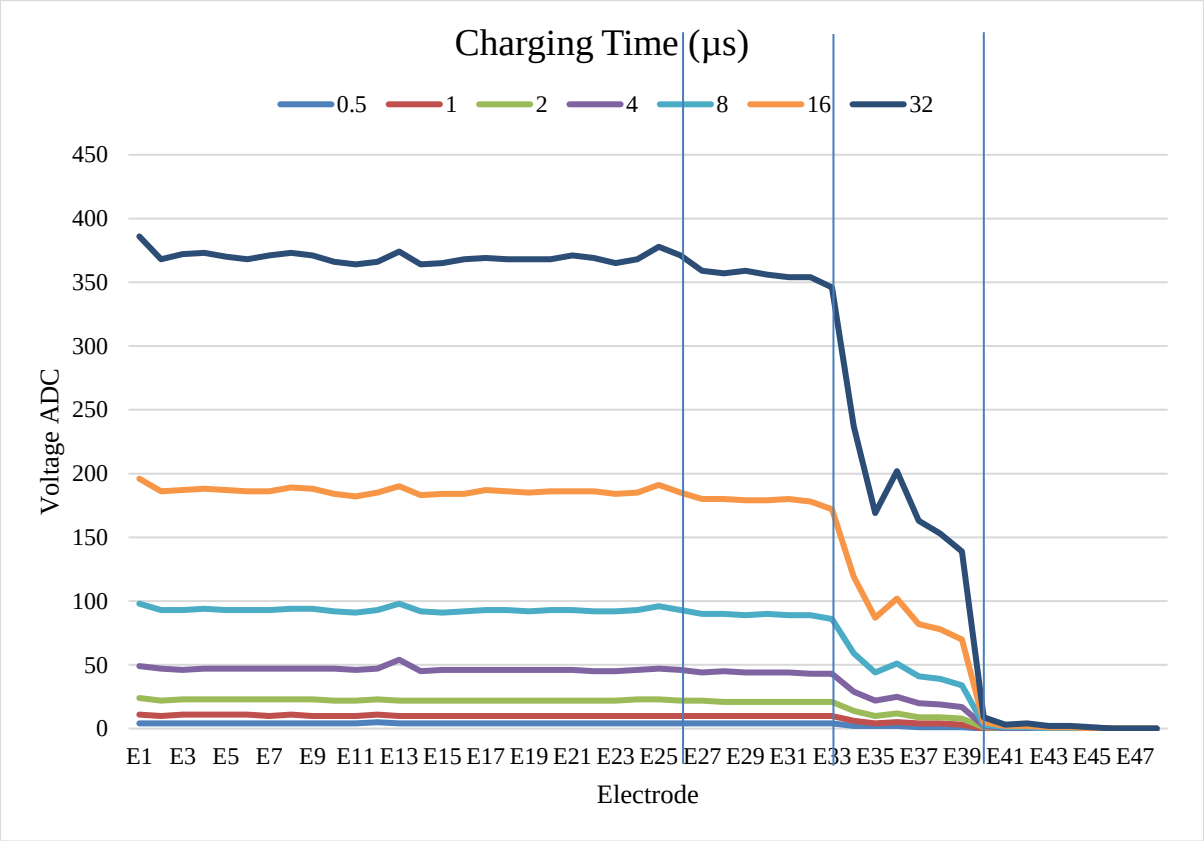

Figure 79: Time tuning - Graph (Voltage (ADC) vs. Time(0.5-32 µs))

The experimental results revealed an increase in the measured voltage in a directly proportional manner with time.

6.5.3 *Combined Tuning Experiments*

Based on the results of current and time tuning experiments, and to select the best combination of current and time in terms of sensitivity, two electrodes were selected as references from air and oil mediums. The absolute difference between the voltages measured by each of the two electrodes (E25 – E27) was used as the sensitivity factor to be monitored while testing all possible combinations. The difference between the two electrodes (delta) is calculated for all possible combinations and shown in Table 29 and the corresponding graph is shown in Figure 80.

Table 29: Combined tuning - Numerical results

	Time (µsec)						
Current (µA)	0.5	1	2	4	8	16	32
1	0.00	0.00	1.00	3.00	4.00	6.00	14.00
2	0.67	1.00	2.00	3.33	8.33	16.00	18.67
3	0.67	1.67	2.67	5.00	13.33	23.67	14.33
4	0.67	2.00	3.67	7.67	16.67	27.00	3.33
5	0.67	2.33	4.67	10.33	20.00	20.00	0.00

6	1.33	2.33	5.67	12.00	22.33	10.67	-0.33
7	1.67	2.33	7.00	9.33	26.67	3.00	0.00
8	2.00	2.33	7.33	11.33	28.33	1.00	0.00
9	2.00	3.33	8.00	12.00	30.00	0.67	0.00
10	2.33	4.00	7.00	16.33	24.67	0.33	0.00
11	2.67	5.33	10.33	15.67	18.33	0.33	0.33
12	3.00	5.67	11.33	18.33	8.33	0.00	0.33
13	3.00	6.67	13.33	19.67	3.00	0.00	0.00
14	3.33	6.33	14.00	22.33	0.33	-0.33	0.00
15	3.67	8.67	14.67	27.33	0.00	-0.33	0.33
16	4.00	9.00	15.33	30.00	0.00	0.00	0.00
17	4.00	10.00	14.33	33.67	-0.67	0.00	0.00
18	4.00	8.67	15.67	29.33	-0.33	0.00	-0.33
19	4.33	9.33	15.00	34.00	-0.33	-0.33	-0.33
20	4.67	9.67	16.00	31.33	-0.33	-0.33	-0.33
21	5.00	10.33	16.67	31.33	-0.67	0.33	-0.33
22	5.00	11.33	17.00	21.00	0.00	0.33	0.00
23	6.00	12.00	18.00	14.00	0.67	0.33	0.00
24	6.33	14.33	16.67	7.00	0.67	0.00	-0.33
25	6.33	14.00	25.00	4.67	0.33	-0.67	-0.33
26	5.67	13.67	26.67	3.33	0.00	-0.67	-0.33
27	5.67	12.33	29.67	2.67	0.33	-0.67	0.00
28	6.00	13.33	25.33	1.00	0.67	0.00	0.00
29	6.33	13.67	25.00	0.00	0.33	0.33	0.33
30	7.00	14.00	26.67	0.33	0.00	0.33	0.33
31	7.67	14.33	25.67	0.67	0.00	0.67	0.67
32	8.00	15.67	26.00	0.33	0.33	0.33	0.33
33	8.33	16.33	26.33	-0.67	0.33	0.00	0.00
34	8.67	16.33	27.00	0.00	-0.33	-0.33	-0.33
35	8.67	16.33	28.33	0.33	-0.67	-0.33	0.00
36	8.67	16.33	27.67	0.33	-1.00	0.00	0.67
37	8.67	16.33	30.00	0.33	-0.67	0.00	1.00
38	9.33	16.00	31.00	0.67	0.00	0.33	0.67
39	10.33	16.33	31.00	0.00	0.33	0.00	0.33
40	10.67	17.00	30.00	-0.67	0.33	0.33	0.00
41	11.00	18.33	29.00	-0.67	0.00	0.00	-0.33
42	10.67	17.67	27.00	0.33	0.00	0.33	-0.67
43	11.00	18.00	25.00	0.00	-0.33	0.00	-0.67
44	11.33	17.33	19.33	-0.33	-0.33	0.00	0.00
45	11.67	19.00	16.00	0.00	-0.67	0.00	0.00
46	12.00	19.33	12.67	0.33	-0.33	-0.33	0.00
47	11.67	20.00	11.00	1.00	-0.33	-0.33	-0.33
48	12.00	20.00	9.00	0.00	0.00	-0.67	0.00
49	12.33	21.33	7.00	-0.67	0.00	-0.67	-0.33
50	13.33	21.33	5.67	-1.00	-0.33	-1.00	-0.33
51	13.00	21.67	5.33	-0.67	-0.33	-0.67	-0.67
52	12.33	20.67	4.33	0.33	-0.33	0.00	-0.33
53	12.33	20.67	3.33	0.67	0.00	0.33	-0.33
54	13.00	21.67	2.33	1.33	0.00	0.67	0.00
55	14.00	23.67	2.00	0.33	0.00	0.33	0.33
56	14.00	29.00	1.67	0.33	0.00	0.33	0.33
57	14.00	29.67	1.67	-0.33	0.00	0.33	0.33

58	14.33	28.67	1.33	0.33	0.00	0.67	-0.33
59	14.67	25.00	1.00	0.33	0.33	1.00	-0.33
60	14.33	25.00	0.67	0.33	0.67	0.33	-0.67
61	14.67	25.00	0.33	0.33	0.67	0.00	-0.67
62	15.00	26.33	1.00	0.00	0.67	-0.33	-1.00
63	16.00	28.00	2.00	0.00	1.00	0.00	-1.00

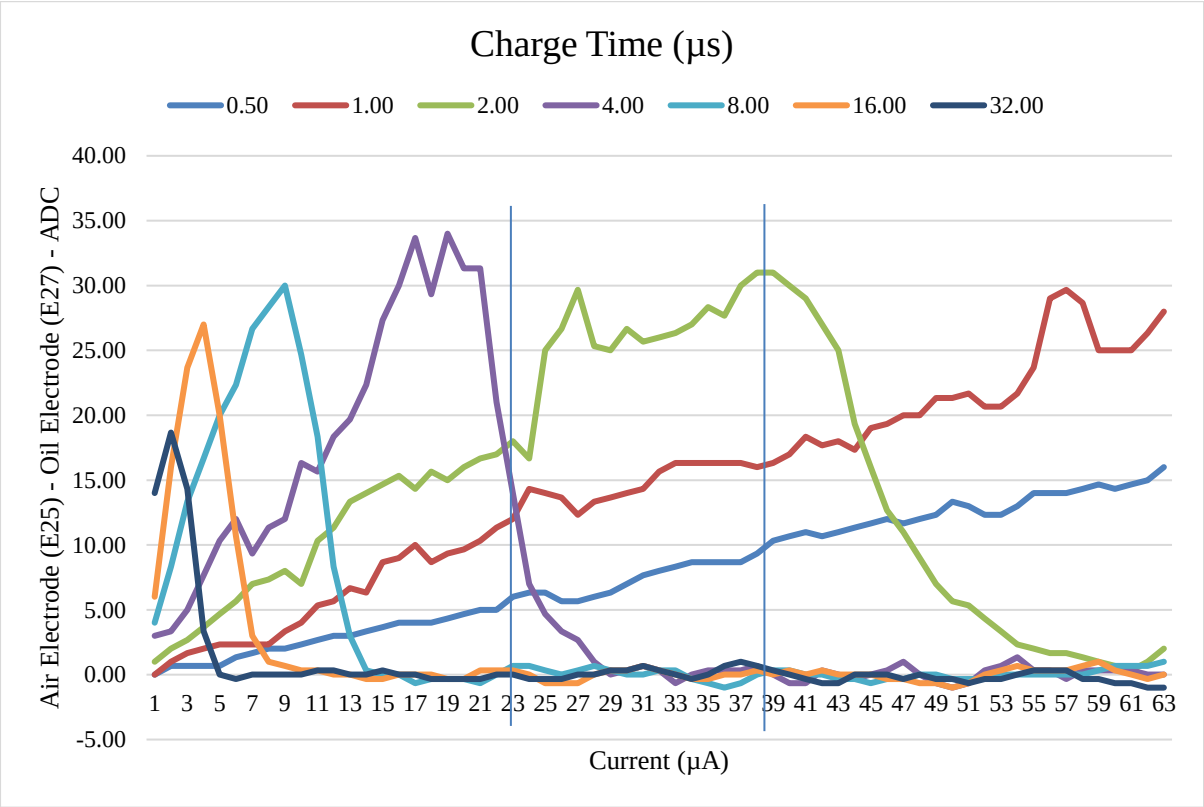

Figure 80: Combined Tuning Graph (delta vs time and current)

Based on the experimental results for the tuning, the combination of 2µsec charge duration time and 32µA of charge current amount was selected since it admitted the maximum difference factor between oil and air while attaining an acceptable power consumption and relatively high sampling rate before reaching the saturation level.

6.6 Capacitive Sensor Enhanced Multi-Layer Design with Pins

Based on all the past observations while working with the different sensor prototypes, we noticed that the major fouling effect is occurring while the sensor is moving down into the liquid. During the downward movement, a set of electrodes are entering the water carrying a thin layer of oil acting as a separator between the electrodes and water. Without having a sufficient amount of time to clean the oil layer from the sensor strips, the oil layer sticks to the sensor strips and highly affects the voltage measurements of the electrodes. In air, this problem is reduced since oil is pulled by gravity and tension with the surface oil downward. The vertical motion of the sensor was recorded several times to monitor the fouling effect. A snapshot from a video recording of the sensor vertical motion showing the fouling effect in water is shown in Figure 81. Note that this effect is minimal while working with low vicious oils.

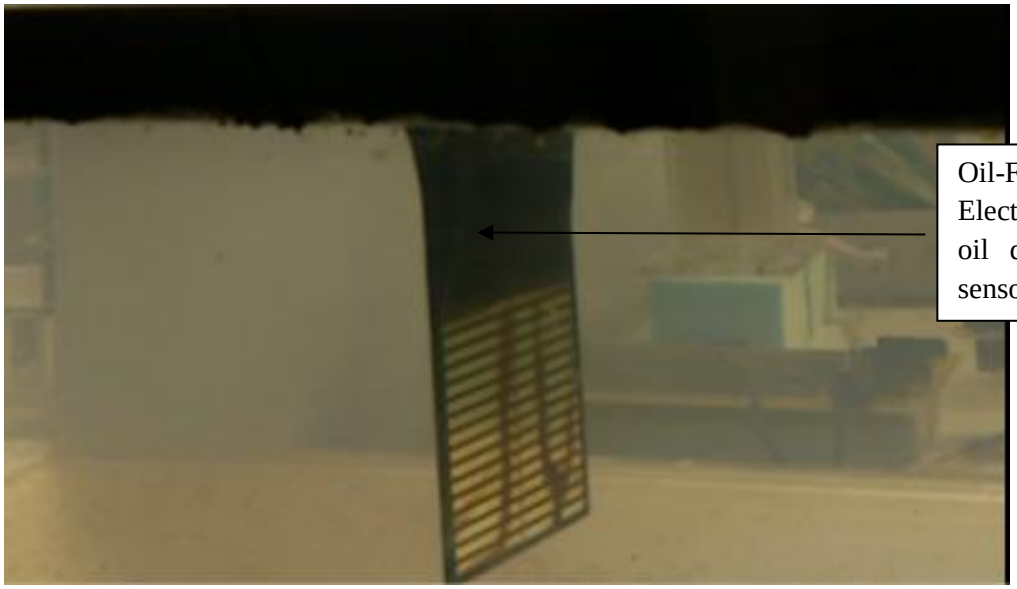

Figure 81: Photo showing oil-fouled electrodes

To reduce the fouling effect on the sensor, and to increase sensor sensitivity, a novel solution was developed, which consisted of adding pins normal to the plane of strips of the sensing array. In addition, sensing electrodes were added to the two sides of the sensor and the connection tracks were embedded in a 4-layer PCB design. The added pins play a major role in penetrating the thick oil layer covering the sensor strips. While the sensor is immersed in the examined liquid containing oil and water layers, the pins located in the water section of the sensor are short-circuited due to water conductivity. The upper pins located in the oil section are totally immersed in oil and thus the measured capacitances are related to the dielectric constant of the oil, which is different from that of water and air. Based on this enhanced design, the actual sensing method used by the sensor can be thought of as a mixture between capacitive sensing and conductive sensing techniques: short-circuiting is done in the water partition of the sensor, and capacitive sensing happens in the air and oil sections of the sensor due to their insulating properties. Figure 82 illustrates the enhanced sensor design showing the following parts: (a): Sensing electrodes, (b): Connection tracks, (c): Anti-fouling pins, and (d): PCB. The implemented sensor prototype with pins is shown in Figure 83.

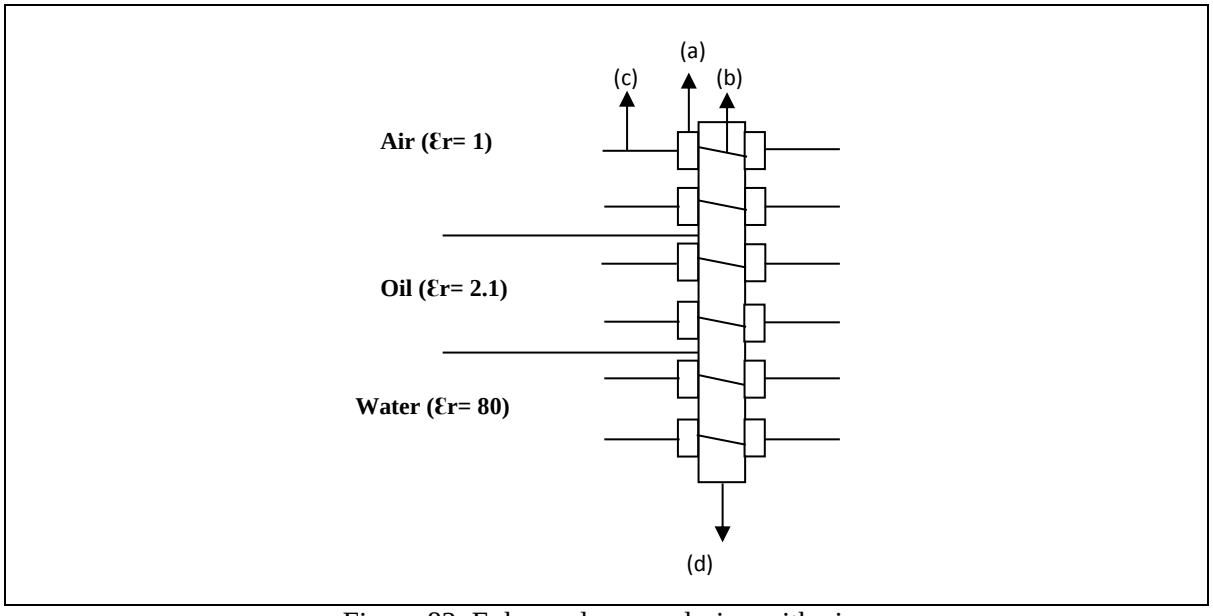

Figure 82: Enhanced sensor design with pins

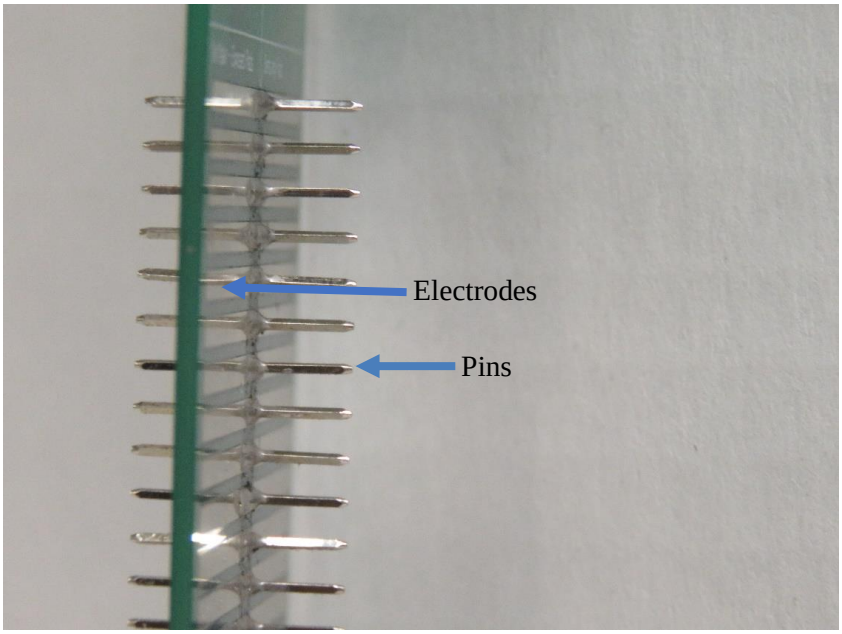

Figure 83: Enhanced sensor design with pins

To assess the performance of the added pins, two sensors with/without pins were tested. To compare the rate of change of the electrodes' measures in the two boards, the average voltage measured by the last three electrodes in each of the two sensors were recorded and plotted (Figure 84).

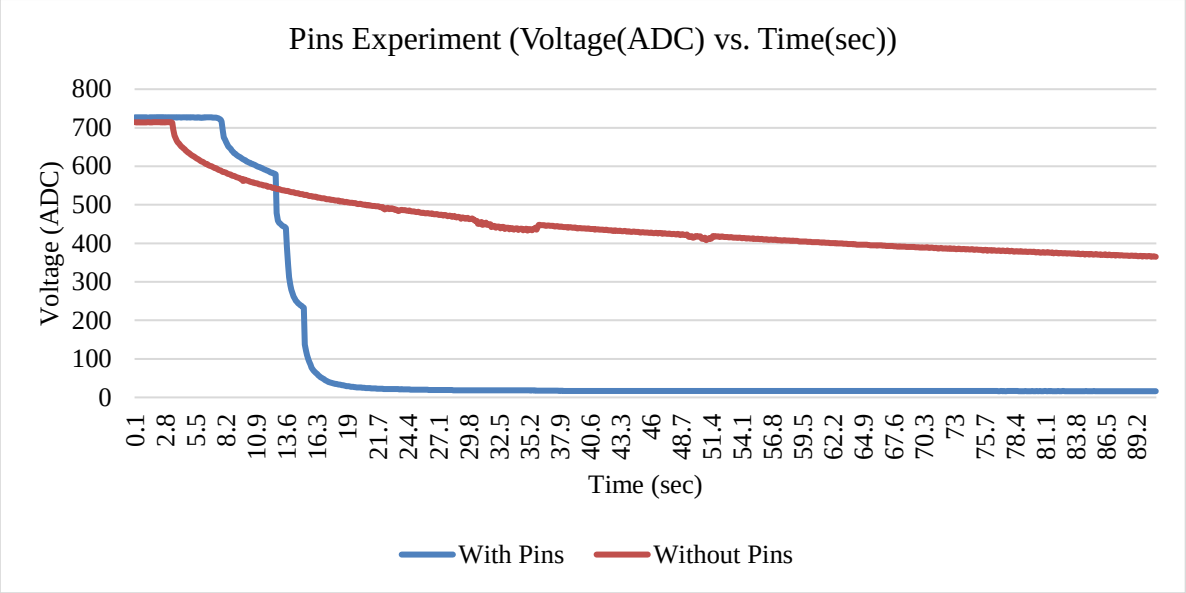

Figure 84: Pins Experiment (Voltage(ADC) vs. Time (sec))

The experimental results shown in Figure 84, show clearly that the voltage measured by sensor with installed pins made a severe drop in the voltage after being immersed in water. This is because the horizontal pins penetrated the oil-fouling layer covering the sensor body, as shown in Figure 85. In contrast, the voltage measured by the second sensor (exposed – no pins), showed a much slower voltage drop. This experiment demonstrated the ability of the horizontal pins to decrease the oil-fouling effect on the sensor performance by increasing the rate of change of the voltage measured by different electrodes when moving between oil and water mediums.

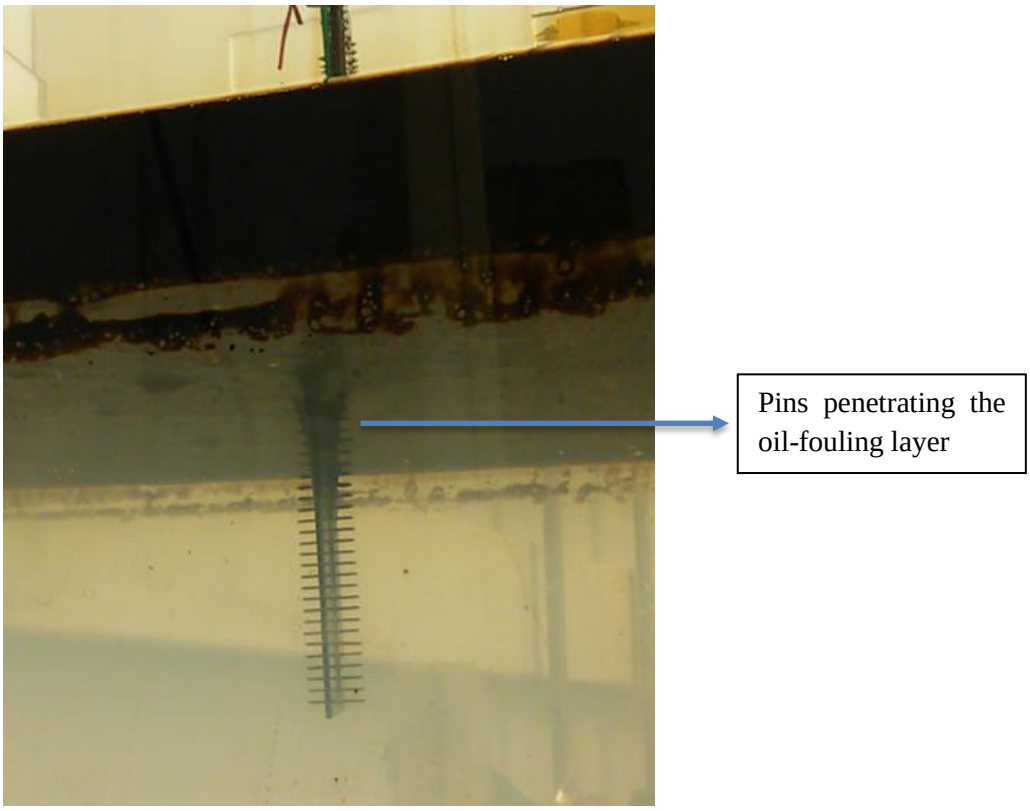

Figure 85: Photo showing pins penetrating the oil-fouling layer

Based on the experimental results, it was concluded that the added pins play a major role in penetrating the thick oil layer covering the sensor strips. While the sensor is immersed in the examined liquid containing oil and water layers, the pins located in the water section of the sensor are short-circuited due to water conductivity. The upper pins located in the oil section are totally immersed in oil and thus the measured capacitances are related to the dielectric constant of the oil, which is different from that of water and air. Based on this enhanced design, the actual sensing method used by the sensor can be thought of as a mixture between capacitive sensing and conductive sensing techniques: short-circuiting is done in the water partition of the sensor, and capacitive sensing happens in the air and oil sections of the sensor due to their insulating properties.

6.7 Additional Attempts to Reduce the Oil-fouling Effect

6.7.1 *Adding High-Frequency Vibration Mechanism to the Sensor*

Although the initial testing phase demonstrated the ability of the capacitive sensor in determining the medium it is in, one problem was observed with the oil soiling of the electrodes in the water under the oil slick level, while the sensor bobs up and down. Although the oil eventually slides off these strips and rises to the surface, the dynamics of the process is relatively slow for thick oils and risks affecting the determination of the oil/water interface. To deal with this issue, the initial sensor prototype was equipped with a vibrating module (Figure 86), to help expedite the removal of oil from fouled strips. To assess the effect of the vibrator module, two experiments were performed; before and after activating the vibrators. The same procedure was used in performing the two experiments. The sensor was immersed vertically from a fixed position into the water through a thin floating oil-layer. The voltage measured by the capacitive stripes was recorded. To interpret the experimental results, the voltage-drop of two stripes passing from the initial position (Air) to the end position (Water), while penetrating the oil layer, were recorded and compared. An instance of the experimental results is shown in Table 30, and the corresponding graphs, displaying the voltage drop of the two stripes with respect to time, are shown in Figure 87, and Figure 88.

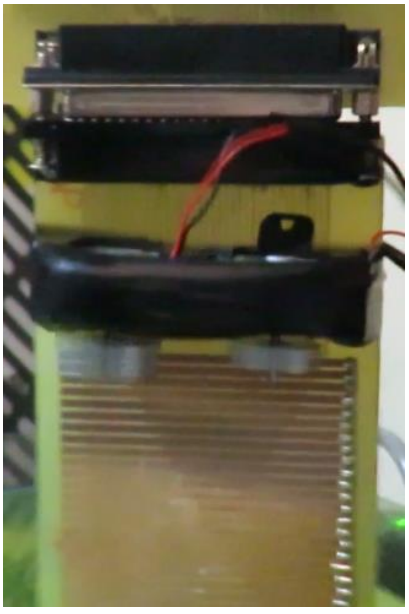

Figure 86: Capacitive sensor with vibration mechanism

Table 30: Vibrator Experiment (Voltage (ADC) vs. Time (sec))

Time (sec)	E1 (ADC)	E1 with vibrator (ADC)	E2 (ADC)	E2 with vibrator (ADC)
1	144	144	161	162
2	136	135	148	148
3	133	137	140	142
4	127	111	132	111
5	132	89	137	54
6	118	76	122	65
7	108	76	88	49
8	90	64	86	40
9	81	65	74	46
10	80	59	66	39
11	76	58	72	35
12	73	54	64	41
13	68	54	58	39
14	69	50	56	36
15	71	49	60	37
16	66	47	58	29
17	62	42	50	33
18	59	44	52	31
19	58	41	54	33
20	59	37	52	30
21	60	38	51	33
22	57	36	49	30
23	54	36	48	28
24	55	33	48	30
25	51	32	50	27
26	51	33	49	27
27	53	33	50	31
28	52	34	50	25
29	50	34	47	27
30	48	1	46	26

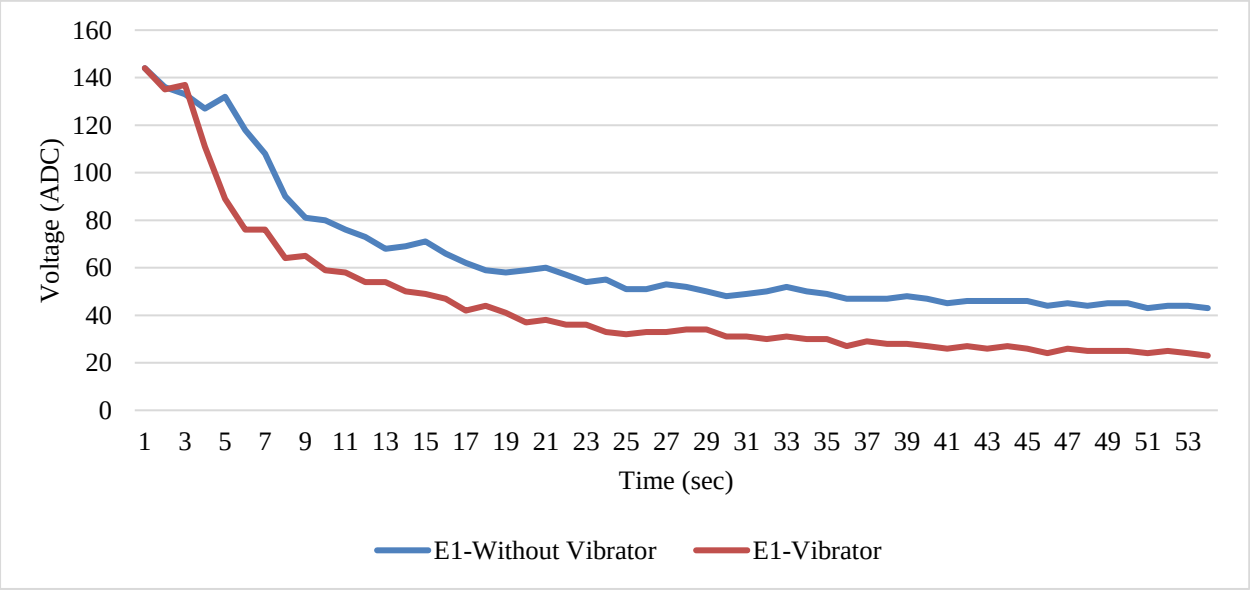

Figure 87: E1 voltage-drop, before & after installing the vibrator (Voltage (ADC) vs. Time (sec))

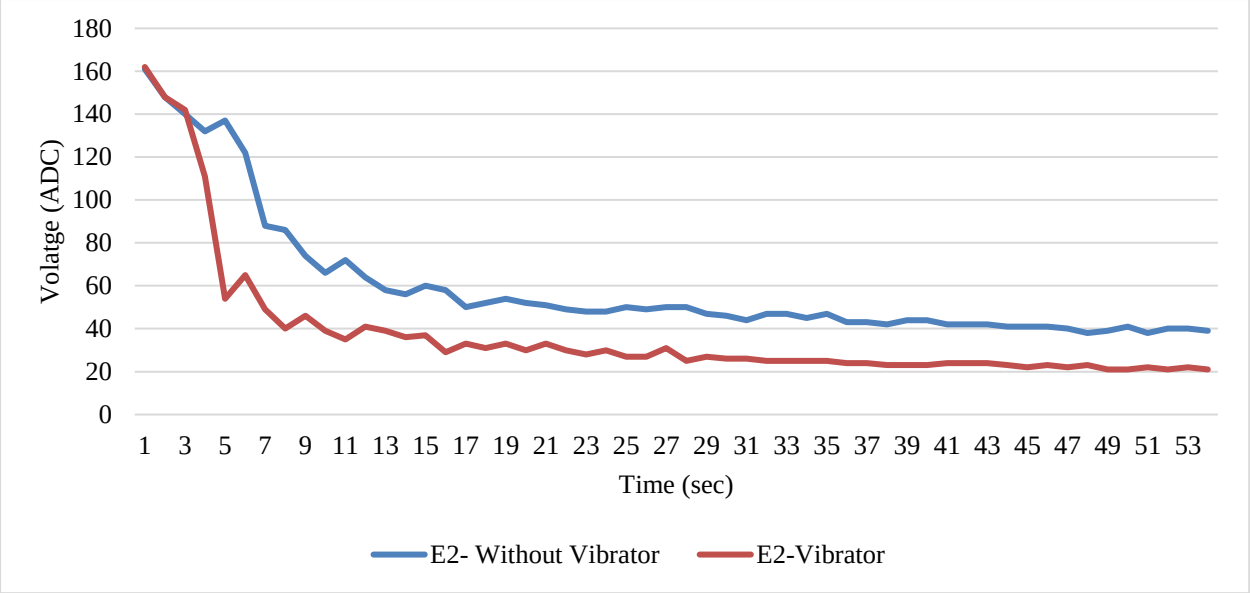

Figure 88: E2 voltage drop before & after installing the vibrator (Voltage (ADC) vs. Time (sec)

The experimental results revealed that the use of vibrators helped increase the rate of the voltage drop of the two electrodes. This result supports the idea of using a vibration system, since speeding up the voltage drop is essential in decreasing the oil-fouling effect.

6.7.2 *Preliminary Work Done on Coating with Nanoprotech Material*

In addition to the proposed vibrator above, several coating materials were tested. First, the initial sensor prototype was coated with a transparent electrical insulation material provided by Nanoprotech composed of the following ingredients: highly purified mineral oil, anticorrosion additives, antioxidant paraffinic, and naphthenic hydrocarbons. The recommended temperature for operation of this material is between -20ºC to +35ºC and it maintains its properties for a temperature range from -80ºC to +140ºC. Spraying the sensor cartridge with the Nanoprotech material (Figure 89) is done manually, and the board is kept to dry in air for around twenty-four hours before the first use. The excess of the spraying process (liquid residue) remaining on the sensor's body is removed, after the drying process is completed. The material is completely transparent, and covers all the components of the sensor including, the pins, stripes, and connection tracks.

To compare the sensor performance before and after applying the Nanoprotech coat, two identical experiments were performed. In the two experiments, the sensor was immersed into the oil/water mixture starting from a fixed position above the water surface. To monitor the effect of the material on the oil-fouling process, the voltage-drop of the last two electrodes (E35, and E36), while passing from the air layer until reaching the water layer, were recorded and analyzed. The experimental results of the immersing experiment are shown in Figure 90.

Figure 89: Nanoprotech – Liquid Electrical Insulation

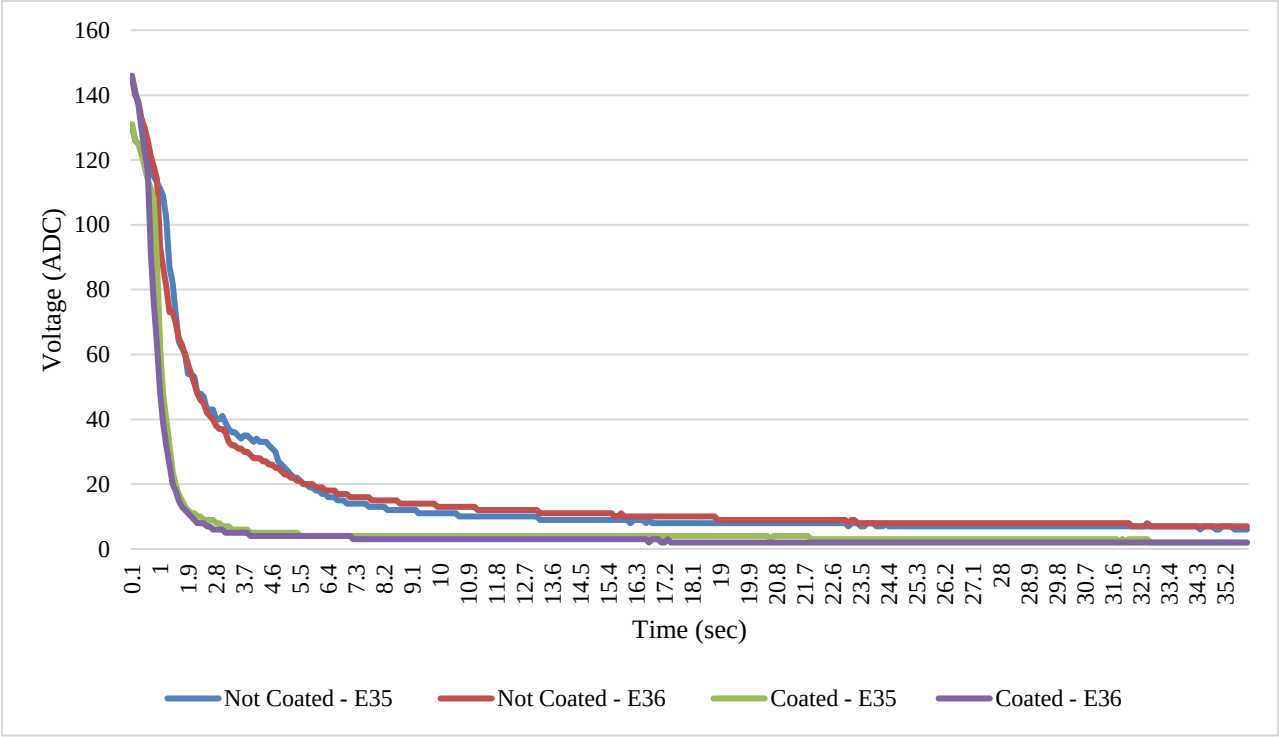

Figure 90: Nanoprotech Coating - Assessment Experiment (Voltage (ADC) vs. Time (sec)

As shown in Figure 90, the Nanoprotech coating increased the rate of drop of the measured voltage, while the sensor being immersed from oil to water. This can be deduced from the severe drop in E35 and E36 voltages, recorded immediately after the immersing started. In contrast, before applying the coat, the rate of change was much slower as shown in the graph. At the end of the experiment, when the voltages are almost stable, values measured by the coated sensor were lower than the values recorded by the non-coated sensor. For instance, the voltages measured by E35 and E36 before coating, were between seven and eight (ADC). After coating, the voltages of E35 and E36 decreased to around two and three (ADC). This decrease validates that the coating played a role in enhancing the conductivity of the electrodes. In addition to the oil-fouling assessment experiments, several experiments were done

to analyze the effect of the coating on the sensor response in all conditions (Air-Oil-Water). Voltages measured by electrodes when immersed in air and water, with and without coating, are shown in Table 31.

Table 31: Voltages in air & water, before and after coating with Nanoprotech insulation material

	Voltage (ADC)			
Electrode	**Air (Not Coated)**	**Air (Coated)**	**Water (Not Coated)**	**Water (Coated)**
E25	138	138.19	3	2
E26	132	132	3	2
E27	132	132.06	2.44	2
E28	134	134.78	2.46	2
E29	133	133.01	2.04	2
E30	134	134.99	2.06	2
E31	133.69	134	2.24	2
E32	135	135	2.02	2
E33	132.05	133	2	2
E34	131	131.99	2	2
E35	131	131.96	2.04	2
E36	148	148.99	2.91	2

As shown in Table 31, the voltages measured by the sensor electrodes are almost equal in Air and Water cases, before and after coating. However, it was noticed that in the water case, voltages measured after coating are slightly lower and more stable than the voltages measured before coating. This result, validates the conclusion made in the previous experiment, indicating that the Nanoprotech coating enhanced the conductivity of the stripes without impacting the sensor behavior in other cases (equal values in Air case). Also, to check the coating effect on oil detection, two identical experiments were performed before and after coating the sensor cartridge. Initially, the sensor was partially immersed in water, where the first five electrodes were surrounded by air. Then, oil was added to the water container from a fixed position above the water surface. The purpose of this method was to monitor the oil effect while contacting the electrodes directly without being altered by the sensor motion. Also, the main aim of this experiment is to check if the coating impacts the oil detection capability. The experimental results including the measured voltages (ADC) and the percent relative changes of the voltages, are shown in Table 32.

Table 32: Relative differences (%) in Oil case, before and after coating with Nanoprotech insulation

	Not Coated			Coated		
	Voltage (ADC)			Voltage (ADC)		
Electrode	**Air**	**Oil**	**Relative Difference (%)**	**Air**	**Oil**	**Relative Difference (%)**
E1	167	160	4.19	168	161	4.17
E2	157	149	5.10	158	150	5.06
E3	156	148	5.13	157	149	5.10
E4	159	150	5.66	160	151	5.63
E5	158	149	5.70	159	149	6.29

The experimental results revealed that the percentage relative changes, due to the oil contact, were similar in both versions (4-6%); coated and non-coated. Thus, it can be concluded, that the coating didn't have any negative effect on the oil detection ability.

The experimental results presented above showed that the Nanoprotech coating helped in reducing the oil-fouling process, while not impacting the air and oil detection capabilities. Also, the use of the Nanoprotech material was observed visually to decrease the wetness of the sensor board while being immersed in water. However, several questions were raised regarding the actual composition of this material, and the reason behind enhancing the conductivity of the electrodes. Clarification of the actual role of the material is needed, based on the fact that this material's primary role is to insulate electrical parts in water and not to enhance the conductivity. However, further investigation is needed in the future work.

6.7.3 *Preliminary Work Done on Coating with Ultra-ever dry Material*

While attempting to reduce oil-foiling of the strips, Ultra-Ever-Dry produced by Ultratech was tested. First, after spraying the sensor with the two product components (base coat and top coat), the sensor was immersed and removed several times in a set of water/oil mixtures, including light, medium and heavy (Fuel) oil samples. As a result, in most of the trials, it was observed that the oil was falling-off immediately after removing the sensor from the examined liquid. However, in some cases, especially when dealing with heavy oil types (Fuel), the material performance was affected.

To analyze the effect more accurately, several experiments were performed. The experiments were done using the same sensor board, before and after applying the coating. The ultra-ever dry material is applied by manual spraying in two stages. In the first stage, the sensor cartridge is sprayed by the bottom coat material. Then, the board is kept drying in air for around 15 minutes. In the second stage, the top coat material is applied to the board by manual spraying. After applying the top coat, the sensor is kept drying in air for around twenty-four hours, before the first use. The spraying process was performed under a specialized fume hood. The fume hood is a self-contained, filtered laboratory enclosure, used to remove hazardous vapors and particles resulting from the spraying process. It is important to note that the spraying was done based on regular motion iterations, to have a homogenous and equally distributed amount of coating material on the sensor surfaces. However, since the spraying was done manually (by hand), some differences in the coating distribution was observed on the sensor surfaces. In the first experiment, the voltages measured by the sensor electrodes were recorded while the sensor was set to a fixed position in air. To assess the impact of this material on the sensor, voltage values obtained after applying the coating are compared to the corresponding values stored before applying the coating. A sample of the experimental results, showing the average of a set of voltages measured by the first twelve activated electrodes, are shown in Table 33, and the corresponding graph is shown in Figure 91.

Table 33: Relative differences (%) and Voltages (ADC), before and after coating with Ultra-ever dry

Electrode	Non-coated (Avg. Voltage (ADC))	Coated (Avg. Voltage (ADC))	Relative Differences (%)
E1	171.00	167.83	1.85
E2	161.79	158.11	2.27
E3	160.05	156.03	2.51
E4	166.00	156.00	6.02

E5	163.12	155.31	4.79
E6	167.02	153.86	7.88
E7	164.48	158.46	3.66
E8	168.98	162.40	3.89
E9	162.60	158.03	2.81
E10	163.72	157.91	3.55
E11	157.72	153.17	2.88
E12	160.93	156.00	3.06

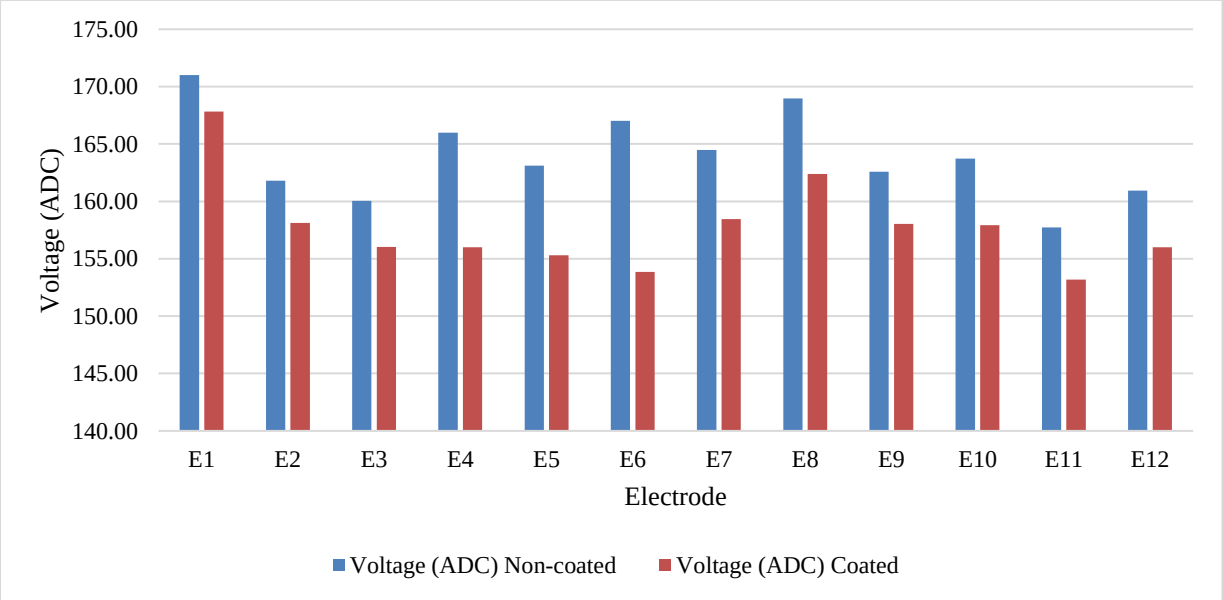

Figure 91: Voltages (ADC) measured before and after coating with Ultra-ever dry (Air) - Graph

The experimental results revealed that the voltages measured by the capacitive stripes in air decreased after applying Ultra-ever dry material. Since the voltage is inversely related to the capacitance, it was concluded that the additional coating layer increased the base capacitance of the stripes.

To assess the voltage-drop numerically, the percent relative differences are calculated and shown in Table 33. The percentage differences varied among the stripes, ranging between 1.85% and 7.88%. This variation is due to the different distribution of the coating material on the sensor surface. The average percentage difference was around 3.77%.

To monitor the effect of the coating material in the oil and water cases, another experiment was performed. In this experiment, the sensor was partially immersed in an oil/water mixture. Before applying the coat, the thirty-six activated electrodes were distributed in the oil/water mixture as follows:

- E1 to E16: Air
- E17 to E21: Oil
- E22 to E36: Water

The voltages measured for the non-coated sensor, before and after immersing in the examined liquid, in addition to the percentage relative differences, are shown in Table 34.

Table 34: Non-coated - Voltage (ADC) & R.D (%). - Partially immersed in oil/water mixture

		Voltage (ADC)		
Case	**Electrode**	**Calibration (Air)**	**Partially immersed in oil/water mixture**	**Relative Difference (%)**
Air	**E1**	171.00	172.00	0.58
	E2	161.79	162.01	0.14
	E3	160.05	160.99	0.59
	E4	166.00	165.13	0.53
	E5	163.12	162.97	0.09
	E6	167.02	166.06	0.58
	E7	164.48	164.94	0.29
	E8	168.98	170.29	0.78
	E9	162.60	164.00	0.86
	E10	163.72	163.43	0.18
	E11	157.72	159.03	0.83
	E12	160.93	160.94	0.01
	E13	148.09	147.86	0.15
	E14	149.65	149.19	0.30
	E15	150.06	149.83	0.15
	E16	154.02	153.03	0.65
Oil	**E17**	152.98	147.97	**3.27**
	E18	155.90	148.99	**4.44**
	E19	154.02	147.88	**3.99**
	E20	157.00	149.01	**5.09**
	E21	153.68	141.99	**7.61**
Water	**E22**	154.00	66.82	56.61
	E23	149.01	48.33	67.56
	E24	151.04	48.15	68.12
	E25	138.94	74.94	46.06
	E26	139.61	45.64	67.31
	E27	140.18	35.21	74.88
	E28	142.98	18.07	87.36
	E29	140.99	21.00	85.11
	E30	143.09	36.58	74.43
	E31	141.99	77.72	45.26
	E32	143.51	17.97	87.48
	E33	140.00	23.29	83.36
	E34	139.43	17.49	87.46
	E35	138.99	12.44	91.05
	E36	153.23	32.11	79.04

The same experiment was repeated after coating the sensor with the ultra-ever dry material. The voltages (ADC) measured by all electrodes, in addition to percentage relative differences are shown in Table 35.

Table 35: Coated (Ultra-ever dry) - Voltage (ADC) & R.D (%). - Partially immersed in oil/water

Case	Electrode	Calibration (Air)	Partially immersed in oil/water mixture	Relative Difference (%)
Air	**E1**	167.83	166.95	0.52
	E2	158.11	157.97	0.09
	E3	156.03	156.00	0.02
	E4	156.00	157.04	0.66
	E5	155.31	156.60	0.82
	E6	153.86	155.15	0.84
	E7	158.46	157.01	0.92
	E8	162.40	163.33	0.57
	E9	158.03	157.81	0.14
	E10	157.91	156.99	0.59
	E11	153.17	152.11	0.70
Oil	**E12**	**156.00**	**153.99**	**1.29**
	E13	**143.23**	**140.06**	**2.21**
	E14	**144.69**	**139.30**	**3.72**
	E15	**144.20**	**139.78**	**3.07**
	E16	**150.06**	**144.17**	**3.93**
Water	**E17**	147.03	126.89	13.70
	E18	144.94	107.01	26.17
	E19	127.00	91.21	28.19
	E20	127.97	92.70	27.57
	E21	147.00	103.11	29.86
	E22	147.09	103.90	29.36
	E23	144.03	103.19	28.36
	E24	146.97	103.74	29.41
	E25	130.43	95.82	26.53
	E26	131.94	95.25	27.81
	E27	137.00	97.62	28.75
	E28	154.00	136.27	11.51
	E29	137.14	95.97	30.03
	E30	133.03	97.48	26.72
	E31	137.00	95.62	30.20
	E32	134.00	94.69	29.34
	E33	135.03	89.08	34.03
	E34	135.71	83.13	38.75
	E35	136.20	78.64	42.27
	E36	152.29	90.60	40.51

To assess the effect of the coating material on each of the three cases (Air/Oil/Water), the average value of the percent relative differences calculated for each case in the two previous experiment (Table 34, and Table 35) are shown in Table 36, and the corresponding graph is shown in Figure 92.

Table 36: Comparison between relative differences in Air/Oil/Water cases before and after coating

	Average Percentage Difference (%)	
	Non-Coated	**Coated (Ultra-Ever Dry)**
Air	0.42	0.53
Oil	4.88	2.84
Water	73.41	28.95

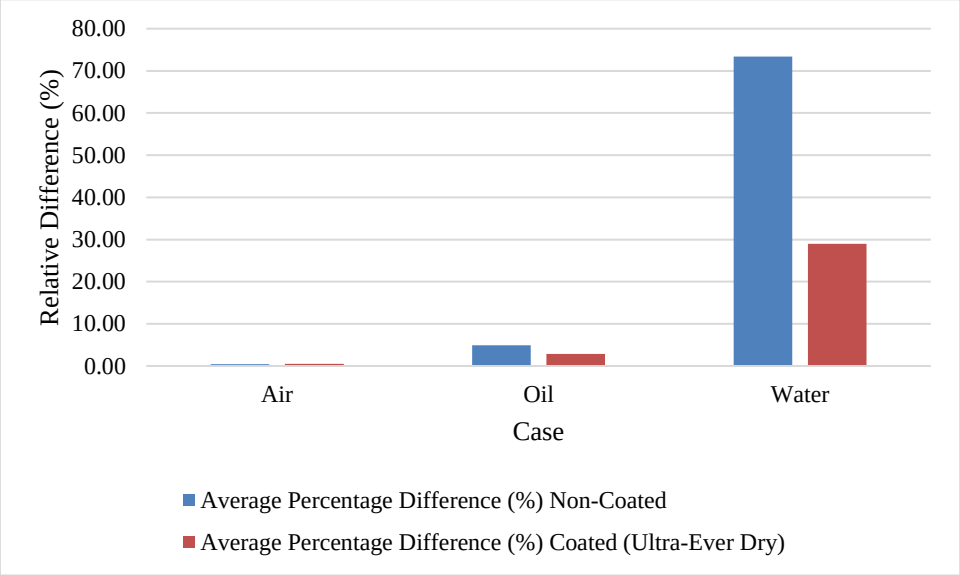

Figure 92: Comparison between relative differences in Air/Oil/Water cases before and after coating

This experiment revealed that after applying the Ultra-ever dry coating, the relative percentage change in the water was reduced. Theoretically, this result was expected since the coating plays a major role in isolating the electrodes from water. Without coating, the electrodes were short-circuited due to the water conductivity, thus, the potential difference was dropped to around zero. In contrast, after the coating was applied, an additional layer (dielectric) was added to the electrodes, increasing the base capacitance, and decreasing the sensor sensitivity. Also, a decrease of the relative change of the electrodes immersed in oil was observed.

Several important notes were recorded while working with the ultra-ever dry material. First, it was noted that the manual spraying technique (by hand) resulted in an irregular distribution of the coating thickness on the sensor surfaces. Thus, a non-uniform coating layer was observed, impacting the base capacitance of the electrodes inconsistently. Based on this, a more consistent method is recommended to be used during the coating process. Also, it was observed that the addition of the Ultra-ever dry coating layer, decreased the sensitivity of the sensor. This conclusion was made after observing the decrease in the percentage relative difference calculated for each of the electrodes while being immersed in water and oil. Further investigation regarding the performance of this coating and super-hydrophobic materials will be done in future work.

As a conclusion, despite the fact that adding the vibration mechanism decreased the oil-fouling effect, it was not considered in the final sensor design since it has a major disadvantage related to the added power consumption and the complexity introduced to the packaging. Also, the super-hydrophobic

(Ultra-ever dry) coating was not considered in the final sensor design since it decreased the sensor sensitivity. Regarding the Nanoprotech coating (Nano electrical insulation), despite the fact that it helped decrease the oil-fouling effect, it was not considered since further investigation is needed to validate the initial observations recorded during the initial experiments. At the end, the best solution to handle oil-fouling was found to be the horizontal pins introduced in the previous section, where no power consumption was added, and no major changes were applied to the sensor design and packaging. It is important to note that chemical coatings will be studied in more details in the future development.

6.8 Battery Testing

Several experiments were performed to test the performance of the selected batteries. The following presented experiment was implemented to assess the selected 9V battery pack composed of 6 AA 1.5V batteries (single use – Energizer) connected in series. The battery pack used is shown in Figure 93, and the experimental parameters are shown in the list below:

- Baud Rate: 115200
- Number of MPR121 controllers: 4
- Charge Current: 32 µA
- Charge duration: 2 µsec
- Sampling time: 1 message every 2 seconds
- Data: One Message containing all voltage readings (48) in String format delimited by ‘,’.
  Message Example:
  "786,750,754,756,755,753,755,757,753,745,736,728,729,699,695,698,702,699,694,680,625,609,605,599,580,543,557,561,556,545,517,465,326,107,87,115,110,108,104,107,103,105,96,88,75,69,56,43"
- Wireless Module Status: ON.
- Experiment Start Time: 10:00 PM
- Experiment Date: 2/10/2017
- Sensor installation: Small tank (Lab). E1 – E13 (Air), E13-E22(Oil), E23-E48 (Water)
- Power Source: 9V made of 6 batteries energizer single-use (1.5V) connected in series.

Figure 93: 9V Battery Pack - AA Batteries

The experiment lasted around 4 hours and the results showed that the selected batteries remained in an acceptable condition providing the circuit with the needed voltage during the entire experiment duration. For more accurate monitoring of the battery voltage value with respect to time, the input voltage was logged every 30 minutes. The numerical voltage values are shown in Table 37 and the corresponding graph is shown in Figure 94.

Table 37: Voltage vs. Time - Battery Experiment

Time (HR: MIN)	**Voltage (V)**
10:05	8.84
10:35	8.47
11:00	8.33
11:30	8.19
12:02	8.07
12:30	7.99
13:07	7.92
13:34	7.86
14:05	7.80
14:36	7.74

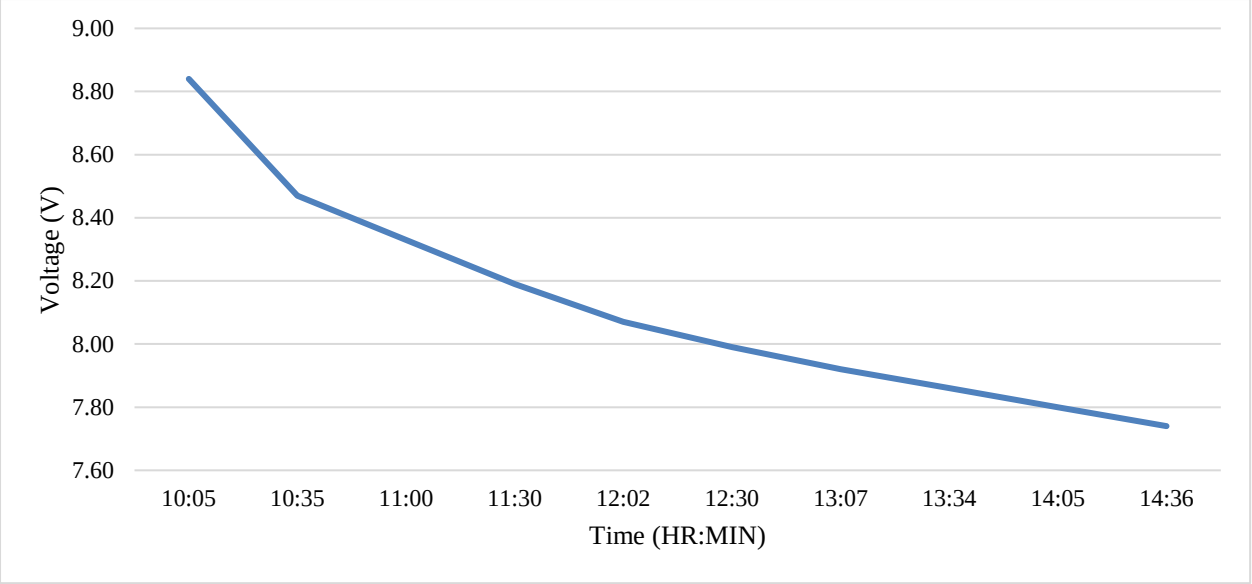

Figure 94: Voltage vs. Time (Graph) - Battery Experiment

As a conclusion, since the batteries remained in good condition for almost 4:30 hours of continuous transmission, with a relatively high baud rate and no heating or disconnection in transmission was recorded, the 9V battery pack was selected for the beta design of the sensor. To increase the battery lifetime, NiMh AA batteries could be used without performing any modifications to the battery pack. Example of the rechargeable NiMh batteries with a capacity of 2500mAh is shown in Figure 95.

Figure 95: AA Rechargeable Batteries (2500 mAh)

6.9 Wireless Transmission Testing

To validate the range of the selected wireless modules, an experiment was performed on the third of October 2017, where all the sensor components were activated and embedded inside the alfa version of the proposed capacitive instrument (version 1). The RF transmitter was activated for the duration of the entire experiment. A message of raw voltage values measured by all electrodes was sent every two seconds. The base station (Laptop + RF Receiver) was placed at a fixed position and the sensor was moved around up to a distance of 200 meters from the base station: no disconnection or delays were recorded. The result of this experiment was considered acceptable, since the signal transmitted by the RF module was received for a distance exceeding the target range of the eventual application.

6.10 Enhanced Algorithms Based on Sensor Movement Tracking

6.10.1 *Movement Tracking in Dynamic Liquid Conditions*

As described before, the aim of the algorithm enhancement is to detect the best set of measurements where we need to apply the oil thickness analysis. This approach is based on detecting the dynamic water conditions and tracking the direction of the wave interacting with the sensor body (upward/downward). When the sensor is moving downward, most of the calculated relative differences increase since more electrodes will be immersed in the examined liquid. Electrodes moving from oil to water, and electrodes moving from air to oil will have more relative differences from baseline calibration values taken in air. In contrast, when the sensor is moving upward, the relative differences will decrease. The average relative difference of all electrodes is calculated at each measurement cycle and used as an indicator for the sensor movement. For the static case, since no movement occurs, the average should be changing within the random error interval with respect to time. In dynamic cases, the average will be increasing or decreasing based on the direction of the sensor movement or waves. If the sensor is fixed in place, the average value is used to track the motion of the liquid in contact with the sensor. To demonstrate this capability, the relative differences of all electrodes at each measurement cycle are stored in a 2D array and converted to a grayscale image, shown in Figure 96, where the y-axis corresponds to the electrode index and x-axis corresponds to time. A clear variation of the color intensity in the image is observed with respect to the vertical movement of the sensor in waves. Brighter intensities reflect an increase in the relative difference due to water contact. According to this graph, the amplitude and frequency of the waves can be determined, since the sampling time and the geometrical sensor properties are known.

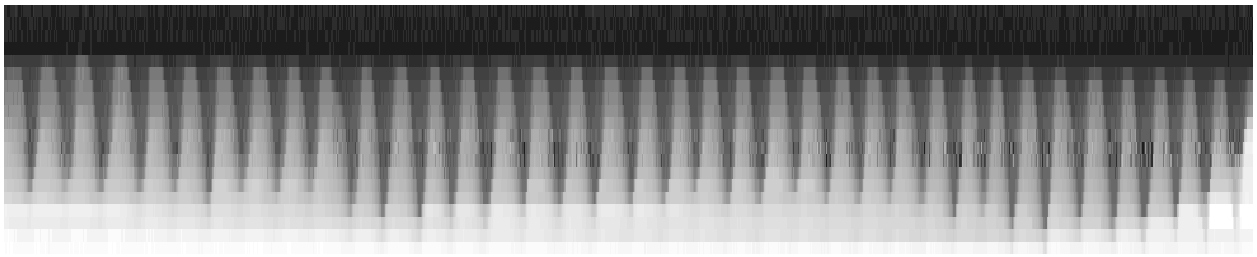

Figure 96: Relative differences converted to grey scale image

To detect the set of measurements taken at the highest point of the sensor movement, the minimum relative difference presented by each electrode during a certain interval of time is selected. In contrast, to detect the measurements taken at the lowest point, maximum relative differences are selected.

6.10.2 *Overall Thickness Measurement Algorithm*

The measurement algorithm aims to find the indices of the electrodes located at interfaces between materials with different dielectric constants. In this application, and based on the sensor geometrical properties, electrodes located at the water/oil interface and the air/oil interface are detected and used to calculate the oil thickness in both static and dynamic conditions. The algorithm has a low dependence on the direct numerical values of the voltage measurements and can work on a device with a limited amount of computational resources.

The system starts by measuring the voltage values of all electrodes in a sequential manner, using the capacitive touch controllers, indexed by the multiplexers. The microcontroller reads the digital voltage values acquired from each electrode and applies several layers of digital filtering to enhance the stability

of the measurements. To normalize the acquired voltage values, relative percentage changes from baseline calibration values are calculated for each electrode. The calibration values are taken when the sensor is completely dry and placed in open air for a sufficient duration of time. The calculated relative percentage changes are used by the algorithm to decide on the state (air/oil/water) of each electrode. Since each ratio is assigned to its electrode index and knowing the geometrical dimensions of the sensor (separation between electrodes and stripe thickness), the actual thickness of oil can be calculated. For instance, the sensor was set to a fixed position in the oil/water mixture, and the relative algorithm based on finding the maximum gradients were tested. The relative differences and the detected Air/Oil and Oil/Water interfaces displayed at the MatLab GUI are shown in Figure 97, where the upper figure shows the relative differences on y-axis and the electrode index on the x-axis. The lower figure shows a one-dimensional array where the electrode index is on the x-axis and the binary value (1=interface, 0=non-interface) used as an interface indicator is set on the y-axis. Several oil thicknesses were recorded and statistical analysis for the obtained measurements are shown in Table 38.

Table 38: Statistical analysis of thickness measured using relative algorithm (static)

Average Thickness (mm)	20.13
Standard Deviation	0.70
Sample Size	496
Confidence Coefficient	1.96
Margin of Error	0.06
Upper Bound	20.19
Lower Bound	20.07
MAX	26
MIN	17

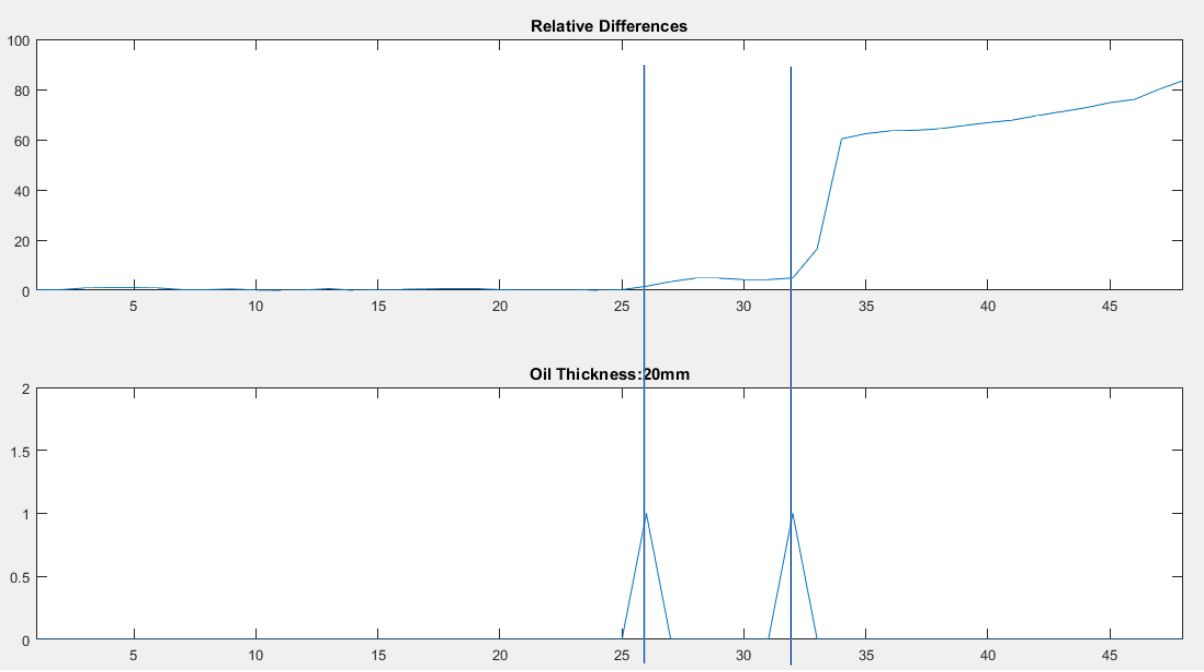

Figure 97: MatLab GUI showing detected interfaces

To handle dynamic cases where the sensor rises or drops relative to the oil layer (due to lift or dip of the vessel, or due to waves) a two-step algorithm is used. The first step is to store a set sensor voltage measurement taken during a specific interval of time. After that, the direction of sensor movement is detected for each of the stored rows. This is done by monitoring the sense of the average value in each measure (increasing/decreasing). Then, two approaches were introduced, the "Highest Point Algorithm" and the "Corrected Lowest Point Algorithm".

For light oil types (ex. Diesel), the "Highest Point Algorithm" is applied; the approach consists of measuring the thickness using the set of values taken when the sensor reaches its highest points (crests) through the stored array. This is done since with light oil fouled stripes that moved from oil to air will clean relatively fast and stripes that are fouled at the bottom side are minimal (if any) since at the highest point most of the fouled striped went back into the oil. This algorithm is used also in static cases since the highest points will be regular points in the array.

The second approach is more suited for the heavy oil types (ex. Hydrocal, Calsol) where the negative impact of fouling is more effective. This approach is called the "Corrected Lowest Point Algorithm". It works by detecting the measurements taken when the sensor reaches the lowest points in the stored array (minimums) and applying a correction method on them to remove the number of fouled electrodes. By using time interpolation, the correction mechanism works by finding the number of fouled electrodes and subtracting it from the detected oil interval before calculating the actual thickness. The reason for adopting this approach because with thick oils when sensor is on top the fouled stripes in the air will take long to clean. Therefore, instead consider the sensor when it is submerged the most since most fouled stripes would be at the bottom in the water. In this case, the algorithm will overestimate the oil thickness due to fouling and would require a correction step where fouled stripes are detected and removed from the thickness. The workflow of the overall algorithm is illustrated in the flowchart presented in Figure 98.

Algorithm detailed description:

Calibration

The calibration voltage values are acquired while the sensor is completely dry and placed in open-air for a preset duration of time. For each electrode, the average of all measured voltages is stored in a one-dimensional array. While operating, the relative voltage difference (R) of each electrode of index 'i' is calculated using the following equation:

$$R\ (\%) = \frac{|Current[i] - Calibration[i]|}{Current[i]} \text{ x } 100$$

Validity Check

At each measurement cycle, a validity check is applied on the acquired values to check if the sensor is in a valid sensing position. A sensing position is set to be valid when the last electrode in the sensor array is immersed in water. The relative change of the last electrode is calculated and compared to a threshold value (50%) to decide if the electrode is in water. If the calculated relative change is greater than 50%, the measure is considered valid. Otherwise, the measure is considered invalid, and not stored in the measurements array. Also, a text message (Invalid) is sent to the base station to inform the user

about the sensor state. This would allow for the detection of the scenario where the sensor is out of the water.

Interface Detection (Detect-Interface)

To detect the interface between two different mediums, the algorithm uses a voting method named "Detect-Interface" and is described as the following:

// Function to get the interface between two different layers

Detect-Interface (Relative Differences Array)

```
// Create a one-dimensional array (Votes) of size N initialized by zeros.
Votes = zeros (1, N)
// Calculate votes of each electrode
index =1
While (index<N)
{
        Votes(index) = mean (RD (index+1: N) – mean (RD (1: index)) – (RD(index)/2)
}
// Get the index of the interface with the maximum value of votes
Max_Value = MAX(Votes)
Interface = getIndex (Max_Value)
// Return the index of the interface
Return Interface
```

Where "N = 48" is the total number of electrodes, "index" is the electrode index, and "RD" is the array holding the relative differences from calibration.

To measure the oil thickness, the interface detection method is applied two times iteratively. After finding the water interface, all of the electrodes below it (greater in index) are removed, and the method is applied on the remaining electrodes to find the oil/air interface.

Highest Point Algorithm

```
Start
While (1)
{
        // initialize counter to zero
        c=0
        While (c< 50)
        {
                // Measure voltages (all electrodes)
                M = Measure ();
                //Get relative Differences (RD), C: Calibration, M: Measured,
                RD = Get Relative Differences (C,M);
                V = Check Validity (RD);
                If (V = True (valid))
                {
                        // add to the 2-dimensional temporary array holding valid relative differences
                        Temp Array (c,:) = RD;
```

```
                    // increment counter
                    c = c+1;
                }// End If
        }//End While - Temp Array Full
        // Initialize temporary vector
        Temporary Vector = zeros (48);
        // Get the minimum relative difference from each column (electrode)
        For (k=0, k<48, k++)
        {
                Temporary Vector (k) = MIN (Temporary Array(:,k));
        }//end For

        // Calculate thickness
        Thickness = Get Thickness (Temporary Vector)
        Overall Thickness = 0.8*Overall Thickness + 0.2*Thickness

        // Clear Temporary Array
        Clear (Temp Array)

        // Clear Temporary Vector
        Clear (Temporary Vector)

// End global While
}//end While
End
```

Get Thickness Method (Thickness = Get Thickness (Temporary Vector))

This function gets the oil thickness based on the "Detect-Interface" method described above. Detecting the oil/water interface, removing oil/water interface and all electrodes below it (greater in index) from Temporary Vector, detect the air/oil interface, and calculate the oil thickness using the detected number of electrodes located between the two interfaces.

Corrected Lowest Point Algorithm

```
Start
While (1)
{
        // initialize counter to zero
        c=0
        While (c< 50)
        {
                M = Measure ();
                RD = Get Relative Differences (C, M); //C: Calibration, M: Measurements
                V = Check Validity ();

                If (V = True) // Valid measure
                {
```

```
                    // add to temporary array
                    Temporary Array (c, :) = RD;
                    // increment counter
                    c = c+1;
                }// End If
        }//End While - Temporary Array is Full

        // initialize empty arrays for maximum, minimum, and amplitude relative differences
        Temporary Max Vector = zeros (48);
        Temporary Min Vector = zeros (48);
        Temporary Amp Vector = zeros (48);

        // Get the maximums, minimums, and amplitudes
        For (k=0, k<48, k++)
        {
                Temporary Max Vector (k) = MAX (Temporary Array(:,k));
                Temporary Min Vector (k) = MIN (Measurements Array(:,k));
                Temporary Amp Vector = Temporary Max Vector (k) - Temporary Min Vector (k)
        }//end For

        //Detect water interface
        Water Interface = Detect-Interface (Temporary Max Vector);

        // Calculate relative change of averages to detect sensor movement
        Relative Change = ((Mean (Temporary Max Vector) – Mean (Temporary Min Vector)) / Mean
(Temporary Max Vector)) (100)

        // Check if relative change > threshold (%)
        If (Relative Change > 3%) // if > threshold, then apply correction step
        {
          // Correct Water interface by removing fouled electrodes
          While (Water Interface > 1)
          {
            If (Temporary Max Vector (Water Interface) > Mean (Temporary Amp Vector (0):
        Temporary Amp Vector (Water Interface -1)))
            {
              Water Interface = Water Interface – 1;
            }//end if
          }//end While
        }//end if
       // Remove Water interface and other electrodes beneath it from Temporary Max Vector and get
oil interface
       Temporary Max Vector = Remove Water Portion (Temp Max Vector, Water Interface)
       // Get oil interface
      Oil Interface = Detect-Interface (Temporary Max Vector);
```

// Get Oil portion and calculate thickness
Oil Interval = Water Interface – Oil Interface;

// Calculate and update thickness
thickness = (Oil Interval) (2) + (Oil Interval-1) (1)
} // end While (1)
End

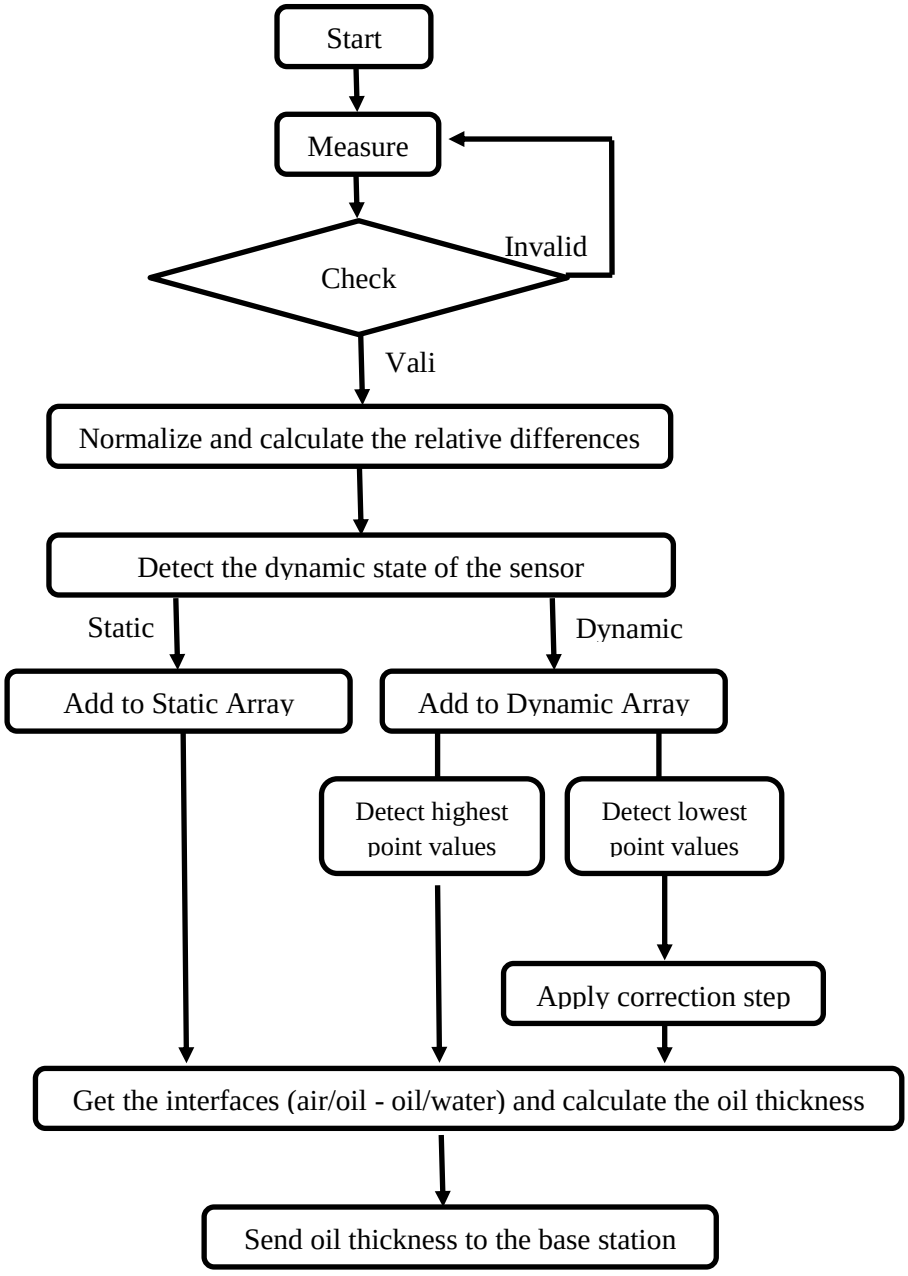

Figure 98: Algorithm flowchart

6.11 Mechanical Design Refinement and Optimization

6.11.1 *Packaging Design*

After optimizing the capacitive sensor design, the design of the mechanical packaging was also refined and adapted to fit the dimensions of the final sensor prototype. One of the most important factors that impact the package dimensions is the size of the batteries used to power the device. Multiple batteries have been contemplated to power the sensor, and accordingly, multiple packages have been designed to meet the different sizes as well as to optimize the final prototype package. Mainly, two types of batteries were considered, the 7.2V 3800mAh Nickel Metal Hydride (Ni-MH) battery, and the 2500mAh 1.2V 'AA' Ni-MH batteries. As the battery life tests conducted showed promising results for the 2500mAh 1.2V 'AA' Ni-MH batteries, the double-sided six-battery holder was selected to be used in the final design for its compact size, availability, and acceptable efficiency. Figure 99 shows the two types of batteries.

Figure 100 and Figure 101 show the designs made for two different placement configurations of the 7.2V 3800mAh Ni-MH batteries. Figure 102, shows the package for the sensor with the 2500mAh 1.2V 'AA' Ni-MH batteries. Figure 103 is a comparison of all 3 packages.

Figure 99: 7.2V 3800mAh Ni-MH (left), 2500mAh 1.2V 'AA' Ni-MH (right)

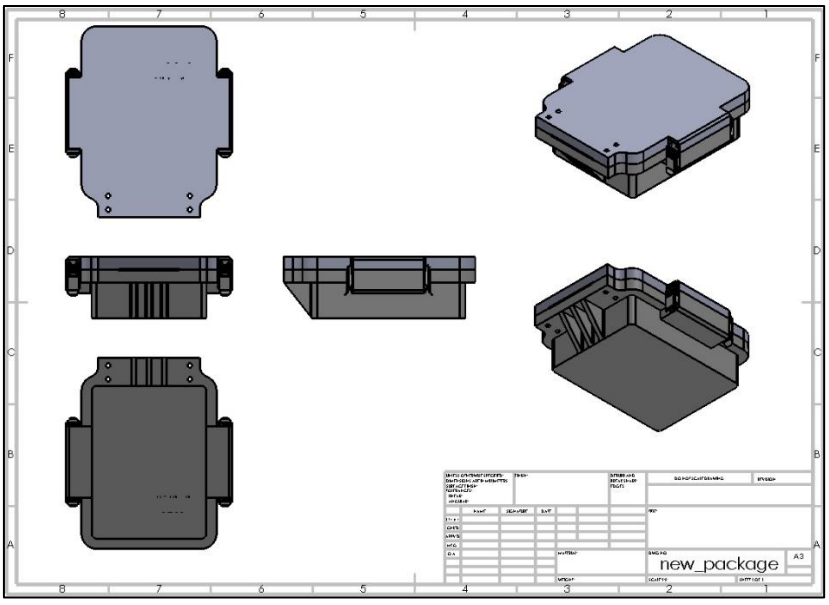

Figure 100: Batteries flat side to side package

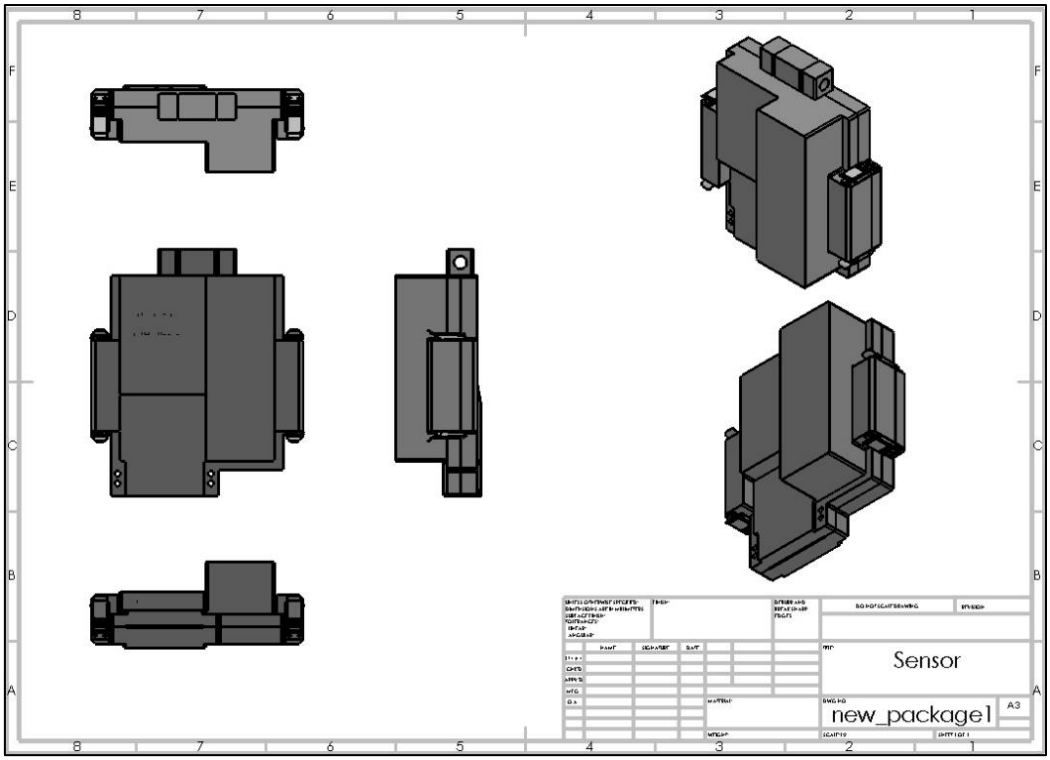

Figure 101: package for batteries on one side and sensor on the other

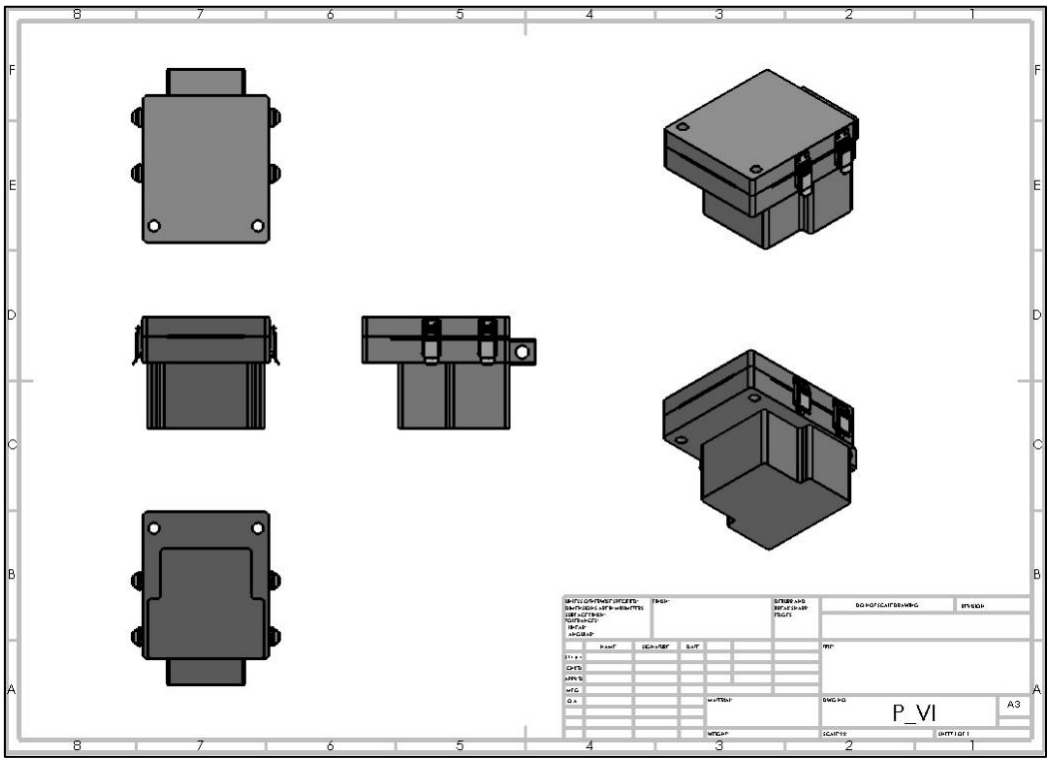

Figure 102: Package of sensor powered by 'AA' Ni-MH

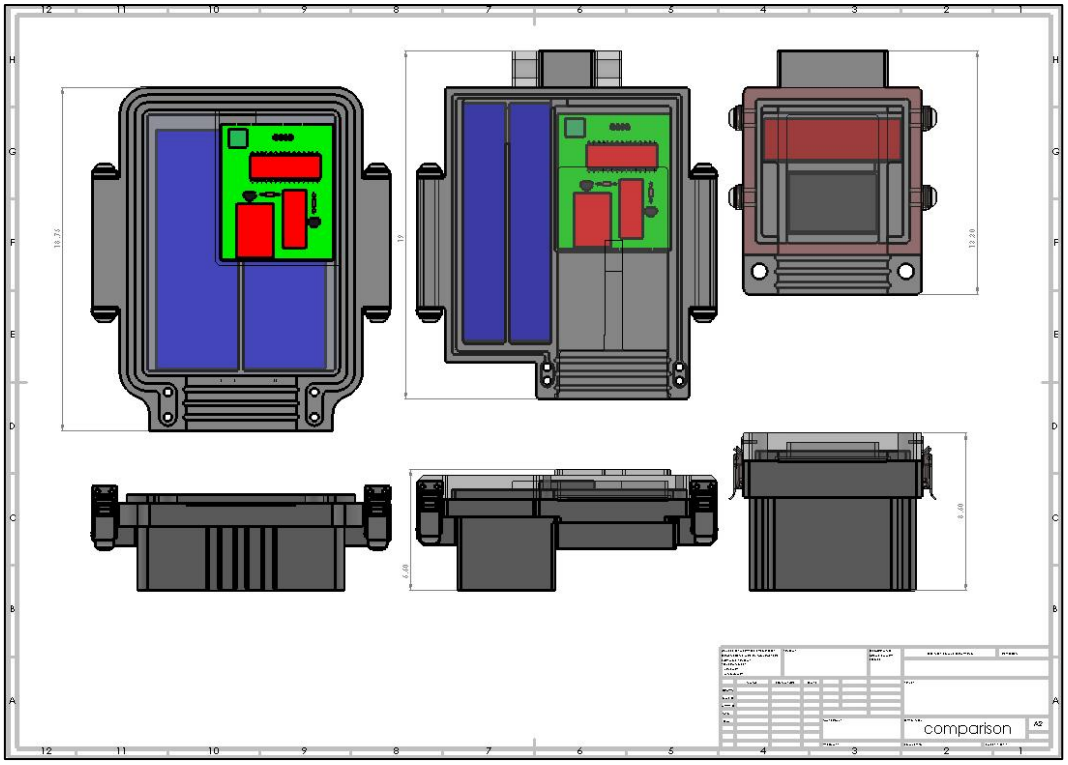

Figure 103: Comparison of final packaging designs for capacitive sensor

Three final packages (Figure 102) in total were manufactured; the packages are the third iteration and are aimed to be relatively compact in size, made to fit the designed mounts for the skimmer tests and the moving bridge tests. The package in Figure 104-Left is mounted on a 3D printed extension bracket in order to fit the large testing tank; the extension is made to be modular in size in order to change height according to the desired distance from oil surface. The blue 3D printed plates allow varying the distance by increments of 1 cm, when added and removed from the assembly during testing. Figure 104-Right shows the implemented package with the control unit and power unit installed. The final version of the packaging design assembled with the sensor cartridge, power unit, and the control unit is shown in Figure 105.

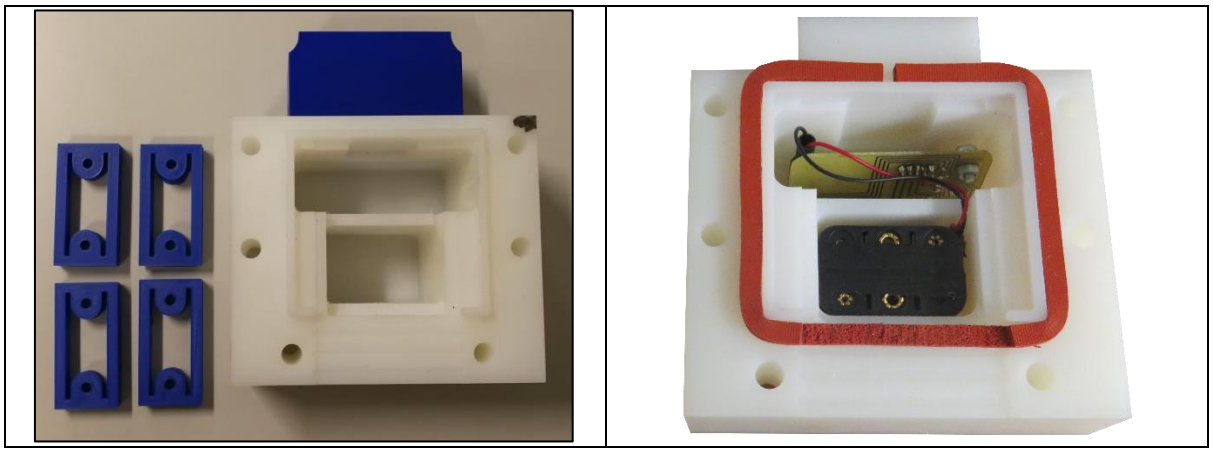

Figure 104: Final package with printed modular extension mount and instrumentation

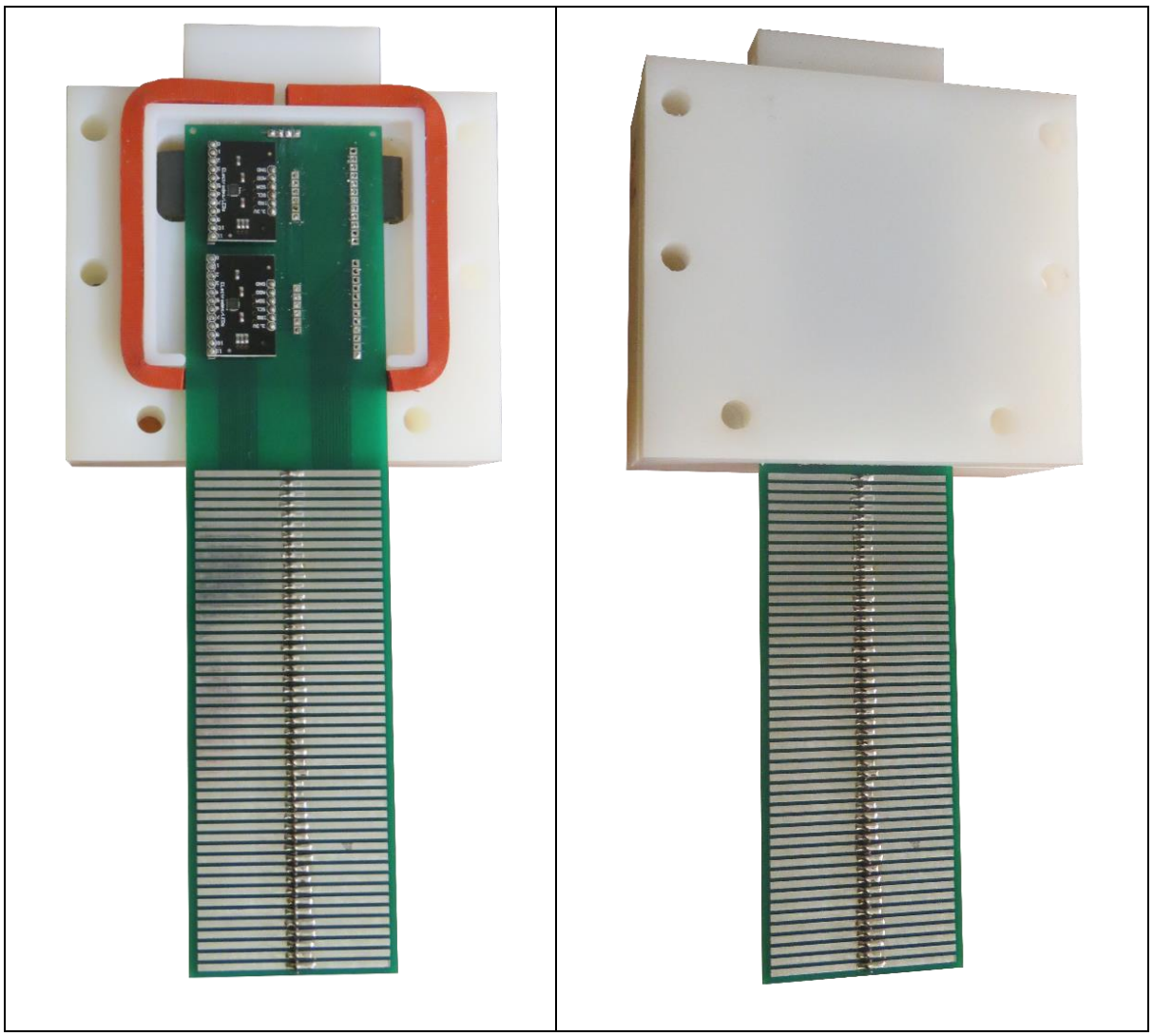

Figure 105: Final capacitive sensor prototype with packaging and instrumentation

6.11.2 *Attachments for Final Testing*

6.11.2.1 Bridge Hinged Mount

For the final sensor design testing, several attachments were manufactured to mount the sensor to the testing equipment. In order to mount the capacitive sensor to the moving bridge at the Ohmsett facility, another attachment was designed to fit to the setup available at Ohmsett. The attachment design is made of two parts: sensor mount fitting the extension on the packaging, and a plate made to size per the dimensions sent from Ohmsett. The two parts are hinged together. Figure 106 is the drawing of the bridge mount connection plate, and Figure 107 is the first designed attachment using a spring lock mechanism, designed to keep the sensor in the water and avoid it lifting due to dragging and waves, Figure 108 shows the final attachment that was adopted, relying on the weight of the sensor mount extension to keep the sensor horizontal during tests.

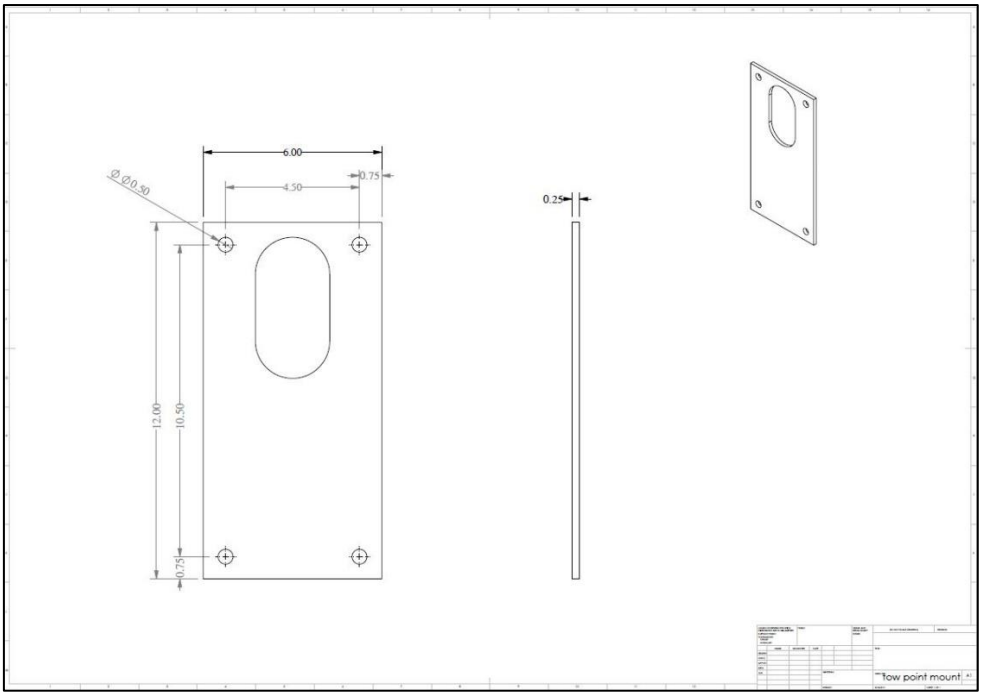

Figure 106: Tow point mount drawing (dimensions in inches)

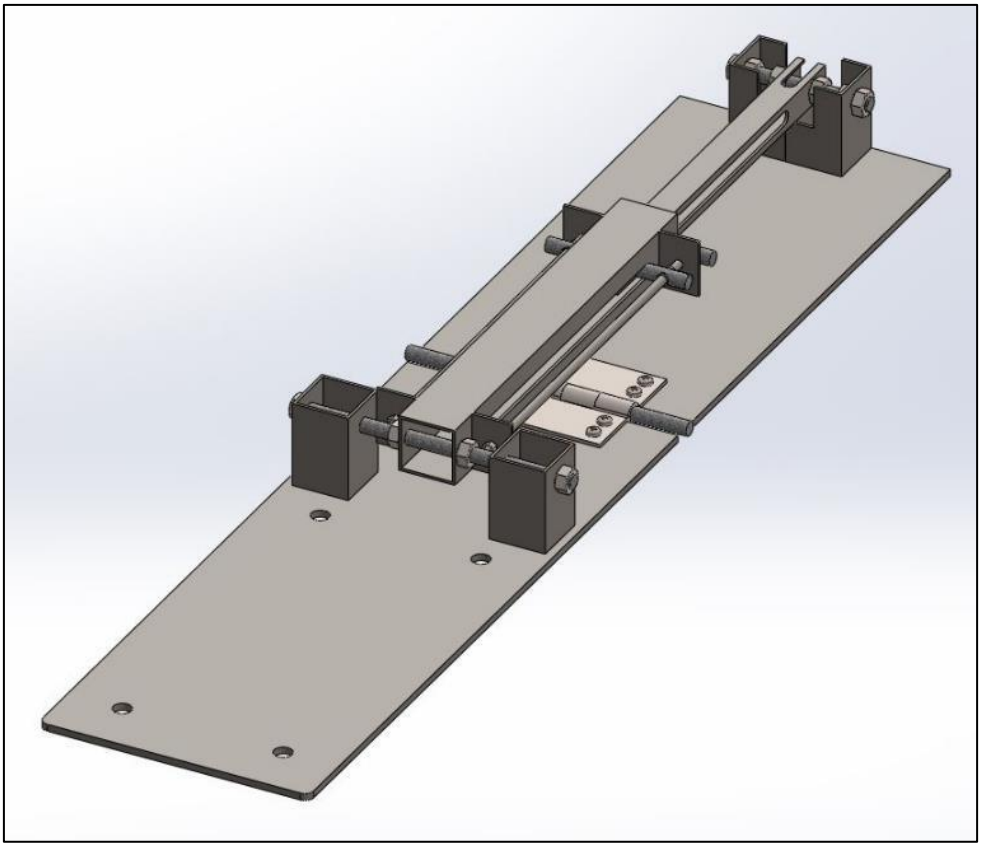
Figure 107: Spring lock attachment computer-aided design

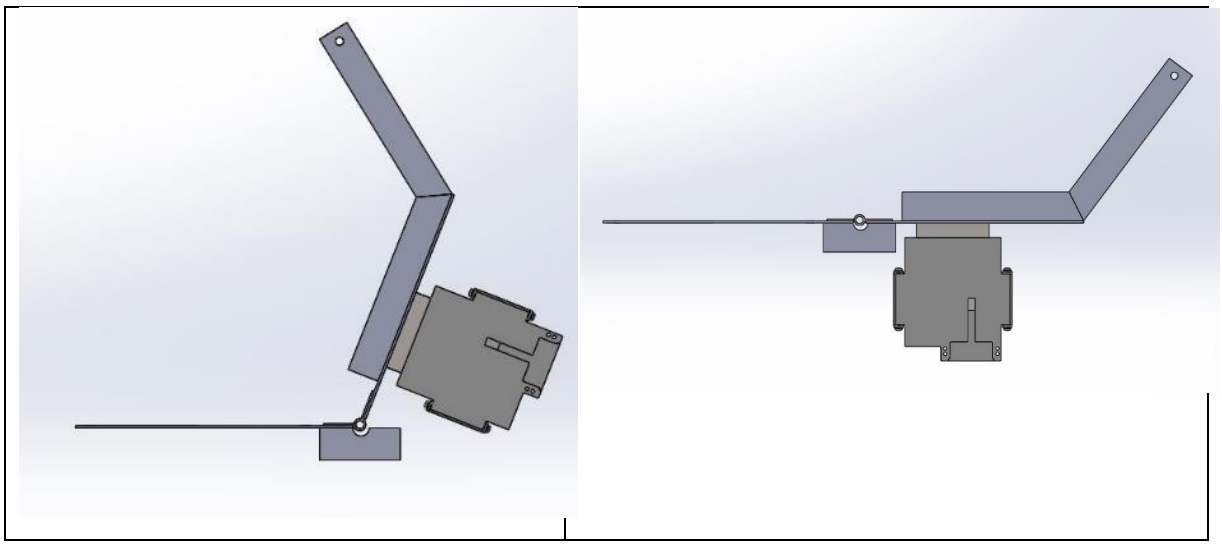

Figure 108: Retracted attachment (right), Released attachment (left) computer aided design

6.11.2.2 Manufactured Bridge Hinged Mount

The hinge mount was manufactured and then modified after manufacturing in order to reduce weight and eliminate non-structural material. Figure 109 and Figure 110 are images of the actual mount after weight reduction. A combination of weldments of U-beams and 2x2 metal pieces were added in order to provide structural support and to restrict the angle at a 0-90 degrees range of motion. The mechanism is naturally open and tends to reopen under the effect of gravity when released, due to the added moment of the cable extension arm pointing down and away from the hinge. The sensor fitting is made of the same 2x2cm metal rod as the stoppers; unlike the CAD design this fitting is non-hollow, and the same geometry is used in the assembly.

Figure 109: Manufactured hinged mount

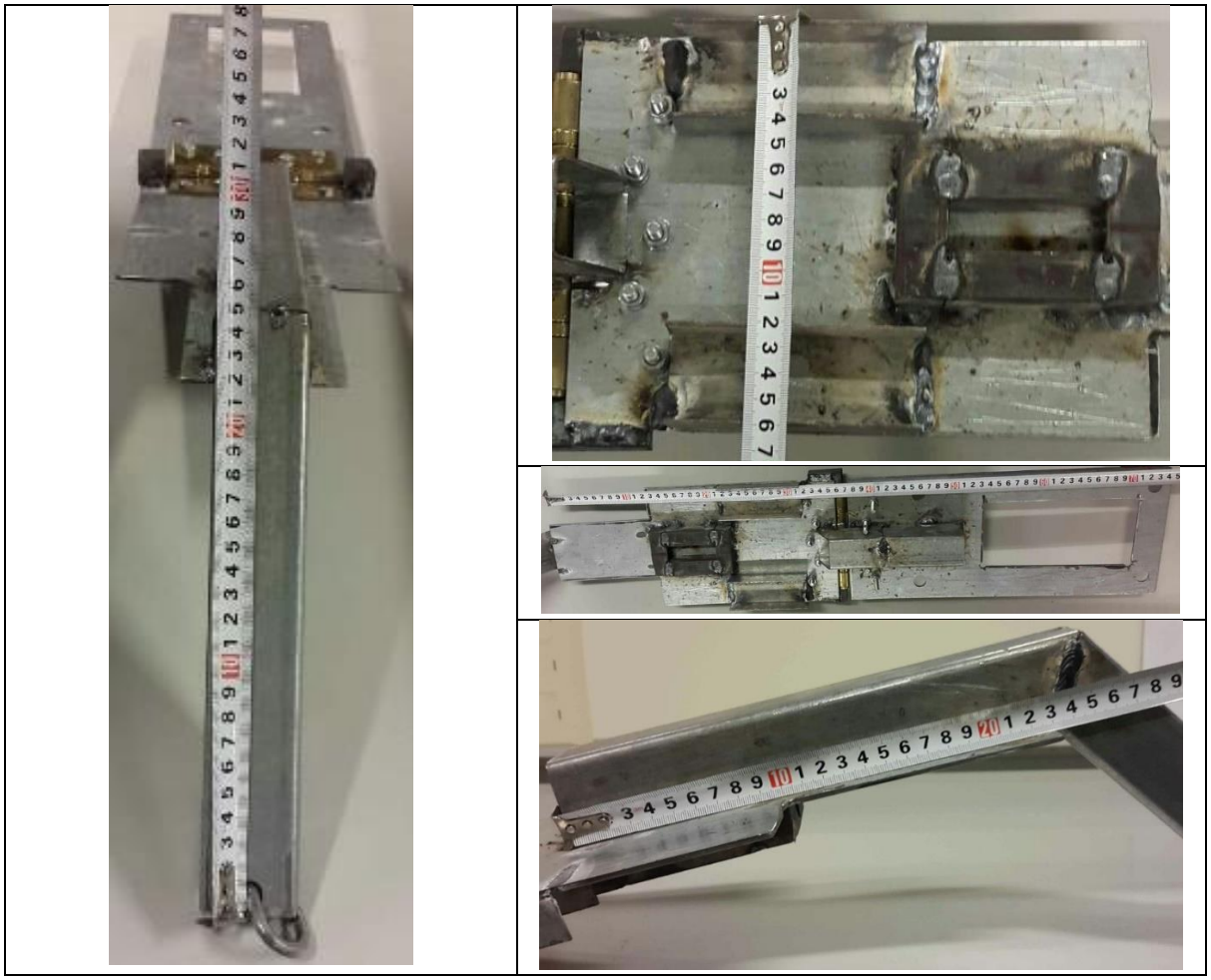

Figure 110: Dimensions after manufacturing

6.11.2.3 Skimmer Mount Design

The mount that goes onto the skimmer is a beam fixed on two of the three floaters at the stainless-steel cylinders above water level by an omega bracket fixture, it is composed of three parts: the beam, the rail, and the slider. The beam is composed of two equal length parts connected by a bracket assembly; to allow for adjustment to the angle of the cylinders, the rail connects to the beam assembly and a slider is mated on the rail to allow for vertical adjustment of the sensor height. Two designs were adopted and manufactured: the first is made of a weld series of metal 4x4cm beams and weighs 9.3kg; a second design is manufactured of aluminum extrusions, which are rectangular in cross-section and are of 4x2cm in area. The use of the aluminum extrusions allows us to avoid welding, as well as cutting down the weight to 4.3kg and a more flexible room for adjustment to the actual size of the skimmer. Figure 111 shows the metal beam design and Figure 112 shows the aluminum design.

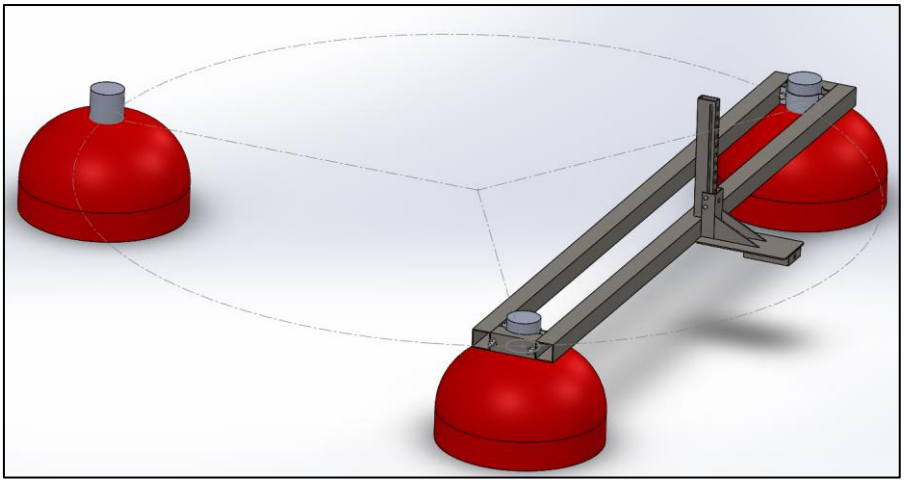

Figure 111: Metal beam mount computer-aided design

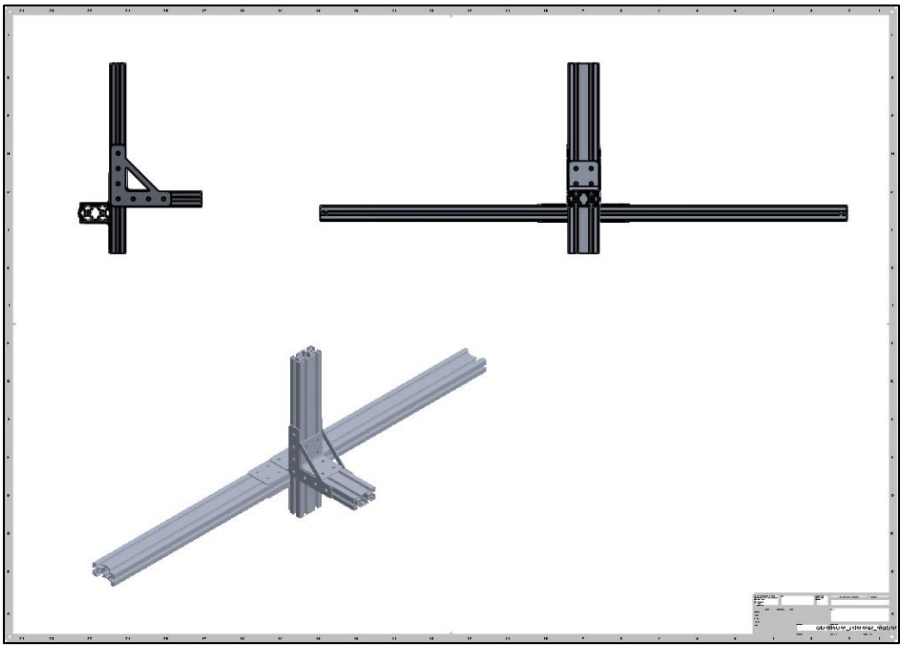

Figure 112: Aluminum extrusion mount computer-aided design

6.11.2.4 Manufactured Skimmer Mount

The skimmer mount was manufactured out of 2x2cm aluminum extrusion slots. Figure 113, Figure 114, and Figure 115 are the final subassemblies of the skimmer mount. It should be noted that during assembly of the aluminum extrusion, the screws used should have low wiggle in order to prevent wedging under sliding friction of the different subassemblies. A preferred way to assemble the parts is to combine the different parts before adding the joiners and brackets since sliding the pan heads is much simpler and more efficient than having to start with the brackets and build the rest into the assembled parts. The assembly order should be the horizontal beam first with the proper distance adjustment onto the buoy floats, the vertical slider second with the sensor holder already mounted, finally the height adjustment would be made by untightening the vertical screws on the vertical side of the triangular brackets.

After testing at the facility, it was noted that the skimmer was lower than expected and the sensor got completely covered by oil; therefore, fixing the mount's vertical position should take into account the sinking effect that will be caused by an increase in oil volume due to either fluid accumulation under flow or change in static environment. In order to prevent dunking of the sensor in oil during use, another phenomenon to be accounted for when fixing the sensor holder is to use the complete range of strips in order to cover thicknesses from higher buoyancy (minimal oil volume) to smaller buoyancy (maximum allowable oil thickness by the sensor). The latter is dependent on the skimmer buoyancy, and the density of oil in the environment.

Figure 113: Manufactured skimmer mount sensor holder

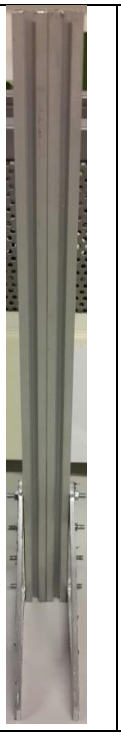

Figure 114: Manufactured skimmer mount right angle slider

Figure 115: Manufactured skimmer mount horizontal fixture

Chapter 7- Ohmsett Testing

Between November 27 and December 1, 2017 extensive testing at Ohmsett was carried out. The testing included:
1- Capacitive sensor indoor testing in a tank (Static, vertical and horizontal motion)
2- Spectro sensor indoor testing in a tank (Static and slight motion)
3- Capacitive sensor outdoor testing in the large tank (dragged by the bridge with no waves, mounted on the skimmer free floating and dragged with and without waves)
4- Spectro sensor outdoor testing in the large tank (free floating with and without waves)

The properties of the oil-types used in the experiments as provided by Ohmsett, are shown in Table 39.

Table 39: Pre-Test Lab Analysis (Ohmsett)

Pre-Test Lab Analysis (T664)						
Test Oil	**S.G. @20C**	**Viscosity @20C**	**I.F.T.**	**S.T.**	**BS&W**	**Date**
Diesel	0.842g/mL	8cP	13.8dynes/cm	30.1dynes/cm	0%	11/1/17
Hydrocal 300 (New)	0.909g/mL	220cP	22.6dynes/cm	33.5dynes/cm	0.8%	11/1/17
Hoops (Weathered)	0.896g/mL	55cP	15.8dynes/cm	33.3dynes/cm	1.4%	11/1/17
Calsol 8240	0.931g/mL	2653cP	31.0dynes/cm	36.4dynes/cm	0.2%	11/1/17
Hoops (fresh)	0.865g/ml	28cP	16.9dynes/cm	31.5dynes/cm	0%	11/1/17
Description	**S.G. @20C**	**Salinity**	**I.F.T.**	**S.T.**	**Average Temperature**	**Date**
Test Basin Water	1.019g/ml	28.3ppt	35.9dynes/cm	65.4dynes/cm	See tests	12/4/17
Lab Tech	Allen Cannone					

This chapter presents the detailed results of all the experiments with the analysis. A video showing the capacitive sensor testing is available at: https://youtu.be/GufzKsxNTyo and a video showing the spectro-based sensor testing is available at: https://youtu.be/gYLgEAgGhe0.

7.1 Dipping Tests (sensor #1 - Capacitive Sensor)

Dipping tests were designed to test the sensor in known slick thicknesses of different values using four different test oils. These tests were performed in the Ohmsett high-bay area using small clear glass tanks (12.875” x 12.875”) with clear sides, where known oil thicknesses were created on approximately a 6 inches (152.4 mm) depth of saltwater. Starting with the oil with the lowest viscosity, thicknesses were increased, as per a test matrix, by dispensing the appropriate volume using graduated cylinders. The oils were dispensed in order of increasing viscosity. The sensor was deployed manually for each condition by the onsite AUB engineers and was displaced in a regular pattern upon entry into the test slick. The sensor was first held steady to obtain an initial static case reading, followed by a dynamic case for a duration of about one minute of reciprocating vertical motion, and then followed by about

one minute of lateral motion in the direction parallel to the oil slick. The experimental setup used in performing the dipping tests (static and dynamic cases) is shown in Figure 116.

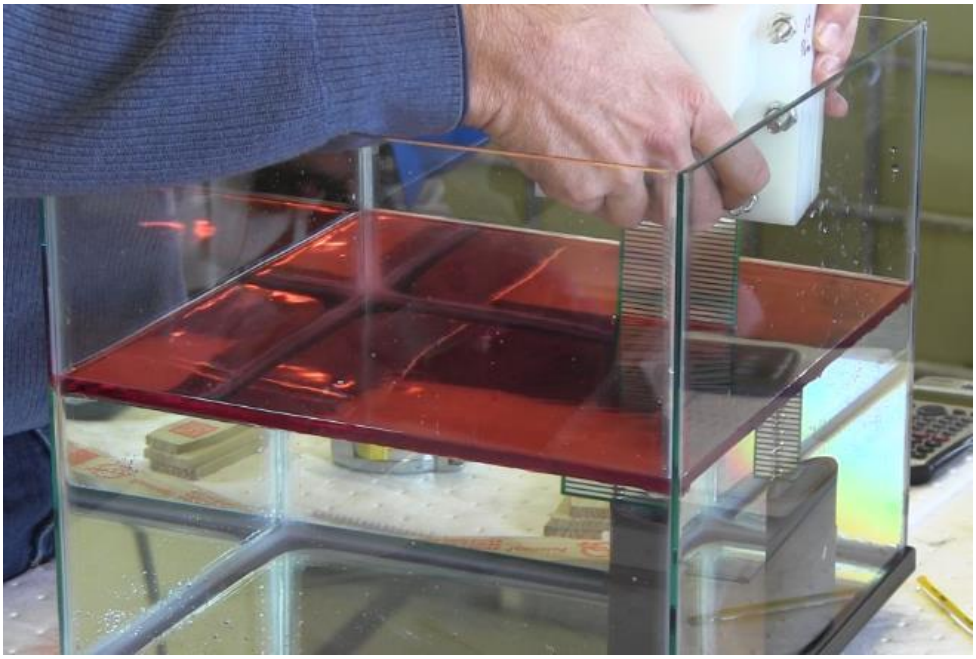

Figure 116: Experimental setup for dipping tests (Ohmsett)

This process was repeated in a relatively consistent manner for each test condition while data was recorded by AUB engineers via wireless communication to a nearby laptop. The series of tests included four oil types: diesel, Hoops Crude oil (weathered), Hydrocal 300 and Calsol 8240. Starting with the thinnest slick, each oil was dispensed to create eight different slick thicknesses ranging from 0.125 to 3 inches (3.175 to 76.2mm). The sensor was removed from the tank when oil was being added but the sensor was not cleaned or modified in any way between tests. The tank was completely emptied and cleaned between the tests using different oil types.

Ohmsett Observations/Notes:

- A miniscus effect above and below the oil slick was observed along the tank wall perimeter potentially skewing thickness.
- When dispensing more viscous oils (Hydrocal 300 and Calsol 8240) residual oil remained on the graduated cylinder walls.

As a result, the residual had a cumulative effect on the total volume dispensed and may have skewed the thicknesses to less than targeted.

The method used to perform the dipping tests is summarized by the following points:

- Prepare slick(s) in small tank (over salt water)
- Manually place sensor into slick at random height without visual or other alignment to the oil slick, and then obtain readings.
- Remove sensor, increase thickness – repeat.

For all of the dipping tests performed, the volume amounts added (Figure 117) to obtain the required thicknesses are summarized in Table 40.

Table 40: Dipping tests - Target thicknesses and Volumes

Target Thickness (mm)	Total Volume (ml)	Volume to Add (ml)
1	339.6	339.6
2	679.2	339.6
3	1,358.4	679.2
4	2,037.7	679.2
5	2,716.9	679.2
6	4,075.3	1,358.4
7	5,433.8	1,358.4
8	8,150.7	2,716.9

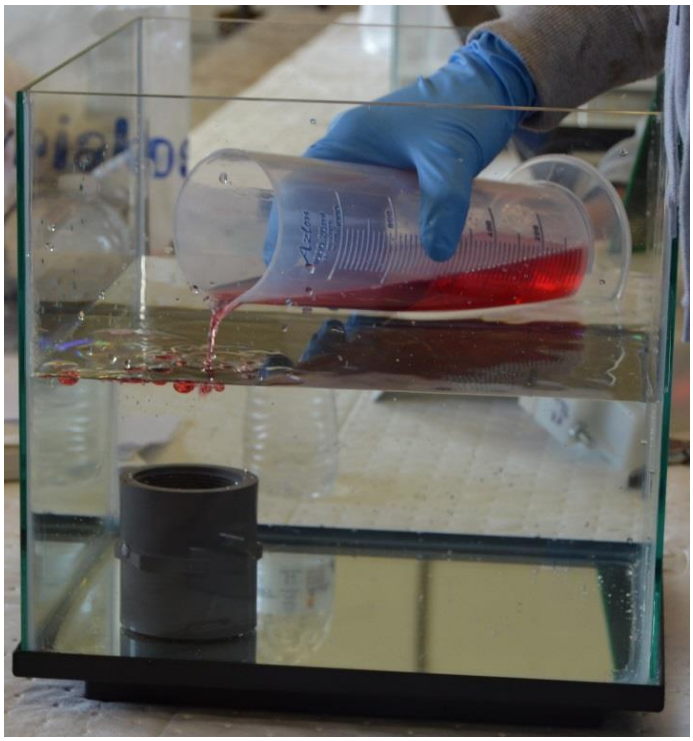

Figure 117: Adding controlled amount of oil - Graduated Cylinders

7.1.1 *Dipping Tests (1-8) - Diesel*

Tests numbered from 1 to 8 used diesel oil with a thickness ranging from 0.125 inches (3.18mm) to 3inches (76.20mm). Water and oil temperature were recorded ranging between 69°F and 71°F. The experimental results showing the measured thicknesses versus the actual thicknesses are shown in Table 41 for the static case and in Table 42 for the dynamic case. The results were obtained based on the "Highest Point Algorithm" developed for light-oil types (ex. Diesel – Hoops). Figure 118, shows the plot of the static and dynamic Diesel experiments with respect to the actual estimated thicknesses.

Table 41: Capacitive Sensor Dipping Tests (1-8) – Diesel / Static

Test Type	Case	Oil Type				
Dipping	Static	Diesel				
Test Number	**Actual Thickness (mm)**	**Average Measured Thickness (mm)**	**Standard Deviation**	**Sample Size**	**Sample Duration (mm:ss)**	**Average Error (mm)**
1	3.18	6	0	19	02:38	2.83
2	6.35	6.01	0.01	22	03:04	0.34
3	12.70	13.9	1.71	30	04:14	1.2
4	19.05	19.88	1.65	28	03:57	0.83
5	25.40	25.66	1.9	27	03:48	0.26
6	38.10	36.24	2.41	20	02:47	1.86
7	50.80	49.95	0.88	18	02:29	0.85
8	76.20	70.41	7.82	21	02:55	5.79
				AVG	**03:14**	**1.745**

Table 42: Capacitive Sensor Dipping Tests (1-8) – Diesel / Dynamic

Test Type	Case	Oil Type				
Dipping	Dynamic	Diesel				
Test Number	**Actual Thickness (mm)**	**Average Measured Thickness (mm)**	**Standard Deviation**	**Sample Size**	**Sample Duration (mm:ss)**	**Average Error (mm)**
1	3.18	10.88	6.98	35	04:58	7.7
2	6.35	6.01	0.01	22	04:23	0.34
3	12.70	13.35	0.97	29	04:06	0.65
4	19.05	18.66	1.5	27	03:48	0.39
5	25.40	25.61	1.8	22	03:04	0.21
6	38.10	29.63	5.72	29	04:06	8.47
7	50.80	36.88	11.78	32	04:32	13.92
8	76.20	76.85	1.38	24	03:22	0.65
				AVG	**04:02**	**4.04**

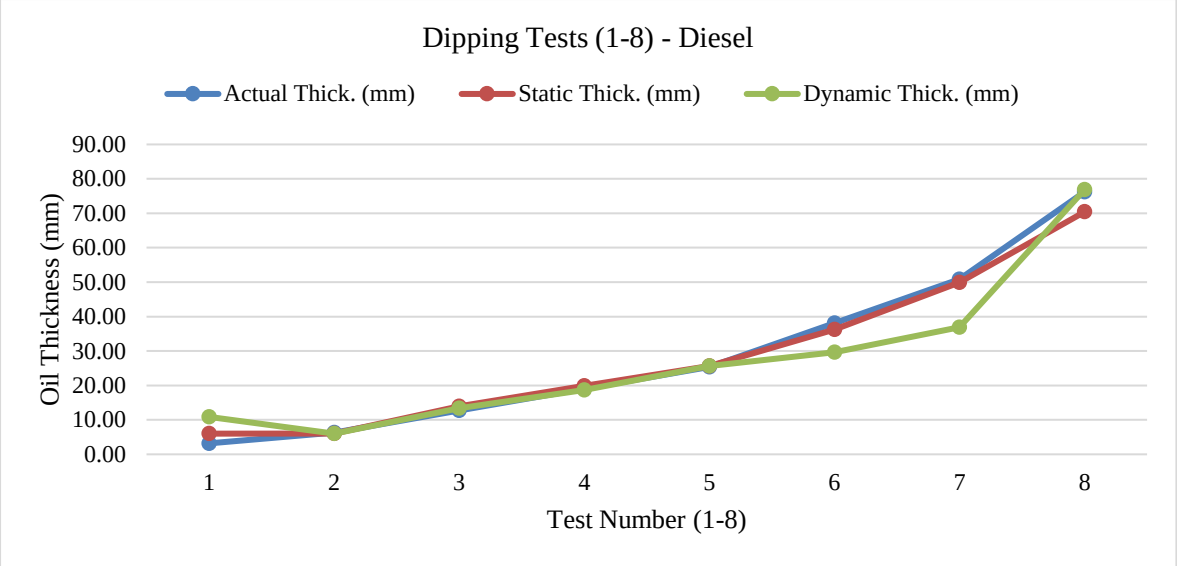

Figure 118: Dipping Tests (1-8) / Diesel (Static & Dynamic Curves)

As shown in Figure 118 and Table 41, the absolute error of the measured thicknesses in the static case didn't exceed the resolution of the sensor (3mm) in all the performed tests (1-8) except in the last test (8) where the average measured thickness is around 70.41mm and the actual was estimated as 76.2mm. It is important to note here that in this case, the absolute error (5.79mm) didn't exceed the error caused by misclassification of two strips (6mm) out of forty-eight strips contained in the sensor PCB. Also, it is important to note that 5/8 static tests showed an extremely high accuracy with an average absolute error less than 1mm.

In the dynamic case, it is noted that as shown in Table 42, and Figure 118, 5/8 of the dynamic tests showed an extremely high accuracy, with an average absolute error less than 1mm. However, as expected, and because of the increased dynamic motion of the sensor (vertical and horizontal movement), the number of misclassified strips increased in some cases causing an increase in the absolute error in comparison to the static case.

Based on the experimental results, it can be concluded that despite the fact that the sensor passed most of the static and dynamic tests with an acceptable accuracy, the misclassification of few number of electrodes in the dynamic tests was leading to a sudden increase in the absolute error because of the relatively high width of the sensor electrodes (3mm) and due to some remaining fouling effect. To solve this problem, it is recommended to decrease the electrodes width to increase the sensor resolution and to lower the impact of misclassified electrodes on the measured thickness. This conclusion is of high importance to be considered in the future development of the device.

7.1.2 *Dipping Tests (9-16) – Hoops (weathered)*

Tests numbered from 9 to 16 used Hoops (weathered) Oil with a thickness ranging from 0.125 inches (3.18mm) to 3 inches (76.20mm). Water and oil temperature were recorded around 70°F (69°F -71.5°F). Some comments recorded during performing these tests are:

- Observed oil coating on sensor below slick (Figure 119)
- Observed meniscus effect on oil containers (skew actual thickness)

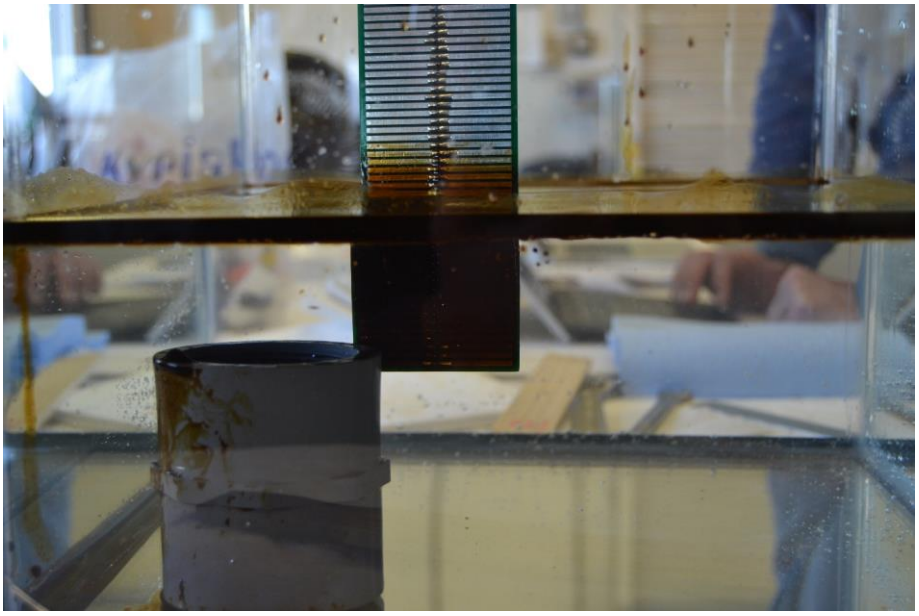

Figure 119: Coating of the sensor body under slick - Hoops (weathered)

The experimental results showing the measured thicknesses vs. the actual thicknesses are shown in Table 43 for the static case and in Table 44 for the dynamic case. The results were obtained based on the "Highest Point Algorithm" developed for light-oil types (ex. Diesel – Hoops). Figure 120, shows the plot of the static and dynamic Hoops (weathered) experiments with respect to the actual estimated thicknesses.

Table 43: Capacitive Sensor Dipping Tests (9-16) – Hoops (weathered) / Static

Test Type	**Case**	**Oil Type**				
Dipping	Static	Hoops (weathered)				
Test Number	**Actual Thick. (mm)**	**Average Measured Thickness (mm)**	**Standard Dev.**	**Sample Size**	**Sample Duration (mm:ss)**	**Average Error (mm)**
9	3.175	15.05	14.72	32	04:31	11.88
10	6.350	8.92	3.25	19	02:37	2.57
11	12.700	12.99	1.03	21	02:56	0.29
12	19.050	19.26	0.78	22	03:04	0.21
13	25.400	24.26	2.92	18	02:29	1.14
14	38.100	35.27	4.65	22	03:04	2.83
15	50.800	51.66	2.52	24	03:21	0.86
16	76.200	70.28	7.79	26	03:39	5.92
				AVG	**03:12**	**3.21**

Table 44: Capacitive Sensor Dipping Tests (9-16) – Hoops (weathered) / Dynamic

Test Type	**Case**	**Oil Type**				
Dipping	Dynamic	Hoops (weathered)				
Test Number	**Actual Thickness (mm)**	**Average Measured Thickness (mm)**	**Standard Deviation**	**Sample Size**	**Sample Duration (mm:ss)**	**Average Error (mm)**
9	3.175	18.06	4.81	26	03:39	14.88
10	6.350	7.61	1.07	26	03:40	1.26
11	12.700	11.74	1	22	03:04	0.96
12	19.050	17.24	2.22	28	03:57	1.81
13	25.400	21.3	2.93	23	03:13	4.1
14	38.100	32.14	2.86	24	04:26	5.96
15	50.800	43.32	5.78	26	03:40	7.48
16	76.200	80.43	6.98	24	04:32	4.23
				AVG	**03:46**	**5.08**

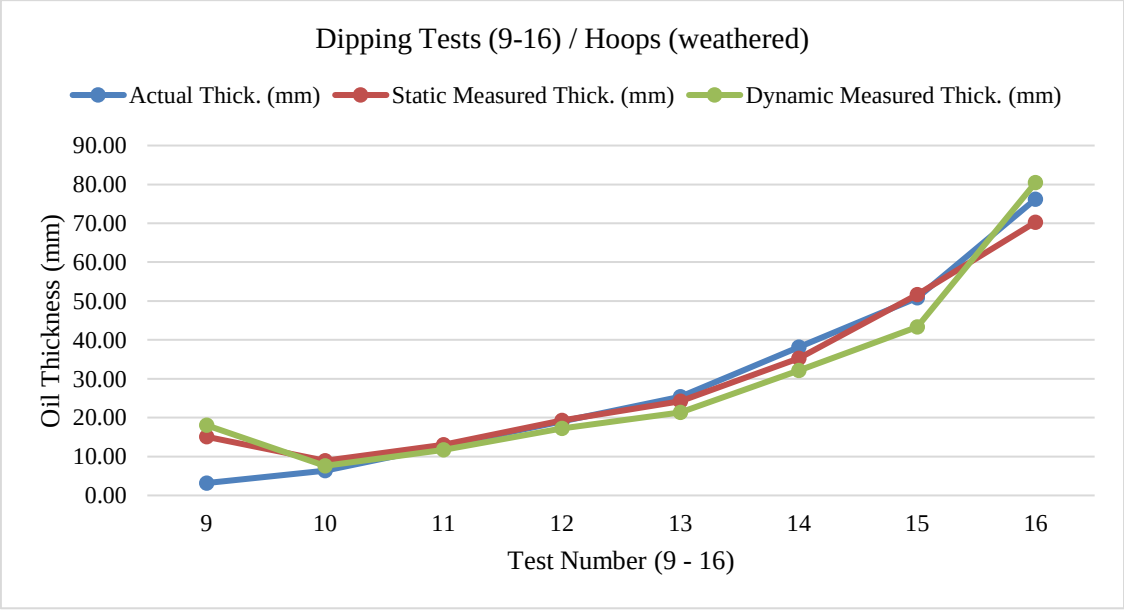

Figure 120: Dipping Tests (9-16) / Hoops (weathered) (Static & Dynamic Curves)

For the static tests, as shown in Table 43, three tests (11, 12, and 15) showed an extremely high accuracy with an absolute error less than 1mm. The remaining tests showed an acceptable accuracy with an error around one to two electrodes out of forty-eight total electrodes producing an absolute error ranging from around 1 to 5mm. It is noted that the larger error occurred at the first test (Test No. 9) where the actual thickness is around 3.18mm. To interpret the cause of the error, we plot the set of measurements acquired while performing the first test (Test No. 9) with respect to time (Figure 121).

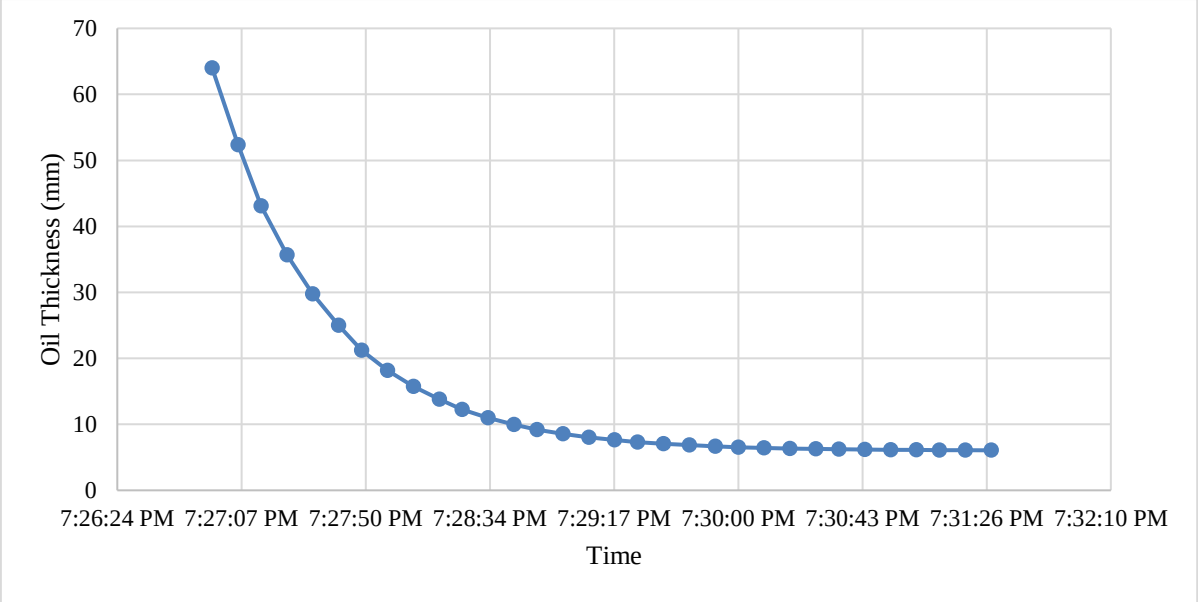

Figure 121: Test 9 (Static) – Hoops (weathered) (3.175mm)

The curve plot shown in Figure 121 describes the reason for having a relatively large thickness measurement average (15.05mm) while the actual thickness is around 3.175 mm. As the sensor is immersed in the liquid for the first time, most of the electrodes are covered with a layer of oil due to the fouling process. Because of the fouling effect, initial readings of the sensor were relatively large (63mm – 52mm – 43mm). Also, the use of a relatively-slow moving average rate contributes to decreasing the change of the sensor measurements. However, it is obvious that the sensor reaches a steady state at around (7:28:35 PM) where all of the remaining measurements are less than 10mm and become almost stable at 6mm. It is worth noting that in static cases the fouling of strips that went through oil and into water can be detrimental since the sensor is not moving to "wash" it off. In a normal operational case the user could be instructed to move the sensor around to reduce this effect; however, in all our tests this was not done in order not to bias the results. It also important to note that based on the sensor resolution which is around 3mm (single electrode width (2mm) + vertical gap (1mm)), this result is considered acceptable. In future development, this problem may be addressed by increasing the sensor resolution and speeding up the measurement change rate in addition to coating the sensor.

For the dynamic case, as shown in Table 43, and Figure 120, the error slightly increased due to sensor movement and fouling. However, with an absolute error equal to less than one electrode (3mm) in three tests (10, 11, and 12) and less than two electrodes (6mm) in another three tests (13, 14, and 16), the result is considered acceptable. It is noted that the larger error occurred at the first test (19), and that during performing these test, significant fouling of the sensor below the slick was recorded. Regarding the first test where the sensor is completely immersed for the first time through the thin oil layer, the fouling effect was very high. Also, as reported by the testers, the actual thickness is slightly skewed by the effect of meniscus effect noted on oil containers.

While most results were extremely satisfying, it was observed that the effect of fouling was maximized while dealing with thin oil layers (test 9). Accordingly, mitigating the fouling issue will be considered a priority in the future development of this measurement device. This can be done by several approaches related to hardware design and algorithm improvements. For example, the anti-fouling mechanical structure, including horizontal pins may be further developed by enhancing the pins manufacturing, adding high-frequency vibrators, and testing hydrophobic chemical coatings.

7.1.3 *Dipping Tests (18-25) – Hydrocal 300*

Tests numbered from 18 to 25 used Hydrocal 300 oil with a thickness ranging from 0.125 inches (3.18mm) to 3 inches (76.20mm). Water and oil temperature were recorded around 70°F (69°F -71°F). A note was reported while performing the first test (Test No. 18) describing that it was difficult to uniformly cover the surface area with oil at this thickness (0.125inches). Measurement results are obtained by the "Corrected Lowest Point Algorithm" used for heavy oils. The experimental results showing the measured thicknesses vs. the actual thicknesses are shown in Table 45 for the static case and in Table 46 for the dynamic case, and the corresponding graph is shown in Figure 122.

Table 45: Capacitive Sensor Dipping Tests (17-25) – Hydrocal 300 / Static

Test Type	**Case**	**Oil Type**				
Dipping	Static	Hydrocal 300				
Test Number	**Actual Thickness (mm)**	**Average Measured Thickness (mm)**	**Standard Deviation**	**Sample Size**	**Sample Duration (mm:ss)**	**Average Error (mm)**
17, 18	3.175	12.09	4.09	21	02:56	8.91
19	6.350	6.76	0.67	19	02:38	0.41
20	12.700	13.35	1.53	16	02:11	0.65
21	19.050	18.97	1.94	19	02:38	0.08
22	25.400	27.78	1.9	21	02:55	2.38
23	38.100	36.43	2.57	19	02:38	1.67
24	50.800	47.48	4.39	22	03:04	3.32
25	76.200	72.36	3.51	24	03:22	3.84
				AVG	**02:47**	**2.65**

Table 46: Capacitive Sensor Dipping Tests (17-25) – Hydrocal 300 / Dynamic

Test Type	**Case**	**Oil Type**				
Dipping	Dynamic	Hydrocal 300				
Test Number	**Actual Thickness (mm)**	**Average Measured Thickness (mm)**	**Standard Deviation**	**Sample Size**	**Sample Duration (mm:ss)**	**Average Error (mm)**
17, 18	3.175	5.97	2.31	26	03:38	2.8
19	6.350	12.01	5.3	27	04:08	5.66
20	12.700	9.13	4.41	22	03:32	3.57
21	19.050	15.3	3.44	19	02:37	3.75
22	25.400	29.67	4.43	19	02:59	4.27
23	38.100	36.85	3.56	24	04:16	1.25
24	50.800	52.03	3.15	25	03:31	1.23
25	76.200	80.08	1.87	24	03:22	3.88
				AVG	**03:30**	**3.30**

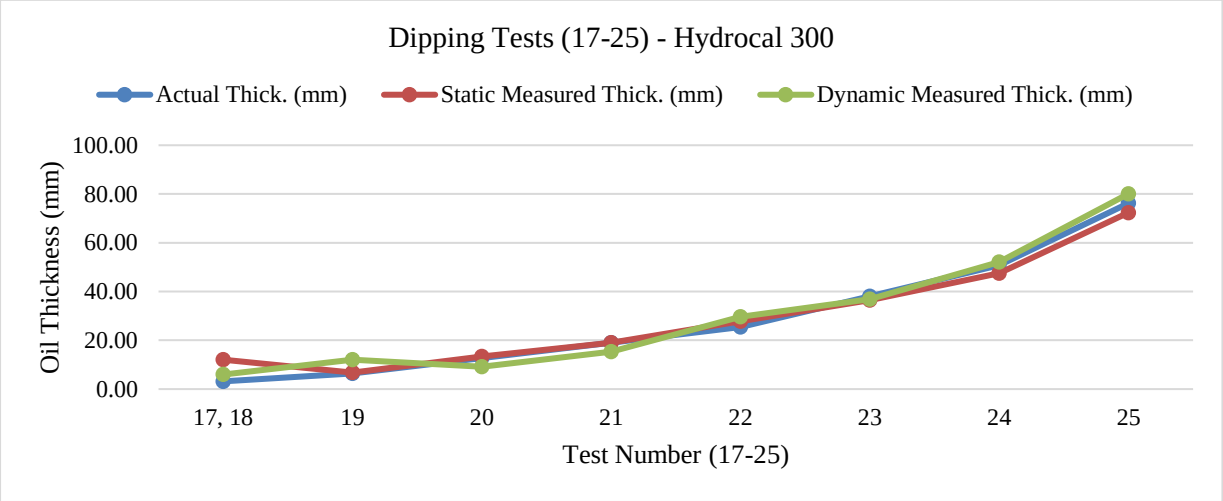

Figure 122: Dipping Tests (17-25) / Hydrocal (Static & Dynamic Curves)

The results of the Hydrocal 300 static experiments shown in Table 45, showed an acceptable accuracy, since all of the tests except for the first one had an absolute error of less than or around 3mm, representing a misclassification of a single electrode. As described before, in this case also, the first test with the smallest oil thickness had the largest error. In the dynamic tests, the "Corrected Lowest Point Algorithm" was proven to produce good results since, as shown in Table 46, all of the dynamic tests showed an average absolute error ranging from around 1mm to a maximum of 5.4mm, representing the misclassification of fewer than two electrodes out of forty-eight. The measurement results of the static and dynamic tests with respect to the actual thicknesses are shown in Figure 122.

7.1.4 *Dipping Tests (26-33) – Calsol 8240*

Tests numbered from 18 to 25 used Calsol 8240 oil with a thickness ranging from 0.125 inches (3.18mm) to 3inches (76.20mm). Water and oil temperature were recorded ranging between 69°F and 70.5°F. Measurements are obtained by the "Corrected Lowest-Point Algorithm" used for heavy oils.

Table 47: Capacitive Sensor Dipping Tests (26-33) – Calsol 8240 / Static

Test Type	**Case**	**Oil Type**				
Dipping	Static	Calsol 8240				
Test Number	**Actual Thickness (mm)**	**Average Measured Thickness (mm)**	**Standard Deviation**	**Sample Size**	**Sample Duration (mm:ss)**	**Average Error (mm)**
26	3.175	8.998	4.415	35	04:57	5.823
27	6.350	10.022	0.878	26	03:48	3.672
28	12.700	10.637	3.277	20	02:47	2.063
29	19.050	26.582	2.419	28	03:56	7.532
30	25.400	30.8	0.767	23	03:13	5.4
31	38.100	37.143	2.014	18	02:29	0.956
32	50.800	47.728	4.633	19	02:38	3.072
33	76.200	73.015	4.447	21	02:55	3.185
				AVG	**03:20**	**3.96**

Table 48: Capacitive Sensor Dipping Tests (26-33) – Calsol 8240 / Dynamic

Test Type	**Case**	**Oil Type**				
Dipping	Dynamic	Calsol 8240				
Test Number	**Actual Thickness (mm)**	**Average Measured Thickness (mm)**	**Standard Deviation**	**Sample Size**	**Sample Duration (mm:ss)**	**Average Error (mm)**
26	3.175	9.886	3.542	26	03:39	6.711
27	6.350	8.882	3.204	26	03:39	2.532
28	12.700	19.946	4.349	30	04:27	7.246
29	19.050	26.018	2.429	26	05:53	6.968
30	25.400	30.658	2.516	25	03:31	5.258
31	38.100	45.322	3.675	30	04:14	7.222
32	50.800	55.234	1.755	23	04:44	4.434
33	76.200	78.29	2.374	23	06:40	2.09
				AVG	**04:35**	**5.30**

Experimental results of testing Calsol 8240 oil in static and dynamic cases showed high accuracy against different thicknesses. For instance, the results of the static case tests shown in Table 47, showed an absolute error ranging from 0.956mm (test 31) to 5.823 mm (test 26). Note that the maximum absolute error in this experiment did not exceed the misclassification of more than two electrodes out of forty-eight. For the dynamic case, despite that the error has slightly increased due to fouling and random sensor movement, the absolute error was also varying in a range between around 2mm to around 7mm, representing one or two misclassified electrodes only. As discussed before, increasing the sensor resolution by making the electrodes thinner, and decreasing the vertical gap between them contributes to decreasing the effect of misclassification. To describe the behavior of all tested cases, Figure 123 shows the measured thicknesses in the static case and the dynamic case with respect to the actual thicknesses.

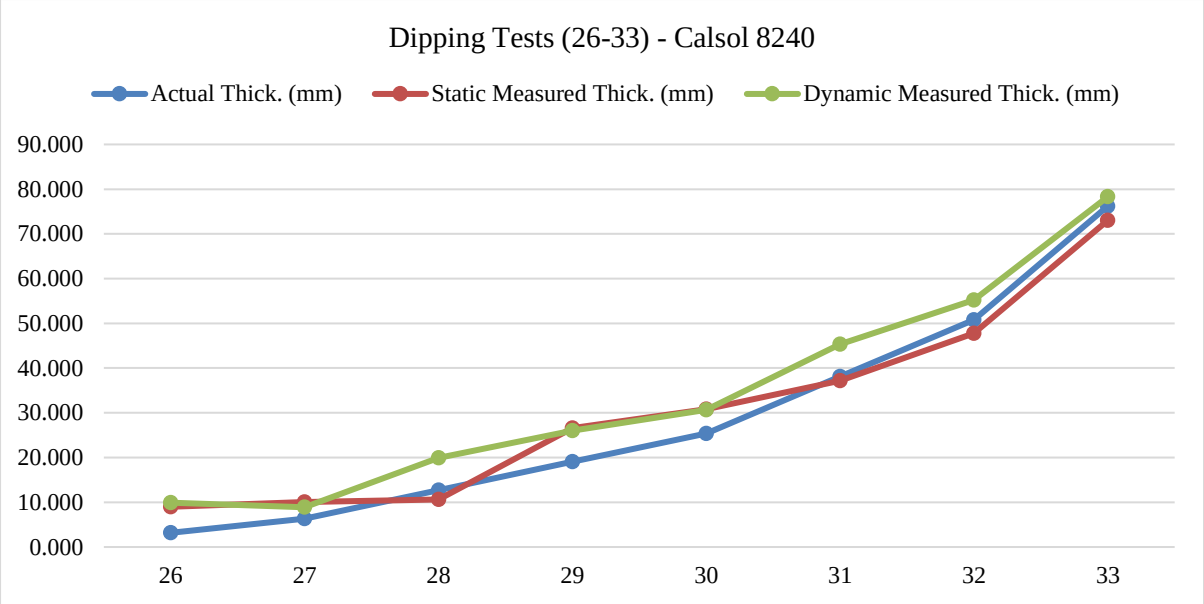

Figure 123: Dipping Tests (26-33) / Calsol (Static & Dynamic Curves)

7.2 Outdoor Bridge Mounted Tests (sensor #1 - Capacitive Sensor)

This test was designed to obtain sensor data while advancing in surface slicks at a range of speeds that are typical when deployed onto spill response equipment or in fast water currents. The test setup was accomplished by preparing a channel along the test basin west wall, using boom attach brackets, end panels and a section of foam filled 24-inch boom (Figure 124). The final channel dimensions were 34 inches wide by 58 ft-6 inches long. This nominal area was used to contain varying slick thicknesses as defined by a test matrix. The slick parameters for this series included thicknesses of 0.25. 0.5, 1.0 and 2.0inches and was repeated using two test oils namely Hydrocal 300 (tests 34 to 61) and weathered Hoops (tests 73 to 86). Test oils were dispensed from totes positioned along the west deck and the volumes determined using physical depth soundings converted to gallons using the manufacturer conversion table. Sensor #1 was attached to the fabricated mount (AUB) which provided the ability to manually rotate the sensor from the deployed position to a raised (above channel barrier elevation) position using a hinge and pull rope. This was monitored during tests by a technician and implemented if needed as a safety to avoid possible collision of the sensor into the barrier. The AUB mount and sensor was attached to an Ohmsett provided mount affixing the sensor to the main bridge providing for vertical adjustment. Figure 124, shows the sensor mounting setup with the sensor raised, boom attached bracket and channel end panel.

Figure 124: Capacitive Sensor – Bridge-mounted Experimental setup

Multiple passes were performed, and sensor data collected while traveling both in the north and south directions at 0.5 and 1.0knots. Passes at 2.0knots and above were performed in the south direction only. A total of 28 Ohmsett data files were recorded when testing in Hydrocal 300 oil and 14 files recorded when testing in Hoops Crude (weathered). Ohmsett files were recorded using LabVIEW software and were subsequently provided to us in an enclosed media drive. The recorded information pertinent to this test includes the speed of the sensor (bridge), the relative bridge position, ambient weather conditions, and the water temperature.

Ohmsett Observations/Notes:

- Wind effects apparently caused the contained slick to stack more towards the downward direction of the wind. When present, the wind was typically from the south direction Figure 125. The wind direction and speeds are provided in the LabVIEW data files for confirmation.
- The target slick thickness was skewed to a lesser thickness especially with 2-inch slicks due to the boom bellying outward, and thereby increasing the surface area (Figure 127).

- While advancing, leading edge of sensor appeared to create a bow wave possibly diverting oil away from the sensor contacts (Figure 126).

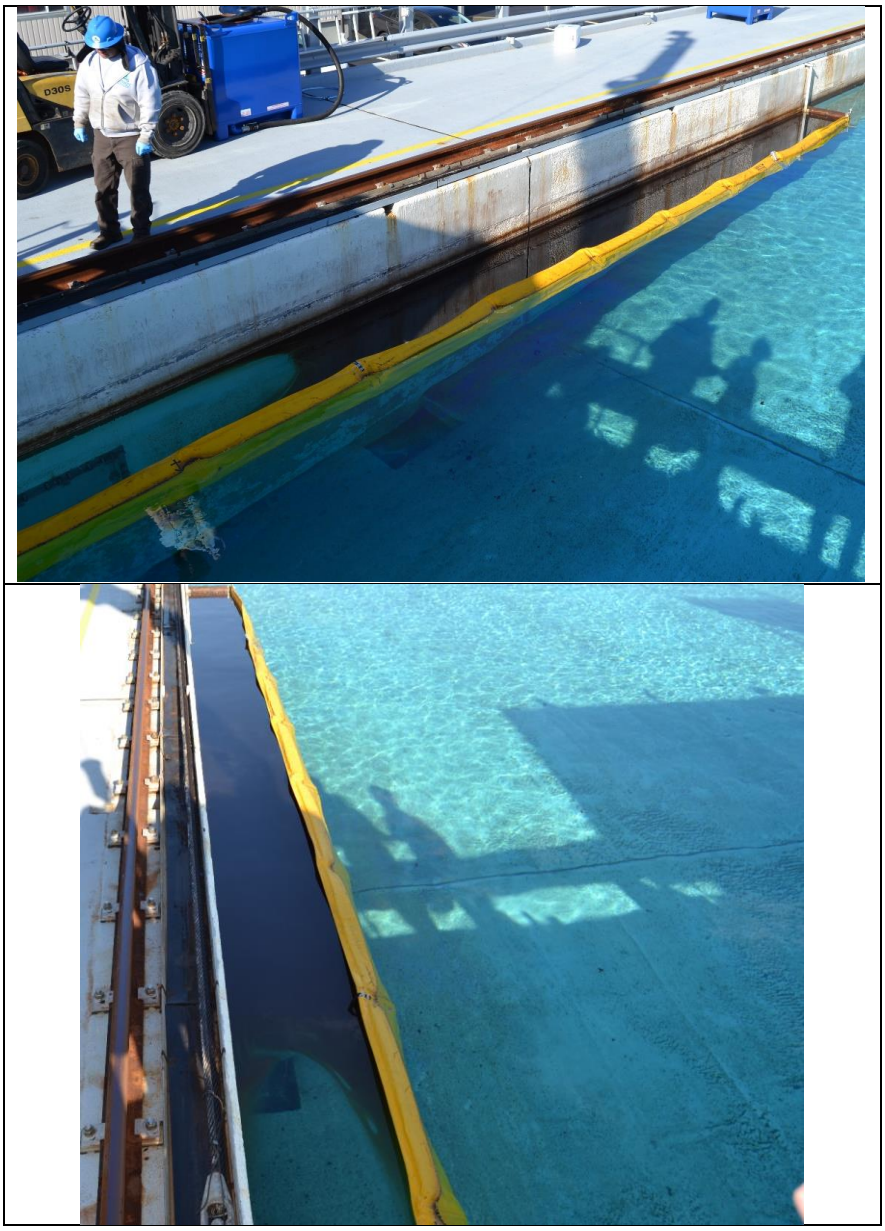

Figure 125: Contained oil in the channel - Wind Effect

Figure 126: Bridge-mounted Sensor while dragging (Snapshot from video# 00131)

Figure 127: Photo showing boom bellying outward

7.2.1 *Dynamic Tests (34, 60) – Hydrocal 300*

Hydrocal 300 dynamic tests were performed using four slick thicknesses, and four advance speeds. The test area is 34" x ~58.5' channel along test basin west wall. The method used in performing the dynamic tests is as follows:

- Prepare defined slick thickness; with the sensor in oil-travel north at test speed, record measurements, stop; reverse direction, record measurements.
- Raise sensor to exit test area, lower sensor into clear basin water, record measurements travel at test speed 30 feet, reverse direction, stop near test area, raise sensor to move into test area, repeat north and south passes and clear water passes 3X.

The ambient weather conditions recorded while performing these tests are shown in Table 49. The results of dynamic experiments are provided in Table 50. Measurements are obtained by the "Corrected Lowest-Point Algorithm" used for heavy oils. For each of the tests, the average of and the standard deviation of the recorded measured thicknesses is provided. Figure 132, shows the plot of the average measured thickness with in comparison to actual (estimated) thicknesses.

Table 49: Ambient weather conditions - Tests (34-60)

Test No.	Avg. Water Temp (°F)	Avg. Wind Speed (mph)	Avg. Wind Direction (°)	Avg. Air Temp (°F)
34	48.63	10.26	103.36	50.95
35	48.78	10.49	102.33	51.16
36	48.78	9.06	114.82	51.33
37	49.01	9.75	111.18	51.66
38	49.43	7.73	124.19	51.83
39	50.04	4.99	125.33	51.87
40	49.31	9.34	134.23	52.22
41	51.73	9.82	130.30	54.07
42	51.62	8.25	139.10	53.59
43	51.75	9.54	126.78	54.04
44	51.91	9.52	137.80	54.08
45	53.02	11.08	137.82	53.38
46	52.39	6.82	142.19	53.21
47	48.64	10.49	142.08	52.50
48	49.34	10.56	148.80	52.38
49	49.67	7.51	149.14	52.49
50	50.11	10.29	136.40	53.29
51	52.96	9.52	136.51	53.32
52	52.45	7.08	158.12	53.75
53	54.14	7.49	153.49	53.31
54	54.98	9.45	150.56	53.85
55	53.82	11.03	157.32	53.89
56	52.48	8.50	161.18	53.78
57	52.42	5.23	143.68	53.92
58	53.07	7.23	129.60	54.16
59	53.00	6.52	144.20	54.17
60	52.70	7.07	123.18	54.13

The measured thickness with respect to time and speed are shown in the figures below (Figure 128-Figure 131) and the average of the acquired measurements in each case are shown in Table 50.

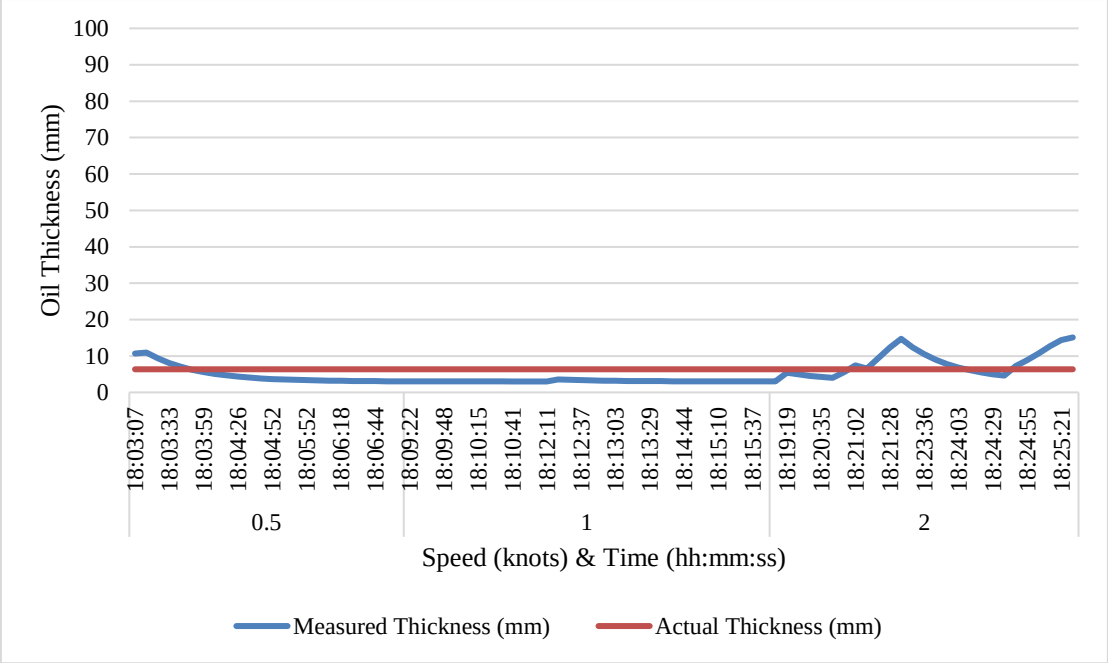

Figure 128: Tests 34 - 40 / Thickness: 6,35mm / Speed: 0.5-1-2 knots

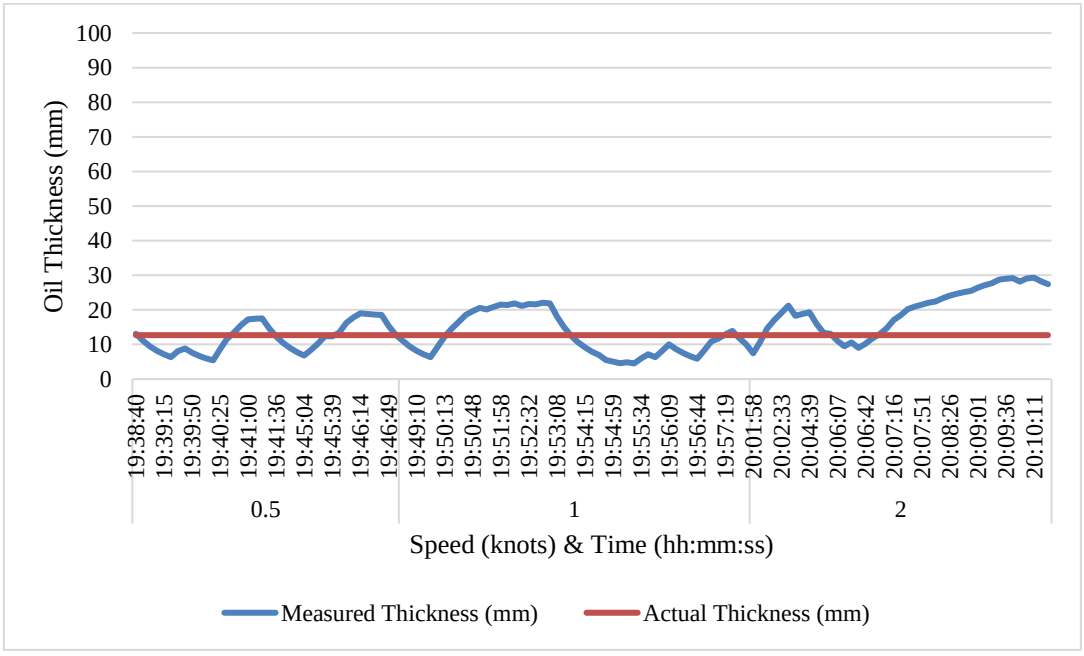

Figure 129: Tests 41 - 46 / Thickness: 12.7mm / Speed: 0.5-1-2 knots

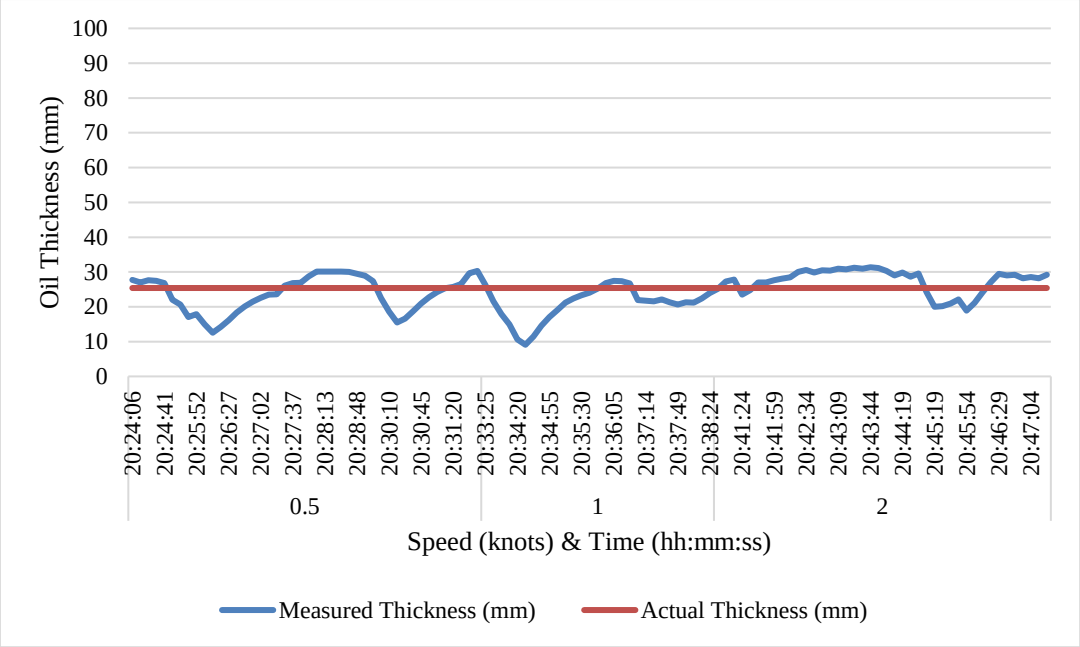

Figure 130: Tests 47 - 52 / Thickness 25.4mm / Speed: 0.5-1-2 knots

Figure 131: Tests 53 - 60 / Thickness 50.08mm / Speed: 0.5-1-2 knots

Table 50: Capacitive Sensor Dynamic Tests (34-60) – Hydrocal 300

Test No.	Bridge/ Sensor Speed (knots)	Actual Thick. (mm)	Average Measured Thick. (mm)	Standard Deviation	Sample Size	Sample Duration (mm:ss)	Avg. Error (mm)	Notes
34, 35	0.50	6.35	9.88	2.45	86	16:09	3.527	Preload: 26 gal, wind effects – slick think at south end
36, 37, 38	1.00	6.35	3.10	0.15	32	06:23	3.253	

39, 40	2.00	6.35	8.10	3.60	27	06:20	1.749	
41, 42	0.50	12.70	11.97	4.26	38	08:18	0.727	Preload: 52 gal
43, 44	1.00	12.70	12.39	5.98	50	08:53	0.313	
45, 46	2.00	12.70	19.89	6.75	43	08:31	7.189	
47, 48	0.50	25.40	23.72	5.19	44	07:40	1.685	Preload: 104 gal
49, 50	1.00	25.40	20.86	4.90	29	04:59	4.537	
51, 52	2.00	25.40	27.43	3.48	42	06:24	2.029	
53, 54	0.50	50.08	33.06	4.71	24	07:42	17.020	Preload: 208 gal - Thickness Measured 1.5 inch (38.1 mm)
55, 56	1.00	50.08	34.10	2.83	29	05:34	15.984	Thickness Measured 1.5 inch (38.1 mm)
57, 58, 59, 60	2.00	50.08	34.60	2.61	22	03:46	15.482	Thickness Measured 1.5 inch (38.1 mm)
					AVG	**07:33**	**6.12**	

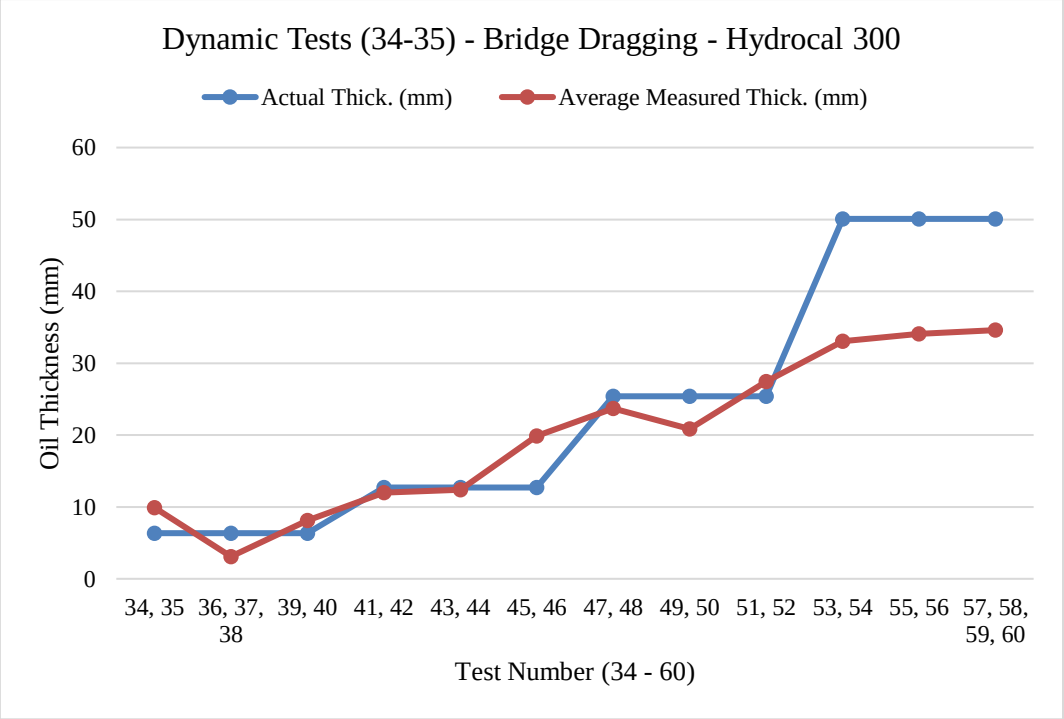

Figure 132: Dynamic Tests (34-35) – Hydrocal

As shown in Table 50, and in Figure 132, the average absolute error in all tests performed while dragging in different speeds ranging from a thickness of 6.35 to 25.04mm ranges between 0.313mm to 7.1mm in the worst case. However, most of these tests showed an impressive accuracy of absolute error less than 6mm, representing the misclassification of fewer than two electrodes out of forty-eight electrodes. Based on the different testing scenarios including different speeds and dragging conditions, this result is considered acceptable. It is obvious that for the last three tests numbered from 53 to 60 where the actual estimated thickness was recorded as 50.08mm, the largest absolute error occurred. However, it is important to note that for this case, and based on the notes provided by Ohmsett, the target slick thickness was skewed to a lesser thickness, especially with 2-inch slicks, due to the boom bellying outward increasing the surface area. Also, Ohmsett staff noted that in this case, the actual

thickness was measured by manual visual tools as 1.5 inches (38.1mm). Based on this fact, and by taking the 38.1mm as the actual thickness, we note that the actual absolute error in these tests was in the range of 4 to 5mm since the measured thicknesses ranged from 33.06 to 34.60mm.

7.2.2 *Dynamic Tests (73, 89) – Hoops (weathered)*

Measurement results obtained from tests (73, 89) were recorded but will not be taken into consideration due to a technical error that occurred in the sensor while performing these tests. Most measurements for these test cases were stuck at the same number indicating a malfunction.

7.3 Skimmer Mounted Tests in Waves (sensor #1 - Capacitive Sensor)

The purpose of this test was to collect slick thickness data when mounted to a typical skimmer while experiencing wave conditions and traveling slowly into and against the waves. The test setup consisted of a boomed area along the test basin west wall measuring 10ft. x 34ft. Sensor #1 was rigidly mounted to a Desmi Termite skimmer frame and positioned between two of the floats, and in front of the skimming weir. The AUB and Ohmsett team provided mounts for vertical adjustment. Prior to testing the skimmer was placed into the test basin and the sensor adjusted such that the waterline was near the center of the measurement range.

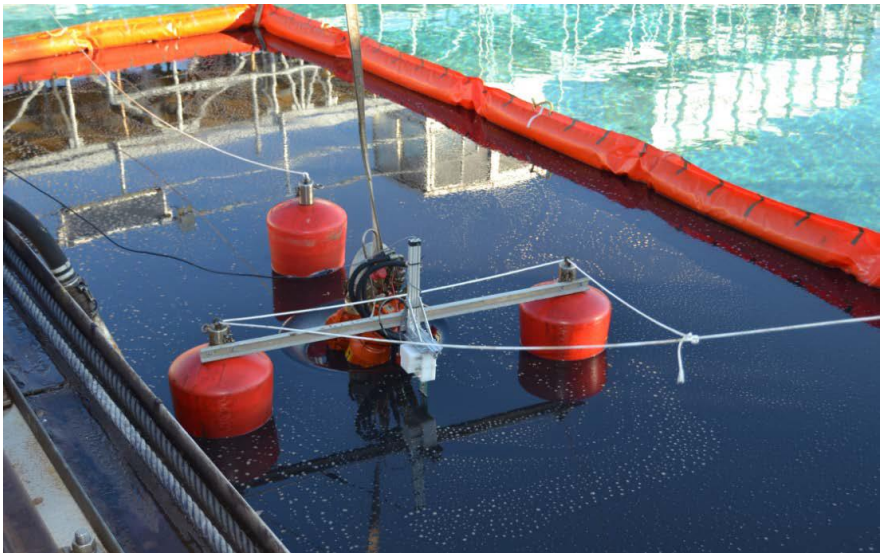

Figure 133: Sensor #1 Mounted to Desmi Termite Skimmer

Figure 133 shows the sensor mounted on the skimmer in the test area. The skimmer was tethered with ropes; one rope routed to each of the main and auxiliary bridges. From these locations, technicians manually controlled the skimmer position and slowly towed the skimmer into the waves. As shown, the waves approached the skimmer from the right (south end of test basin). For these series of tests, Hydrocal test oil was provided at two slick thicknesses: 1 and 3inches. Multiple wave conditions were generated and adjusted during tests to provide wave heights not exceeding the operational range of the sensor. A total of three Ohmsett data files were recorded (tests 90-92) in which surface profile data was captured. Surface profile data, (for wave analysis) was captured using a downward looking distance sensor (named banner west) located on the main bridge. Video and still photos documented the response of the skimmer to the waves. Since the sensor was rigidly mounted to the skimmer, it was subject to the response of the skimmer in waves with respect to pitch, heave, and roll.

Ohmsett Observations/Notes:
Testing performed using hardwire communication – due to wireless not functioning.

Skimmer-mounted Tests numbered from 90, 91, and 93 were performed using Hydrocal 300 oil, two thicknesses, and varied wave conditions. The method used to perform these tests is described as the following:

- Sensor #1 (Capacitive) mounted to skimmer via bracket provided by the AUB team.
- Establish initial sensor depth with a skimmer installed in water.
- Main and auxiliary bridges positioned at opposite ends of the test area.
- The skimmer will be tethered – a control rope going to each bridge.
- Obtain stationary readings; begin wave condition, run test for approximately 15 minutes, manually maneuver skimmer in the area as directed.

The wave properties used in the three tests are summarized in Table 52. Ambient weather conditions are shown in Table 51.

Table 51: Ambient weather conditions - Tests (90-92)

Test No.	Avg. Water Temp (°F)	Avg. Wind Speed (mph)	Avg. Wind Direction (°)	Avg. Air Temp (°F)
90	45.87	7.53	311.70	49.20
91	46.92	10.12	319.09	51.64
92	51.23	10.34	321.88	52.83

Table 52: Skimmer-mounted tests - Wave conditions

Test	Wave Type	Wave Setting	H 1/3 (in.)	Mean Wave Height (in.)	Avg. Wave Period (s)	Average Wave Length (ft.)
90	Sine	15 cpm, 3"	3.412	2.776	4.194	61.026
		25 cpm, 3"	5.265	4.652	2.534	30.543
91	Harbor chop	45 cpm, 3"	8.795	5.752	n/a	n/a
		30 cpm, 3"	4.467	3.588	n/a	n/a
92		15 cpm, 3"	3.533	2.812	n/a	n/a
		25 cpm, 3"	2.683	1.896	n/a	n/a
		25 cpm, 3"	2.72	2.189	n/a	n/a
		35 cpm, 3"	5.094	3.426	n/a	n/a

7.3.1 *Skimmer-mounted Tests - Test No. 90*

- Description: Skimmer mounted, manual pull-in Wave
- Oil Thickness: 1 inch (25.4mm)
- Wave Condition: 9:00am – 1ST setting: 15 cpm, 3" / 2nd setting: 25 cpm, 3"

For the first test, three log files were recorded. The average measurement thickness calculated from each wave experiment, in addition to the starting and ending times are provided in Table 53. Figure 134, shows the measured thickness with respect to time.

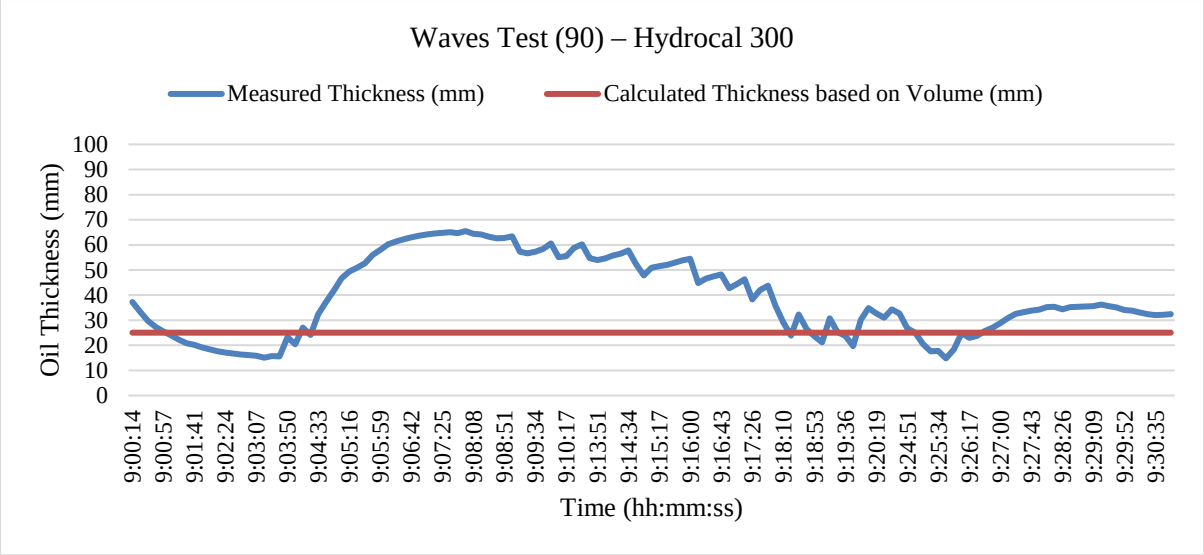

Figure 134: Capacitive Sensor Waves Test (90) – Hydrocal 300

Table 53: Results for Skimmer-mounted (Capacitive - Test 90)

Wave No.	Start Time	End Time	Actual Thick. (mm)	Average Measured Thick. (mm)	Standard Deviation	Sample Size	Sample Duration (mm:ss)	Absolute Error (mm)
1	9:00:14	9:10:50	25.4	43.30	19.24	60	10:36	17.90
2	9:13:51	9:30:57	25.4	35.58	10.91	75	17:06	10.18

The result of the sine test 90 shown in Table 53 and Figure 134, revealed that the sensor's accuracy was impacted mostly by the start of the wave and then the absolute error of the measurement decreased with time even when the second wave was actuated. This is related to two main factors. First, the fouling effect of heavy oil caused by oil accumulation on the sensor body increases the measured thickness especially at starting phase of the wave, where a sudden transition from calm to wave conditions occurs. The second factor is related to smoothing rate used in the algorithm. Smoothing is controlled by the moving average attributes, and based on the current settings, the implemented moving average rate is relatively slow. Speeding up the change rate may contribute to enhancing the recovery process.

7.3.2 *Skimmer-mounted Tests - Test No. 91*

Test No. 91, Harbor chop test. The Wave Condition:

- 10:00 am – 15cpm, 3" (too aggressive, reduced cpm to 30)

Figure 135, shows the measured thickness with respect to time, and average results are shown in Table 54.

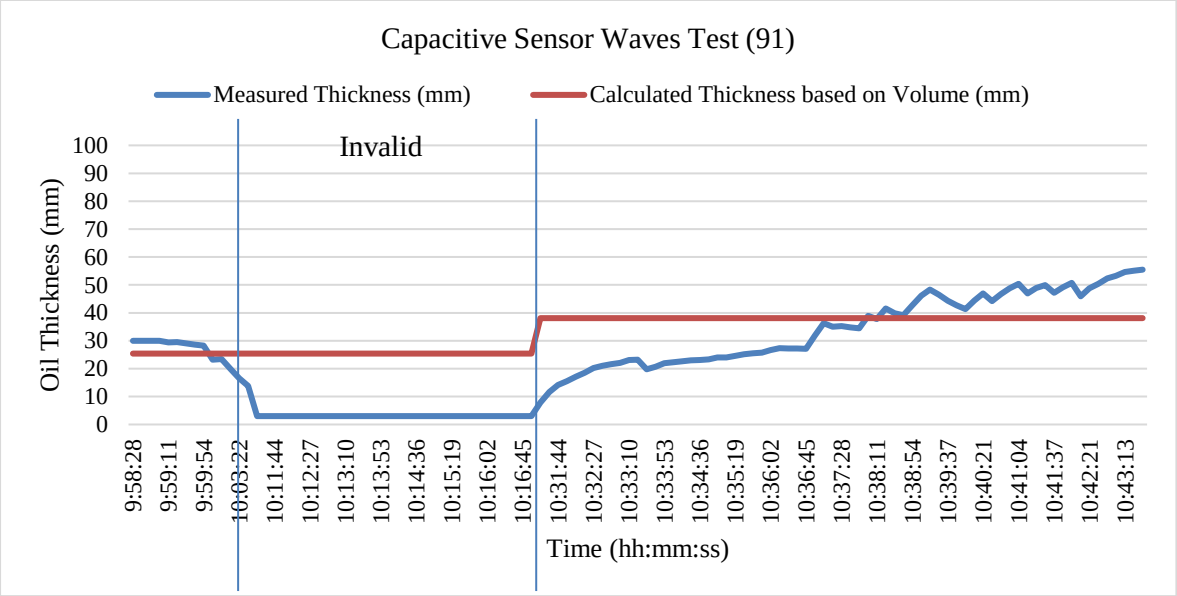

Figure 135: Capacitive Sensor Waves Test (91) – Hydrocal 300

Table 54: Results for Skimmer-mounted (Capacitive - Test 91)

ID	Start Time	End Time	Actual Thick. (mm)	Avg. Meas. Thick. (mm)	Stand. Dev.	Sample Size	Sample Duration (mm:ss)	Absolute Error (mm)	Note
1	09:58:28	10:03:33	25.4	25.837	5.53	14	05:05	0.437	Calm
2	10:11:22	10:16:56	25.4	3	0	32	05:34	-	Sensor dunk into water (3mm – invalid measure)
3	10:31:22	10:43:30	38.1	34.56	12.84	69	12:08	3.54	

The results of the test 91 (Table 54) showed a very high accuracy at the beginning five minutes in calm conditions with an average absolute error of 0.437mm. After the wave was created, based on the notes recorded by the Ohmsett staff, the sensor was dunking into the water. During this time, sensor recorded 3mm for a set of measurements. Actually, the constant 3mm measures are considered invalid since the sensor is located under the oil layer while dunking. After that, starting from 10:31:22, the sensor was producing valid measures. Based on the average of the valid measures taken in the third case, the average absolute error was also acceptable (3.54mm). It is important to note here that the dunking problem is one of the important points that should be taken into consideration in the future development of the device.

7.3.3 *Skimmer-mounted Tests - Test No. 92*

Test No. 92, Harbor chop test. The Wave Condition:

1- 10:55 am – wave started, 15cpm, 3”
2- 11:08 am – increased to 25cpm, 3”
3- 11:18 am – changed to 25cpm, 4.5”

4- 11:21 am – changed to 35cpm, 4.5”
5- 11:25 am – wave stopped

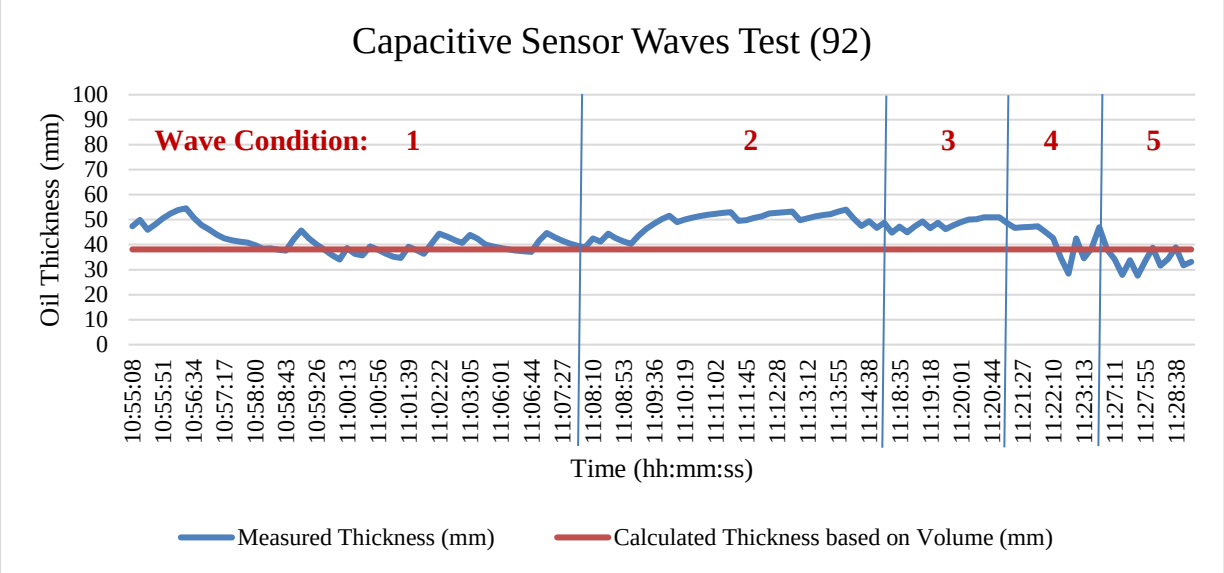

Figure 136: Capacitive Sensor Waves Test (92) - Hydrocal 300

Table 55: Results for Skimmer-mounted (Capacitive - Test 92)

ID	Start Time	End Time	Actual Thick. (mm)	Avg. Meas. Thick. (mm)	Stand. Dev.	Sample Size	Sample Duration (mm:ss)	Absolute Error (mm)	Wave Condition
1	10:51:00	11:03:16	38.10	46.16	7.58	69	12:16	8.07	wave started, 15 cpm, 3”
2	11:05:39	11:14:59	38.10	46.79	5.42	53	09:20	8.69	increased to 25 cpm, 3”
3	11:18:24	11:20:55	38.10	48.33	2.11	15	02:31	10.23	changed to 25 cpm, 4.5”
4	11:21:06	11:23:58	38.10	41.91	6.46	12	02:52	3.81	changed to 35 cpm, 4.5”
5	11:26:24	11:37:21	38.10	41.22	5.39	60	10:57	3.22	stopped
						AVG	**7:35**	**6.80**	

The measured thickness with respect to time and wave conditions is shown in Figure 136. The experimental average results shown in Table 55, shows that the average absolute error of the measured values in the first two cases were similar (8mm). However, the error increased to around 10 mm when the amplitude of the wave was increased to 4.5” in the third case. However, in the last two cases, the average error was highly reduced with the stopping of waves. It is important to note here, that despite the fact the sensor accuracy was affected by the presented wave conditions, the absolute average error

in terms of the sensor resolution was considered acceptable (10mm = 3 strips). Again, it can be concluded that fouling effect must be further mitigated by future enhancements.

We note that the skimmer was powered off during the skimmer tests. Based on the behavior of the skimmer while operation, vibrations may be introduced into the sensor body which may indirectly help in decreasing the fouling effect.

7.4 Slick Thickness Testing (sensor #2 – Spectro Sensor)

The Spectro sensor is designed to identify and measure relatively thin slicks less than 3 millimeters. Tests conditions provided for sensor #2 were primarily created in open-top totes and the slick thicknesses defined using mass balance. Two open top totes were used to provide a known surface area for testing. Each was near filled with saltwater from the Ohmsett test basin and placed in the high bay area for use. One tote was used to provide a known slick thickness for calibration purposes and the second for varying slick thicknesses for measurement. Two oils, diesel and Hoops Crude (fresh) were supplied to create the range of slicks required as per the test matrix. The sensor was calibrated for each oil type used by taking measure at 0mm, 1mm and 3mm.

Ohmsett Observations/Notes:

- 100 and 200um slick thicknesses were difficult to establish, voids and variations were present.
- Use of dark oil (Hoops Crude) reduced the measurement range due to lack of transparency. The matrix was modified to use a narrower range of thicknesses; 100 to 700um.

7.4.1 *Spectro Sensor Tank Test - Diesel*

Spectro sensor Thickness Measurement Tests (high bay - slick prepared in 38. 5” x 44.0” x 30” poly tank). The testing method is summarized as follows:

- Prepare slick in defined tray on basin water
- Place sensor onto slick, obtain readings.
- Add oil to the slick, obtain readings

The experimental results showing the average estimated thickness versus the actual thickness (estimated by volume) are shown Table 56 and the corresponding graph is shown in Figure 137.

Table 56: LED-based Sensor - Diesel / Tank Experiment (Measured Thicknesses)

Test	Thick. (µM)	Average Measured Thickness (µM)	Abs. Error (µm)	S.D.	Sample Size	Sample Duration (mm:ss)	Notes
63	500	1422.79	922.79	954.35	63	02:06	Thin slick difficult to accomplish
64 - Trial 1	1000	1485.94	485.94	863.82	65	02:08	Sensor moving around
64 - Trial 2	1000	1544.56	544.56	1288.49	48	01:34	Sensor moving around
65 - Trial 1	2000	1882.72	117.28	1043.50	87	02:52	Sensor moving around
65 - Trial 2	2000	2162.05	162.05	815.72	91	03:00	Sensor moving around
66	3000	2745.70	254.3	395.76	105	03:30	adding oil from 2mm to 3mm.
		AVG	**414.48**		**AVG**	**02:31**	

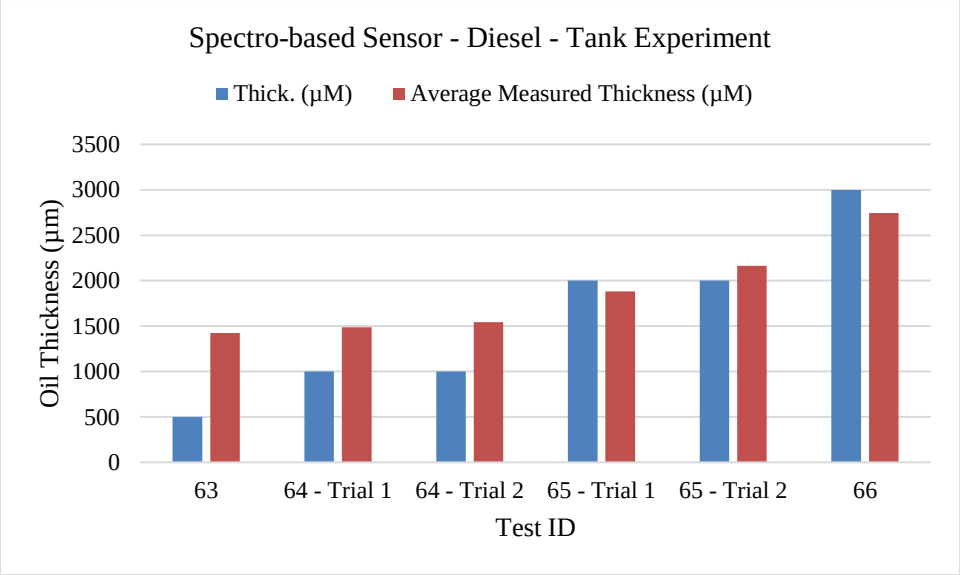

Figure 137: Spectro-based Sensor - Diesel / Tank Experiment (graph)

As shown in figures above, the results showed an acceptable accuracy with an absolute error of 200 - 300µm in the last three tests where the actual thickness was estimated at 2000 and 3000µm. However, the average error was around 500µm at the 1000µm thickness test and increased when testing thinner thicknesses. For interpreting this result, it is important to note that thicknesses below 500µm were difficult to establish in all cases since the oil had an irregular distributed film as shown in the picture of Figure 138 and therefore the actual thickness was larger.

Figure 138: LED-based Sensor - Diesel Test (Tank)

7.4.2 *Spectro Sensor Tank Test – Hoops (fresh)*

The same experimental setup and method were used to test the spectro sensor against Hoops (fresh) oil. The experimental results are shown in Table 57, and the corresponding graph in Figure 139.

Table 57: LED-based Sensor - Hoops / Tank Experiment (Measured Thicknesses)

Test	Thickness (µM)	Average Estimated Thickness (µM)	Abs. Error (mm)	S.D.	Sample Size	Sample Duration (mm:ss)	Notes
68 - trial 1	100	981.82	881.82	10.51	54	02:06	Fouling (lens)
68 - trial 2	100	815.03	715.03	244.39	126	04:12	after cleaning lens and dipping
69	200	894.96	694.96	110.26	70	02:18	Hoops was observed not uniform
70	300	549.45	249.45	389.42	145	05:12	Oil pushed in and out and moved around
71	500	792.78	292.78	310.97	107	03:56	moving around and clearing oil then moving in.
72	700	841.32	141.32	314.31	237	09:58	moving sensor
		AVG	**495.89**		**AVG**	**04:37**	

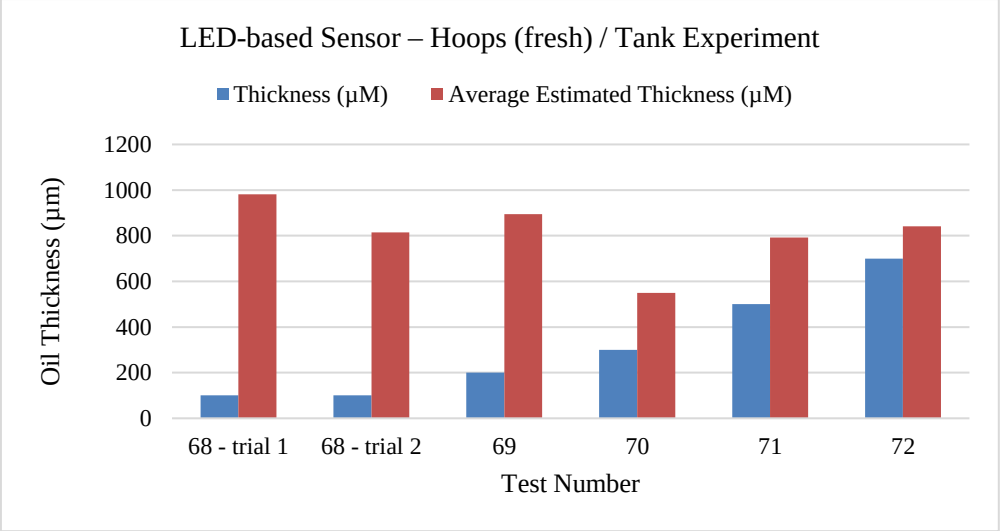

Figure 139: LED-based Sensor – Hoops (fresh) / Tank Experiment (Graph)

In this experiment, because of the dark color of the Hoops (fresh) oil, fouling of the light-emitter lens was clearly observed (Figure 140). It was observed also that the oil was not uniformly distributed (Figure 141).

Figure 140: Lens fouling – Hoops (fresh)

Figure 141: Non-uniform Distribution (Hoops)

For the last three tests (70, 71, and 72), the measurement accuracy was acceptable with an average absolute error ranging from 141µM to 249µM. However, for the first three tests, the calculated error with the theoretically calculated thickness was relatively high (around 700 µM). However, this result is not conclusive since ground truth cannot be verified at these thicknesses. It is worth noting that during testing it was observed that when clear water patch passed under the sensor it gave low (down to 0 in some cases) measures and when oil slick passed under the thickness increased.

7.4.3 *LED-based Waves Test - Diesel*

The LED-based sensor floating experiment was performed within in open-water testing area; tested in thin "slicks" in test basin 10' x 30' area. The method used in implementing the tests is as follows:

- Deploy sensor #2 into area after preparing slick
- Allow it to drift. (have lightweight rope /string for control and retrieval)

Test No. 92, Wave Condition:

1- 10:55 am – wave started, 15cpm, 3"
2- 11:08 am – increased to 25cpm, 3"
3- 11:18 am – changed to 25cpm, 4.5"
4- 11:21 am – changed to 35cpm, 4.5"
5- 11:25 am – wave stopped

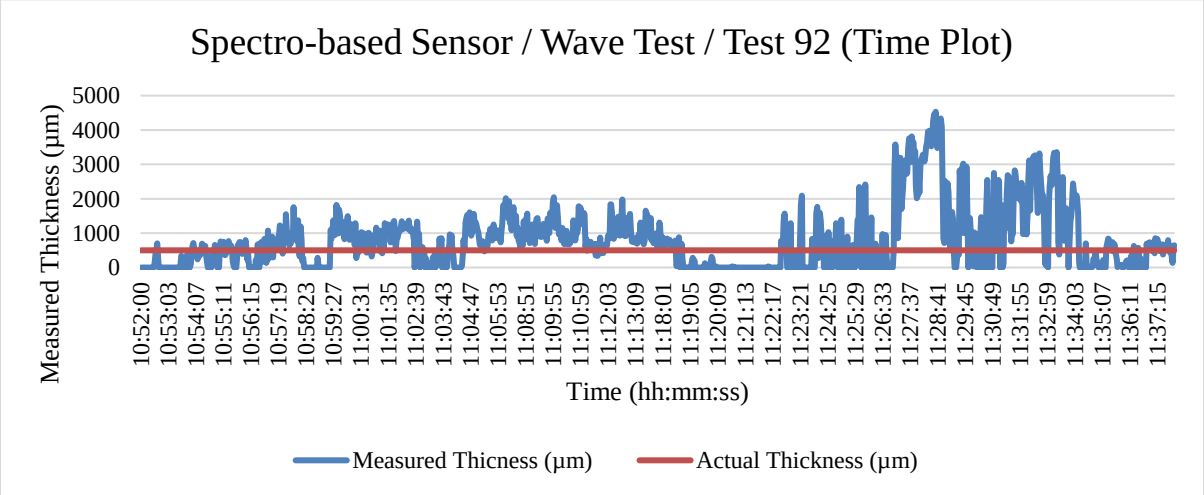

Figure 142: Spectro-based Sensor - Test 92 - Waves (1, 2)

Table 58: Spectro-based Sensor - Diesel / Waves Experiment

ID	Start Time	End Time	Avg. Meas. Thick. (µm)	Actual Thick. (µm)	Abs. Error (µm)	S.D.	Sample Size	Sample Duration (mm:ss)	Wave Condition
1	10:52:00	11:05:57	545.81	500	45.81	471.43	419	13:57	10:55am, wave started, 15cpm, 3”
2	11:07:49	11:13:43	1072.61	500	572.61	391.05	175	05:54	11:08am, increased to 25cpm, 3”
3	11:17:33	12:17:33	274.11	500	225.88	381.54	104	0:03:26	11:18am, changed to 25cpm, 4.5”
4	11:21:01	11:24:59	273.72	500	226.27	515.91	120	0:03:58	11:21am, changed to 35cpm, 4.5”
5	11:25:01	11:37:55	1246.72	500	746.72	1259.33	120	0:12:54	11:25am, stopped

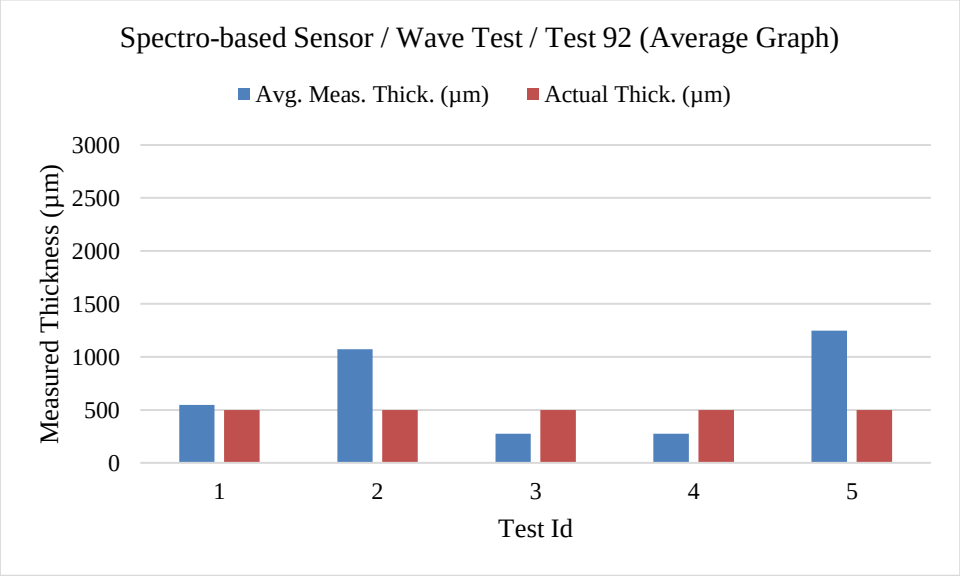

Figure 143: Spectro-based Sensor - Test 92 - Average graph

The measured thicknesses with respect to time are shown in Figure 142, and the average thickness with respect to each wave condition is shown in Figure 143. As shown in some cases the sensor measures 0 which is expected as visually it was evident there were clear patches within the ring due to the non-uniform spread of the oil. The average of the measured oil thicknesses in each of the five wave conditions is presented in Table 58. It is noted that in this experiment, measurements obtained from the Spectro-based sensor (Table 58) showed high standard deviation values in all cases. This result was expected due to the behavior of the sensor in waves. However, for a baseline value of around 500µM, the sensor was able to measure 545µm in test 1 and around 247µm in tests 3 and 4. The other tests showed an average measurement ranging from 1072µm to 1246µm. As the main aim of the test was to assess the ability of the sensor to detect thin oil slicks, this result proved the ability of the sensor to

detect and estimate the oil slick even with a slightly increased error in harsh dynamic conditions. It is worth noting that in such a test the ground truth cannot be controlled and thicker/darker oil from the nearby test seeped into the ring with diesel as shown in Figure 144.

Figure 144: Experimental area - Test 92

Chapter 8- Conclusion, Recommendations and Future Development

We believe that most of the project objectives were met but there is still room for improvement. Several prototypes of the two sensors were developed and one of each of the latest models was kept at Ohmsett. Overall, the testing at Ohmsett was very successful in testing the limits of both sensors and identifying areas of improvement. We believe both sensors accomplished most aspects of TRL 5.

Based on the assessment of the experimental results obtained from the tests done at the Ohmsett facility and aiming to improve the performance of the presented sensors in real working conditions, we propose to consider several enhancements to the two sensing devices as a future development plan.

For the capacitive sensor, several important points will be addressed, including the following:

1- Although the fouling effect was significantly mitigated by the knife design, pins and the algorithms, it remained the main source of error, especially when dealing with heavy oils and highly dynamic conditions (waves and splashing). To handle this problem, we suggest improving the mechanical design of the anti-fouling mechanism used in the capacitive sensor, including the implementation of the staggered horizontal pins, using hydrophobic coating materials, and/or the inclusion of a vibrator on the sensing board to help remove fouling.

2- Another limitation that appeared during the testing of the capacitive sensor against waves is the dunking of the sensor package in the examined liquid. One suggested remedy is by changing the design of the device in a way where the processing unit will be completely separated from the sensing unit. By doing so, the sensing unit length will be extended to be longer and extending significantly outside the oil surface, allowing the sensor to move freely through the oil/water mixture. Another option is to mount the device on a float, which would allow motion in only a vertical direction.

3- Use case Specifics: it was observed that there is a need for two types of capacitive sensors. One designed specifically to be handheld and standalone giving measures directly on a screen and another one to be mounted on skimmers.

4- We believe the sensor can be further developed to reach TRL 6 but there are operational considerations that need to be addressed such as protection from floating debris, faster response rate, and easier deployment.

5- To enhance the sensor resolution, and to decrease the impact of electrodes misclassification on the measured thickness, we suggest changing the electrodes design by decreasing the single electrode width and the vertical gap distance between the electrodes. This will increase the sensor resolution and accuracy.

6- Other limitations appeared during the testing such as failure of wireless connectivity and processing/memory limitations. We suggest replacing the main processing unit by a more advanced module, providing more advanced processing and storage capabilities. To attain low cost, compact size, and simplicity, we propose to use the “RASPBERRY Pi ZERO” module instead of the Arduino modules. To ensure a reliable wireless connection, the RF modules will

be replaced with more advanced units allowing the real-time configuration of the wireless settings. As a backup for communication, a cable connection will be provided as a built-in feature in the device.

7- As an enhancement, we propose to store all the raw data of the sensor for future debugging and analysis, an SD card slot will be installed in the device allowing the insertion of memory cards with several GBs into the device. Also, the memory cards will be used to record measured thickness values, GPS coordinates, and any other required notes during the tests.

For the LED-based spectrometer device, several enhancements will be taken into account in the future design including the following:

1- It was observed that the light-source unit located underwater was highly affected by the fouling of oil while inserting and removing the device from the water/oil mixture. To avoid this problem, an alternative design relying on light/laser reflection will be tested. Based on the concept of light reflection, the light source unit will be placed above the water surface and aiming downwards, and the light sensor will be measuring the intensity of light beams reflected from the liquid surface. The main advantage of this approach is that it provides protection to the light emitter and receiver lenses from oil/water contamination. In addition, laser instead of LED emitters should be considered.

2- It is suggested that the buoy design be enhanced to isolate the sensor/emitter lenses from liquid splashing while operating in harsh dynamic environments.

3- We suggest to include an array of light emitters and receivers instead of a single light emitter/receiver. The use of arrays, in this case, will contribute to decreasing the high-frequency measurement fluctuations caused by bubbles and irregular oil films floating on the water surface.

4- The calibration of the sensor to different oils should be made more flexible to allow more/less data points.

5- We believe the sensor can be further developed to reach TRL 6 but there are operational considerations that need to be addressed such as easier deployment, protection from floating debris, and reducing the buoy size.

6- Similar to the electrical design enhancements discussed in the capacitive sensor section, we suggest that the wireless communication, storage, and processing features be enhanced.

References

[1] F. Aguilera, J. Méndez, E. Pásaroa, and B. Laffona, "Review on the effects of exposure to spilled oils on human health," J. Appl. Toxicol., vol. 30, no. 4, pp. 291–301, 2010.

[2] F. Nunziata and M. Migliaccio, "Oil Spill Monitoring and Damage Assessment via PolSAR Measurements," Aquat. Procedia, vol. 3, pp. 95–102, 2015.

[3] C. Federici and J. Mintz, "Oil Properties and Their Impact on Spill Response Options Literature Review," CNA Anal. Solut., no. 1, pp. 1–92, 2014.

[4] ITOPF, "Aerial Observation of Marine Oil Spills," no. 1, p. 12, 2011.

[5] V. Karathanassi, "Spectral Unmixing Evaluation for Oil Spill Characterization," Int. J. Remote Sens. Appl., vol. 4, no. 1, 2014.

[6] O. P. N. Calla, H. K. Dadhich, S. Singhal, "Oil Spill Detection using Multi Frequency Microwave Sensor Onboard Satellite; SSM/I and AMSR-E," IGARSS, pp. 3710–3713, 2013

[7] O. P. N. Calla, N. Ahmadian, and S. Hasan, "Estimation of emissivity and scattering coefficient of low saline water contaminated by diesel in Cj band (5.3 GHz) and Ku band (13.4 GHz)," Indian J. Radio Sp. Phys., vol. 40, no. 5, pp. 267–274, 2011.

[8] H. Denkilkian, A. Koulakezian, R. Ohannessian, M. S. Chalfoun, M. K. W. Joujou, A. Chehab, and I. H. Elhajj, "Wireless sensor for continuous real-time oil spill thickness and location measurement," IEEE Trans. Instrum. Meas., vol. 58, no. 12, pp. 4001–4011, 2009.

[9] A. Massaro, A. Lay-Ekuakille, D. Caratelli, I. Palamara, and F. C. Morabito, "Optical performance evaluation of oil spill detection methods: Thickness and extent," IEEE Trans. Instrum. Meas., vol. 61, no. 12, pp. 3332–3339, 2012.

[10] F. N. Toth, G. C. M. Meijer, and M. Van Der Lee, "A planar capacitive precision gauge for liquid-level and leakage detection," IEEE Trans. Instrum. Meas., vol. 46, no. 2, pp. 644–646, 1997.

[11] S. C. Bera, J. K. Ray, and S. Chattopadhyay, "A low-cost noncontact capacitance-type level transducer for a conducting liquid," IEEE Trans. Instrum. Meas., vol. 55, no. 3, pp. 778–786, 2006.

[12] B. Kumar, G. Rajita, and N. Mandal, "A Review on Capacitive-Type Sensor for Measurement of Height of Liquid Level," Meas. Control, vol. 47, no. 7, pp. 219–224, 2014.

[13] T. Yeh and S. Tseng, "A Low Cost LED Based Spectrometer," Journal of the Chinese Chemical Society, 2006, 53, 1067-1072, 2006

[14] Texas Advanced Optoelectronic Solutions Inc., "TSL230R−LF, TSL230AR−LF, TSL230BR−LF Programmable Light-to-frequency Converters," TAOS079A, October 2006.

[15] RLX COMPONENTS s.r.o. Electronic Components Distributor, "Light to Frequency Board (MIKROELEKTRONIKA)," [Online]. Available: http://rlx.sk/en/measurement-boards/448-light-to frequency-board-mikroelektronika.html. [Accessed: Feb-2017].

[16] Mikroelektronika, "Light to Frequency Additional Board – User Manual," 2017.

[17] Electronics Katranji Trading (EKT), "412 CH GPS SKM53 MODULE," [Online]. Available: http://www.ekt2.com/products/productdetails/412_CH_GPS_SKM53_MODULE. [Accessed: Feb-2017].

[18] Electronics Katranji Trading (EKT), "412 Arduino NANO 3.0 328 CH340," [Online]. Available: http://www.ekt2.com/products/productdetails/412_ARDUINO_NANO_3.0_328_CH340. [Accessed: Feb-2017].

[19] Electronics Katranji Trading (EKT), "412 Arduino WIRELESS TRANSCEIVER 2.4Ghz," [Online]. Available:http://www.ekt2.com/products/productdetails/412_ARDUINO_WIRELESS_TRANSCEIVER_2.4Ghz. [Accessed: Feb-2017].

[20] Electronics Katranji Trading (EKT), "8 D37 MALE PCB," [Online]. Available: http://ekt2.com/products/productdetails/8_D37_MALE_PCB. [Accessed: Feb-2017].

[21] Electronics Katranji Trading (EKT), "8 D37 FEM PCB," [Online]. Available: http://ekt2.com/products/productdetails/8_D37_FEM_PCB. [Accessed: Feb-2017].

[22] Nano Protech, "Super Electrical Insulation Nano Protech," [Online]. Available: http://www.nanoprotech.mk/home-page/super-electrical-insulation/. [Accessed: Feb-2017].

[23] Freescale Semiconductor, "Proximity Capacitive Touch Sensor Controller MPR121," Technical Data Sheet, 2013.

[24] "Ultra Ever Dry | Slovenija". Ultraeverdry.si. N.p., 2017. Web. 29 Mar. 2017.

[25] "Ultratech | Ultra-Ever Dry | Ultratech International". Spillcontainment.com. N.p., 2017. Web. 29 Mar. 2017.

[26] Hartigan, J. A., and M. A. Wong. "Algorithm AS 136: A K-Means Clustering Algorithm." Journal of the Royal Statistical Society. Series C (Applied Statistics) 28, no. 1 (1979): 100-08. doi:10.2307/2346830.

[27] SparkFun Electronics, "SparkFun Capacitive Touch Sensor Breakout – MPR121," [Online]. Available: https://www.sparkfun.com/products/retired/9695. [Accessed: Feb-2017].

[28] DESMI, "Skimmers/TERMITE", [Online]. Available: http://www.desmi.com/skimmers/termite.aspx. [Accessed: Jan-2018]

Appendix

Note: All dimensions are in centimeters

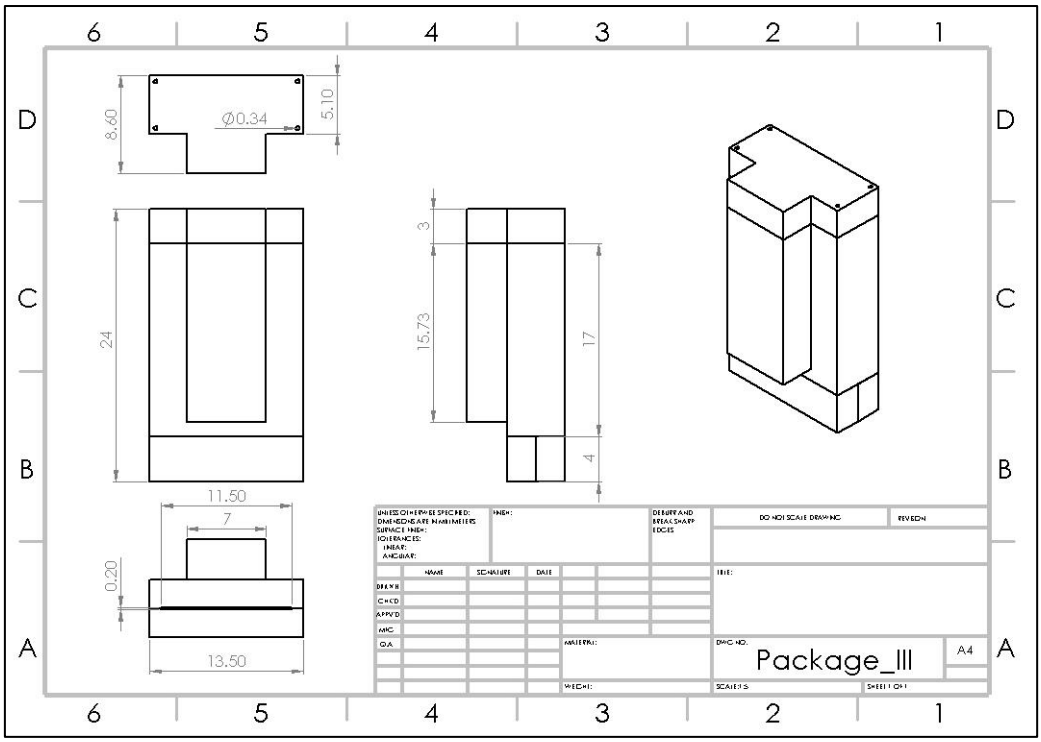

Figure 145: Capacitive sensor package iteration 1

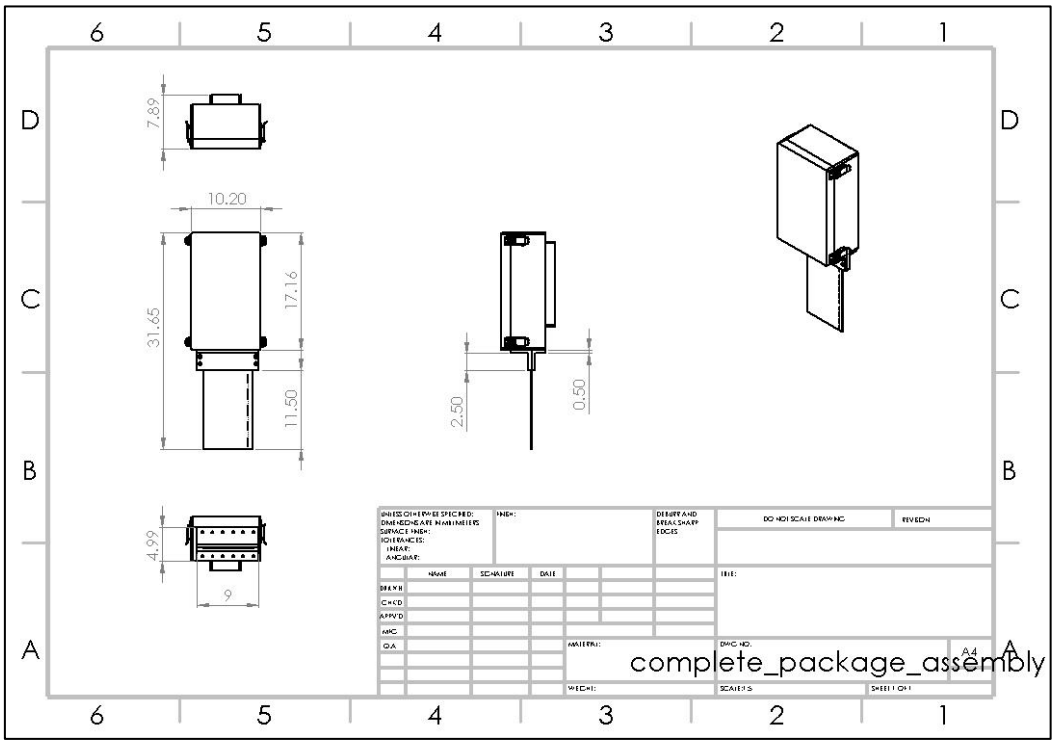

Figure 146: Alpha capacitive sensor package (assembly)

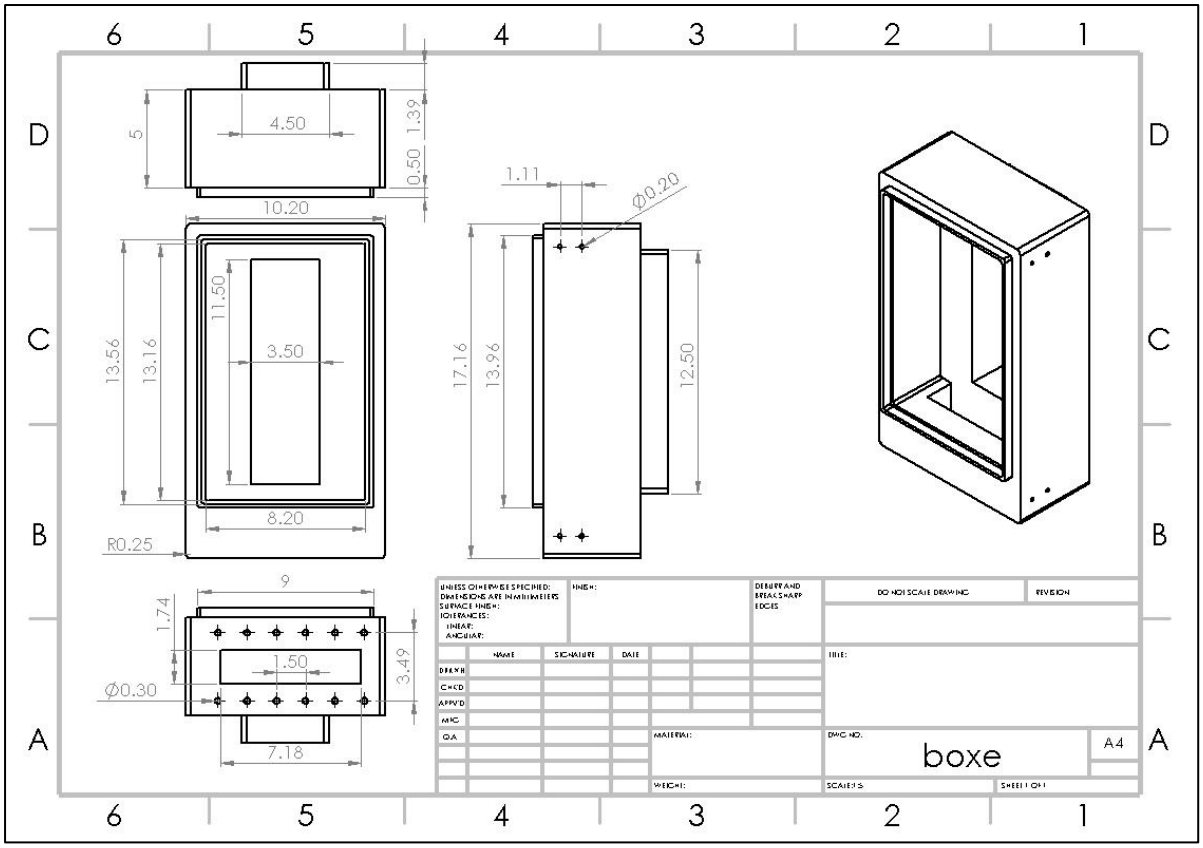

Figure 147: Alpha capacitive sensor package (controller board compartment)

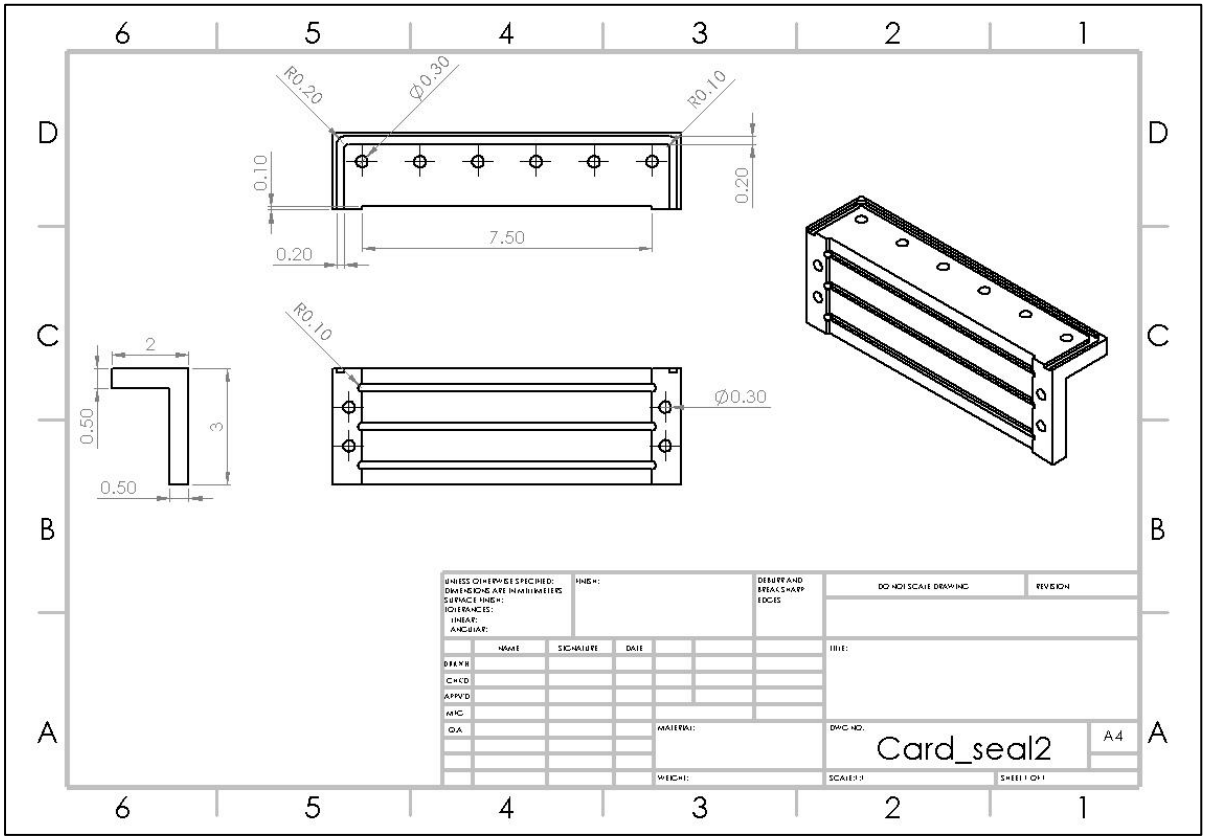

Figure 148: Alpha capacitive sensor package (sensor card lip seal)

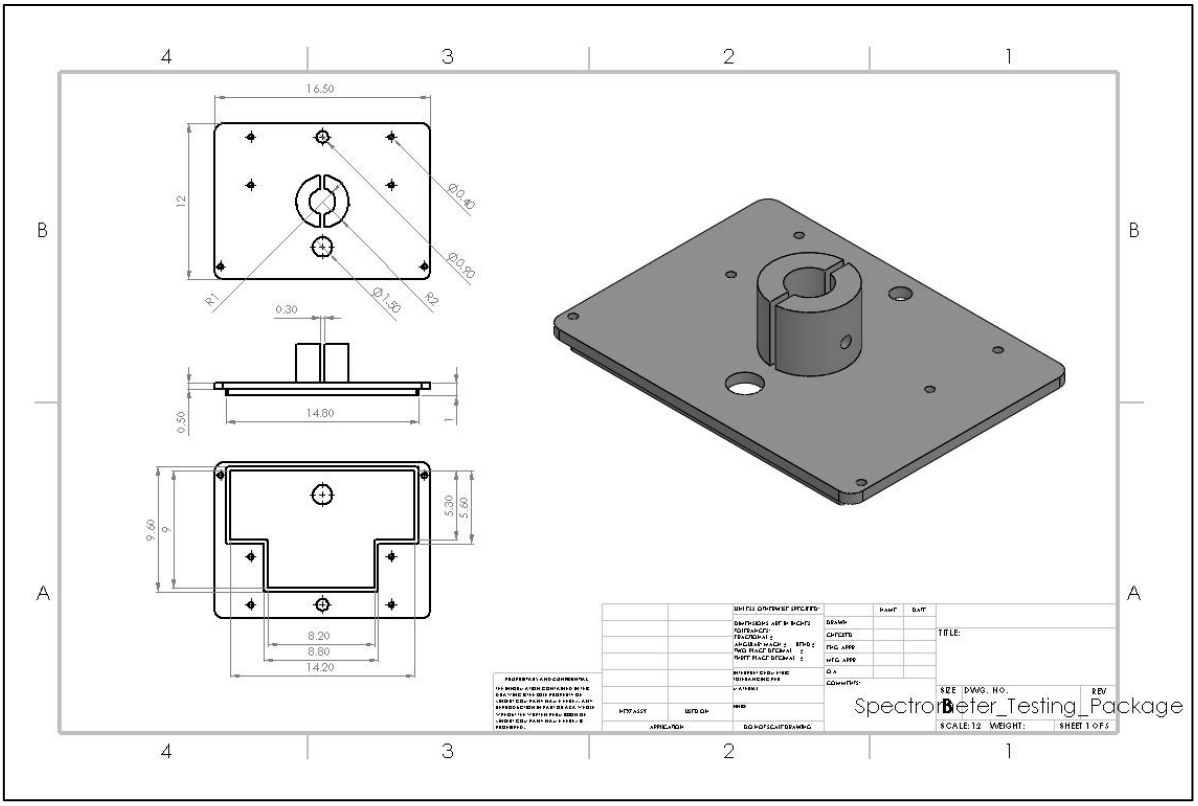

Figure 149: LED based sensor top cap

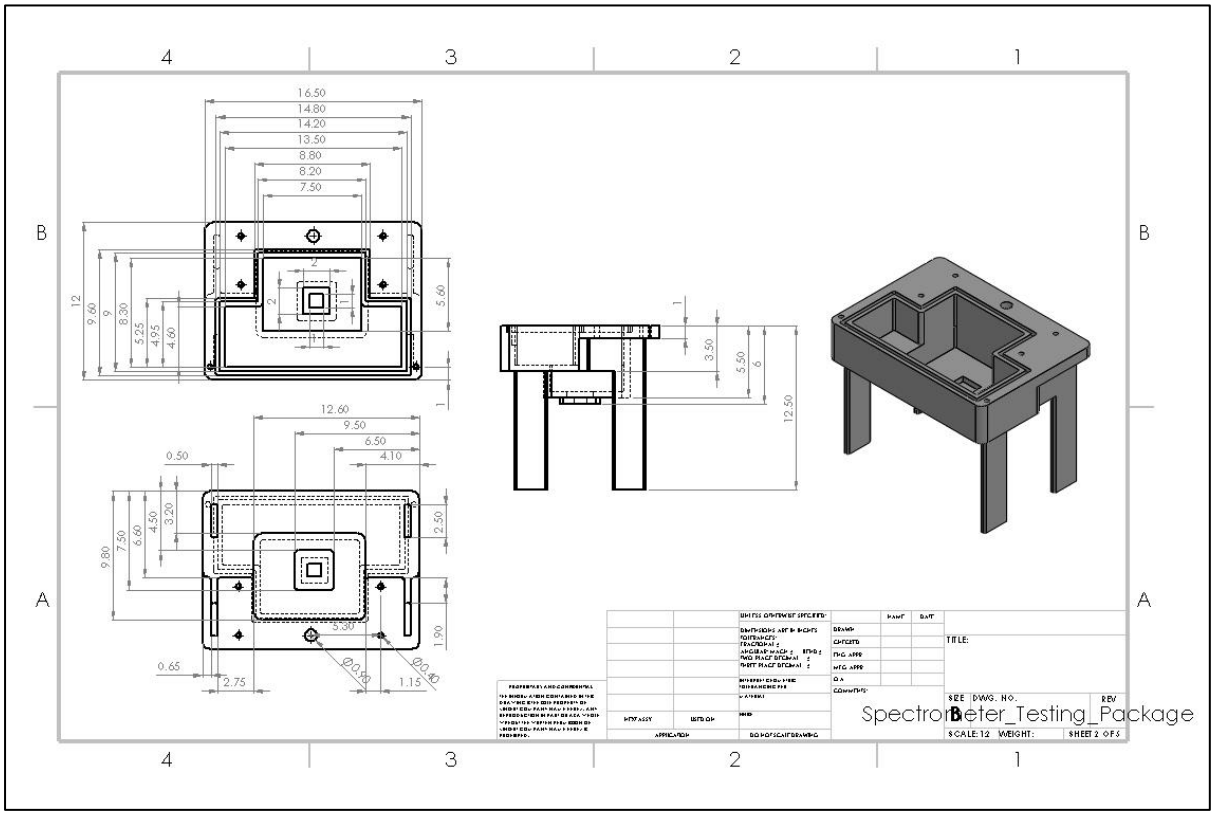

Figure 150: Spectro sensor holder

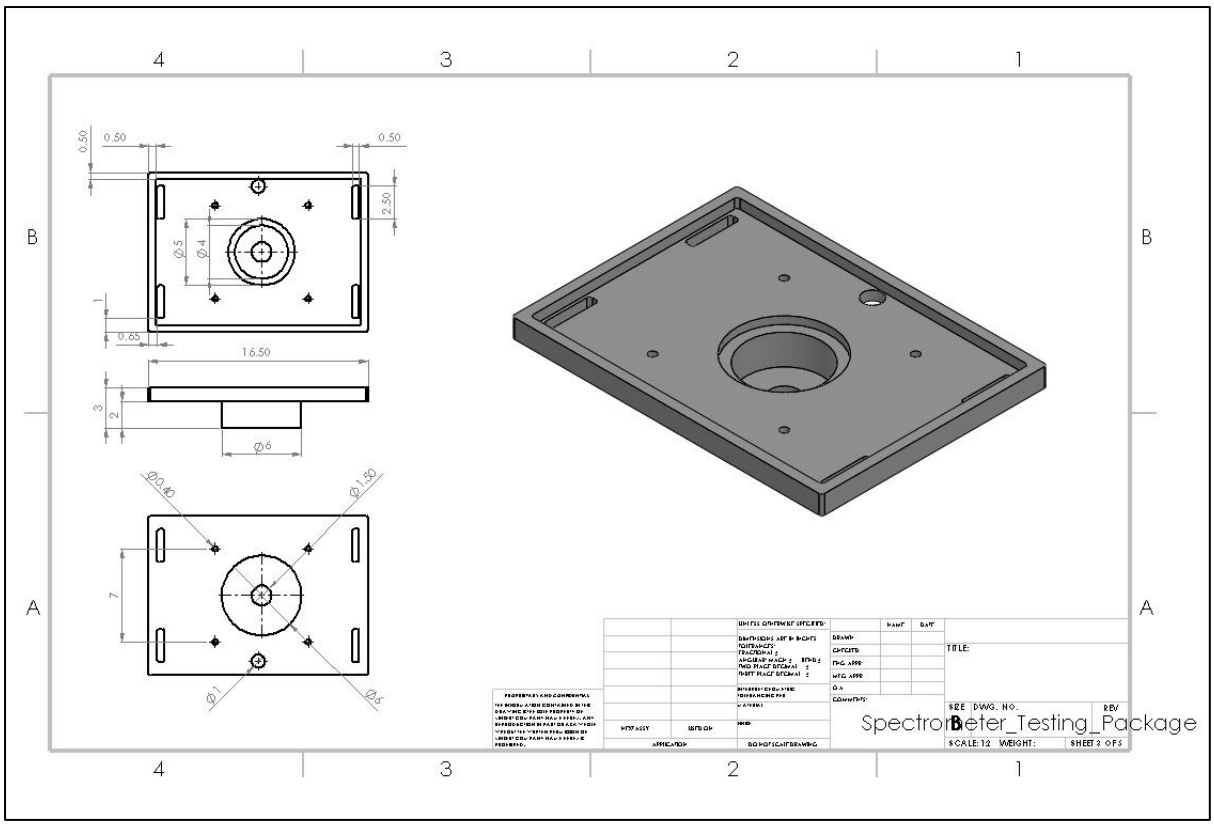

Figure 151: LED case

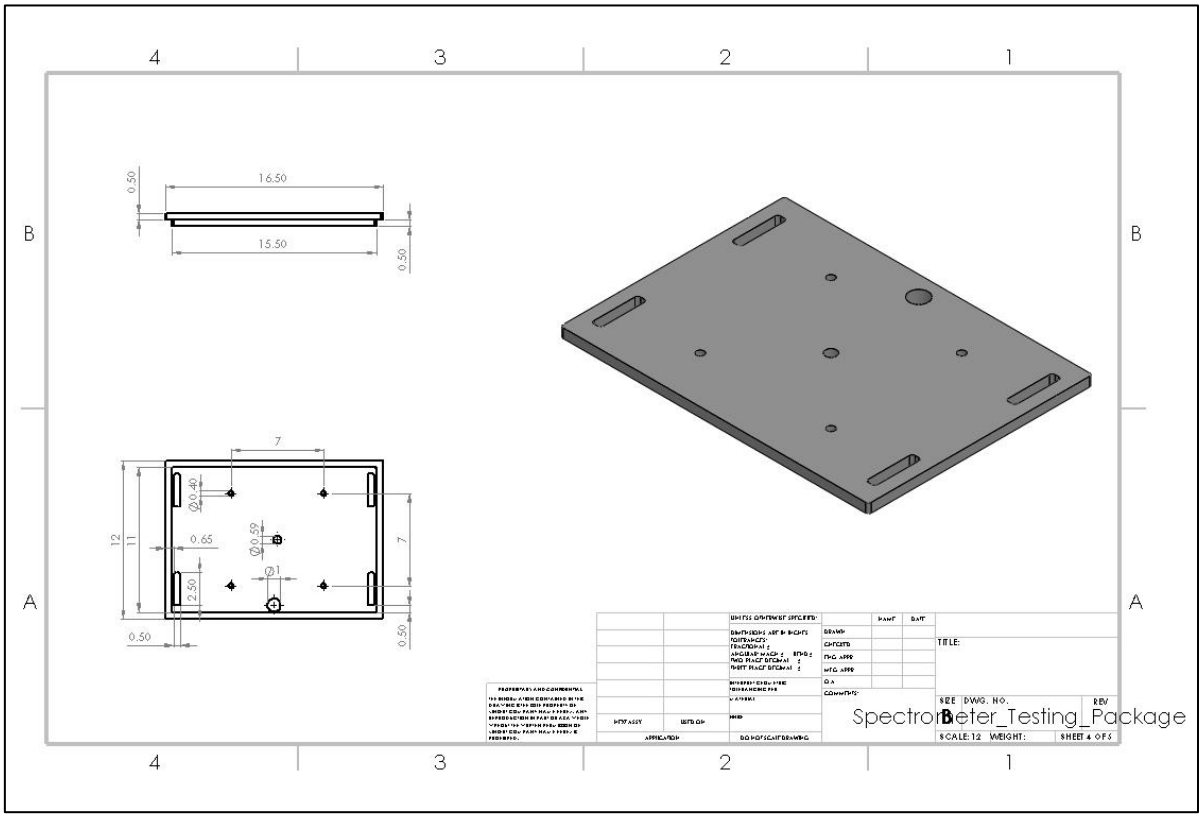

Figure 152: LED case cap

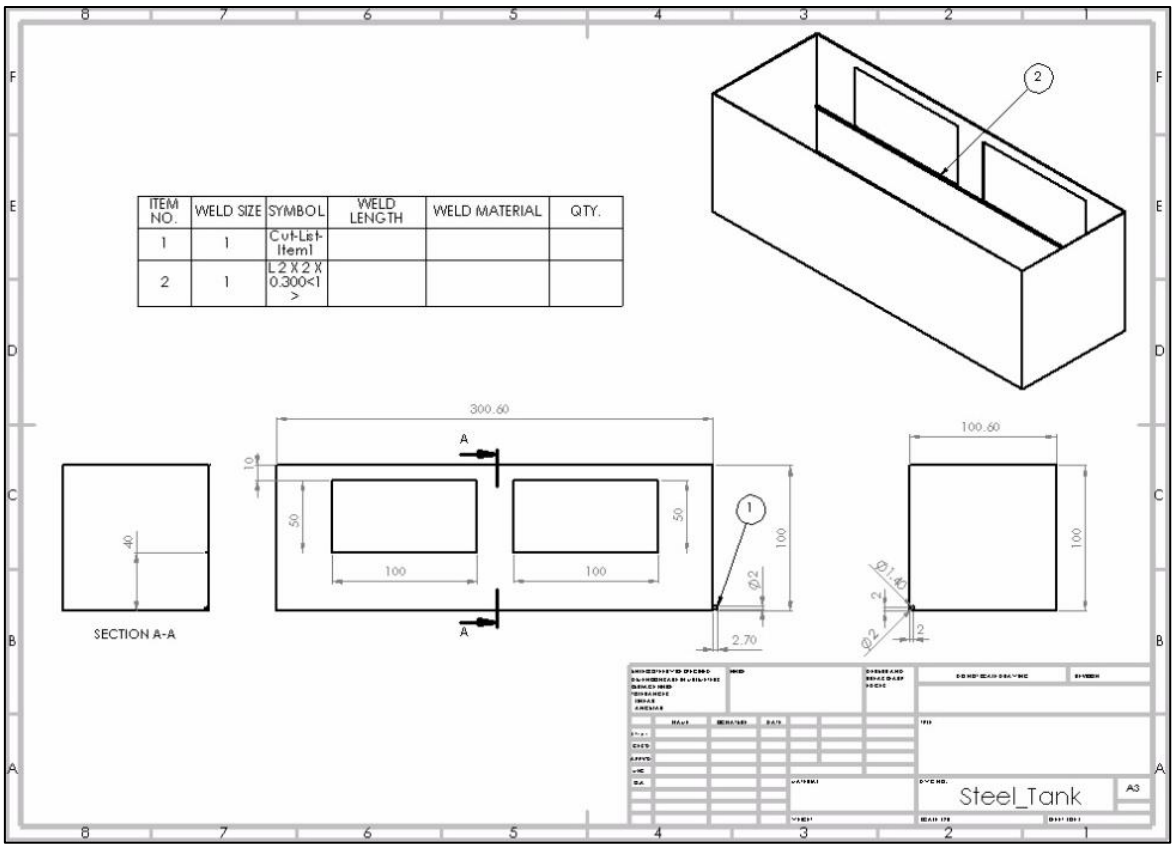

Figure 153: Outdoors lab tank